FLOW INDUCED ACOUSTIC RESONANCES

IN HEAT EXCHANGERS

by

GEORGE J. RAE

A thesis submitted to the Council for National Academic Awards in partial fulfillment of the requirements for the degree of Doctor of Philosophy.

SPONSOR: School of Mechanical and Offshore Engineering
Robert Gordons Institute of Technology
Schoolhill
Aberdeen

COLLABORATING ESTABLISHMENT:
Babcock Power Research Centre
High Street
Renfrew

March, 1986.

FLOW INDUCED ACOUSTIC RESONANCES IN HEAT EXCHANGERS

by

GEORGE J. RAE

SUMMARY

This thesis describes an investigation into the acoustic phenomenon in in-line tubular heat exchangers subjected to cross flow. The flow through such a heat exchanger can result in the production of very high noise levels, which occur as a result of the excitation of an acoustic standing wave in the cavity between the tube rows. This acoustic vibration can occur in large and small heat exchangers alike, resulting in drastically impared performance and working life.

The phenomenon associated with such vibration is poorly understood and considerable anomalies still exist in published literature. There are several theories which attempt to describe this mechanism, however, none of these can satisfactorily account for its complex nature.

The objective of the present work was to carry out an investigation to assess this acoustic phenomenon. The initial stages of this work produced an experimental rig to allow the phenomenon to be fully investigated, this included the examination of the effect of row depth and bank geometry on the acoustic resonance. The next step was to determine the role played by acoustic damping. This included making measurements of the damping under flow conditions and establishing its dependancy on velocity. A method of increasing the acoustic damping of a given bank was developed and incorporated in a tube bank. The results obtained from these experiments revealed that the acoustic system behaved in a manner which was consistent with that of a self excited system.

Finally an appropriate mathematical model of the system was developed. The model, which considers an acoustic feedback effect, was found to give quite an accurate representation of the system, and has the ability to account for all the observations made in this investiagation. This, together with the experimental results, enabled a series of guidelines to be presented as a basis for the design of such a tube bank.

CONTENTS

NOMENCLATURE

A_o	Constant	dimensionless
A	Aspect Ratio	dimensionless
a	Width of acoustic cavity	m
B_o	Correction factor	dimensionless
B	Bandwidth	Hz
C	Constant	dimensionless
c_o	Speed of sound in free space	m/s
c	Speed of sound	m/s
D	Damping parameter	dimensionless
d	Tube diameter	m
F_o	Friction factor	dimensionless
$F_X(f)$	Fourier spectrum of signal X(t)	
$F_{XX}(f)$	Power spectrum of signal X(t)	
$F_{XY}(f)$	Cross spectrum between X(t) and Y(t)	
f_n	Natural frequency	Hz
f_s	Sampling frequency	Hz
f_t	Tube natural frequency	Hz
f_v	Vortex shedding frequency	Hz
f	Acoustic frequency	Hz
G_o	Mass velocity	kg/s
g,h	Constant	dimensionless
H	Height	m
$H_{XY}(f)$	Transfer function from X(t) to Y(t)	
K, K_o	Constant	dimensionless
L	Heat exchanger width normal to the tubes and flow	m

l_l	Longitudinal pitch	m
l_t	Transverse pitch	m
M_o	Dimensionless exponent	
M_N	Mach number	dimensionless
M_t	Mass per unit length of tube (including added mass)	kg/m
M	Mass parameter	dimensionless
m	Mode number or mass	dimensionless or kg
N	Number of tube rows or data points in DFT	
n	Dimensionless exponent	
P	Pressure	N/m^2
Q	Amplification factor	dimensionless
R	Gas constant	J/kg K
Re	Reynolds number	dimensionless
S_A	Acoustic Strouhal number	dimensionless
T	Grotz and Arnolds damping parameter, temperature (Table 1), length of time record (chapter 6)	dimensionless, °C, seconds.
t	Turbulent intensity (chapter 5 and 7), time	dimensionless, seconds
U_m	Velocity at minimum cross sectional area	m/s
U	Velocity, approach velocity	m/s
V_S	Transverse velocity fluctuation	m/s
V	Voltage	volts
V_r	Reduced velocity	dimensionless

$W(t)$	Weighting function	
X_L	Longitudinal tube pitch to diameter ratio	dimensionless
X_T	Transverse tube pitch to diameter ratio	dimensionless
x	Distance in a direction parallel to the flow	m
y	Distance in a direction transverse to the flow and axis of the tubes	m
Z	Impedance	
α^1	Constant	dimensionless
α	Constant $\alpha^1 d \mid \rho U_m$	m/N
β	Stability criterion	
ΔP	Pressure drop	N/m^2
δ	Logarithmic decrement	dimensionless
ψ	Chen's damping parameter	
λ	Wave length	m
θ	Angle of rotation of separation point	radians
γ^2_{xy}	Coherence between X(t) and Y(t)	
ϕ	Phase angle	degrees
ρ	Fluid density	kg/m^3
τ	Time	seconds
ω	Angular frequency	radians / s
ζ	Damping ratio	dimensionless
σ	Parker's constant	dimensionless
γ	Ratio of specific heats	dimensionless
μ	Dynamic viscosity	Ns/m^2

1. INTRODUCTION

Flow induced acoustic resonances can occur in a multitude of different heat exchangers, ranging from large nuclear heat exchangers to small process shell and tube heat exchangers. Basically these heat exchangers all consists of tubes which convey a "tube side fluid" and a shell which encases the tubes and a "shell side fluid". The transfer of heat occuring between the two fluids via the tube walls.

The acoustic resonance in such a heat exchanger is usually only encountered when the shell side fluid is a single phase gas. The resonance when excited is established within the tube bundle in a direction perpendicular to the flow and the tube axis, as shown in figure 1.1. The mode of vibration usually associated with this phenomena is one of the transverse modes. The sound produced by this resonance is practically a pure tone and has been reported to be as high as 165 dB (re 2×10^{-5} Nm^{-2}). Such intense sound levels in a heat exchanger will not only disturb the operating conditions, but can vibrate the whole heat exchanger structure causing tube and shell failures.

It has long been recognised that these resonances could be excited in heat exchanger tube bundles, a problem which has become more evident as design trends have changed towards more compact units (smaller tube spacings)/

spacings)with higher shell side velocities. There is however still a basic shortage or reliable data and satisfactory methods for predicting resonance conditions. Classically it is assumed that the resonance is excited when the vortex shedding frequency and the acoustic frequency become coincidental. Many experimenters however have found this method to be totally unreliable. In a paper by Roger and Penterson (ref. R2) it is stated that, in the case of boilers, even though the vortex shedding frequency may match a transverse acoustic frequency, a standing wave develops in less than 5% of the cases of indicated resonance. The unreliability of this method has led to the development of several other theories explaining the existence of the resonance. One of the more novel ideas was presented by Cohen and Deane (ref. C10) who investigated the acoustic resonance phenomena in public utility power boilers, and noted, that with the trend towards larger units an increase of standing wave vibration had occurred. They concluded that, calculating resonance conditions by using vortex shedding frequency formulaes was not a dependable method, and suggested a minimum duct width of 22 ft for resonance to occur. The relevant theories associated with this phenomenon will be discussed in more detail in the literature survey.

This work was initiated so that the excitiation mechanism might be identified and the relevance of an alternative /

alternative approach suggested by Bryce and Murray (ref. B15) established.

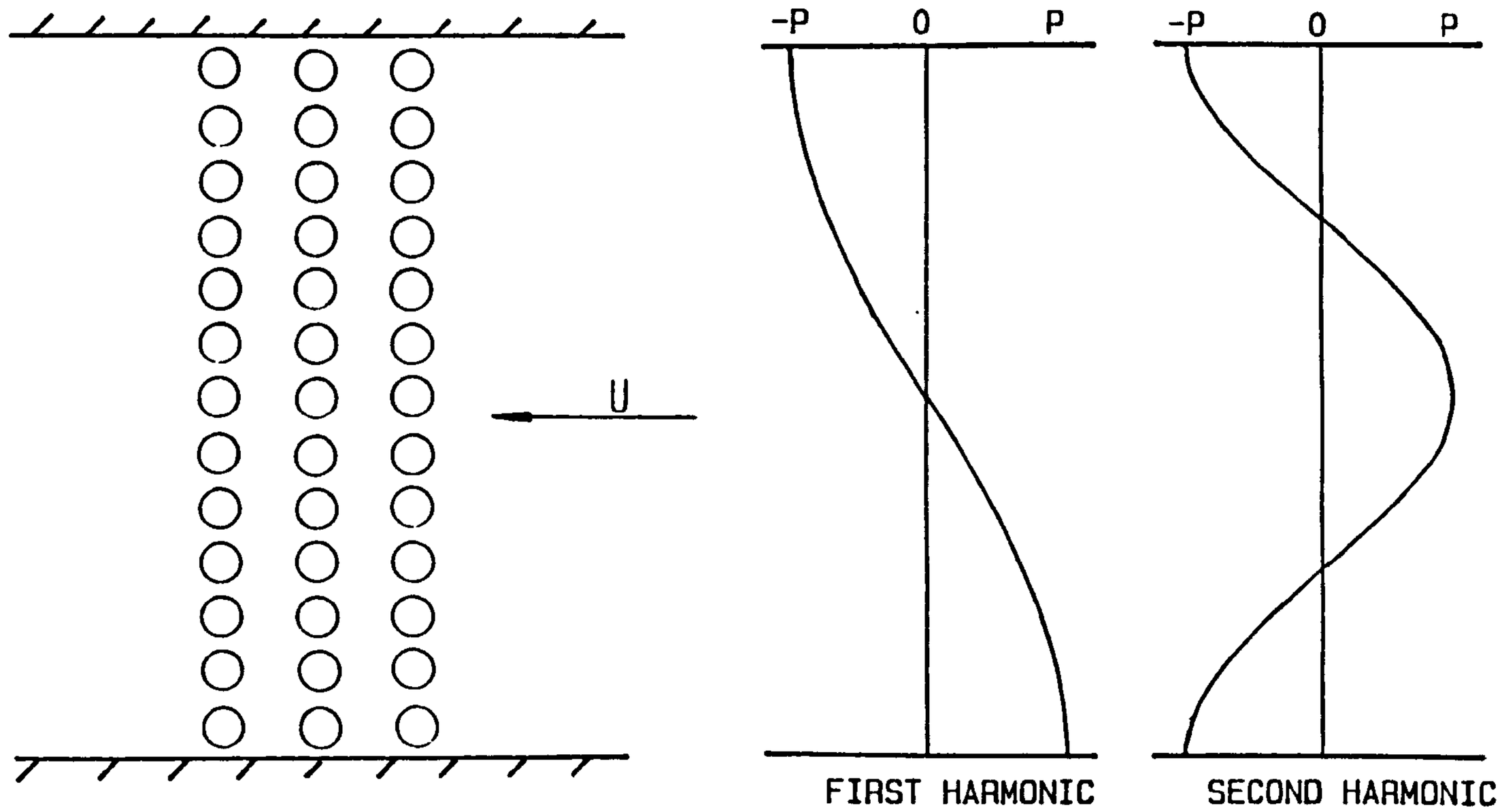

DIAGRAM ILLUSTRATING THE FIRST TWO HARMONICS OF ACOUSTIC VIBRATION IN A HEAT EXCHANGER TUBE BUNDLE

FIGURE 1.1

2. LITERATURE SURVEY

2.1 INTRODUCTION

The occurence of flow induced vibration in heat exchangers is now a widely documented phenomenon. Nevertheless, it is still the second most common cause of heat exchanger failure, corrosion being the most common (ref. B12). Heat exchanger failure, in industrial units, caused by flow induced vibration usually results from a flow over the tubes (shell side flow) rather than a flow through the tubes (tube side flow).

In this review of literature the mechanisms associated with flow induced vibrations will be divided into two different, but not necessarily unrelated categories, of acoustic vibration and tube vibration. The topic of tube vibration shall be discussed initially followed by a review of the various different theories associated with the excitation of acoustic vibration. Several theories exist which describe the nature of each of these phenomena, the more relevant of these will be discussed.

2.2 TUBE VIBRATION

2.2.1. VORTEX SHEDDING

The nature of the flow about a cylinder subjected to a cross flow of fluid is largely determined by the Reynolds number based on the cylinder diameter. When this parameter is sufficiently small (Re < 1) the flow is steady and the streamlines can be calculated using potential flow theory.

As the Reynolds number is increased a pair of fixed vortices will form directly behind the cylinder (see fig. 2.1 (b)). A further increase will result in the wake becoming unstable and beginning to oscillate. These oscillations will appear at some point downstream of the cylinder and move upstream with increasing Reynolds number. When the oscillations reach the cylinder this will result in the fixed vortices breaking away and moving downstream in a staggered array, this is know as the Von Karman vortex street and is illustrated in fig. 2.1 (d). Initially this vortex street will be laminar until a Renolds number of approximately 150 is reached, beyond which, the vortices will become turbulent (fig. 2.1 (e)). In the range $300 < Re < 1.3 \times 10^5$, which is known as the sub critical regime, the frequency of vortex shedding continues to increase in direct proportion to the velocity, when a Reynolds number of approximately 1.3×10^5 is reached the transition from laminar to turbulent/

turbulent boundary layer will occur. At this point the flow separation points move downstream, the vortex shedding becomes disorganised and the drag coefficient drops sharply. The start of the transition from laminar to turbulent boundary layer may be found to occur anywhere in the region $1.0 \times 10^5 < Re < 3.5 \times 10^5$, depending on free stream turbulence and surface roughness. Relatively few experimenters have investigated the supercritical region, but those who have (ref. R3) report that once the turbulent boundary layer is fully established ($Re = 3.5 \times 10^6$) the vortex street is found to reappear.

The vortex shedding phenomena is characterised by a non-dimensional parameter known as the Strouhal number, S, which is named after the author of the first paper on vortex induced oscillations.

The Strouhal number is defined as

$$S = \frac{f_v.d}{U}$$

The well established value of Strouhal number for a single cylinder, subjected to a cross flow fluid, is 0.2 for a sub critical Reynolds number. Figure 2.2 illustrates the Reynolds number effect on Strouhal number, for a single cylinder, and this shows S to be constant in the range $10^2 < Re < 10^5$ (ref. C14).

When a vortex is shed from a cylinder, the flow pattern around the cylinder becomes unsymmetrical, giving rise to an aerodynamic lift force. There also exists /

exists a fluctuating drag force, the frequency of which is twice that associated with the fluctuation lift force. This is because, in the lift direction, one cycle is the interval between two vortices shed consecutively from the same side of the tube (during that interval a vortex has been shed from the other side of the tube). In the drag direction a cycle is the interval between each vortex shed, irrespective of the tube side, therefore the force occurs at twice the frequency. However the fluctuating drag force is an order of magnitude smaller than the lift force.

Consider a cylinder suspended in a fluid and the fluid flow velocity, perpendicular to the cylinder axis, is increased. When the vortex shedding frequency approaches the natural frequency of the cylinder, the vortex shedding frequency becomes motion dependent, and 'locks in' to the frequency of vibration. Bishop and Hassan (ref. B20) found that the total alternating transverse force was greater for an oscillating cylinder than for the same cylinder rigidly mounted. Similarly Toebes (ref. T1) noted that the spanwise correlation of the wake increased for an oscillating cylinder. Thus the 'lock in' phenomena is a feedback mechanism by which the tube motion can lock the vortex shedding frequency to the frequency of motion, and increase the force causing that motion. The velocity range over which vibration will occur as a result of this phenomena, is dependent on/

on the tubes damping and mass parameter. These two non-dimensional numbers are often brought together to form a non-dimensional damping parameter which is equal to $\frac{M_t \delta}{\rho d^2}$. As this parameter is reduced in magnitude, the velocity range over which instability will occur is increased. If however this parameter is sufficiently high it will prevent vortex induced oscillation altogether (ref. D3). Fitz-Hugh (ref. F1) states that, for practical cases, vibration will almost certainly occur if $f_t = f_v \pm 20\%$.

As the amplitude of cylinder vibration increases beyond approximately 0.5 d the symmetric pattern of vortex shedding begins to break up, and when the amplitude increases beyond 1.0 d the lift coefficient decreases to zero (ref. B11). This implies that vortex induced vibration of a cylinder has a self limitating amplitude of approximately 1.0 d.

In an array of cylinders vortex shedding may be characterised by a Strouhal Number in much the same way as an isolated cylinder. Usually, however, this Strouhal number is based on the flow velocity at the minimum gap between the tubes. The Strouhal number, defined in this way, is found to vary with array geometry.

The correlations of Fitz-Hugh and Chen are probably the most widely used for design purposes and these are illustrated in figures 2.3 and 2.4 respectively./

respectively. Figure 2.3 (a) is the correlation for in-line tube bank geometries and 2.3 (b) is for staggered geometries. The X and Y axis of these correlations represent longitudinal and transverse pitch/diameter ratios, and the areas of differing Strouhal number are marked by the contours. The correlations in figure 2.4 (a) and 2.4 (b) are again for in-line and staggered bank geometries. The X and Y axes in these correlations represent transverse tube pitch diameter ratio and Strouhal number respectively. The lines on these correlations indicate geometries of constant longitudinal tube pitch diameter ratio. Comparison of the correlations of Chen and Fitz-Hugh shows that several contradictions exist. Also in the complex maps of figure 2.3 (a) a high proportion of the points do not conform to the Strouhal number zones in which they lie. In the case of the in-line tube bank arrangements, both of the correlations are largely based on the same data. The differences between the correlations at small tube pitch diameter ratios is largely due to the extrapolation to a zero Strouhal number at $\frac{l_t}{d} = \frac{l_l}{d} = 1.0$ which was made by Chen. If recent data is introduced to the staggered correlations it is generally found to be in good argeement with existing data (ref. H1). A study of staggered banks by Baulay (ref. B6) however, does suggest that these correlations fail at small tube pitch to diameter ratios. In the case of the in-line correlations however,/

however, recent data bears no simple relationship to the existing points. Some typical examples of such work shall now be examined.

A study of both in-line and staggered arrays was reported by Baylac et al (ref. B7). For staggered arrays only two geometries, of large pitch ratio, were considered. In these banks the peak in the velocity power spectrum was found to increase continuously with velocity, until the acoustic frequency was reached. For the case of one of their staggered arrays ($X_T = X_L =$ 3.02) they reported the existance of a second peak in the power spectrum which was only visible in the first four rows of their nine row bank. They concluded that for this bank two Strouhal numbers existed corresponding to the two frequencies, and the lower of the two, gave good agreement with the results of Chen. For the case of in-line bank arrangements they studied six different geometries and reported a need to split in-line geometries into two groups, that of large longitudinal pitch diameter ratios ($X_L > 2$) and that of small longitudinal spacings ($X_L < 2$). For arrangements of large longitudinal spacing their results exhibited only one peak in the power spectrum with a corresponding Strouhal number which was in good agreement with that of Chen. In the case of two of their arrangements ($X_T = X_L = 2$ and $X_T = X_L = 2.12$) they observed a large shift in Strouhal number from approximately /

approximately 0.17 to 0.25 at the onset of acoustic resonance, and they concluded that this was due to the "lock-in" phenomena. In the case of banks with small longitudinal spacings they studied two arrangements that of $X_T = X_L = 1.51$ and $X_T = 3.02$, $X_L = 1.5$. For the larger of these they reported a difficulty in defining a precise Strouhal number since the peak in the spectrum was wide. In the smaller bank two peaks were observed whose frequency increased linearly with velocity. The acoustic resonance was excited when the higher of the two reached the acoustic frequency. None of the results for smaller longitudinal spacings bore any resemblance to those predicted by Chen. In an examination of the cross correlation coefficient behind a tube they found that the transverse pitch ratio was the controlling parameter of the degree of correlation. As the transverse pitch ratio was decreased they found the correlation length to increase. They concluded that while transverse pitch ratio seemed to be the controlling parameter for the degree of correlation, the longitudinal pitch ratio had the predominant effect on the Strouhal number.

A paper by Batham (ref. B4) reported an investigation of the pressure distribution on tubes in in-line arrays subjected to cross flow. He found, in the bank with a square pitch/diameter ratio of 2.0, the flow was essentially two dimensional with two apparent peaks /

peaks in the pressure spectrum. These peaks were found to be dependant on angular displacement around the tube and he suggested that the peak corresponding to the lower Strouhal number was due to periodic oscillation of the reattaching shear layer, while the higher Strouhal number was due to vortex shedding. He noted that the Strouhal numbers obtained, showed poor agreement with those given by Chen, which were 30% larger. The spectrum of noise measured upstream of the bank revealed Strouhal numbers twice that of the vortex shedding wake, Batham therefore concluded that the noise was generated by the fluctuating drag excitation. In the 1.25 square pitch diameter ratio bank he observed a highly three dimensional flow, with no apparent peak corresponding to vortex shedding. However a narrow bandwidth peak corresponding to an acoustic instability was present. He noted that the pressure distribution around the tubes was very sensitive to movements of upstream tubes and suggested that instability in such a bank could be caused by a Coanda switching mechanism.

Although in the preceeding discussion the experimenters have generally compared their data to that of Chen, it should be added that the Strouhal number for closely packed banks do not agree with the Fitz-Hugh correlation either. There is also general agreement that in very closely packed banks the distinct /

distinct peak corresponding to vortex shedding breaks down into broadband turbulence making the Strouhal number virtually impossible to define by indirect methods (ref. B1, B4, B11, B12, H1).

The discrepancies mentioned previously are too large to be explained by experimental error or Reynolds number effects. There does however seem to be an explanation for these descrepancies and this is discussed below.

In a study by Bai (ref. B1) he reported measurements in both in-line and staggered geometries. In the closely packed in-line banks, he noted that the peak in the turbulence spectrum did not coincide with the cavity frequency at onset of acoustic resonance and, the measured Strouhal number did not agree with the Chen correlation. In less densely packed banks Bai noted that the vortex frequency was equal to the cavity frequency at the onset of resonance and the measured Strouhal numbers agreed reasonably well with that of Chen. Similarily with the staggered bank geometries the Chen correlation was in good agreement.

In a paper by Bryce and Murray (ref. B15), measurements taken from a model of a cross inclined heat exchanger are reported. The results of figure 2.5 were obtained when the bank contained a few isolated tubes with carefully controlled natural frequencies and damping. When the bank was exposed to a high density gas /

gas flow, (25kg/m³ typically) significant amplitudes of tube vibration were encountered when the vortex shedding frequency, as determined by hot wire anemometry, was in the vicinity of the tube natural frequency. That is the Strouhal number obtained by turbulence spectra and that derived from tube vibration measurements were the same. By contrast figure 2.6 shows some data relating to the onset of acoustic resonance in a test bank geometrically identical to that of fig. 2.5. The vortex shedding frequency (measured by hot wire anemometry) at the point of onset of acoustic resonance and the frequency of the acoustic resonance (measured by microphone downstream of the test section) were determined as the number of tube rows in the bank was varied. As can be seen this ratio varies from around 0.8 down to 0.4, thus showing no simple relationship between the vortex shedding frequency and the acoustic frequency at the point of onset of acoustic instability. They also presented results in which the method of fixing the tubes to the tube plates was altered, and these are illustrated in fig. 2.7. One can see from the results that when the tubes were wedged in place the first mode was not excited, and the onset velocity for the second and third modes is slightly higher than that for the welded tube ends. The Strouhal number as determined by hot wire anemometry is the same in both cases.

Fitzpatrick /

Fitzpatrick (ref. F2) reported on an investigation of the acoustic resonance phenomena within four in-line tube banks of various different geometries. Figure 2.8 shows the results he found if the bank depth was varied. As can be seen the effect of increasing bank depth can vary the acoustic Strouhal number quite considerably. He also observed peaks in the turbulence spectrum which varied linearly with velocity, but bore no simple relationship to the cavity frequency at the onset of acoustic resonance.

Murray (ref. M4) argued that the occurence of acoustic resonances in heat exchanger banks, is not a reliable means of determining Strouhal numbers. Also, if acoustic resonance data is ignored, a more orderly correlation of Strouhal number, as a function of geometry, appeared to exist, although data was sparse. A Fitz-Hugh type correlation for in-line tube banks was presented, in which all data pertaining to acoustic resonances had been removed, and more recent tube vibration data had been included. This correlation is shown in figure 2.9 and a more orderly pattern can be seen to have emerged. Two points should be made regarding this data. Firstly, the data of Funakawa (ref. F5) reported Strouhal numbers based on the approached velocity, rather than the velocity between the tubes as used here. Accordingly, the appropriate geometrical factor had been applied to bring all data to /

to a common basis. Secondly the data of Clasen and Gregorig (ref. C8) had to be altered. This data was more difficult to convert to a consistent basis, since they presented their data as Strouhal numbers based on the velocity at onset of tube vibration, rather than the velocity for peak response as is now more common. In an attempt to correct this, their Strouhal numbers have been decreased by 20% in each case. While this does aid comparison, it is certainly not precise, and some inconsistency in the comparison of their data with others may therefore be expected. However, in the case of two of their geometries (data points underlined) the original velocity/amplitude plots were available, and the Strouhal numbers, based on the peak response conditions, have been derived. In certain array geometries there is some evidence of the existance of two different excitation frequencies. This is particularly clear in the work of Clasen and Gregorig (ref. C8) and Funakawa (ref. F5), who looked at banks with large transverse/small longitudinal pitch geometries. While further work is certainly required to clarify this, it would appear that the higher of these frequencies relates to a somewhat lower level of excitation.

Finally we may conclude that, the occurence of acoustic resonance in heat exchanger banks is not predicted reliably by the use of a single Strouhal number /

number for a given bank geometry. Correspondingly, much of the disorder in Strouhal number correlations results from the inclusion of data derived from acoustic resonances.

VERY LOW Re

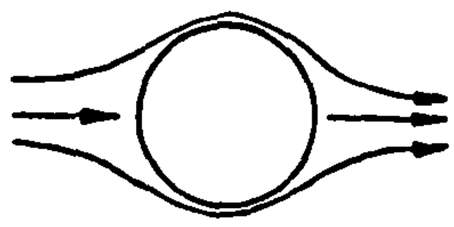

LARGE LATERAL VORTICITY PENETRATION (INCLUDING SPANWISE BOUNDARY INFLUENCE).

TWIN VORTEX STAGE

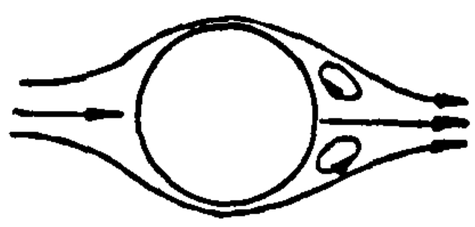

LAMINAR; STEADY IN PRACTICE. UNSTABLE UNDER ARTIFICIAL EXCITATION -- THEORETICALLY AND EXPERIMENTALLY

INCIPIENT KARMAN RANGE
30-40 < Re < 80-90

LAMINAR WAKE INSTABILITY

PURE KARMAN RANGE
80-90 < Re < 150-300

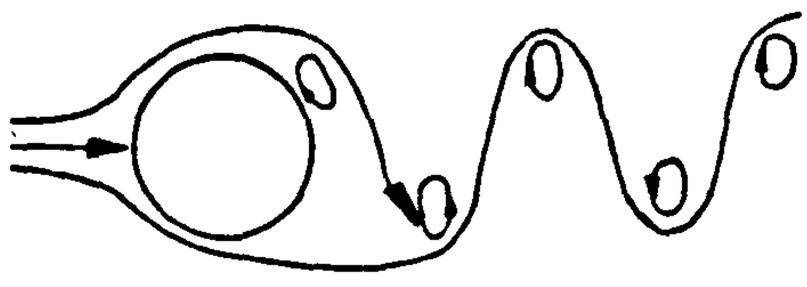

LAMINAR INSTABILITY OF DOUBLE VORTEX SHEET IN PRESENCE OF CYLINDRICAL BOUNDARY.

SUBCRITICAL RANGE

150 / 300 < Re < 100000 / 130000

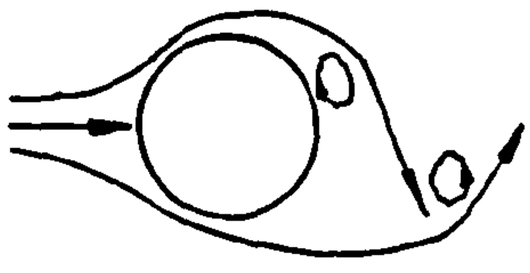

FORWARD PROGRESSION OF TURBULENCE AND INCREASING 3-DIMENSIONALITY
NEARLY CONSTANT STROUHAL NUMBER CORRESPONDING TO DOMINANT DOUBLE SHEET INSTABILITY.

MODERATE SENSITIVITY TO FREE STREAM TURBULENCE AND SURFACE ROUGHNESS

CRITICAL AND POST-CRITICAL RANGE

100000 / 130000 < Re < 3500000

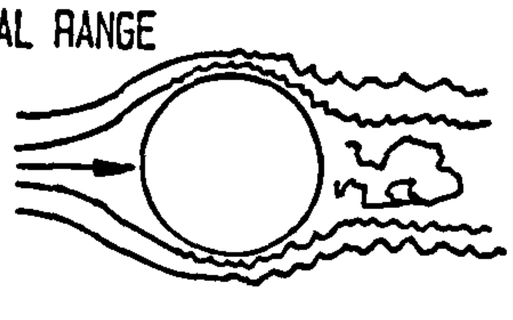

RAPID NARROWING OF WAKE
PROBABLE TIMEWISE AND SPANWISE MIXTURE OF VARIOUS SEPARATION PATTERNS.
STRONG SENSITIVITY TO FREE STREAM TURBULENCE AND SURFACE ROUGHNESS.
LOSS OF DOMINANT PERIODICITY

TRANSCRITICAL RANGE
3500000 < Re < ?

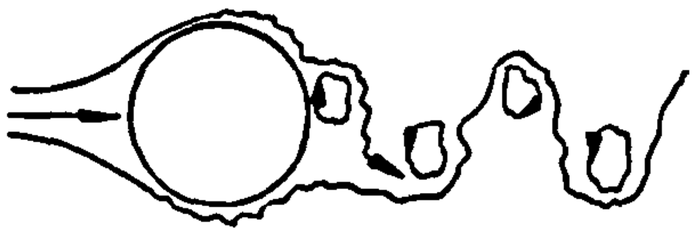

TRANSITION TO TURBULENT LAYER ON FRONT FACE OF CYLINDER, PROBABLY FOR 0 < 80
PROBABLE INSTABILITY OF TURBULENT DOUBLE SHEET. RECOVERY OF PRONOUNCED PERIODICITY CORRESPONDING TO MEDIUM WIDTH OF WAKE

SUMMARY OF CHARACTERISTICS OF MAJOR Re REGIMES

FIGURE 2.1

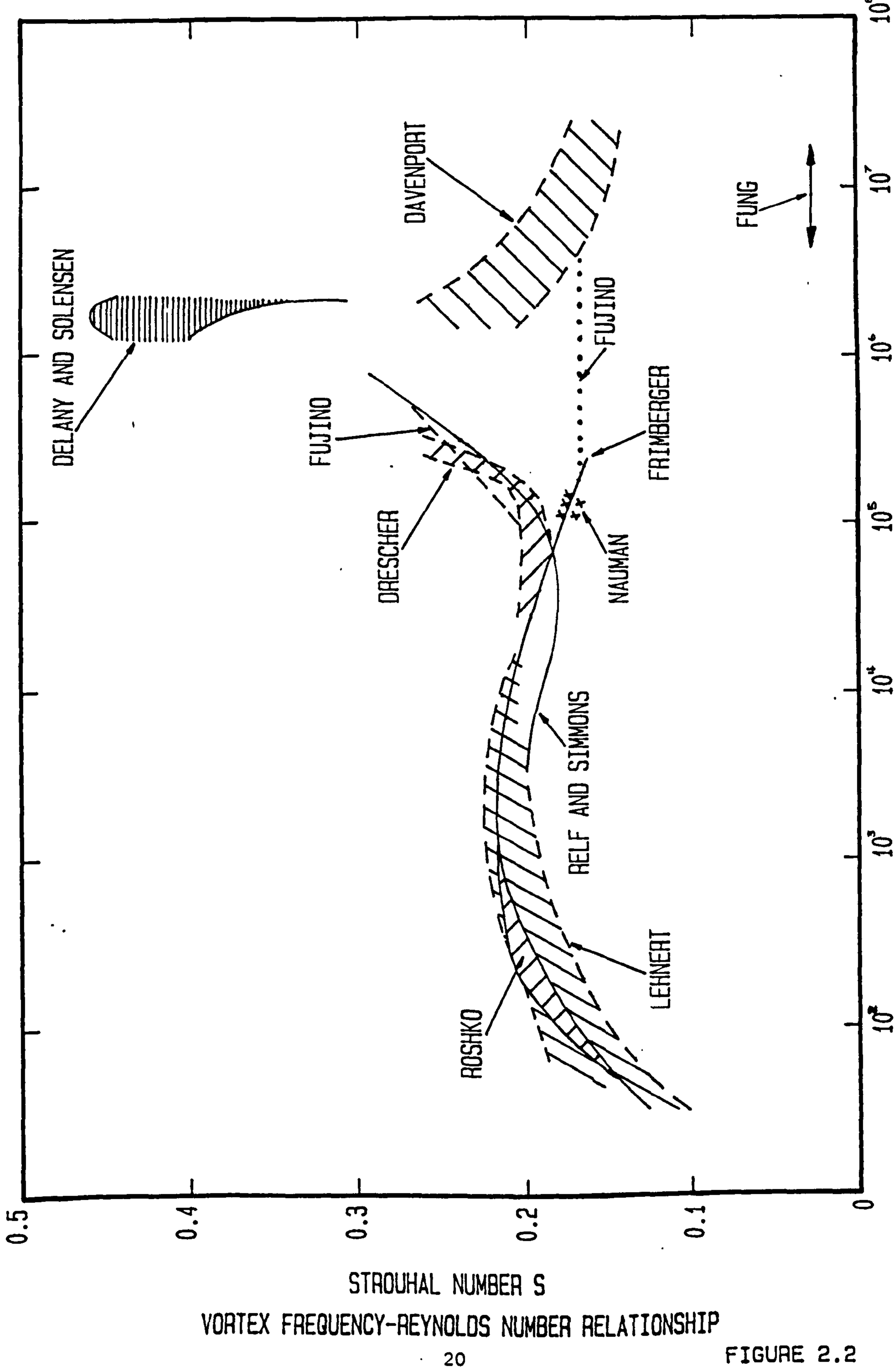

VORTEX FREQUENCY-REYNOLDS NUMBER RELATIONSHIP

FIGURE 2.2

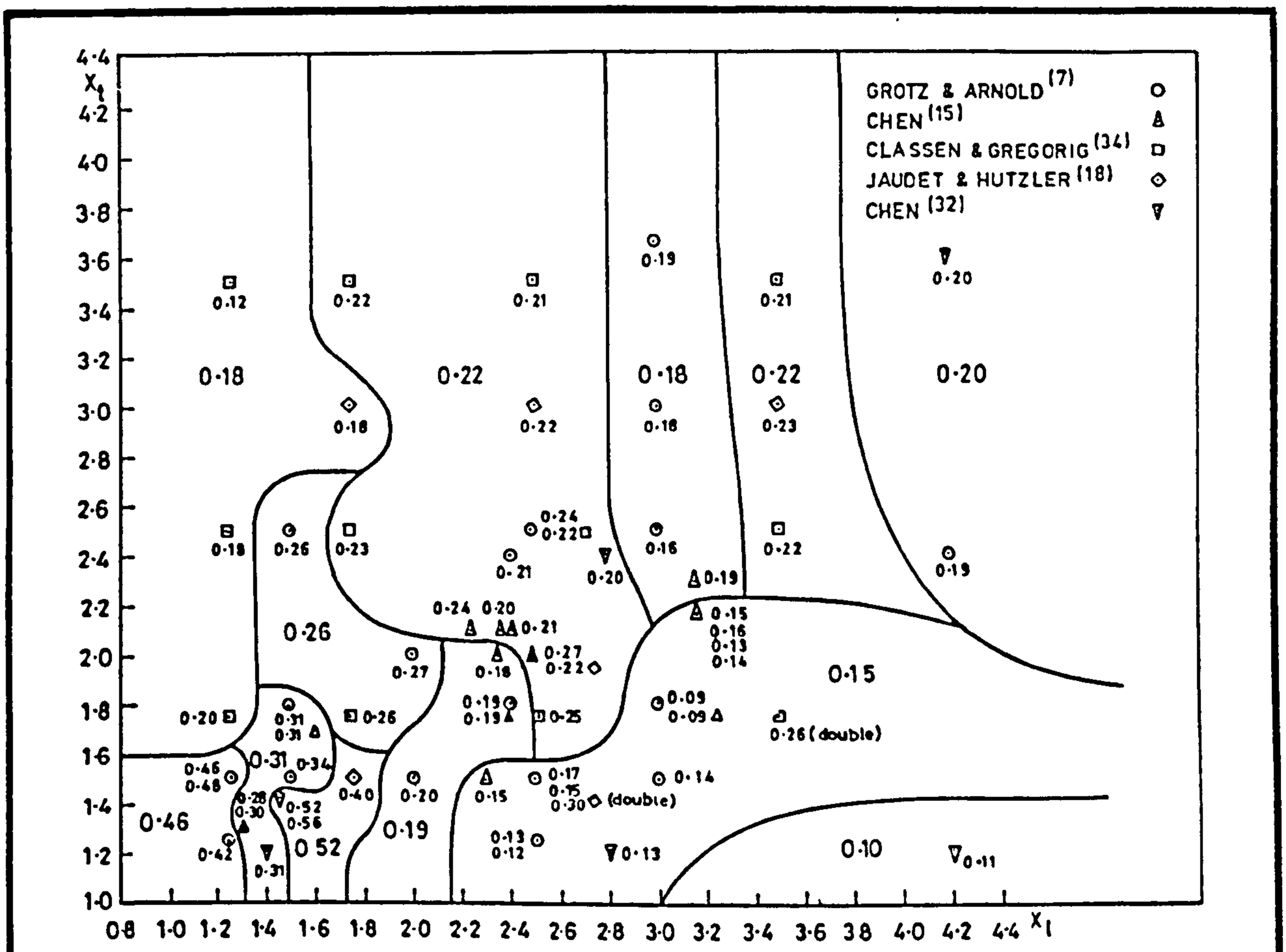

[A] STROUHAL NUMBER CORRELATION FOR IN-LINE ARRAYS

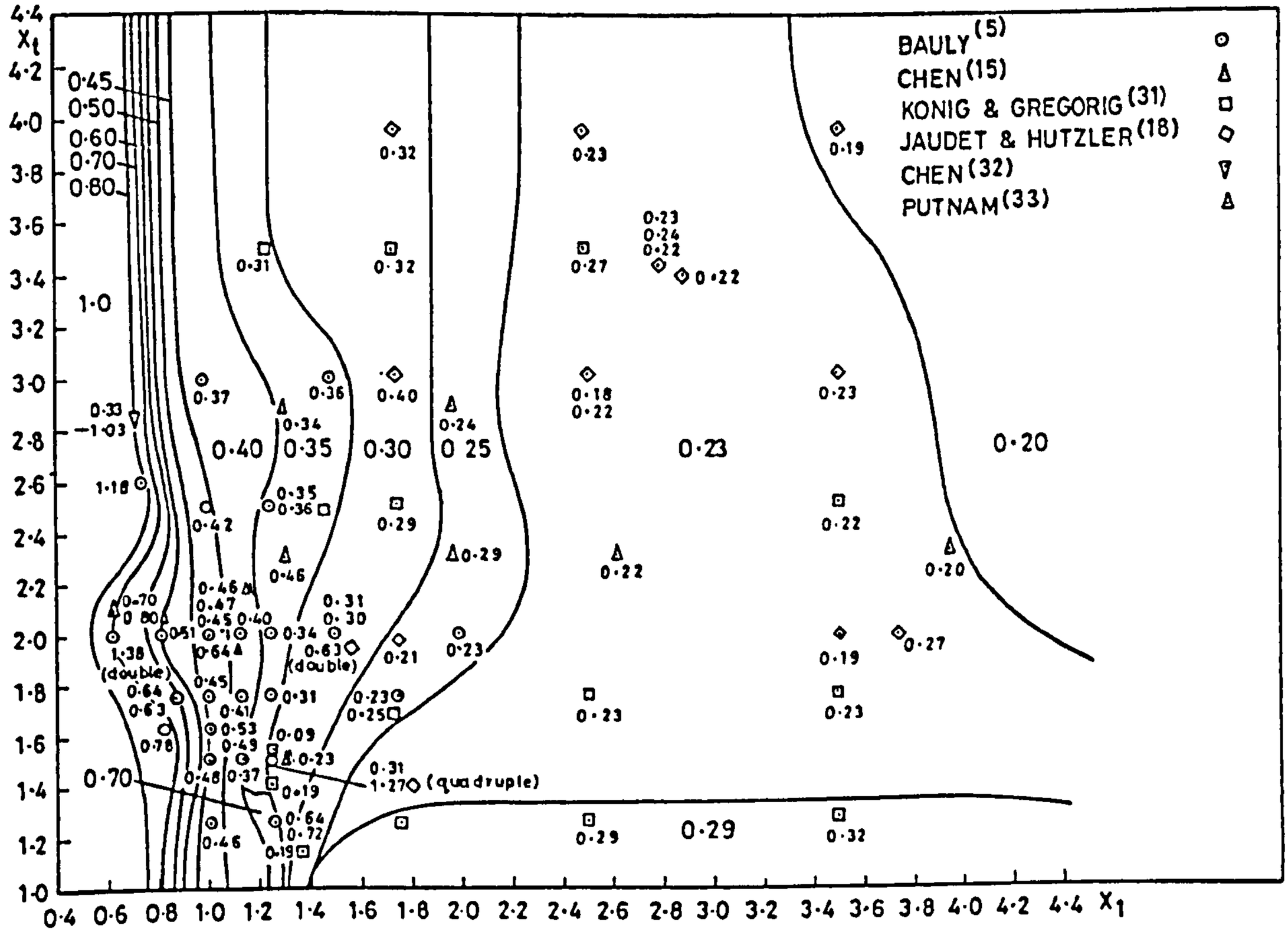

[B] STROUHAL NUMBER CORRELATION FOR STAGGERED ARRAYS

FIGURE 2.3

[A]

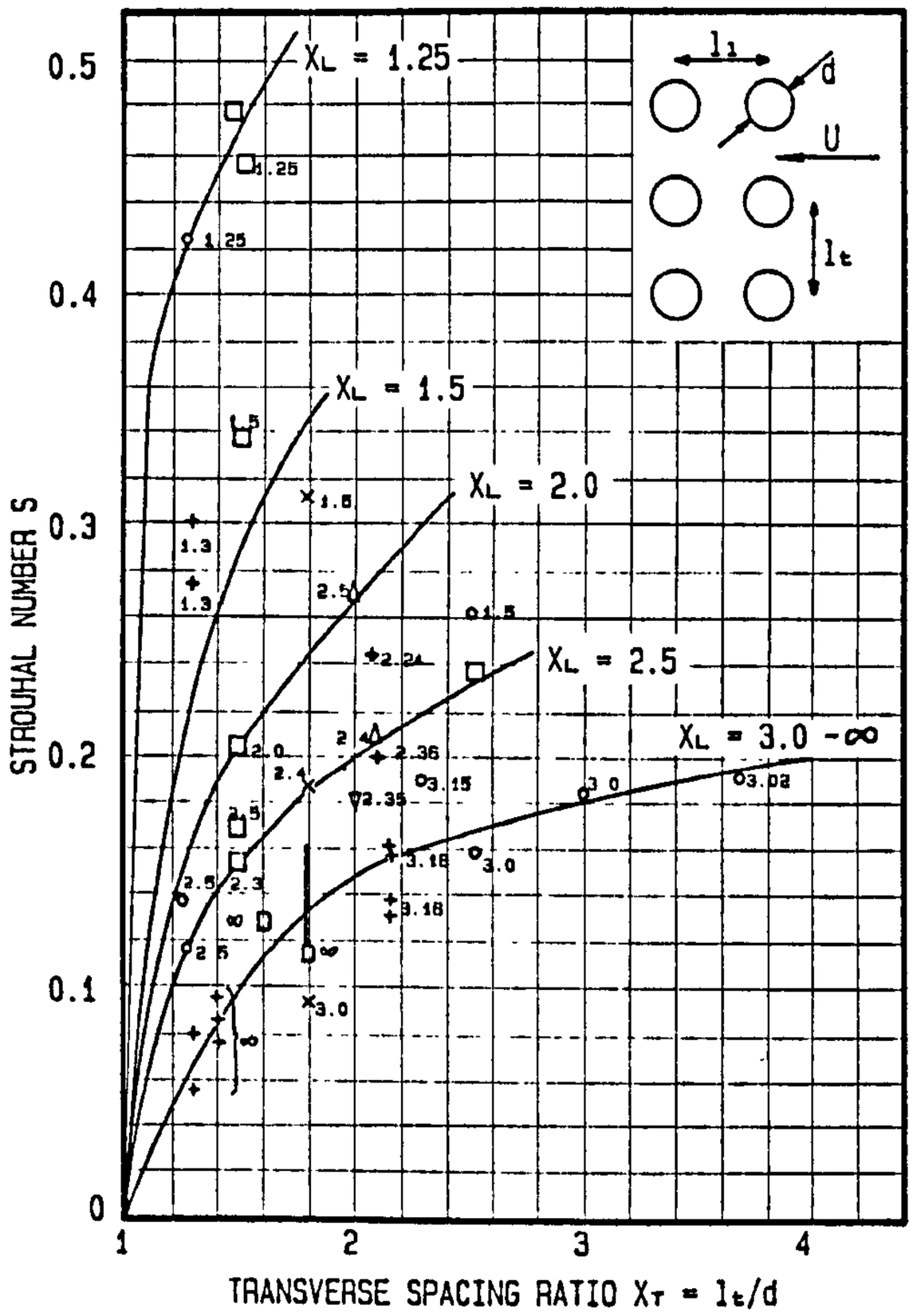

D - LIVESEY/DYE
+ - CHEN
ALL OTHER POINTS FROM
GROTZ and ARNOLD

GRAPH OF STROUHAL NUMBER AGAINST TRANSVERSE SPACING RATIO FOR IN-LINE ARRAYS

[B]

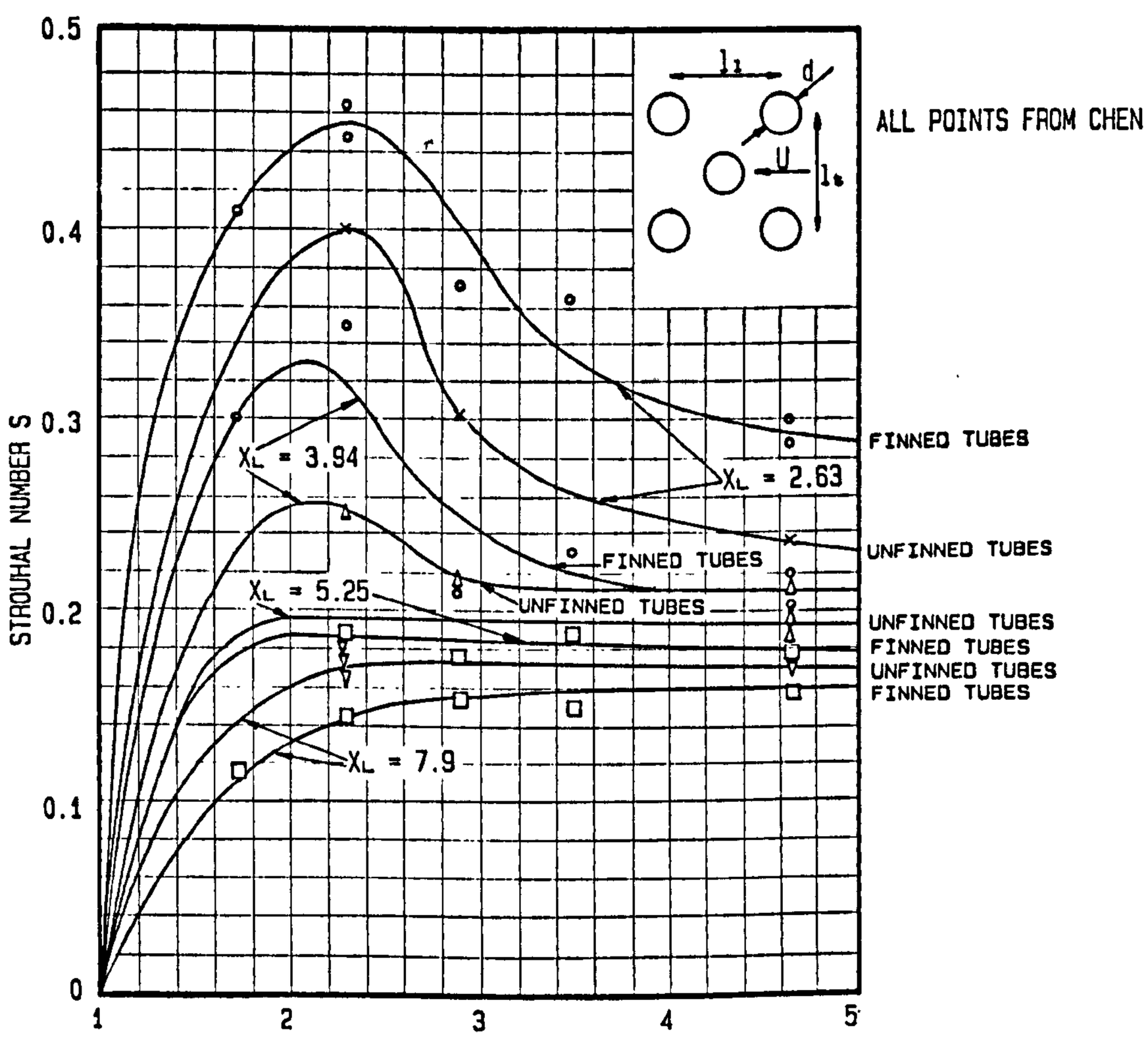

ALL POINTS FROM CHEN

GRAPH OF STROUHAL NUMBER AGAINST TRANSVERSE SPACING RATIO FOR STAGGERED ARRAYS

FIGURE 2.4

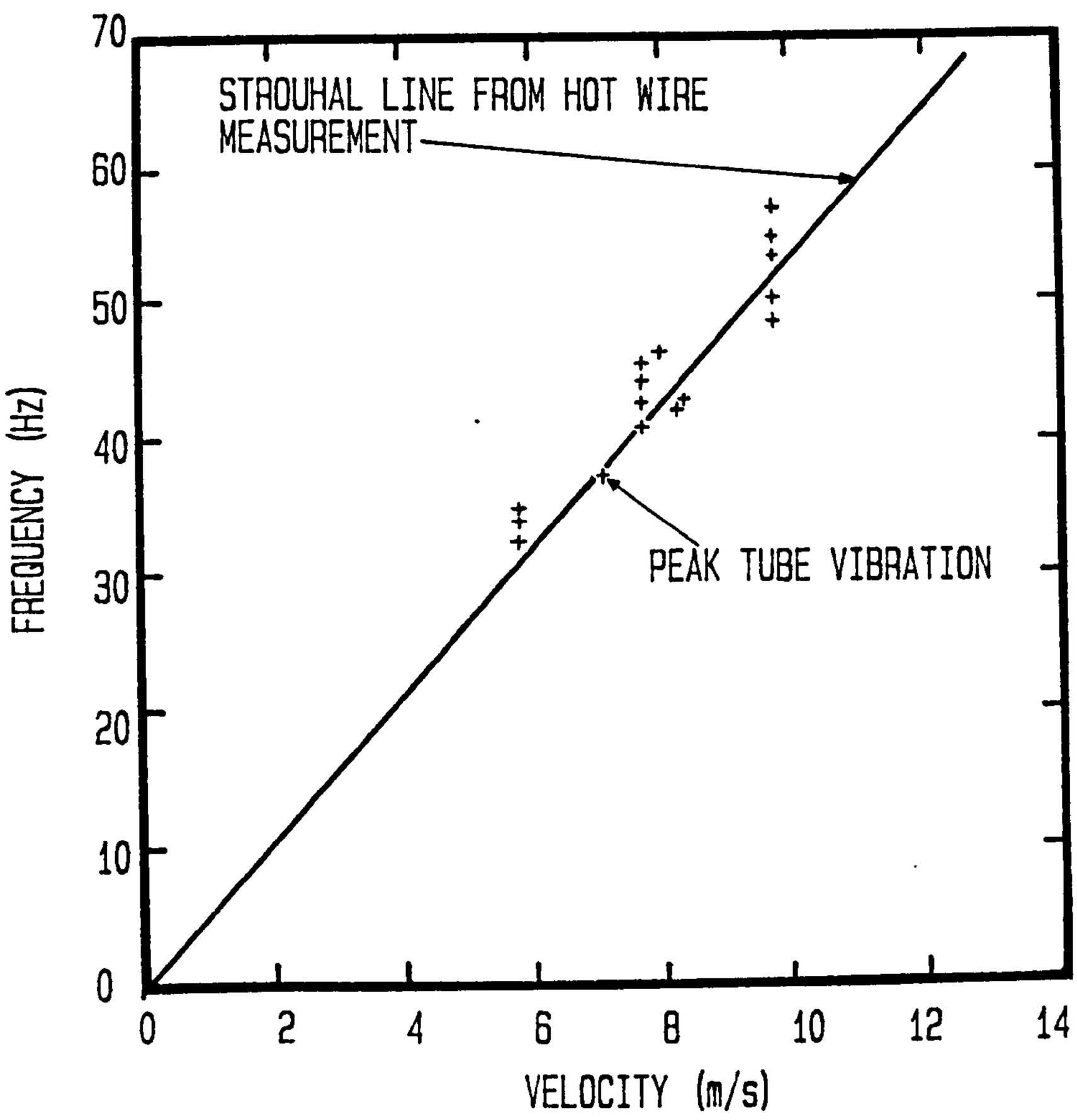

COMPARISON OF HOT WIRE ANEMOMETER AND TUBE RESPONSES

FIGURE 2.5

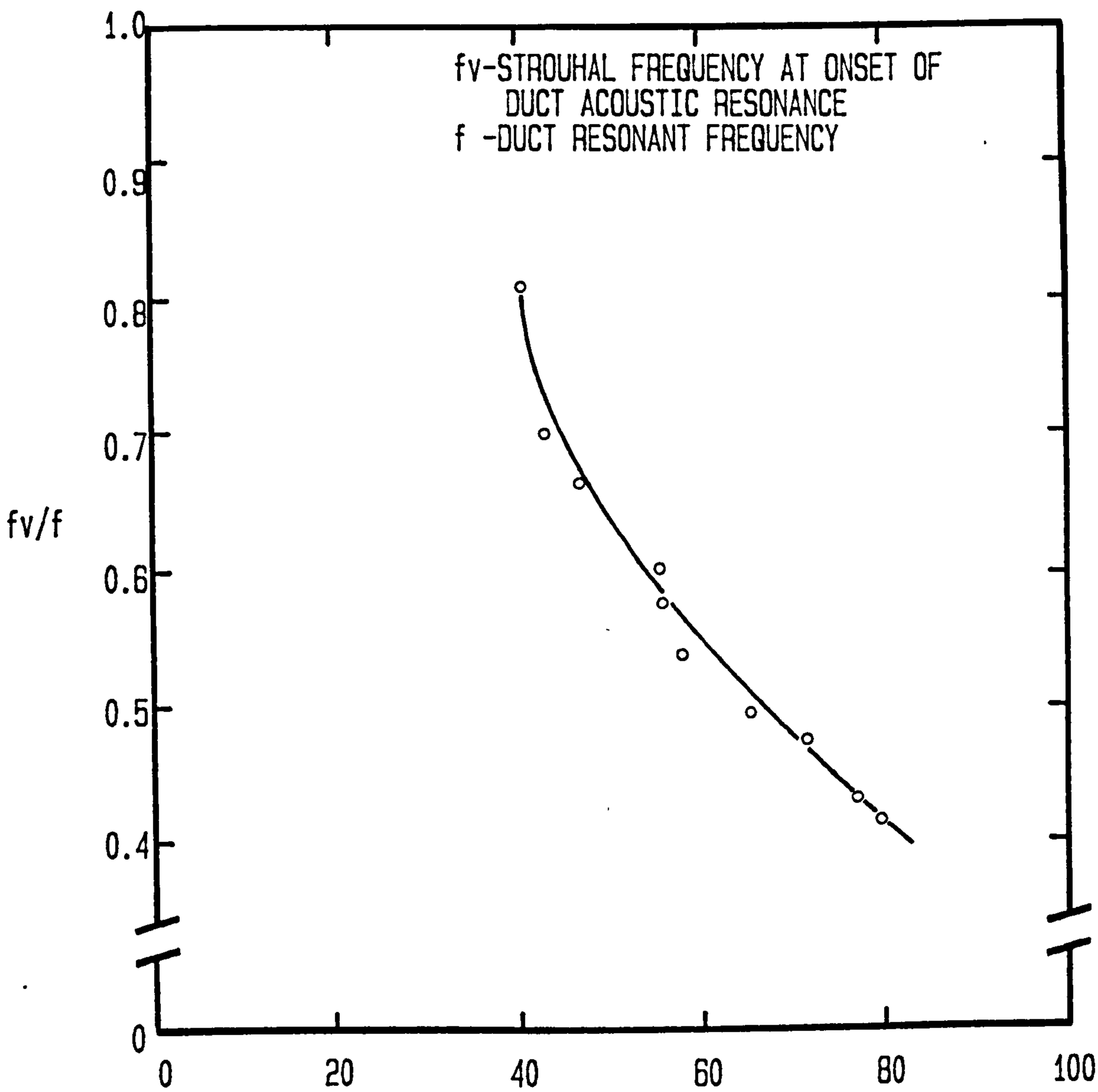

RATIO OF TURBULENCE FREQUENCY TO DUCT FREQUENCY AT ONSET OF DUCT ACOUSTIC RESONANCE VERSES ROW DEPTH OF TEST BANK

FIGURE 2.6

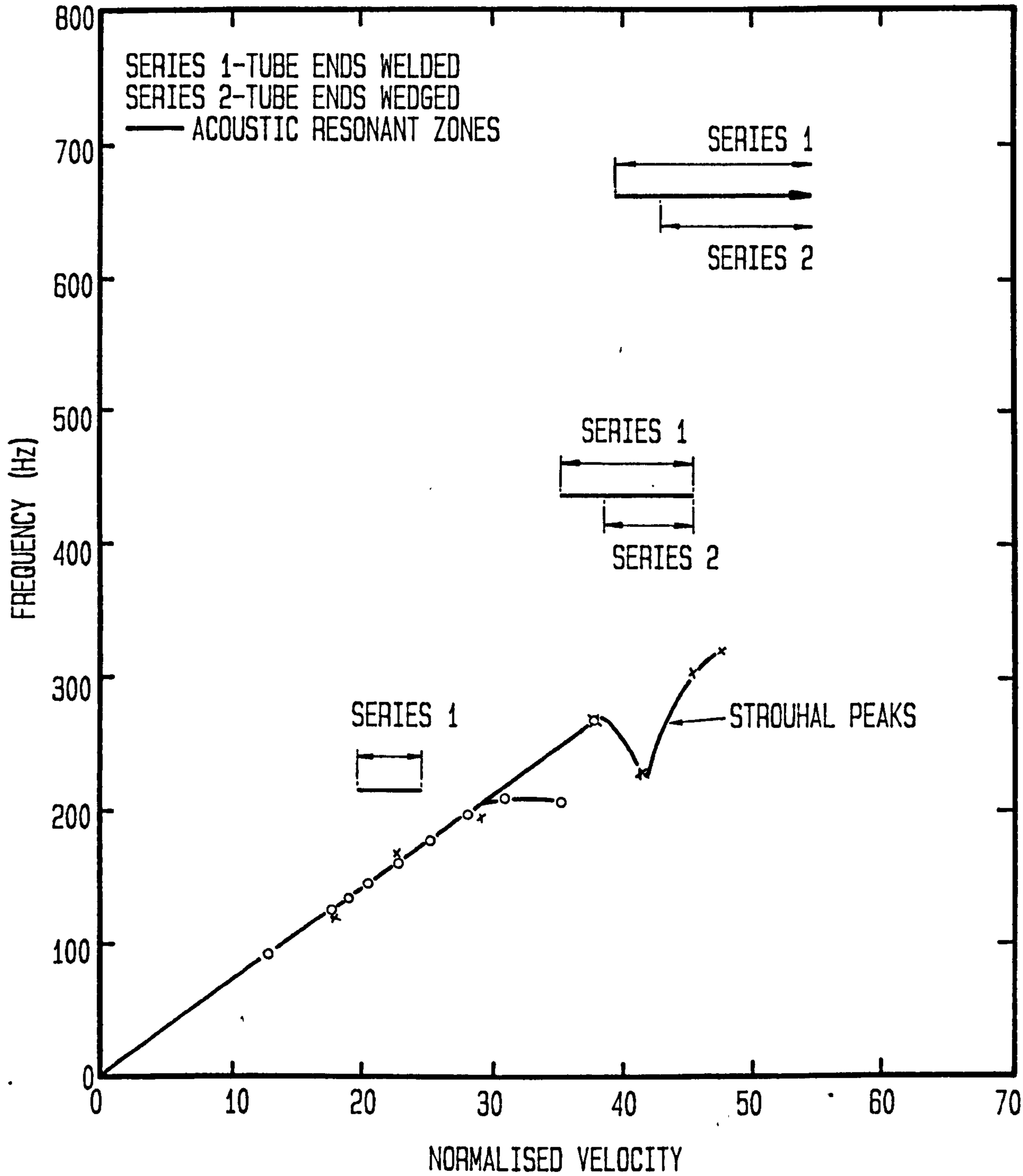

STROUHAL LINE AND ACOUSTIC RESONANCE ZONES FOR STRAIGHT TUBE BUNDLE WITH VARIOUS TUBE FIXINGS

FIGURE 2.7

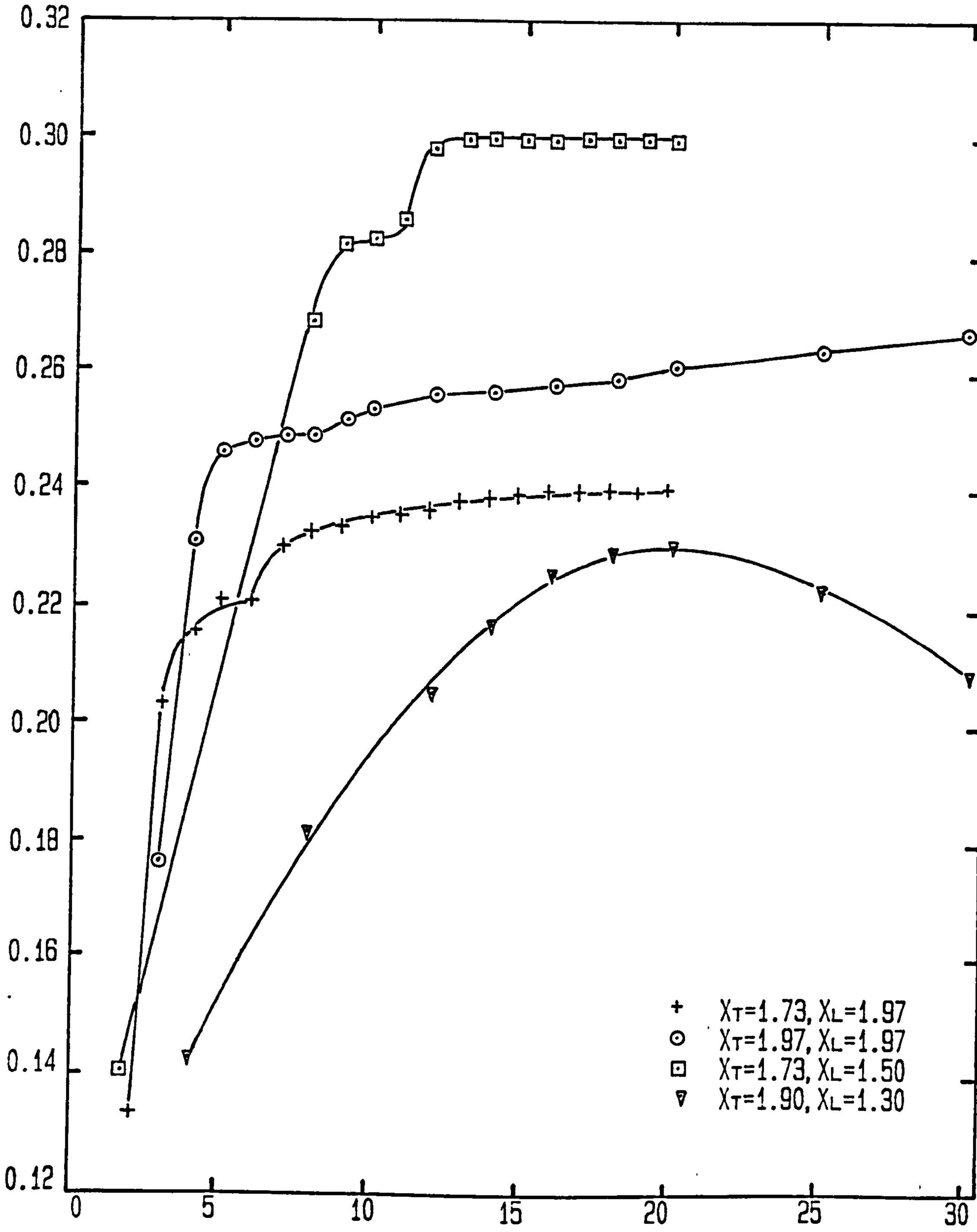

THE EFFECT OF NUMBER OF TUBE ROWS ON ACOUSTIC STROUHAL NUMBER

FIGURE 2.8

NON-ACOUSTIC STROUHAL CORRELATION FOR IN LINE TUBE ARRAYS

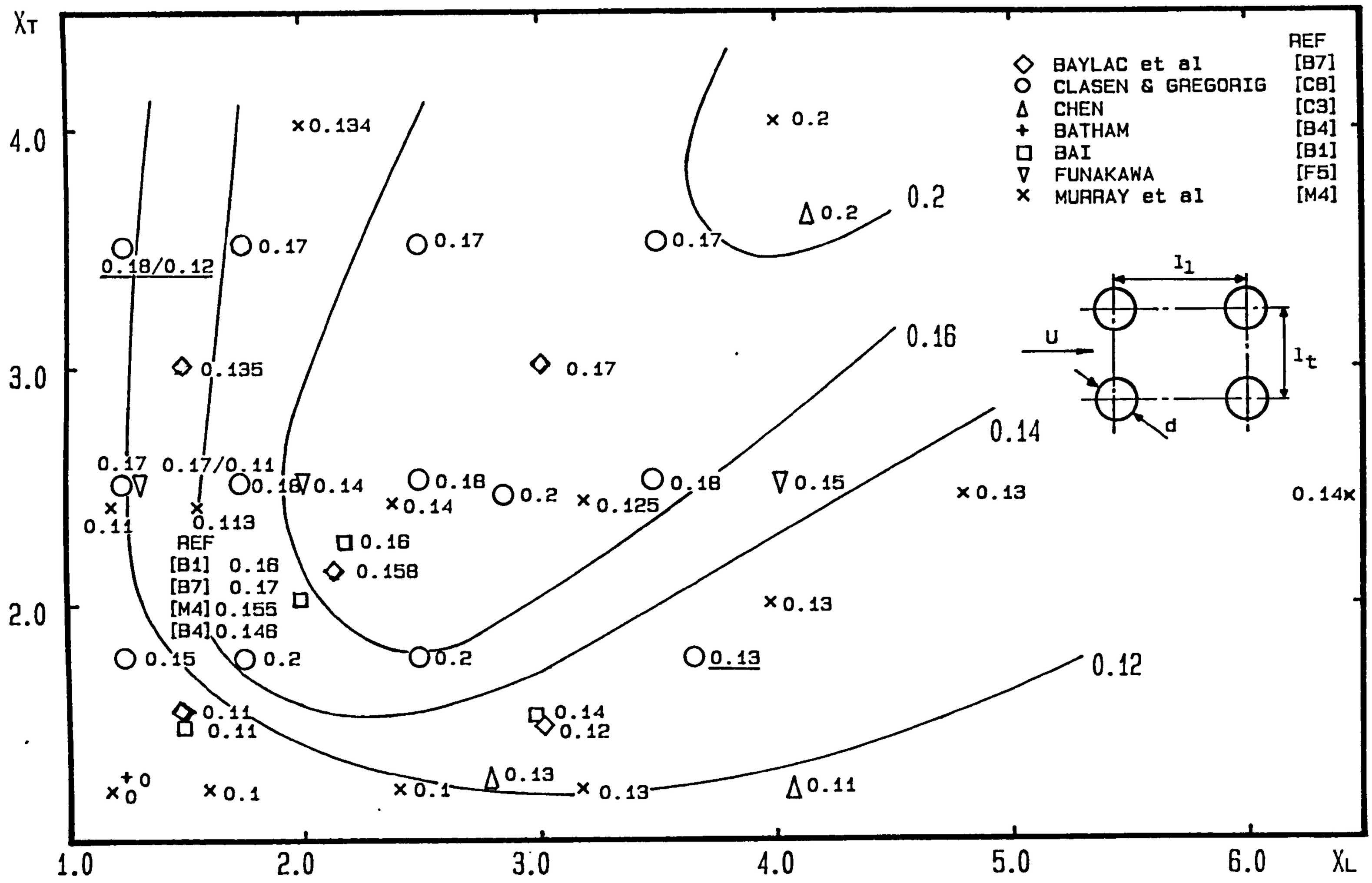

FIGURE 2.9

2.2.2 TURBULENT BUFFETING

Vibration induced by turbulent flow is perhaps the most common form of flow induced vibration experienced in every day life, for example gusts of wind swaying trees and rattling windows etc.

A structure which is placed in a flow retards the flow over its surface and some of the momentum of the flow is converted to pressure on that surface. Most practical flows are turbulent in nature, and in such a flow there exist many oscillatory components spread over a broad range of frequencies. Deterministic analysis for each oscillatory component would prove very tedious, therefore it is more practical to treat the flow statistically and deal with time averaged quantities. The theory of random vibrations provides the techniques for proceeding with this statistical approach, and is more fully described in ref. B11.

The response of a structure subjected to a random excitation can be considered in three parts, that of the non-resonant or buffeting response, the mean response and the resonant response. The mean response is the average displacement of the structure produced by the mean flow during the test interval, and is represented by section A in figure 2.10. The non-resonant response is the vibration at frequencies well removed from the natural frequency of the structure, while the resonant response is the vibration of/

of the structure near the natural frequency (sections B & C respectively in fig. 2.10).

If the power spectrum of the velocity fluctuations, in which the body is placed, is approximately of a constant magnitude (as in a normal turbulent flow, see fig. 2.11a) then, for a lightly damped structure, most of the response will lie in the vicinity of the resonant peak, as shown in fig. 2.11c. If however, the flow contains stronger frequency components which are well removed from the natural frequency of the structure, fig. 2.11b, this will produce significant non-resonant buffeting of the structure.

A structure exposed to turbulence will respond in a manner similar to that illustrated in fig. 2.11c, this shows the response to have a bandwidth which is dependent on the structural damping. The time series of such vibration is illustrated in fig. 2.12 and this shows the response to be modulated. This modulation, or beating,is produced by the interaction of the components of turbulence with the frequencies within the resonant bandwidth of the structure. Vibration due to this excitation can occur at all flow velocities, although the time averaged amplitudes are usually low at low velocities and can be expected to increase with velocity.

As mentioned previously the theory of random vibrations /

vibrations provides the techniques for predicting these vibration levels. This theory assumes that the fluid pressures are independant of the motion of the structure, and the fluid pressures are stationary in the sense that averages made over many cycles are independant of the start of averaging. The first assumption precludes the analysis of structures which are fluid dynamically unstable or experiencing vortex induced vibrations.

If the turbulence properties are known at one point on a structure, then they can be predicted for another point, although the accuracy of the prediction generally decreases with increasing separation of the two points. The spatial dependance of the fluctuating pressures along the structure is given by the correlation function, which gives an indication of the magnitude of the turbulent eddies. The area under the correlation function is defined as the correlation length. Now if the correlation function is integrated over the structural mode shape of interest, then the joint acceptance is obtained. The joint acceptance is a measure of the efficiency of the pressure forces to excite a mode of vibration. For example, if the correlation length is much greater than the structural tube length, then the oscillating pressure forces will act in phase along the length of the tube. A driving force which is uniform along the length of the structure /

structure cannot excite the even sinusoidal modes, (m = 2, 4, 6.....) and only the odd modes will be excited. Hence the value of the joint acceptance, for the even modes, will be zero. Alternatively if the correlation length is small compared with the structural dimensions, as is often the case with turbulence, then the response will become independant of the details of the correlation function and mode shape. (ref. B11) In this situation, the joint acceptance becomes proportional to the ratio of the correlation length to structural length.

With knowledge of the joint acceptance and the power spectrum of the turbulence, the power spectrum of the generalized force can be assembled, and hence the power spectrum of the response can be determined. Once this has been determined it only remains to integrate the response over the required frequency range to obtain the mean square response. This method of prediction does have its downfalls, as accurate estimates of the power spectrum of the turbulence and joint acceptances are rarely available.

For the case of a tightly packed bank of tubes, the turbulent intensity will rise rapidly as the flow enters the tube array, until it reaches a steady state level. In such an array the vortex shedding peak will be very broad unlike the characteristic peak for a single cylinder. Hence for the purposes of random vibration /

vibration analysis the turbulence is often estimated as being a broad humped response with the peak corresponding to the vortex shedding frequency. (ref. B11).

Finally if a structure is placed in the disturbed wake of some other object, then resonant and/or non-resonant response can be obtained, for instance, the vortex street shed from one object (which may be quite stable) can interact with a second downstream object to produce considerable vibration.

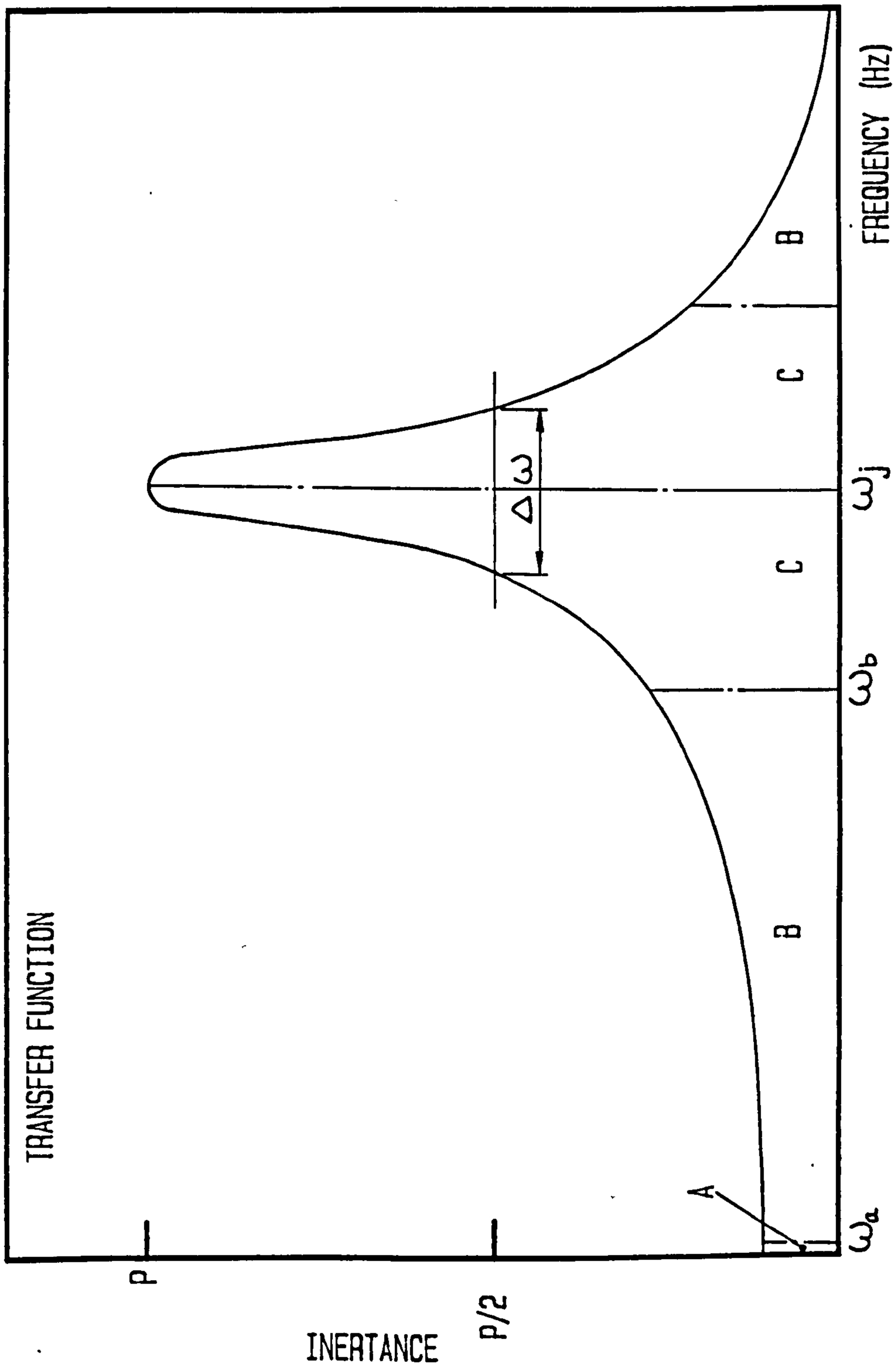

TYPICAL TRANSFER FUNCTION $(1/|Z|^2)$ FOR A LIGHTLY DAMPED STRUCTURE WITH A NATURAL FREQUENCY ω_j

FIGURE 2.10

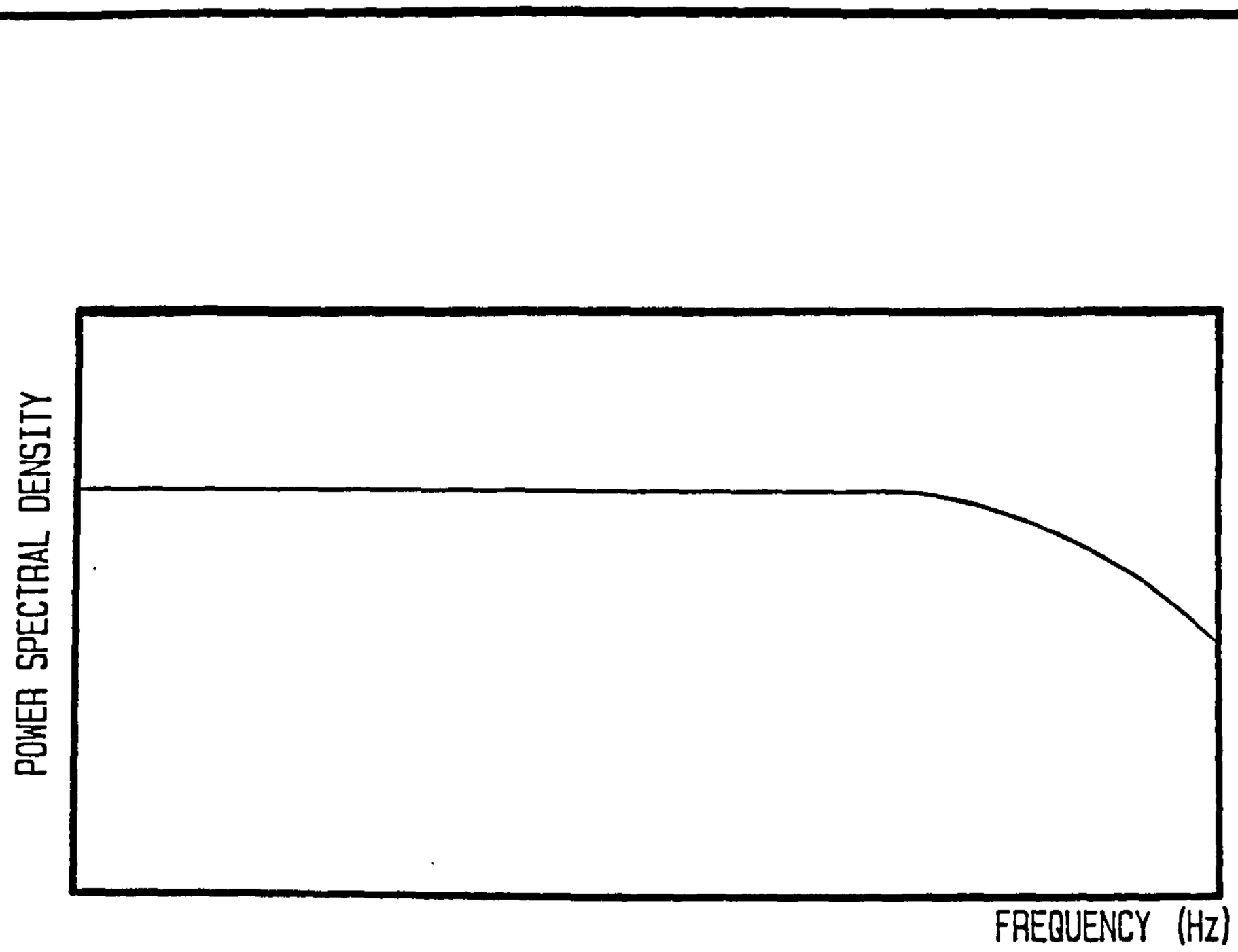

POWER SPECTRUM OF THE VELOCITY FLUCTUATIONS FOR A NORMAL TURBULENT FLOW

FIGURE 2.11 [A]

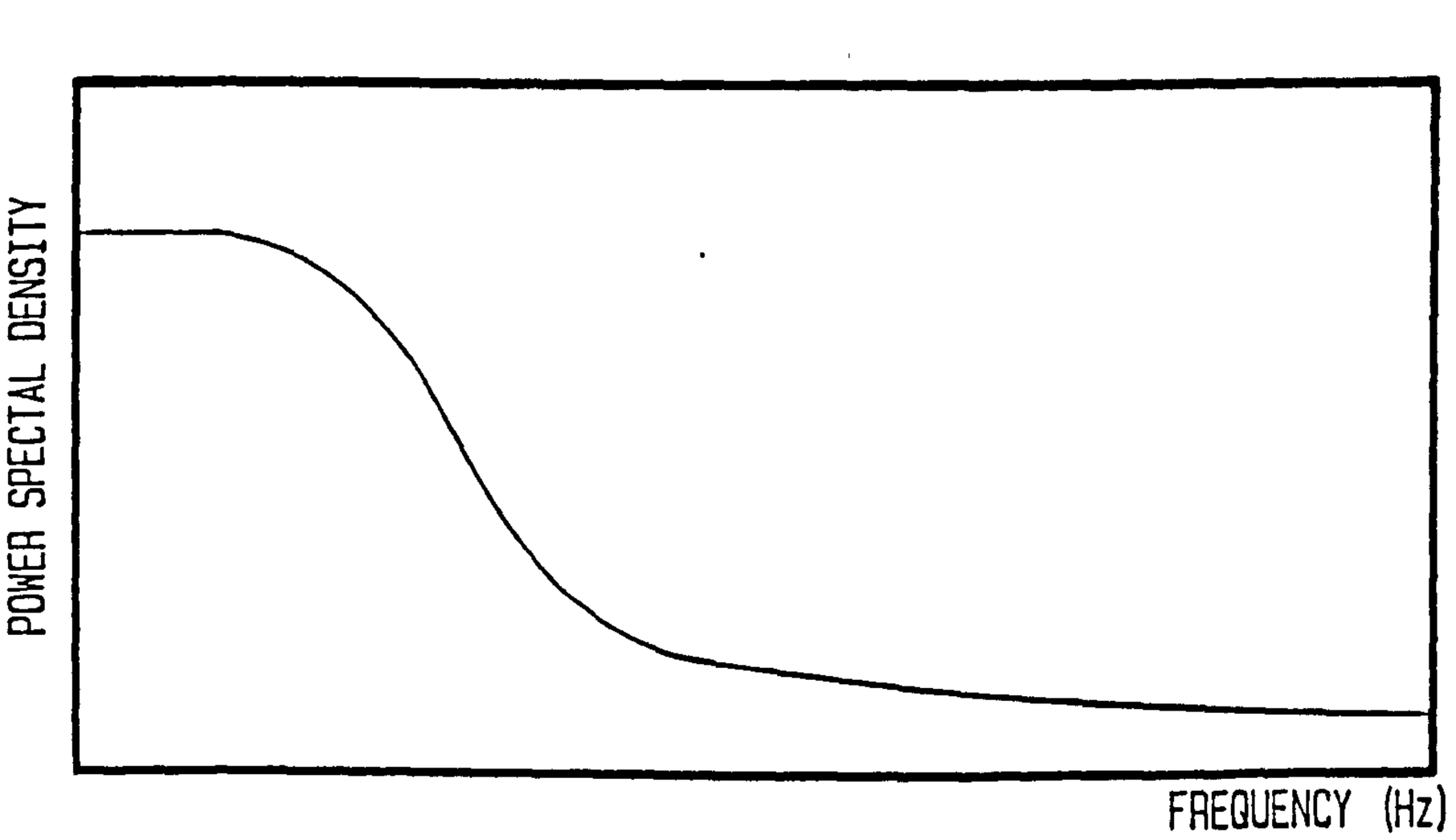

POWER SPECTRUM OF THE VELOCITY FLUCTUATIONS FOR A FLOW WITH SIGNIFICANT LOW FREQUENCY COMPONENTS

FIGURE 2.11 [B]

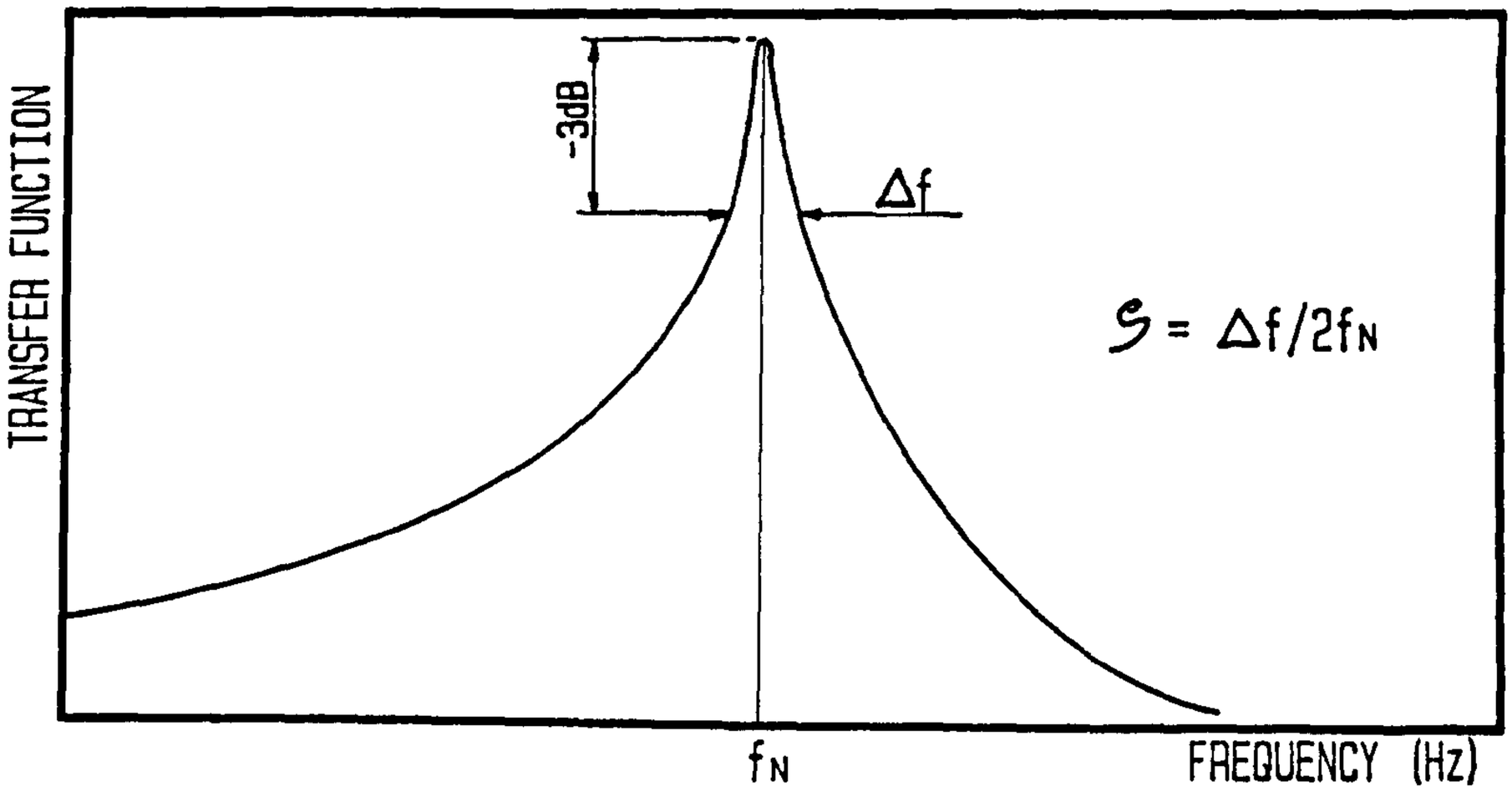

TYPICAL RESPONSE OF A LIGHTLY DAMPED STRUCTURE TO A RANDOM EXCITATION

FIGURE 2.11 [C]

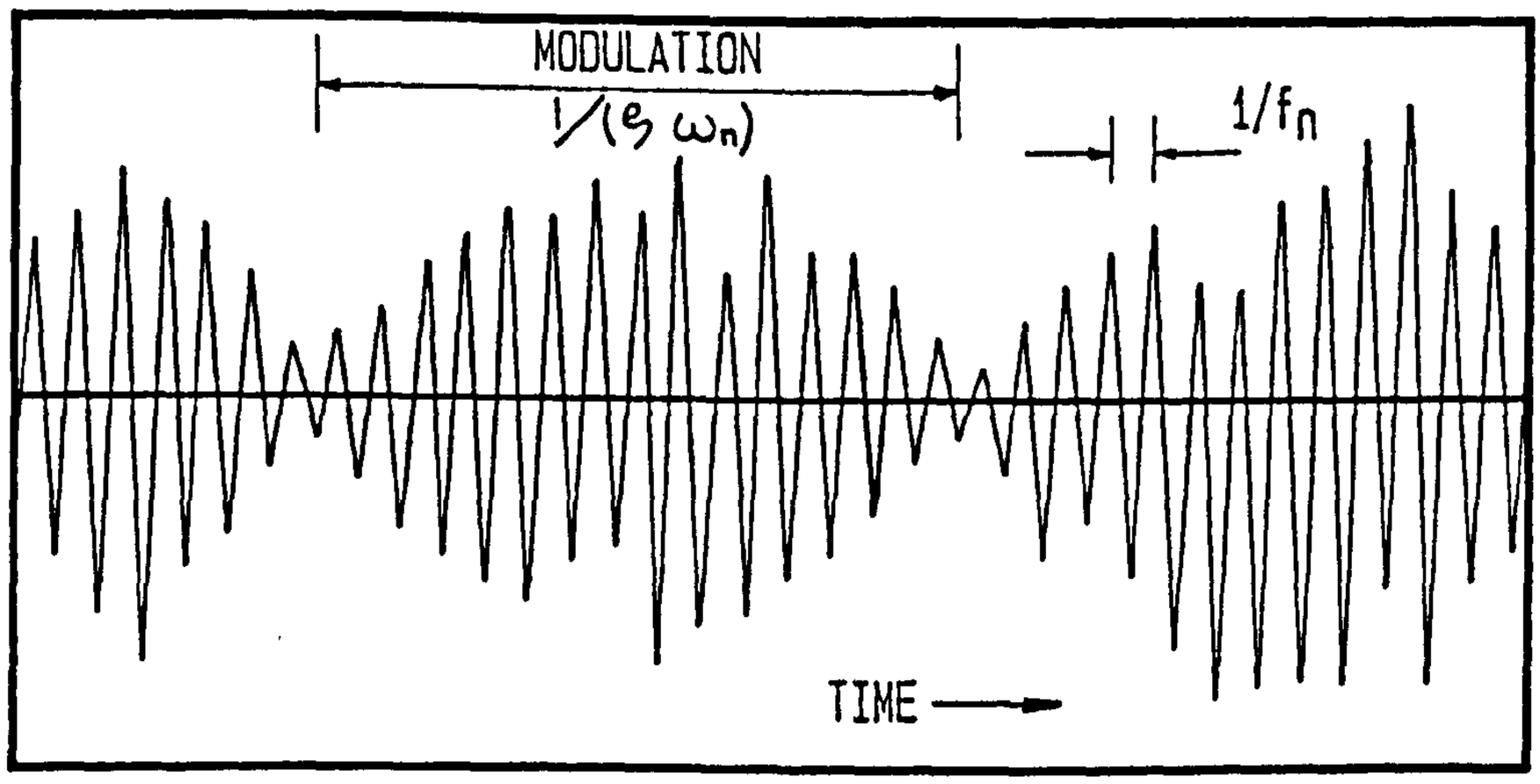

TIME HISTORY RESPONSE OF A LIGHTLY DAMPED SYSTEM TO A RANDOM EXCITATION

FIGURE 2.12

2.2.3 FLUIDELASTIC INSTABILITY

The most familiar examples of fluidelastic vibrations are perhaps those of aircraft wing flutter and the galloping of transmission lines which have become iced. These examples involve single bodies which are isolated in a uniform flow field, and excitation is due to variations in lift force as the direction of incidence of the flow changes. Since the change in angle of incidence is due to the vibratory motion of the body then these oscillations are of a self excited nature. However the cross section of a cylinder rules out such excitation for a single tube, because a change in angle of incidence will not result in a change of lift coefficient.

In an array of tubes the situation is somewhat different and fluidelastic vibration is possible. The displacement of one tube in an array, from its equilibrium position, alters the flow field, thus upsetting the force balance on its neighbouring tubes, and inturn causes them to change their positions. This results in vibration of the tubes, and if, during one cycle of vibration, the energy extracted from the fluid is greater than the energy dissipated by damping, then a fluidelastic vibration will be established.

This mechanism is characterised by a critical velocity, below which the tube is stable, and above which unstable vibration occurs (With tubes vibrating in/

in orbital patterns). The critical velocity is determined by the following equation:

$$\frac{U_m}{f_t d} = K \sqrt{\frac{M_t \delta}{\rho d^2}}$$

Where K is a constant with a value of 9.9 (ref. C1) for a single row of tubes and 3.3 for tube banks (ref. P5, Z3).

This vibration mechanism has received a great deal of attention in recent years, this probably being due to its particular application to Pressurized Water Reactor design, and fairly clear guidelines now exist (ref. P5). The reason for this phenomenon being of particular interest in PWR design is due to the fact that the tubes in heat exchangers with such high density flows do not experience vortex excited instability prior to the onset of fluidelastic vibrations. This is perhaps more easily explained by figures 2.13 and 2.14. Figure 2.13 shows the results of experiments conducted using several vibrating tubes of different mass parameter (ref. M4). These results are shown in the form of an amplitude against reduced velocity plot. The tubes were individually inserted in the middle row of the third column in an array having a longitudinal and transverse pitch of two tube diameters. It can be seen from figure 2.13 that, as the mass parameter is varied, the reduced velocity at which fluidelastic/

fluidelastic instability occurs, moves from below that at which vortex excitation occurs to well above. As can be seen from this diagram these tests produced a well defined vortex shedding peak response at a constant value of reduced velocity. Figure 2.14 (ref. H3) illustrates the conceptial boundaries for tube vibration due to fluidelastic instability and vortex shedding excitation, and an estimate of the sort of flows for which they would be applicable is drawn. As can be seen the high density flows will experience fluidelastic instability before the vortex shedding frequency reaches the tube natural frequency. Lower density flows however, experience vortex shedding excitation prior to the onset of fluidelastic instability.

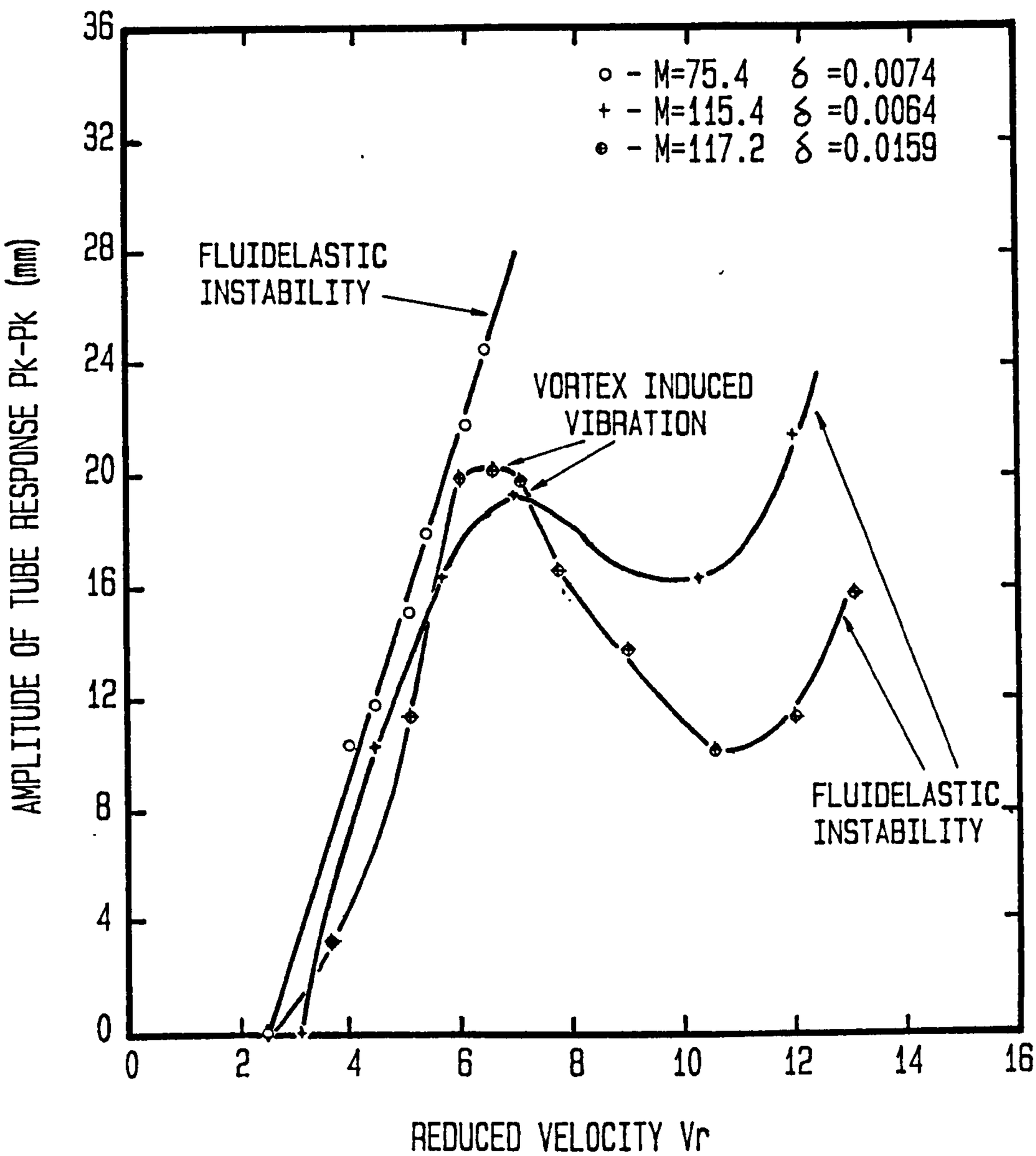

TUBE RESPONSE AS A FUNCTION OF REDUCED VELOCITY

FIGURE 2.13

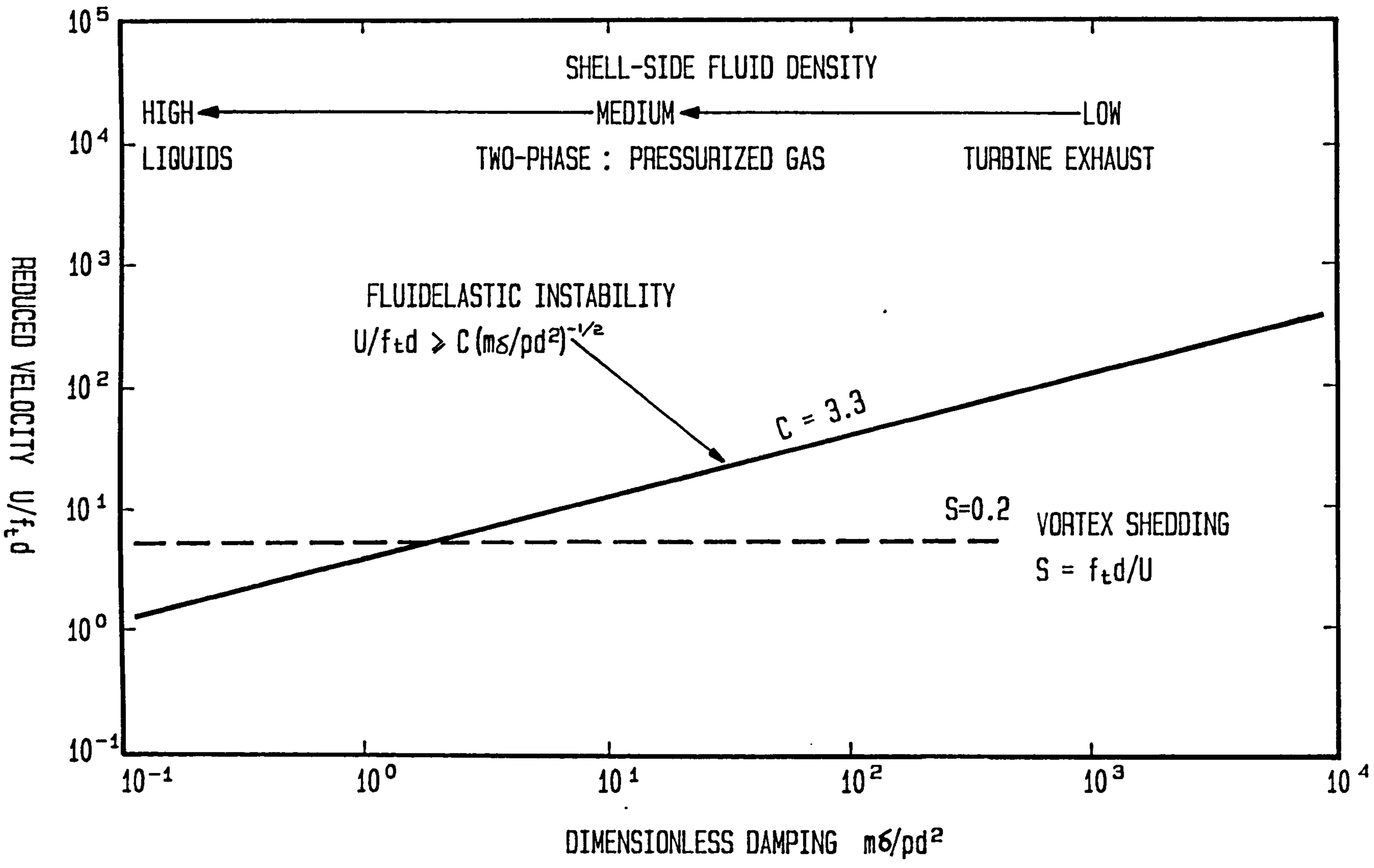

CONCEPTUAL BOUNDARIES OF FLOW INDUCED TUBE VIBRATION

FIGURE 2.14

2.2.4. THE JET SWITCH MECHANISM

Several experimenters have observed that, in closely packed tube arrays, tube vibration in a direction parallel to the flow may be induced by a Coanda switching mechanism. Roberts (ref. R1) has shown that in tube arrays where the tube to tube spacing is less than $X_T = 2.2$, then the jets issuing between these closely packed cylinders couple in pairs, and changes in tube position cause the jets to switch and produce cylinder oscillation. Since the drag force on a cylinder will change significantly as the jets switch, then this can input energy into the cylinder vibration.

However jet switching has only been observed for reduced velocities in the order of 100 and, due to the finite time required for the jet switching to occur, it is not expected at reduced velocities below 75 and, is not expected to affect staggered or irregular tube arrays.

In a paper by Connors (ref. C11) he reported that, due to the highly specialized set of circumstances which were required for the jet switch mechanism to occur, it was of secondary importance in the self excited vibration of tube arrays.

2.3 ACOUSTIC VIBRATION

2.3.1. VORTEX SHEDDING

Classically it is assumed that the acoustic resonance within heat exchanger tube banks is excited by vortex shedding. This can occur when the frequency of vortex shedding is near one of the natural frequencies of the duct containing the tubes. The vortex shedding will then 'lock-in' to the gas column frequency, with the resultant excitation of an acoustic resonance.

This theory has been used quite extensively for predicting the vortex shedding frequencies, and therefore obtaining the Strouhal number, however as explained in section 2.2.1 this method of reasoning cannot satisfactorily account for the observed phenomenon.

Despite the large discrepancies which have been noted in using this method of prediction, it still remains the most widely accepted explanation of the mechanism responsible for acoustic resonance.

Many experimenters have noted that the lower modes of acoustic vibration are not always excited. This has led them to propose a damping criterion which predicts the modes of vibration that are likely to be critically damped, and therefore fail to appear. Perhaps the best known of these theories are those of Grotz and Arnold (ref. G7) and that of Chen (ref. C3). The damping parameter/

parameter developed by Grotz and Arnold describes the slenderness of the resonance chamber, and is described in more detail in section 2.3.2. The damping parameter developed by Chen is as follows:

$$\Psi = \frac{Re}{S} \frac{(X_L - 1)}{X_L} \frac{1}{X_T}$$

It is stated by Chen (ref. C3) that if the value of Ψ does not exceed 600 then the sonic vibration will be critically damped. However in a later paper by Chen (ref. C7), the damping factor was reassessed for application in real heat exchanger units, and the value of Ψ was increased to 2,000. In this paper he states that the critical value of 600 can only be applied in ideal situations, where a smooth velocity distribution exists. In the case of a practical boiler unit however, the flow distribution is generally non uniform, and this has a tendancy to prevent the formation of regular vortex streets, which Chen considers a prerequisite for acoustic vibration. He therefore concludes that a non uniform flow distribution introduces an additional damping in the flow. Therefore the higher value of damping factor must be used.

2.3.2. GROTZ AND ARNOLD

SELF EXCITED VIBRATION THEORY

In a report by Grotz and Arnold (ref. G7), in which they investigated the flow induced vibration phenomena, it was suggested that acoustic resonances in heat exchangers were of a self excited nature. From their experimental results they concluded, that due to the large variations in Acoustic Strouhal number, and its dependence on geometry, vortex shedding was not the mechanism responsible for the resonance. They then described the existence of another mechanism which may be described in the following manner. It is assumed the motion of a particle as it passes between two tube rows is as illustrated in figure 2.15. The flow is accelerated and decelerated as it passes through the tube rows. Due to the large positive pressure gradient as it passes through the diffuser section of a tube row, this will cause the flow to separate from the wall of one tube, thus forming a vortex, and to closely follow the wall of the adjacent tube. The flow will then continue until it is directed by the next tube row and, the formation of the vortices in this row. Thus the flow follows the undulating path illustrated in figure 2.15. (Note the vortex shedding throughout the bank is assumed to be in phase). Following this reasoning they formed an equation relating the frequency/

frequency of these undulations, with the velocity and longitudinal tube pitch of the bank. This is as follows:

$$\frac{U_m}{f\ l_1} = 2.0$$

When the frequency of these undulations coincides with the natural frequency of the resonant chamber between the tube rows, then a larger flow vibration at that frequency will follow. This will tend to enhance the vortex shedding at that frequency.

During their tests they found that in some cases the lower modes of vibration did not appear, they concluded that there must exist a value of damping which, if exceeded, then the fundamental frequency of the resonant chamber would not be excited. From this observation they defined a damping parameter, T, which they named the slenderness ratio, and is defined as follows:

$$\frac{T}{m} = \frac{L}{a}$$

This parameter describes the slenderness of the resonant chamber, and from their results they concluded, that if T/m exceeds 80 then, the mode will not be excited.

Finally they stated that, the forcing function or disturbances/

disturbances which excite and sustain the acoustic vibration is itself dependent on the oscillations, so the acoustic vibrations are self excited, and self sustained.

From the theory put forward by Grotz and Arnold, it may be deduced that the frequency of these undulations will be of the same frequency as the vortex shedding, because during one cycle of these undulations two distinct vortices will have been shed from that tube. Thus Grotz and Arnold's theory should predict the same Acoustic Strouhal number as the classical model, in which the vortex shedding coincides with the acoustic resonance frequency. Following the same reasoning this model should be able to predict the vortex shedding frequency for a given bank geometry. However a more complex relationship between vortex shedding and geometry seems to exist.

UNDULATORY MOTION OF AIR STREAM FLOWING BETWEEN TUBE ROWS

o - PARTICLE POSITION AT TIME τ

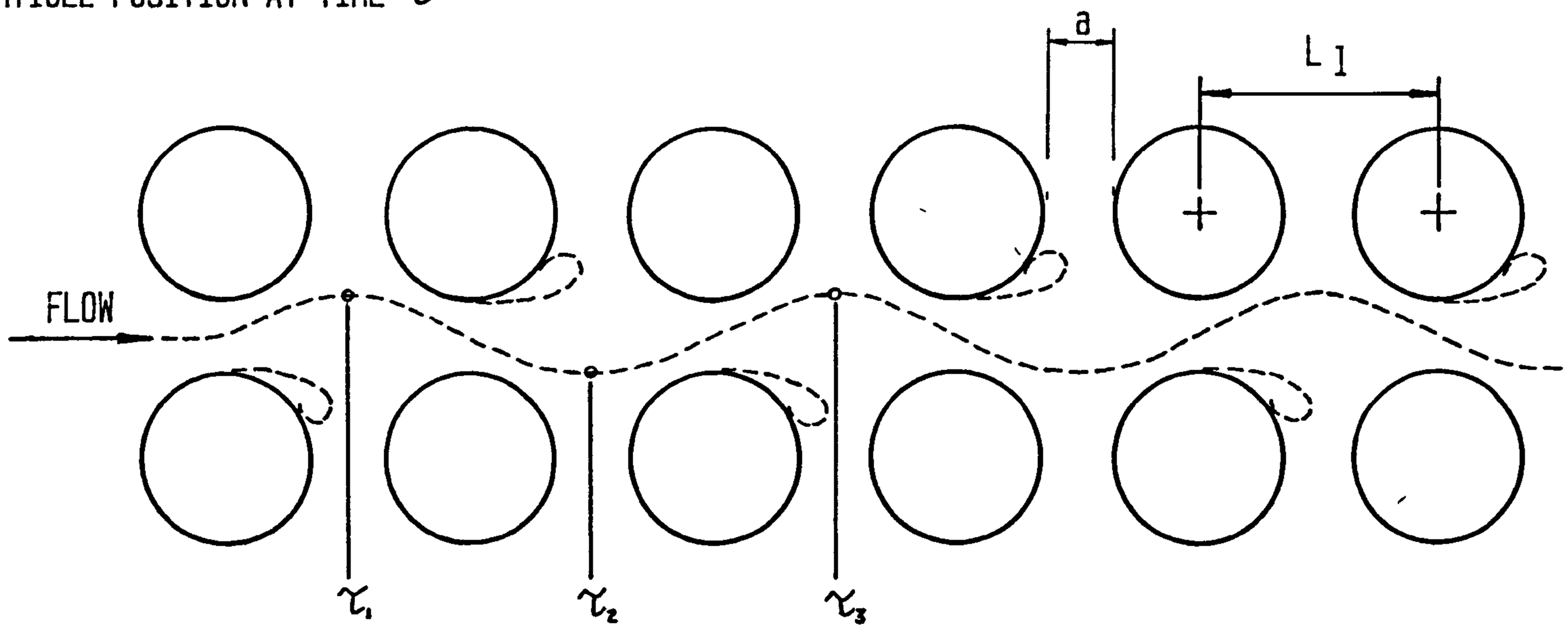

$$U = \frac{2 \cdot L_1}{\tau_3 - \tau_1} \qquad \text{also} \quad f = \frac{1}{\tau_3 - \tau_1} \qquad \therefore \frac{U}{f \cdot L_1} = 2.0$$

FIGURE 2.15

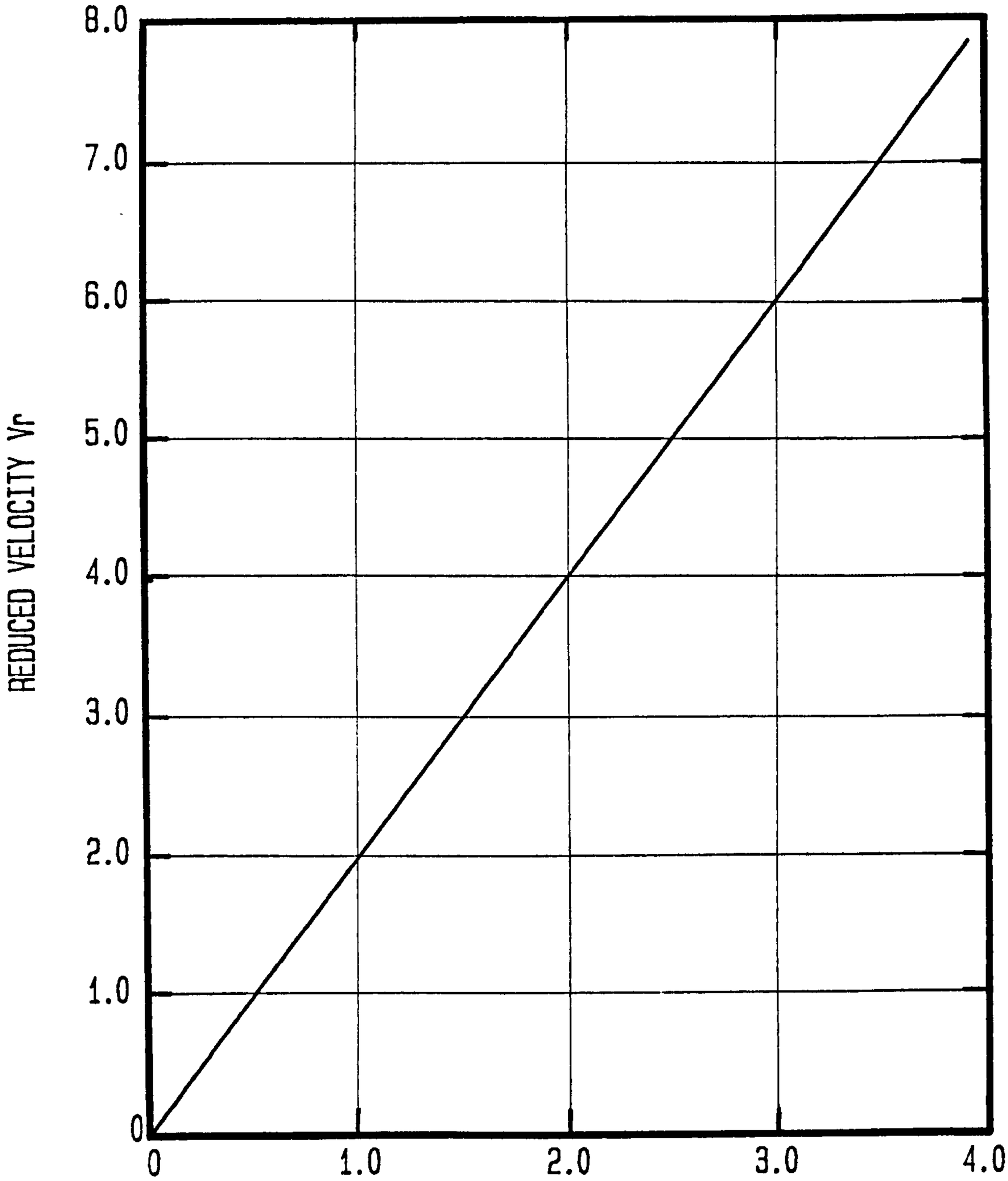

GROTZ AND ARNOLD'S STABILITY CRITERION

GRAPH OF REDUCED VELOCITY AGAINST LONGITUDINAL PITCH TO DIAMETER RATIO

FIGURE 2.16

2.3.3. OWEN'S BUFFETING THEORY

Essentially the theory presented by Owen (ref.01) is a method of explaining the existance of tube vibration and acoustic resonances by the action of turbulent eddies. The argument put forward in his paper is as follows. The turbulent energy of the flow is increased at each row of tubes, and some of this energy is dissipated by viscosity as it travels between tube rows. It is inconceivable that the turbulent energy could increase without limit, so, at some point sufficiently far from the point of entry to the tube bank, the rate of energy generation must become equal to the rate of energy dissipation. At this point the flow will have acquired an almost complete randomness with regard to space and time, and may now be described as turbulent. The fluid now flows through the bank with turbulent energy being generated and dissipated with a periodicity equal to the longitudinal pitch of the bank. This leads to the supposition that the flow will contain energetic eddies which will have a physical scale similar to that of the longitudinal pitch of the bank.

Owen then develops an equation relating the rate of energy generation to energy dissipation, and uses this to show that the eddies should be of a size similar to the longitudinal pitch. Furthermore since these eddies travel downstream with the mean velocity a corresponding/

corresponding peak in the turbulence spectrum will exist, which will increase in frequency as the velocity is increased.

Owen then goes on to explain why the tube response is so sharp by concluding that the tube will be aerodynamically selective, and will respond to that group of eddies whose dimensions are comparable to the tube diameter. Now since, in practical heat exchangers, the longitudinal pitch is of the same order as the tube diameter, a force spectrum will be produced with an even sharper peak corresponding to the energetic eddies. Also since the inherent damping of boiler systems, both mechanical and acoustical, will be low, this will also help to sharpen the response spectrum. Finally he says that the response history due to this excitation, for mechanical or acoustic vibration, will be of a definite frequency slowly modulating in amplitude and phase in a random manner.

Owen's arguements have explained the existence of an excitation which behaves in a manner identical to vortex shedding. He dismisses the existence of vortex shedding in deep banks and assumes that such a phenomenon could not exist because the flow would be completely random. However Owen's theory cannot explain why these broad peaks in the turbulence spectrum and the acoustic resonance occur at different Strouhal numbers, or why some modes of acoustic vibration are missed./

missed. It would also prove very difficult to explain the row depth effect on the Acoustic Strouhal number using this theory. As previously stated Owen supposes that the acoustic response will be modulated corresponding to a random excitation, so one would expect to see a response spectrum with a finite bandwidth which corresponds to the damping present. However in practice the acoustic resonance has been found to appear as a pure tone of constant amplitude.

The equation for predicting acoustic instability in accordance with Owen's theory is as follows:

$$\frac{f\ l_l}{U_m}\ \frac{l_t}{d} = K_o\left(1 - \frac{d}{l_t}\right)^2$$

Where K_o is a constant for all sufficiently widely spaced extensive tube arrays.

This equation can be reduced for $0.6 > d/l_t > 0.2$ to the form

$$\frac{f\ d}{U_m} = 0.5$$

This equation is the same as that proposed by Grotz and Arnold, and the stability criterion is illustrated in figure 2.16.

2.3.4. ALTERNATING RAREFRACTION AND COMPRESSION OF THE GAS

Hill and Armstrong (ref. H2) carried out a series of experiments involving staggered tube bank arrangements, in which they observed two powerful pure tones (typically 100 dB), corresponding to the first and second transverse modes of the tunnel.

The banks were composed of two columns of plain copper tubes which had a fixed transverse pitch diameter ratio of 2.4 and a variable longitudinal pitch diameter ratio. From their results they concluded that vortex shedding played no essential role in the excitation of the acoustic resonance. They further argued that the resonance was excited as a result of the repeated compression and rarefraction of the air as it passed through the tube rows. It follows from this argument that the velocity for the onset of acoustic resonance is given by:

$$U = f \quad l_1$$

However this theory is rejected by many experimenters (ref. B6, F2, O1, D3, etc), although it is known, from Bernoullis equation, that variations in flow area and hence flow velocity, will give rise to periodic pressure variations, the sinuous streamlines produced do/

do not provide a source of sound in a stationary flow field. Therefore they cannot account for the observed phenomenon. (ref. 01)

3.0 OBJECTIVES

The main objectives of this work were as follows:

a) To design and construct a wind tunnel suitable for the full investigation of the acoustic resonance phenomenon.

b) To develop a method of measuring the damping of the acoustic modes within the tube bank, under static and flow conditions.

c) To develop a method of varying the acoustic damping of these modes in a controlled manner.

d) To compare the results with those obtained by other experimenters and assess the existing theoretical models.

e) To develop a suitable mathematical model of the acoustic system.

4.0 DESIGN OF WIND TUNNEL

4.1 INTRODUCTION

In order to effectively investigate the parameters associated with this phenomenon it was necessary to design and construct a suitable facility for doing so. As the principal objectives of this work was to determine the nature of the aero acoustic system, and the role of acoustic damping, the wind tunnel was designed so that the damping would initially be small.

This chapter describes the modelling parameters and design considerations which are taken into account in the design and construction of the wind tunnel.

4.2 MODELLING CRITERIA

When constructing a model of a heat exchanger the effects of scaling must be considered. The non-dimensional parameters which are generally associated with cross flow in heat exchangers are as follows:

Reynolds Number	(Re)
Strouhal Number	(S)
Mass Parameter	(M)
Geometry	(X_T, X_L)
Bank Depth	(N)
Turbulent Inensity	(t)
Acoustic Damping	(Q)
Mechanical Damping	(ζ)
Mach Number	(M_N)
Aspect Ratio	(A)

In the majority of modern heat exchangers the tube outside diameter will be in the range from 15mm to 50mm, and the tube pitch/diameter ratio for in-line or pseudo in-line (cross inclined) tube bundle is between 1.25 and 2.5. The acoustic resonance is usually observed in heat exchanger units which have a single phase pressurized gas as a coolant. In this study the heat exhanger was modelled using air at atmospheric pressure, to represent the coolant, and 19mm outside diameter/

diameter tubes. The effect of scaling and using air to simulate the coolant will cause a mismatch of Reynolds Number. Reynolds number effects however are not thought to be significant in the range $10^2 < Re < 10^5$.

The aspect ratio of a circular cylinder in a flow, is normally required to be greater than twelve (ref. F2) to eliminate three dimensional effects introduced by wall confinement at the cylinder extremeties. A bank of 15 columns normal to the flow and 50 rows in depth is considered to be sufficiently representative of a heat exchanger tube bundle (ref. B19).

Taking these factors into account it was decided to build the tunnel of rectangular cross section measuring 0.4m x 0.6m. This allows at least 15 columns of tubes and an aspect ratio of twenty one.

It was estimated that the turbulent intensity in the tunnel would be small, nevertheless it has been shown that within the first few rows of a bank the turbulent intensity will reach a constant value irrespective of the value upstream.

The mass parameter and mechanical damping of the tubes was not modelled accurately. It was however recognised that these parameters may have some effect on the acoustic system, nevertheless in this situation they will be considered as being aerodynamically passive and therefore will not contribute to the excitation /

excitation of the acoustic resonance.

The Mach number is a measure of the influence of compressibility on the flow. In this study the Mach number was limited to values less than 0.16, at these values compressibility does not ordinarily influence the analysis.

Very little data is available as to the value of acoustic damping which might be encountered in practical plants. However it is sufficient to add that this parameter was kept small. The reason behind this decision is discussed in Ch. 4.5 on the acoustic properties of the wind tunnel.

4.3 WIND TUNNEL LAYOUT

A schematic diagram of the wind tunnel layout is shown in figure 4.1. This illustrates all the major sections of the tunnel together with the fan and silencer. Air enters the wind tunnel by way of the nozzle, passes through a settling length and into the test section. The purpose of the settling length is to minimise any local turbulence in the flow that might have developed at entry. In the test section air passes through the tube bundle and into the diffuser section at the rear. This diffuser section serves to reduce the velocity at the tunnel exit thus minimising the pressure loss. At exit from the tunnel the air enters the fan (which is driven by an electric motor) and is discharged through a silencer to the butterfly valve. It is this valve which allows the air velocity through the tunnel to be regulated.

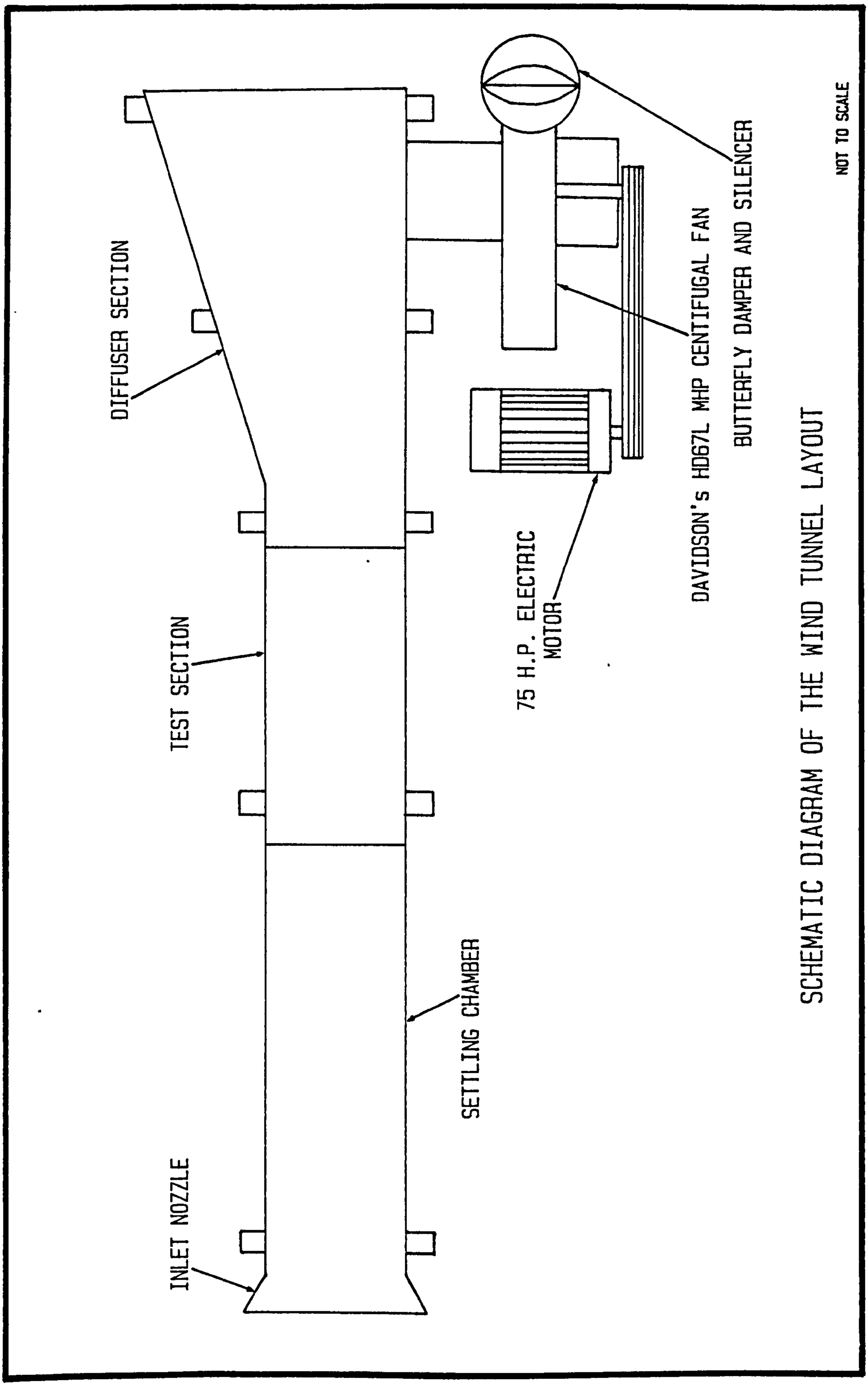
SCHEMATIC DIAGRAM OF THE WIND TUNNEL LAYOUT
BUTTERFLY DAMPER AND SILENCER
DAVIDSON'S HD67L MHP CENTIFUGAL FAN
75 H.P. ELECTRIC MOTOR
DIFFUSER SECTION
TEST SECTION
SETTLING CHAMBER
INLET NOZZLE
NOT TO SCALE

FIGURE 4.1

4.4 THE TEST SECTION

The test section was designed to house a tube array which would have a variable row depth and geometry. This was achieved by building the array of individual frames, each frame repesenting 1 row of the tube bank. A typical frame is shown in figure 4.2. These frames can be individually inserted or removed to vary the bank depth, and spacers may be inserted between them in order to vary the longitudinal pitch. With this design it is necessary to build a set of frames for each transverse pitch ratio to be investigated.

The test section was constructed so that the top could be removed to facilitate the fitting and removal of the tube frames. In figure 4.3 there is an illustration of the test section which highlights the position of the frames together with the rear slide arrangement. It was by means of this slide arrangement that the tube bank was kept tightly packed.

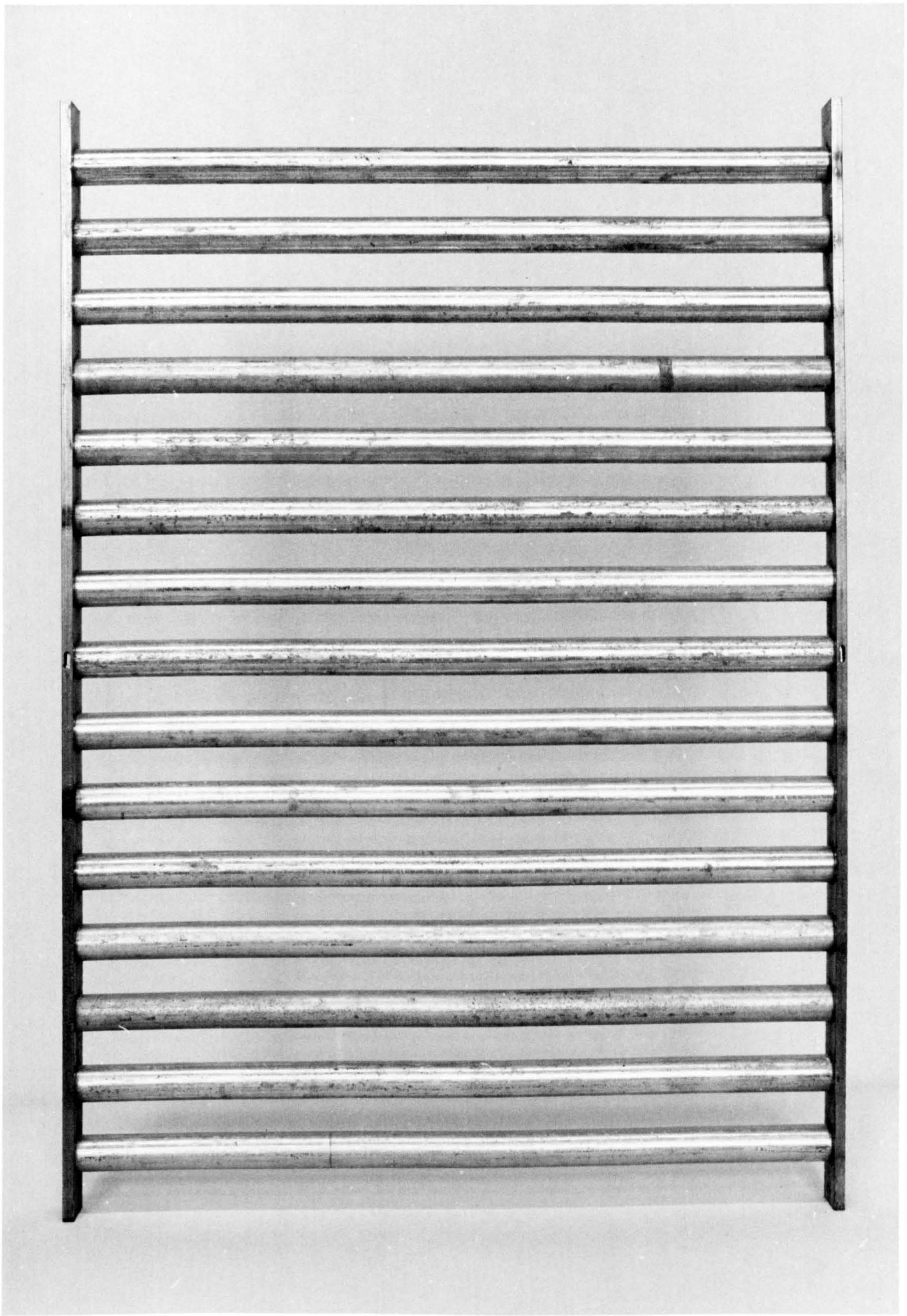

PHOTOGRAPH OF A TYPICAL ROW OF TUBES

FIGURE 4.2

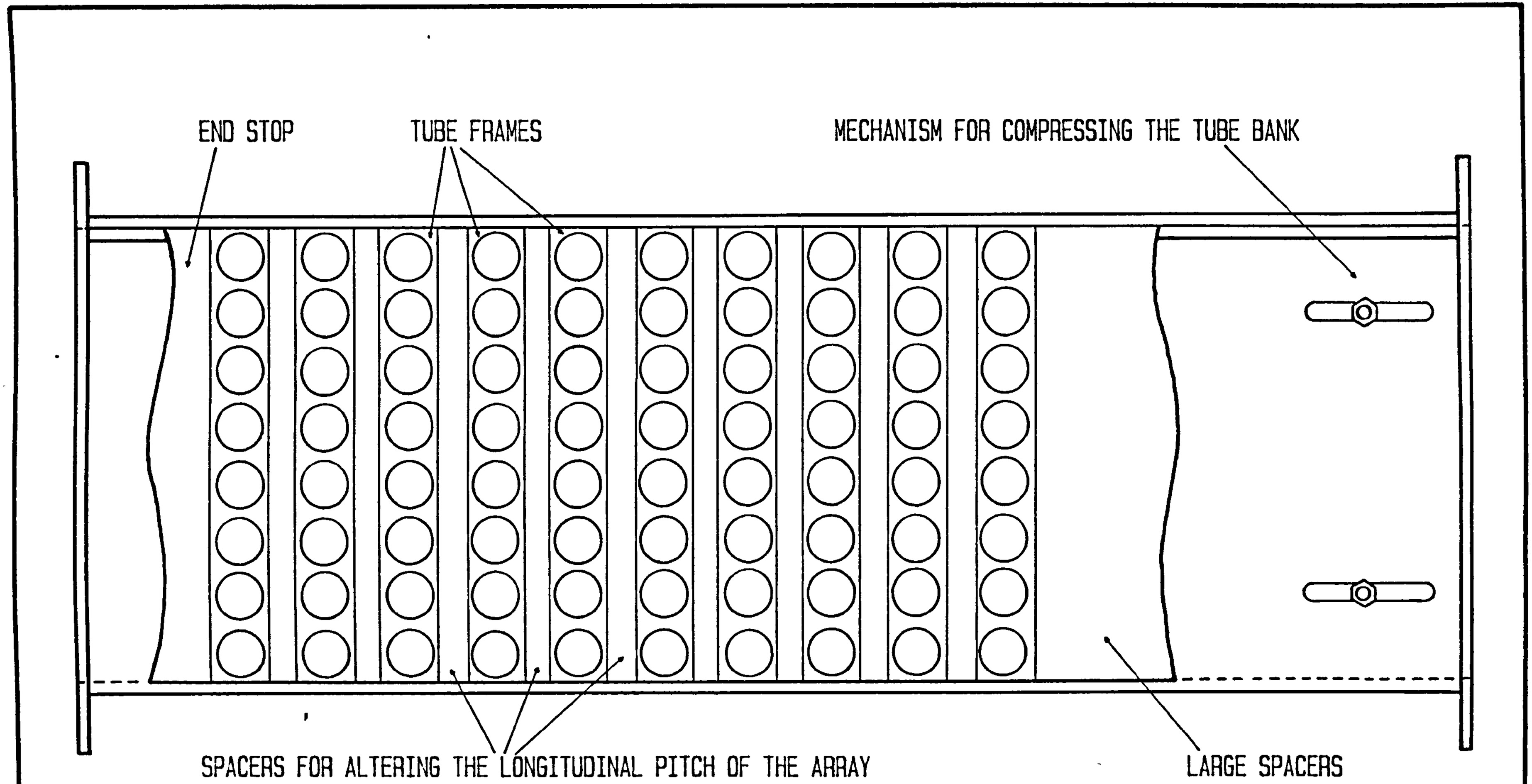

CUT-AWAY DIAGRAM OF THE TEST SECTION

NOT TO SCALE

FIGURE 4.3

4.5 ACOUSTIC PROPERTIES OF THE WIND TUNNEL

The mode of vibration which is usually associated with acoustic resonances in heat exchangers is that of a pure transvers mode (ie no longitudinal modes). This means that the frequency of acoustic vibration may be calculated using the formula stated below (ref. C3, F2, G7).

$$f = \frac{C}{2l}$$

The speed of sound through an array of tubes is lower than it would be if no tubes were present. This is due to scattering and inertial effects caused by the presence of the tubes. Parker (ref. P1) gives the following expression for calculating this reduction in the speed of sound.

$$C = C_o \ (1 + \sigma)^{-\frac{1}{2}}$$

where σ is the fraction of the space occupied by solid bodies.

Using these equations the fundamental frequency of acoustic vibration for each geometry may now be calculated.

It has been noted by several experimeters that some modes of acoustic vibration fail to be excited. In ref. C3 and G7 theories are developed which predict the modes of acoustic vibration which will be critically damped./

damped. These theories were discussed in the previous chapter and therefore shall not be restated at this point, however the results obtained using these equations are summarized in table 1. As shown in table 1 the slenderness ratio, described by Grotz and Arnold, predicts that the fundamental mode shall be excited in all the bank geometry except the 1.34 x 1.34 array. In this array it is predicted that the second harmonic will be the first to be excited.

On the other hand Chen's damping criterion has two different values for critical damping, the value being dependant on the velocity profile at entry to the bank. Chen's guidelines, as stated in ref. C7, suggest that the value of damping factor (ψ) to be used in this situation is 600. The results of these calculations are, for this situation, the same regardless of which value of ψ had been taken and it predicts that the fundamental mode will be excited in each geometry. The Strouhal numbers used in these calculations were taken from Chen's correlation because these values were used in the derivation of this theory.

Making use of the relevant theories the acoustic Strouhal Numbers were calculated for each tube bank to be investigated. This, however, gave a large variation of acoustic Strouhal Number for each bank, so the tunnel was designed to include the lowest acoustic Strouhal number (i.e. highest velocity). Since this parameter determines the velocity which has to be met for/

for resonance to occur the pressure drop across the tunnel can now be calculated. The pressure drop, which is proportional to the row depth was calculated for each tube bundle, and an estimate for the pressure drop across the rest of the tunnel was made. Allowances were also made for the increase in pressure drop across the bank which would occur when the resonance was excited. The pressure drop across the tube bundle was calculated using the theory presented by McAdam (ref. MC2) and is as follows:

$$\Delta P = \frac{4 F_o B_o N G_o}{2\rho}$$

$$\text{Where } F_o = A_o \left(\frac{\mu}{d\ G_o}\right)^{m_o}$$

$$A_o = \left(0.044 + \frac{0.08\ X_L}{(X_T - 1)^n}\right) \text{ for in-line arrays}$$

$$n = 0.43 + (1.13/X_L)$$

$$m_o = 0.15$$

Table 2 summarizes the results of these calculations and using this information it was possible to choose a suitable fan and motor. A centrifugal fan was used because of the high pressure drop and relatively low flow rate which had to be met. The specifications for the fan are shown in figure 4.4.

The wind tunnel, centrifugal fan and motor were mounted on antivibration mountings. The fan was also vibrationally isolated from the tunnel by way of a flexible/

flexible section, see figure 4.1.

As mentioned in section 4.2 the value of acoustic damping was kept as low as possible. The main reasons for this was to allow investigation of the system behaviour under minimum damping conditions and to make the task of producing a significant increase in the damping easier. The damping was kept low by ensuring that the energy transmitted through the walls was low. This was achieved by ensuring that the scale factor was low, the test section walls had no disturbing mode shapes in the vicinity of the acoustic frequency, and by constructing the tunnel from 6mm thick mild steel plate. The test section was modelled using a finite element program (PAFEC). In figure 4.5 the predicted mode shapes and natural frequencies of the section walls are shown. As can be seen from this diagram very little movement occurs in the walls of the tunnel, therefore these mode shapes will not significantly effect the transmitted energy. By making the walls from 6mm steel plate ensured a very high wall density which will reduce the amount of energy transmission.

GEOMETRY		GROTZ AND ARNOLD SLENDERNESS RATIO		CHEN DAMPING FACTOR ψ
X_T	X_L	MODE NO. 1	MODE NO. 2	MODE NO. 1
1.34	1.34	93.8	46.9	3619
1.34	1.67	47.0	23.5	29650
1.34	2.00	31.4	15.7	78139
2.00	1.67	47.0	23.5	7634
2.00	2.00	31.4	15.7	21548
2.00	2.34	23.6	11.8	46166

TABLE 1

GEOMETRY		$(1-\sigma)^{-\frac{1}{2}}$	C	f	S_{min}	U_m	A_o	F_o"	N	ΔP	V.F.R.
X_T	X_L	unitless	ms^{-1}	Hz	unitless	ms^{-1}	unitless	x 10^2 unitless	rows	ins. W.G.	C.F.M.
1.34	1.34	0.84	288.6	241	0.31	14.7	0.467	10.7	50	11.2	1902
1.34	1.34	0.84	288.6	482	0.31	29.4	0.467	9.6	50	40.3	3804
1.34	1.67	0.87	297.4	248	0.20	23.5	0.485	10.4	50	27.7	3032
1.34	2.00	0.88	303.8	253	0.17	28.3	0.512	10.6	50	41.0	3652
2.00	1.67	0.93	319.5	266	0.26	19.0	0.178	3.9	50	6.8	4821
2.00	2.00	0.92	316.0	263	0.25	20.0	0.204	4.5	50	8.6	5088
2.00	2.34	0.91	311.3	259	0.19	26.6	0.231	4.8	50	16.6	6771

$C_o = \sqrt{\gamma RT} = 343.7\ ms^{-1}$ $\quad B_a = 1.0$ since no baffles $\quad M_o = 0.15$

$\rho = 1.203\ kg/m^3$ $\quad \mu = 1.817 \times 10^{-5} Ns/m^2$

TABLE 2

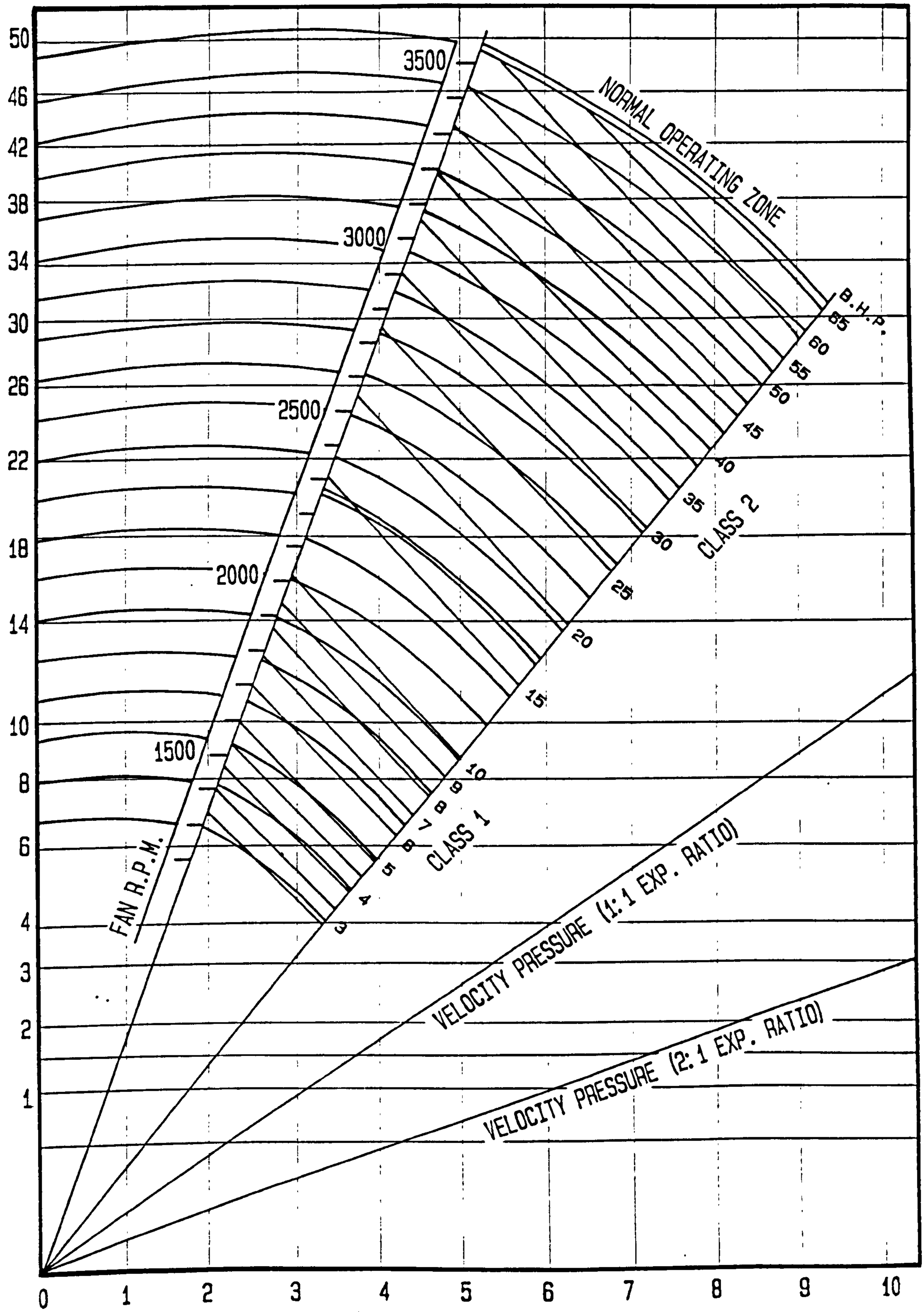

ESTIMATED PERFORMANCE CURVES OF SIROCCO MHP BLOWERS TYPE AND SIZE HD67L (BELT DRIVEN)

FIGURE 4.4

TITLE WIND TUNNEL TEST

PAFEC 75

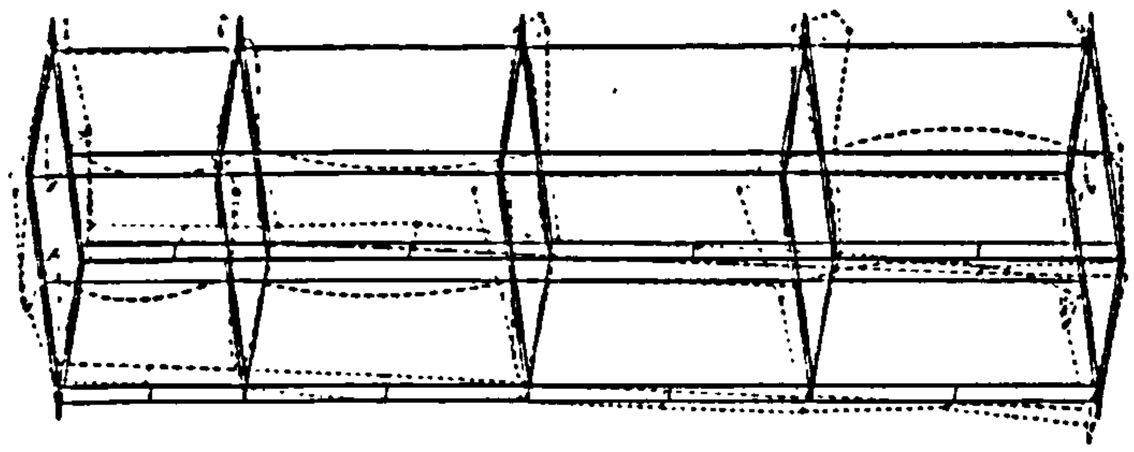

VIEW FROM X = 1.000
Y = 4.513
Z = 5.006

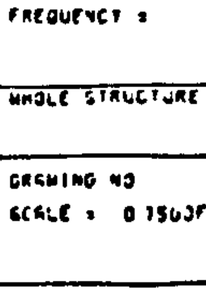

MODE SHAPE NUMBER 35
FREQUENCY = 252.0 HERTZ

WHOLE STRUCTURE DRAWN

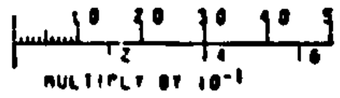

mm.
STRUCTURAL UNITS

DRAWING NO 1
SCALE = 0.1500E -1 1

TITLE WIND TUNNEL TEST

PAFEC 75

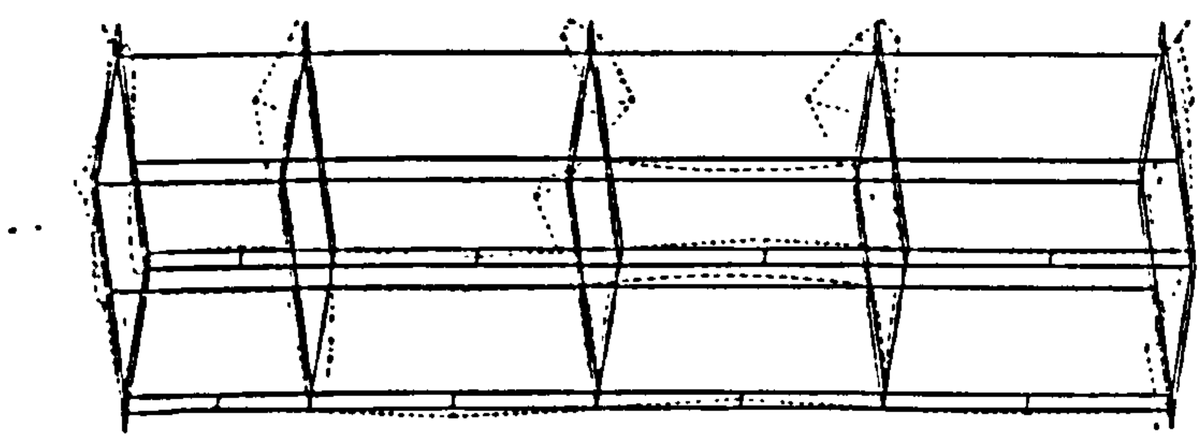

VIEW FROM X = 1.000
Y = 4.513
Z = 5.006

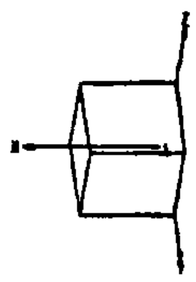

MODE SHAPE NUMBER 36
FREQUENCY = 253.1 HERTZ

WHOLE STRUCTURE DRAWN

FIGURE 4.5 [A]

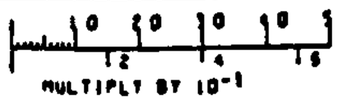

mm.
STRUCTURAL UNITS

DRAWING NO 2
SCALE = 0.1500E -1 1

THE TEST SECTION's NATURAL FREQUENCIES AND MODE SHAPES

TITLE WIND TUNNEL TEST

PAFEC 75

VIEW FROM X = 1.000
Y = 4.515
Z = 5.008

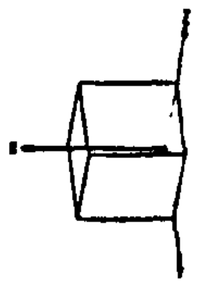

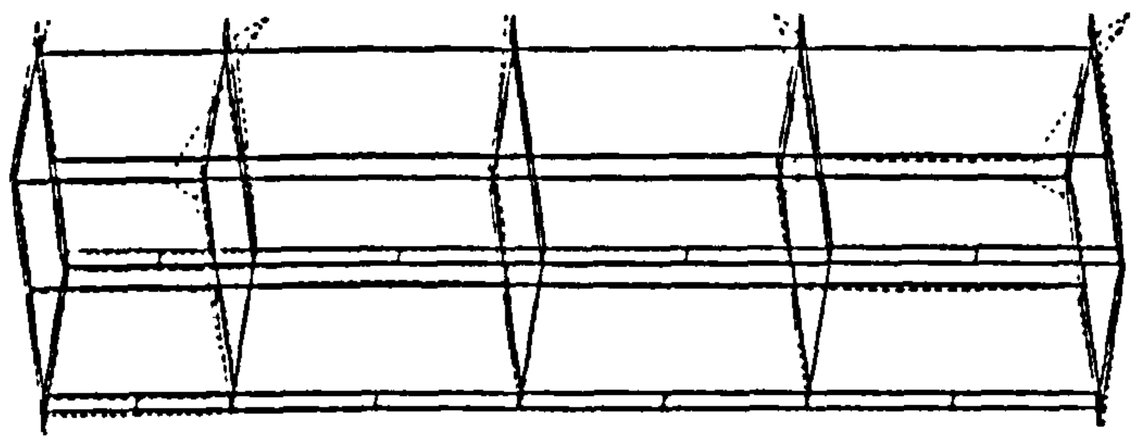

MODE SHAPE NUMBER 37
FREQUENCY = 253.1 HERTZ

WHOLE STRUCTURE DRAWN

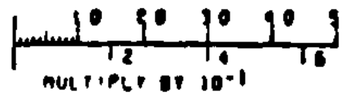

MM.
STRUCTURAL UNITS

DRAWING NO. 3
SCALE = 0.7500E -1 1

TITLE WIND TUNNEL TEST

PAFEC 75

VIEW FROM X = 1.000
Y = 4.515
Z = 5.008

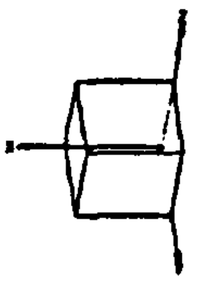

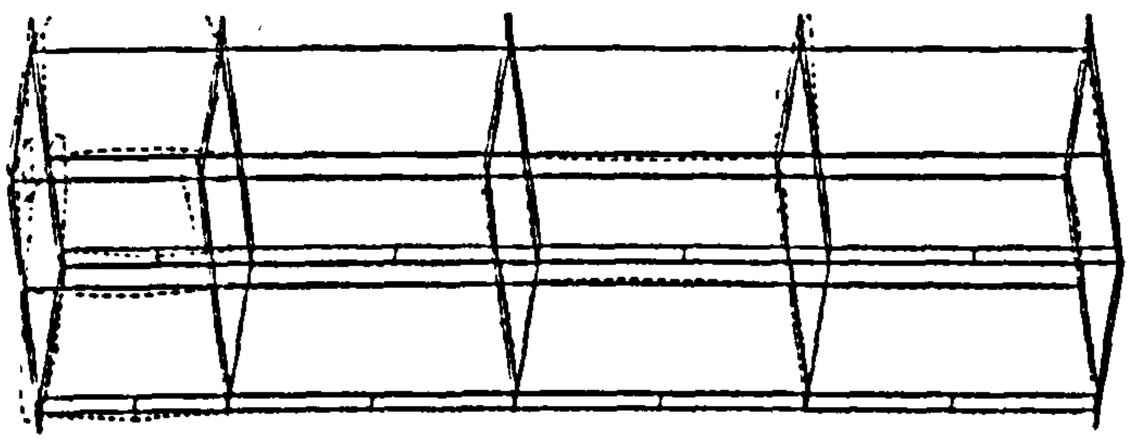

MODE SHAPE NUMBER 39
FREQUENCY = 281.1 HERTZ

WHOLE STRUCTURE DRAWN

FIGURE 4.5 [B]

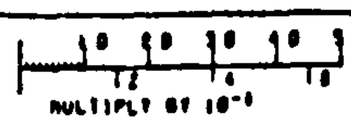

MM.
STRUCTURAL UNITS

DRAWING NO. 4
SCALE = 0.7500E -1 1

THE TEST SECTION's NATURAL FREQUENCIES AND MODE SHAPES

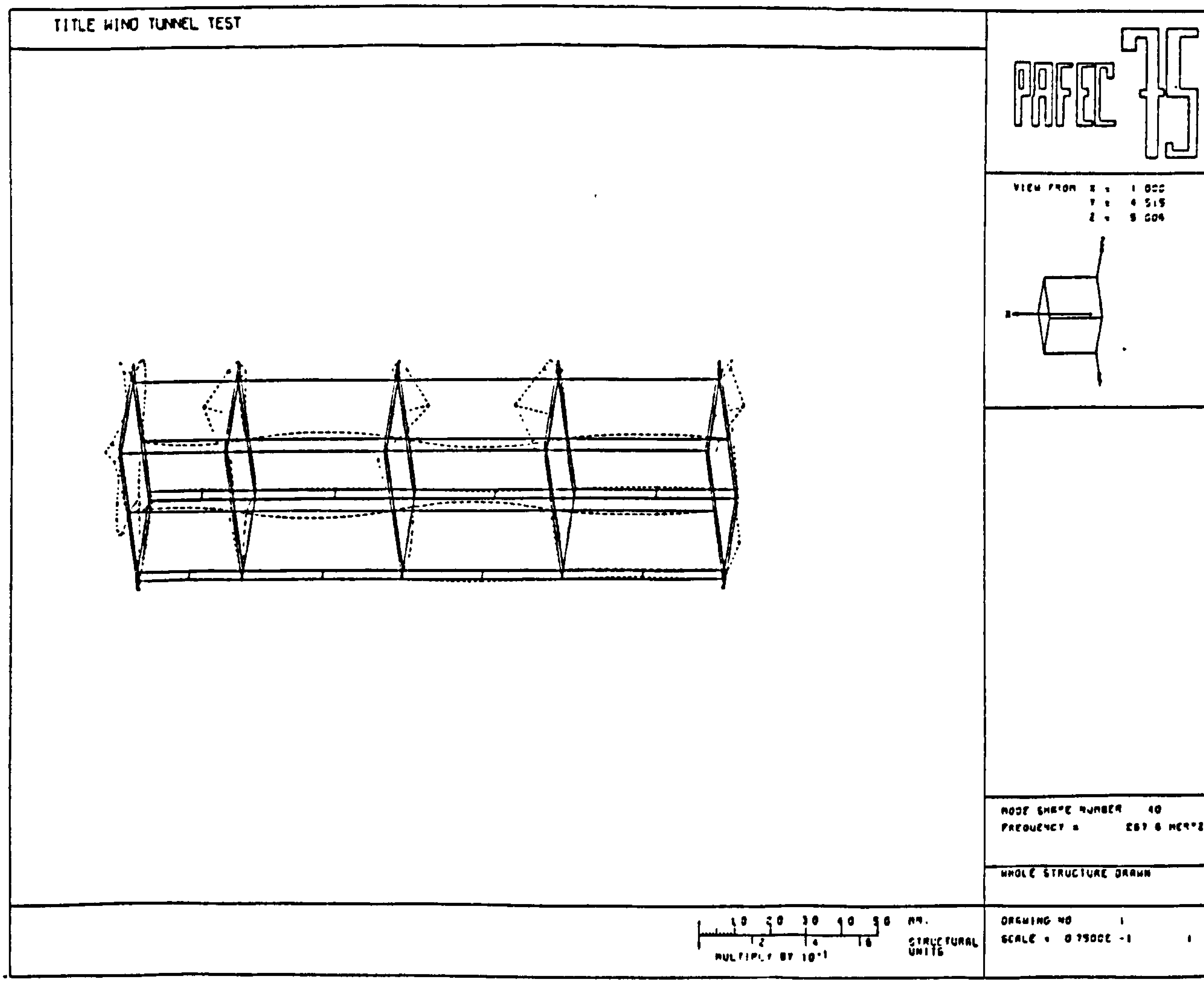

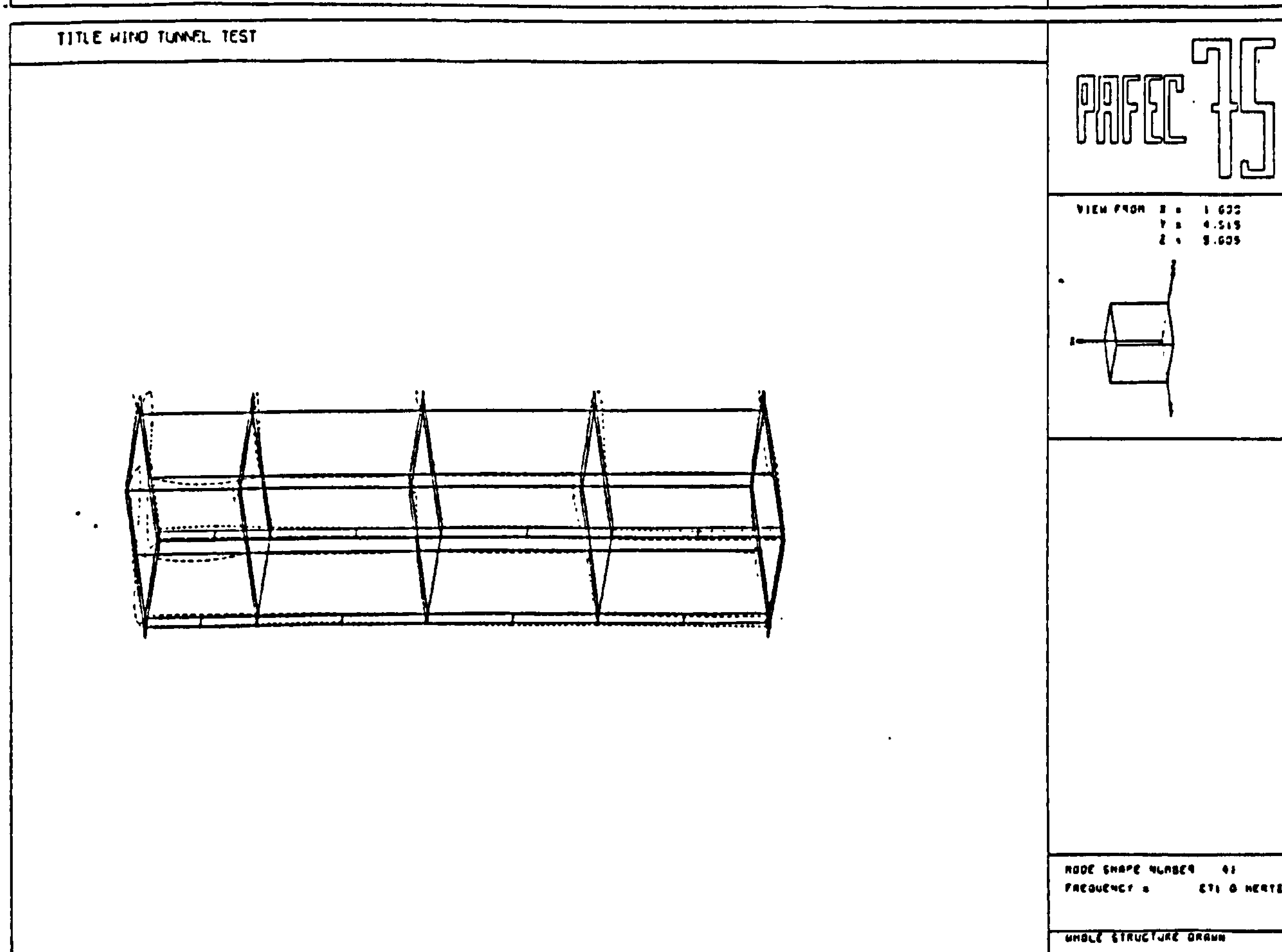

FIGURE 4.5 [C]

THE TEST SECTION's NATURAL FREQUENCIES AND MODE SHAPES

TITLE WIND TUNNEL TEST

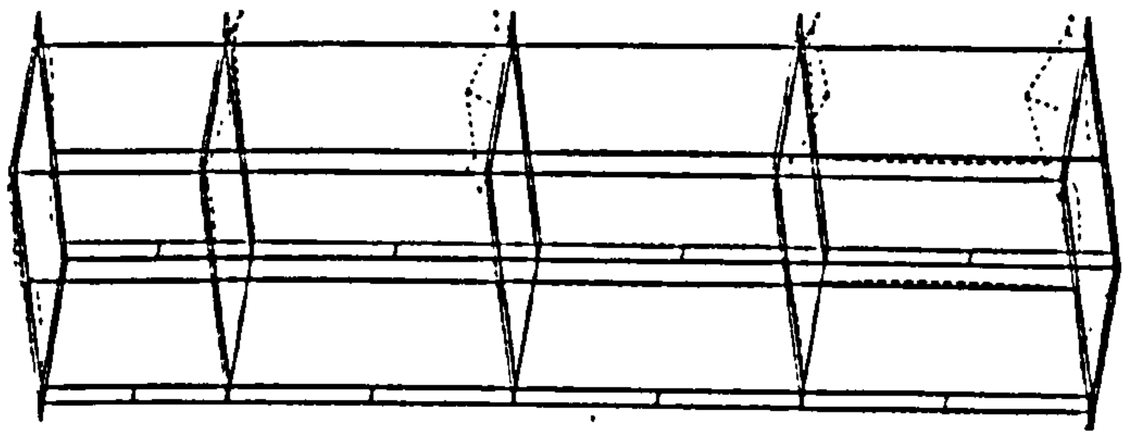

PAFEC 75

VIEW FROM X = 1.000
Y = 0.515
Z = 5.000

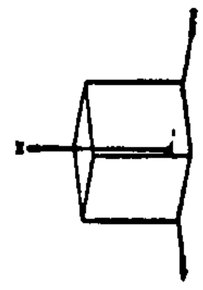

MODE SHAPE NUMBER 42
FREQUENCY = 699.2 HERTZ

WHOLE STRUCTURE DRAWN

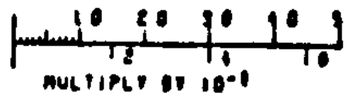

DRAWING NO 3
SCALE = 0.7500E -1

TITLE WIND TUNNEL TEST

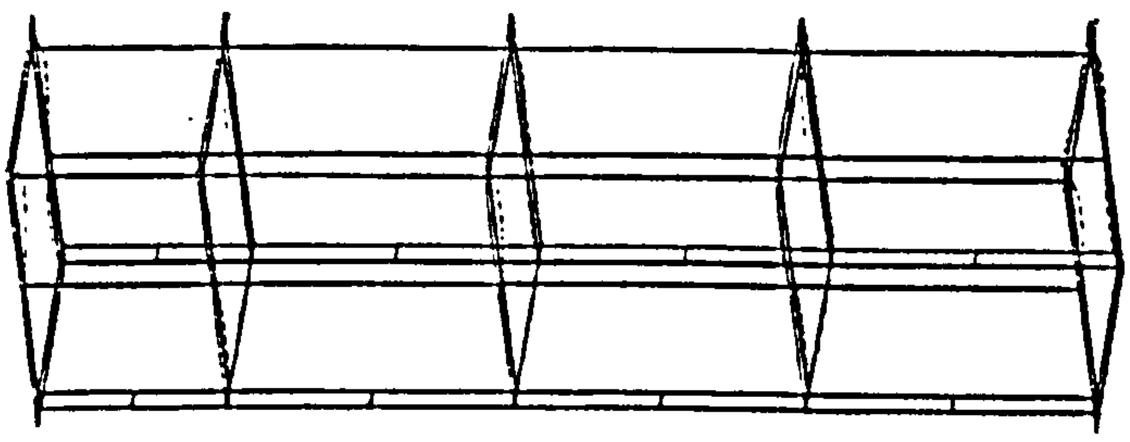

PAFEC 75

VIEW FROM X = 1.000
Y = 0.515
Z = 5.000

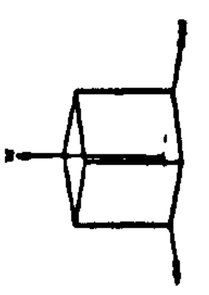

MODE SHAPE NUMBER 43
FREQUENCY = 699.9 HERTZ

WHOLE STRUCTURE DRAWN

FIGURE 4.5 [D]

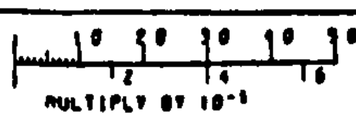

DRAWING NO. 4
SCALE = 0.7500E -1

THE TEST SECTION's NATURAL FREQUENCIES AND MODE SHAPES

TITLE WIND TUNNEL TEST

PAFEC 75

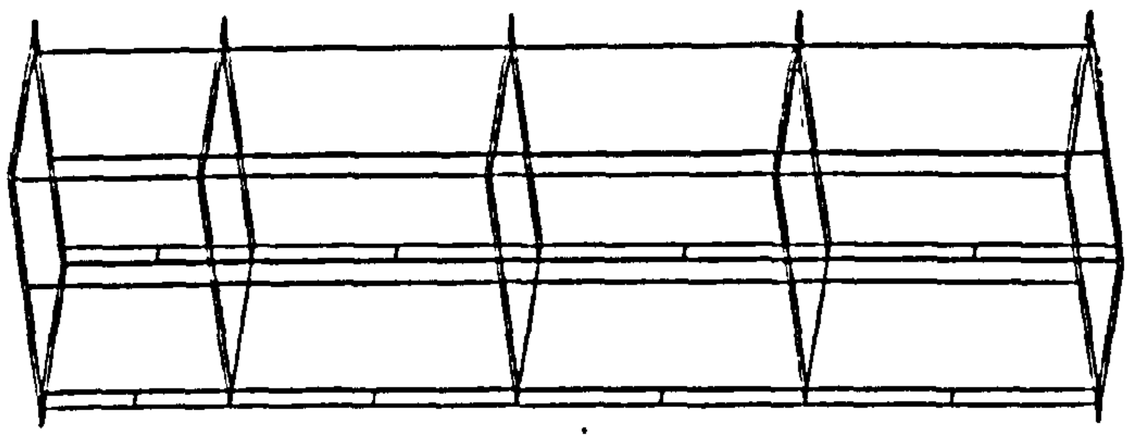

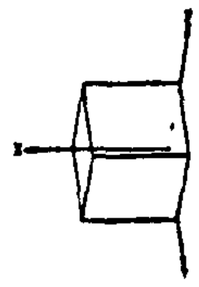

MODE SHAPE NUMBER 44
FREQUENCY = 697.3 HERTZ

WHOLE STRUCTURE DRAWN

DRAWING NO 5
SCALE = 0.75000E-1

TITLE WIND TUNNEL TEST

PAFEC 75

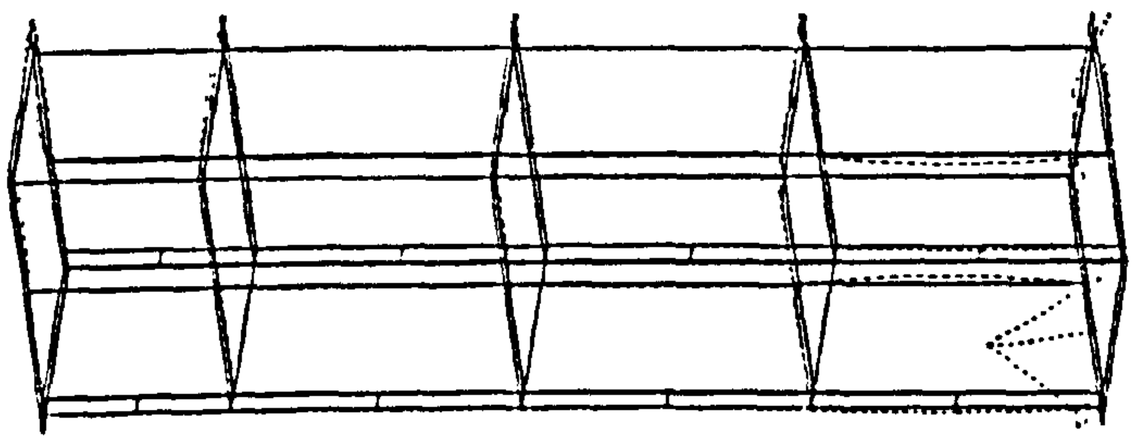

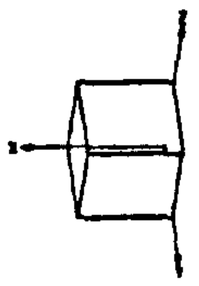

MODE SHAPE NUMBER 45
FREQUENCY = 303.9 HERTZ

WHOLE STRUCTURE DRAWN

DRAWING NO 6
SCALE = 0.75000E-1

FIGURE 4.5 [E]

THE TEST SECTION's NATURAL FREQUENCIES AND MODE SHAPES

5.0 INSTRUMENTATION

5.1 INTRODUCTION

This chapter describes the various instruments used for measurement of flow rate turbulent intensity, acoustic damping and sound pressure level.

5.2 INLET NOZZLE

The mean air flow rate in the tunnel was monitored by measuring the pressure drop across the inlet nozzle. This nozzle was constructed in accordance with the guidelines presented in B.S. 848 and N.E.L. Report no. 39 (ref B16 and P2). The average static pressure downstream of the nozzle was obtained by means of four pressure tappings placed around the circumference of the duct. These were in turn connected to an inclined manometer, see fig. 5.1. The nozzle was calibrated using the method suggested in B.S. 848 and the calibration chart is shown in fig. 5.2.

ALL DIMENSIONS IN mm

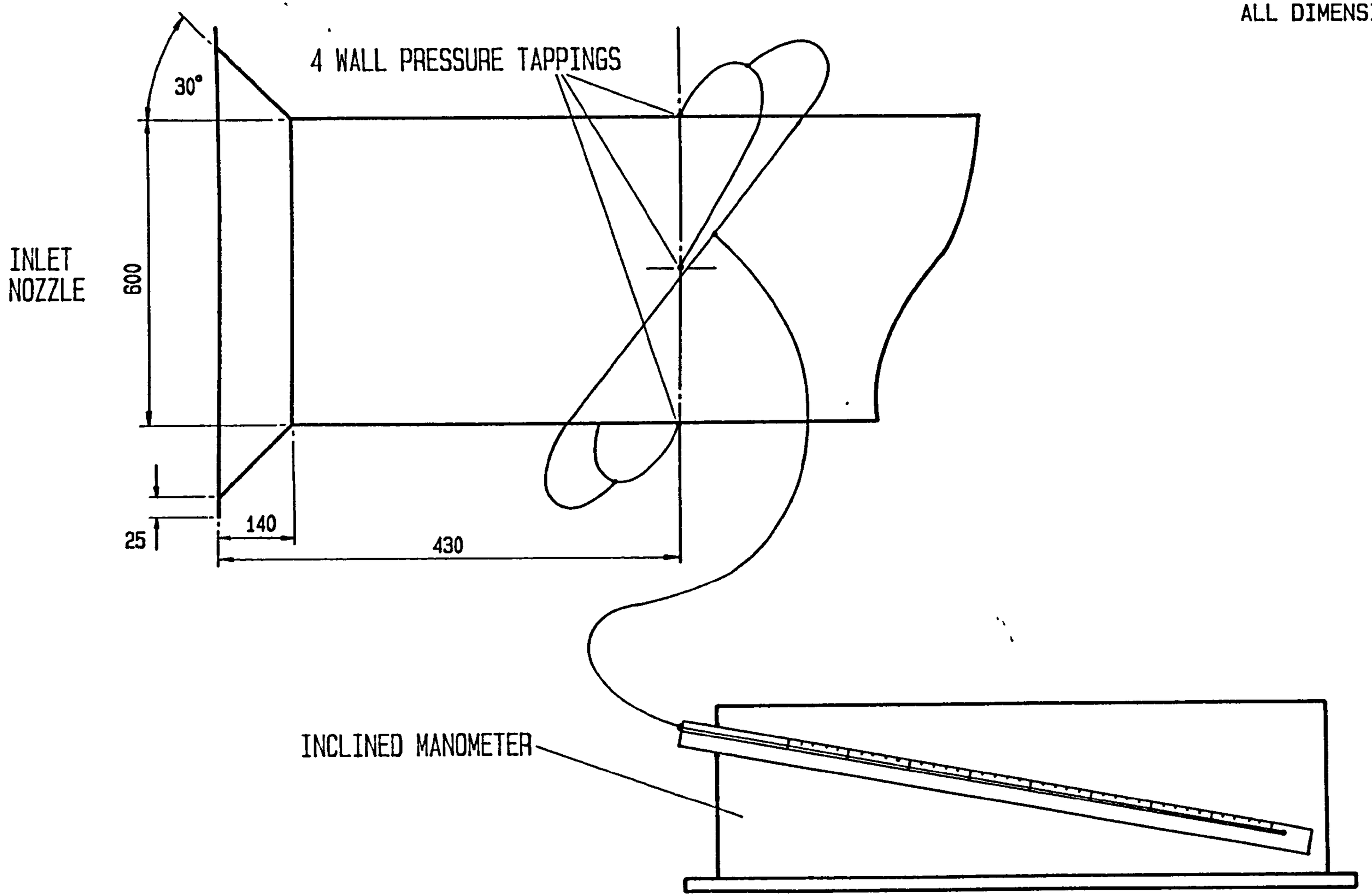

SCHEMATIC DIAGRAM OF CALIBRATED INLET NOZZLE

NOT TO SCALE

FIGURE 5.1

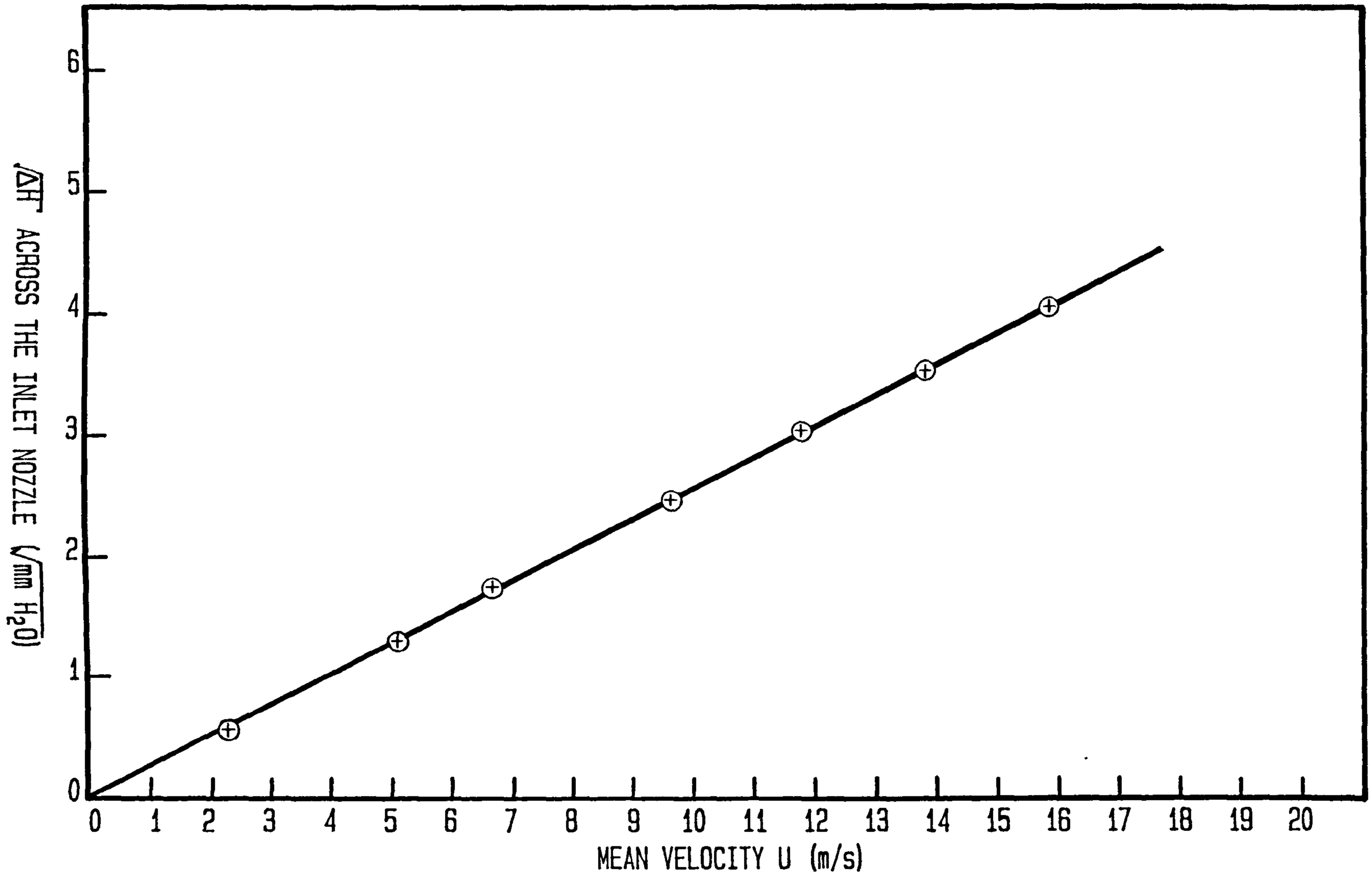

CALIBRATION CHART FOR THE INLET NOZZLE

FIGURE 5.2

5.3 MICROPHONE

It was uncertain what value of sound pressure level (S.P.L.) would be experienced during resonance, and as no reliable empirical method for calculating the S.P.L. exists, a rough estimate had to be made. Previous experimenters have reported resonances of magnitude ranging from 120dB to 160dB (re 2 x 10^{-5} N/m^2). Using this information as a guide a suitable transducer was chosen. A condenser microphone was considered to be best in view of its excellent dynamic range and very low internal noise level. A schematic diagram of this microphone is shown below:

SCHEMATIC CONSTRUCTION OF A CONDENSER MICROPHONE

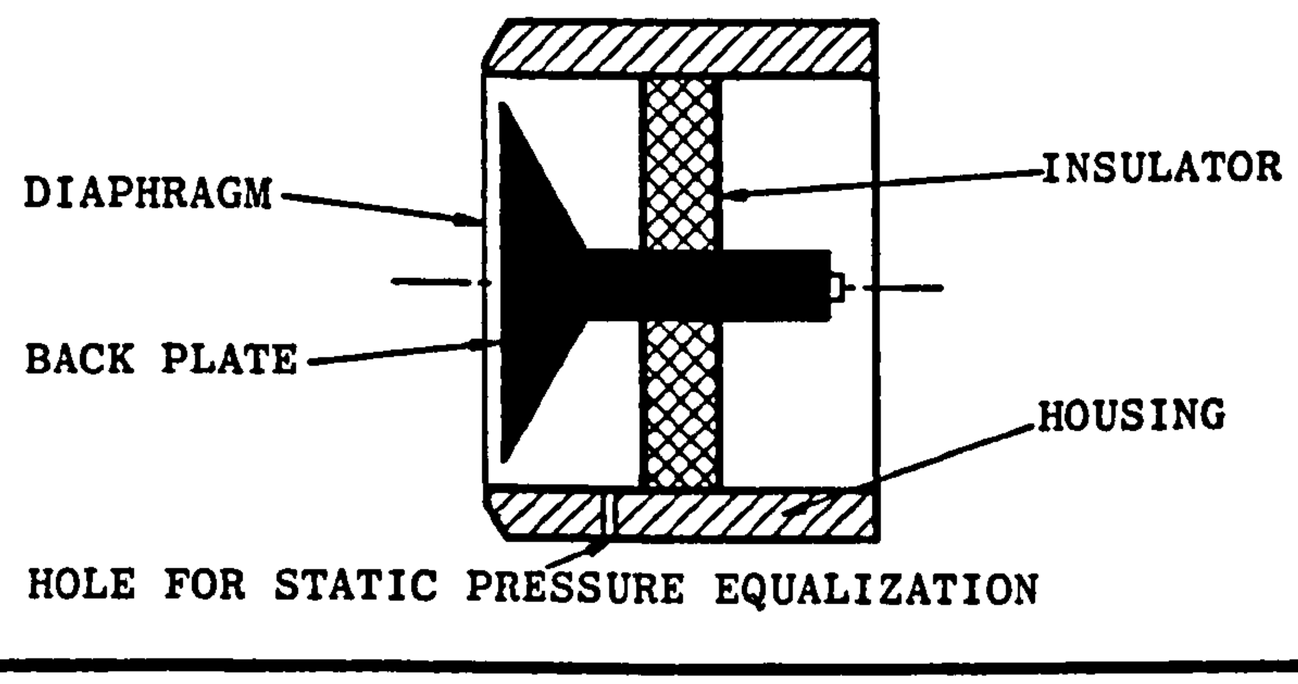

The condenser microphone basically consists of a thin metal diaphragm and a rigid back plate, which constitutes the electrodes of an air dielectric capacitor. A charge is applied to the capacitor by a 200V d.c. polarization voltage. Variations in capacitance, caused by the varying sound pressure on the/

the diaphragm, are now transformed into voltage variations. The bandwidth of the microphone response is determined by the input impedance of the preamplifier at low frequencies and the total capacitance of the system at high frequencies. Figure 5.3 shows the microphone cartridge, the preamplifier and the extension cable. The preamplifier is placed in close proximity to the microphone cartridge in order to reduce stray capacitance, and increase the upper limiting frequency of the response. The complete experimental set-up used for measuring the sound pressure level is illustrated in fig. 5.4. This system was calibrated using a B & K pistonphone type 4220.

B & K CONDENSER MICROPHONE

FIGURE 5.3

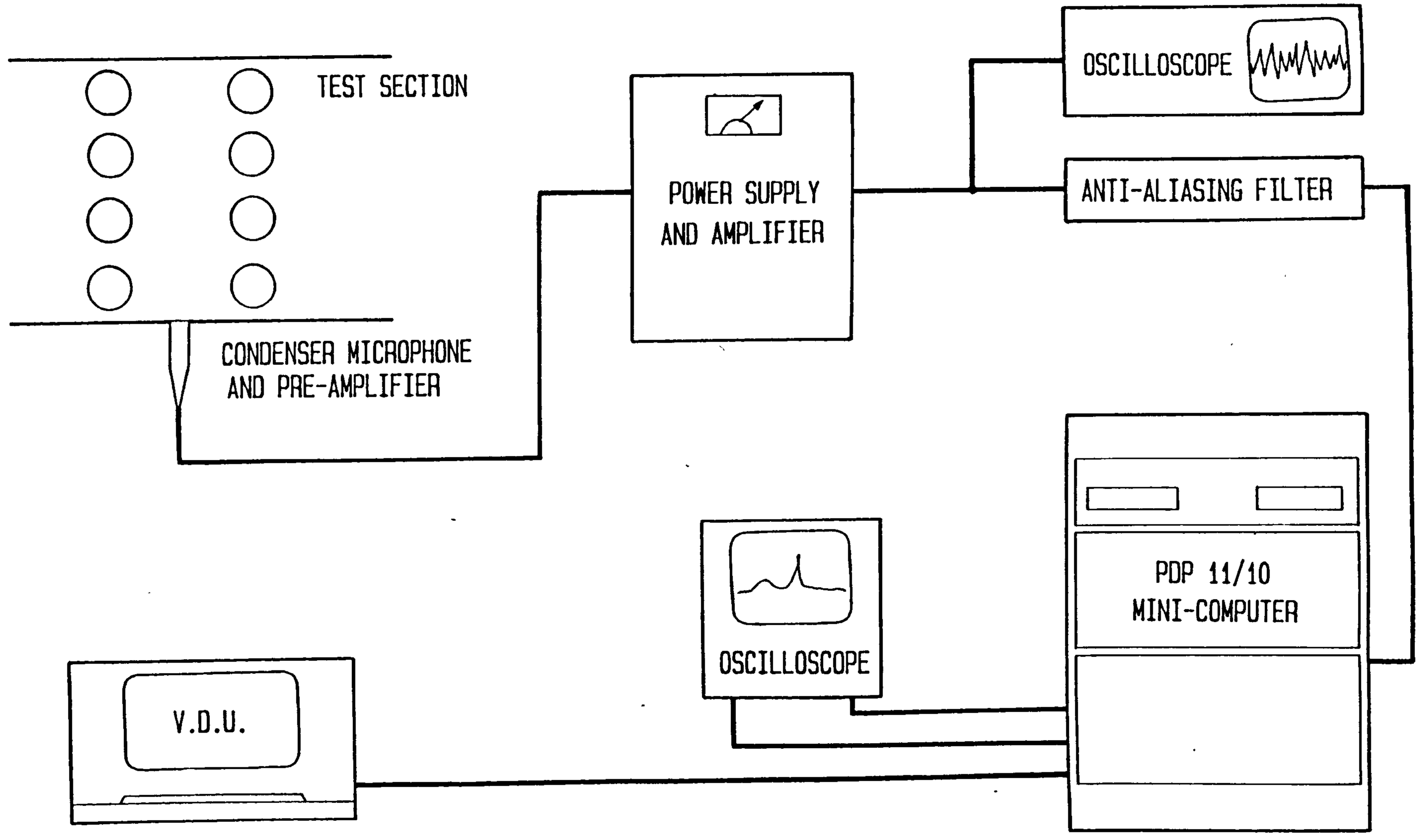

FIGURE 5.4

THE EXPERIMENTAL SET-UP USED TO COMPUTE THE IN-BANK PRESSURE SPECTRUM

5.4 HOT WIRE ANEMOMETER

A hot wire anemometer system was used for making measurements of turbulent intensity and fluctuating velocity. The hot wire system makes use of a heated resistance sensor placed in the flow under measurement and consequently cooled by it. The magnitude of this convective loss is dependent on a number of parameters such as temperature, pressure and velocity. If only the velocity changes, or if the influences of the other parameters are eliminated through the use of suitable circuitry, then the instantaneous heat loss of the sensor is a measure of the instantaneous velocity.

The circuit used for measuring the thermal loss was the constant temperature anemometer circuit (C.T.A.). In principle this consists of a Wheatstone bridge and a servo amplifier. (See diagram below).

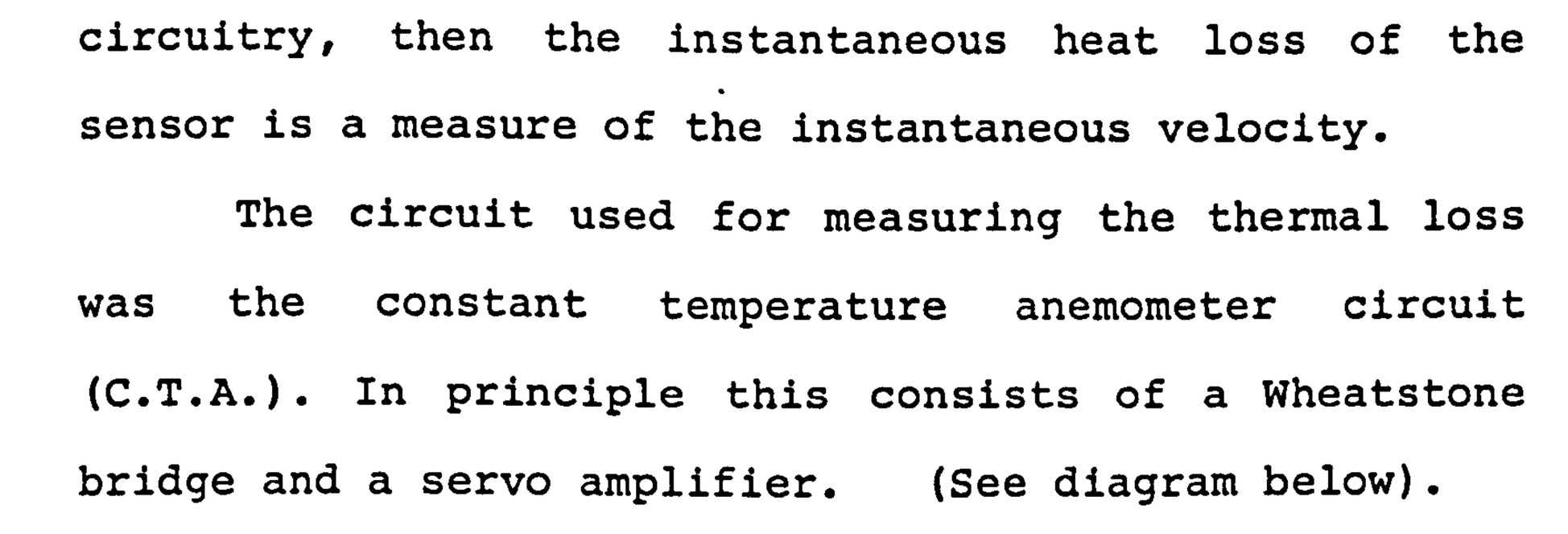

SIMPLIFIED DIAGRAM OF A CONSTANT-TEMPERATURE ANEMOMETER

The active bridge arm contains the probe and one of the two top resistors. The passive bridge arm contains the other top resistance, the comparison resistor and a few compensating networks, which eliminate the influences of the cable parameters. The output voltage of the anemometer system is a nonlinear function of the flow velocity, the transfer characteristics of which are shown in figure 5.5.(a).

This non-linear relationship makes the calculations of turbulent intensity a complicated process, since the slope of the characteristics varies with velocity. These calculations can be simplified by making use of a linearizer. This piece of apparatus converts the transfer characteristics of the anemometer system from those shown in figure 5.5. (a) to that in figure 5.5. (b). A comparison of expressions for calculating the turbulent intensities using both systems readily shows the amount of simplification accomplished.

(a) Nonlinearised anemometer

$$\frac{\sqrt{\bar{u}^2}}{\bar{U}} = \frac{2}{n\ (1 - (V_o/\bar{V})^2} \frac{\sqrt{\bar{v}^2}}{\bar{V}}$$

(b) Linearized anemometer

$$\frac{\sqrt{\bar{u}^2}}{\bar{U}} = C\frac{\sqrt{\bar{v}^2}}{\bar{V}}$$

The set-up for measuring the fluctuating velocities and turbulent intensities are shown in figures 5.6 and 5.7 respectively. The hot wire system, with linearizer, was calibrated using a pitot static tube and manometer. As can be seen from figure 5.6 the linearizer was not incorporated in the system when making the fluctuating velocity measurements. Although it is realised that the anemometers non-linearized response can lead to the production of spurious harmonics, it was felt that due to the relatively small amplitude of the response being measured this problem would not effect the results.

[A]

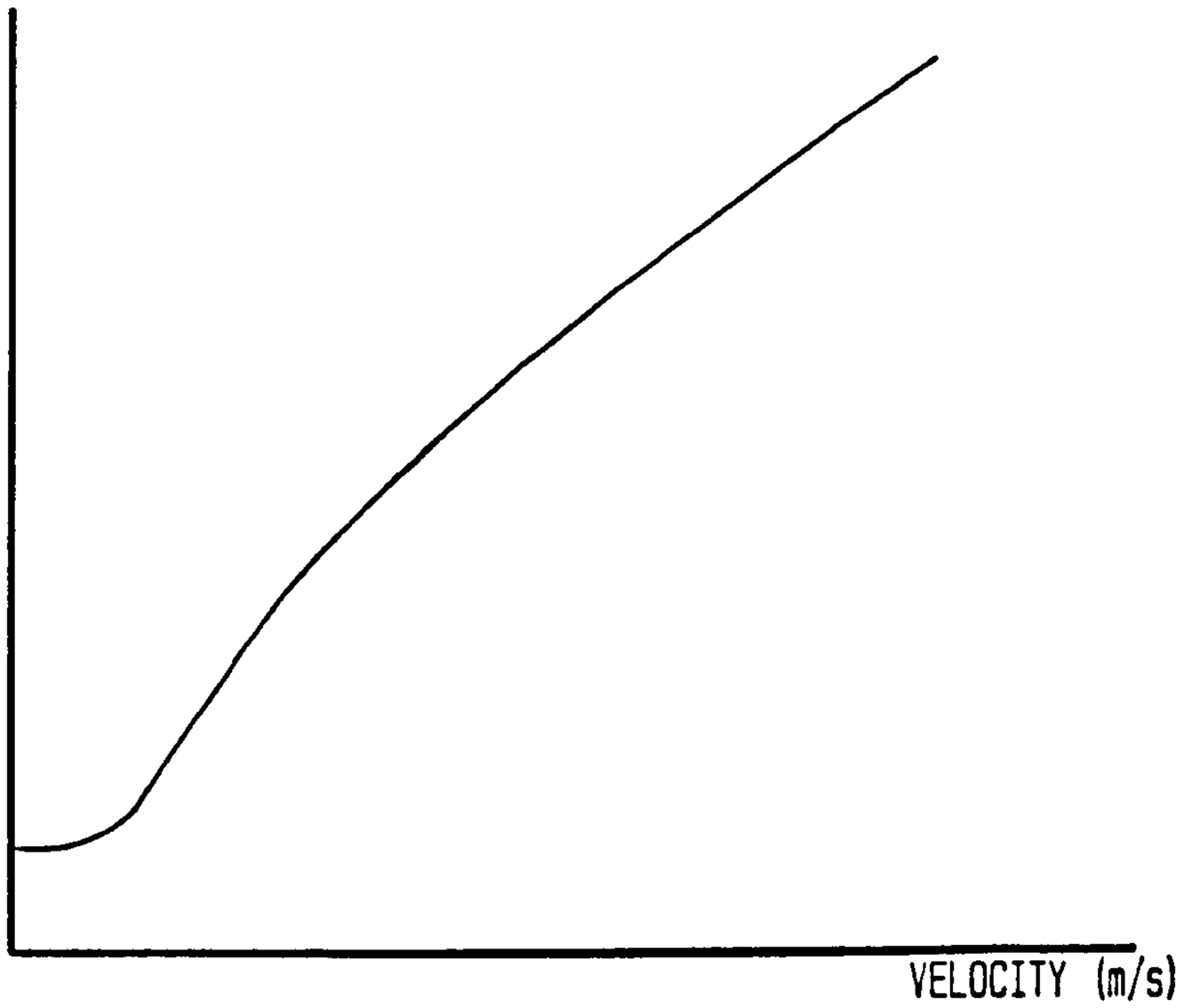

TRANSFER CHARACTERISTICS OF A HOT WIRE ANEMOMETER

[B]

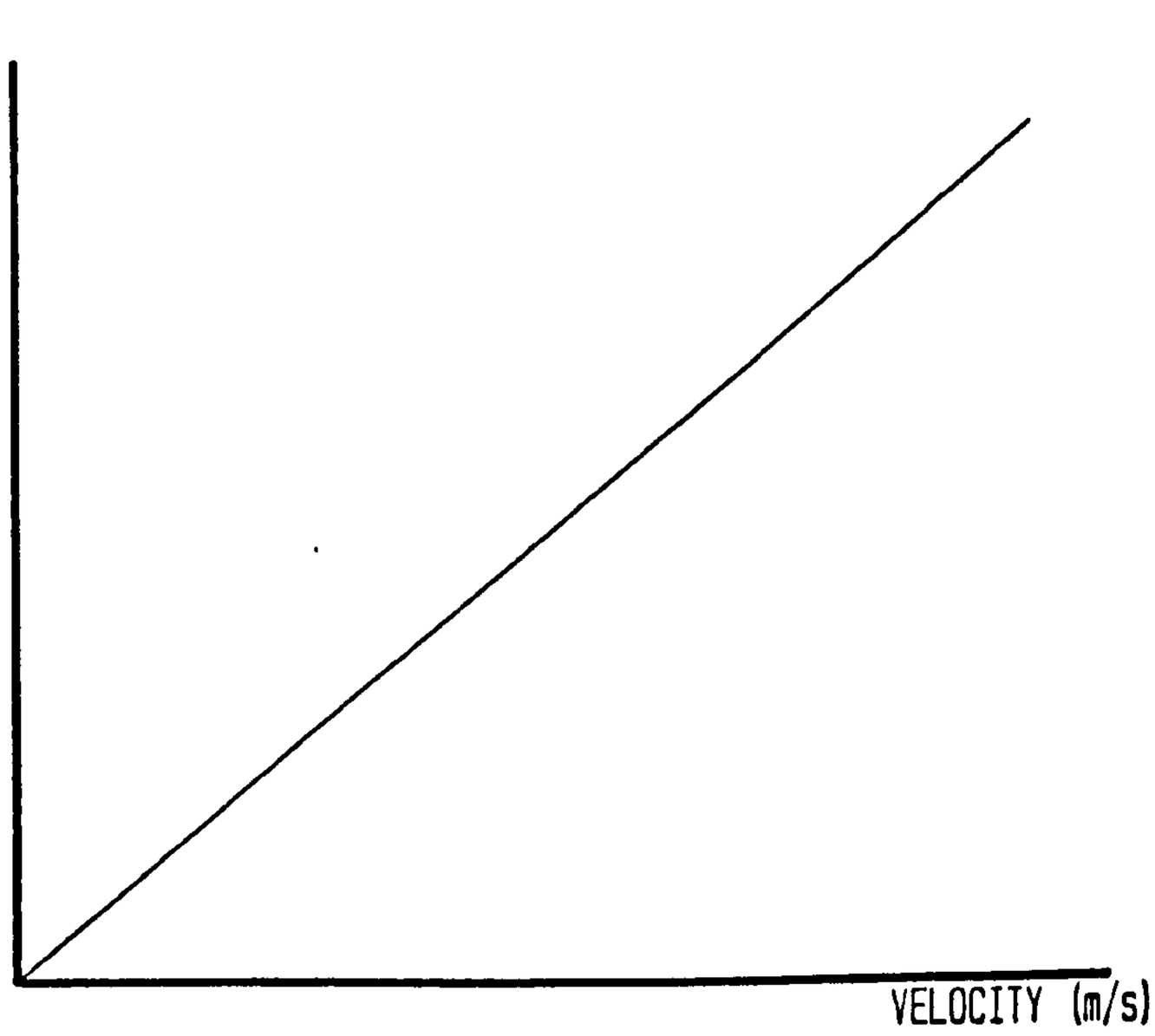

TRANSFER CHARACTERISTICS OF A LINEARIZED HOT WIRE ANEMOMETER

TRANSFER CHARACTERISTICS FOR A LINEARIZED AND NON-LINEARIZED HOT WIRE ANEMOMETER

FIGURE 5.5

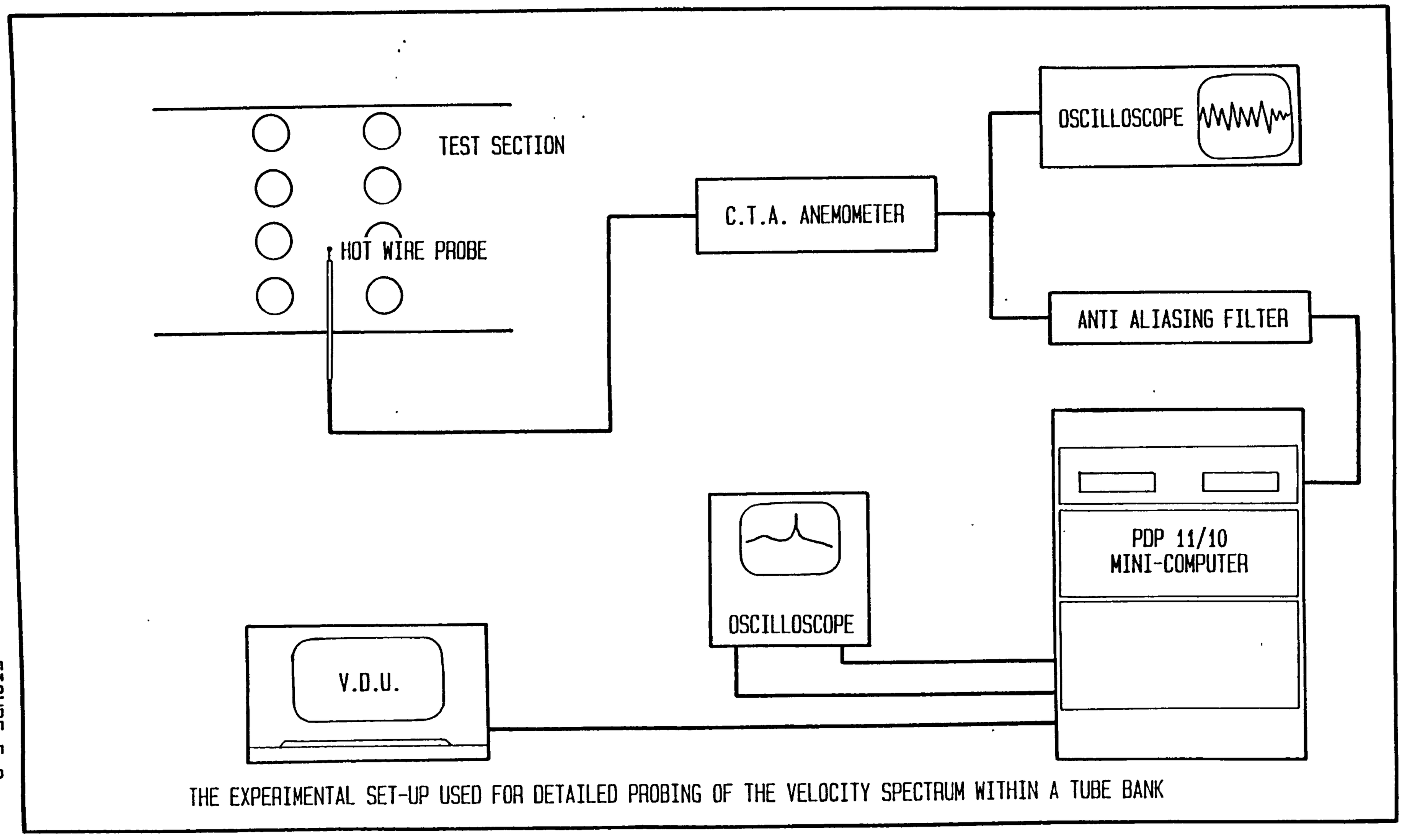

FIGURE 5.6

THE EXPERIMENTAL SET-UP USED FOR DETAILED PROBING OF THE VELOCITY SPECTRUM WITHIN A TUBE BANK

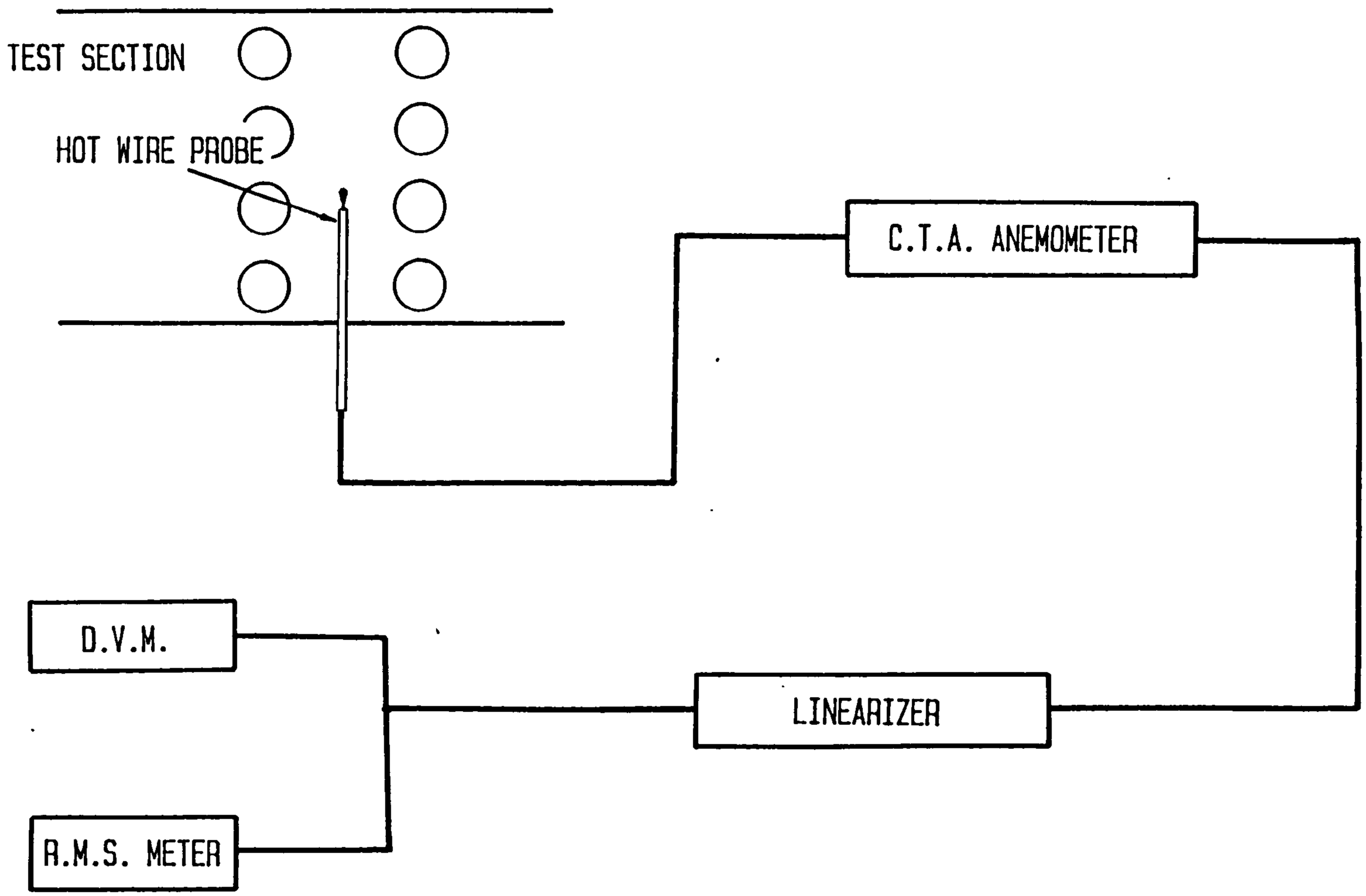

FIGURE 5.7

THE EXPERIMENTAL SET-UP USED IN THE MEASUREMENT OF TURBULENT INTENSITY

5.5 ACOUSTIC DAMPING MEASUREMENTS

It was required that measurements of the acoustic damping be made under flow conditions. This was achieved by obtaining the transfer function between an external excitation and the response of the acoustic system. Mathematical details of this procedure and that used to obtain the acoustic damping values are shown in Chapter 6.5. A schematic diagram of the test section with equipment employed in making these measurements is shown in figure 5.8. As can be seen from this diagram a piston was mounted in the top of the test section to provide the acoustic excitation and the response was measured by a microphone. The piston was driven by a shaker, fed with band limited random noise, and an accelerometer fixed on the piston gave a measure of the excitation. The transfer function, dampings, etc were calculated using the PDP-II computer.

The principal design criterion for the piston was that it should have a minimum weight (to minimise the shaker power required to drive it) and that its natural frequency should be above the area of interest thus minimising spurious resonances and phase distortion. The pistons were constructed from perspex and their physical dimensions together with their natural frequencies are shown in table 3. This shows the fundamental frequency of the six inch square piston to be well above the frequency range of interest so this/

this piston can be considered as being rigid. The natural frequency of the eight inch square piston however, is very close to that of the acoustic frequency. In this situation the piston can no longer be assumed to move rigidly. This problem was overcome by increasing the pistons natural frequency using the web arrangement shown in figure 5.9. This arrangement gave additional stiffness and was found to increase the natural frequency sufficiently to remove the phase distortion.

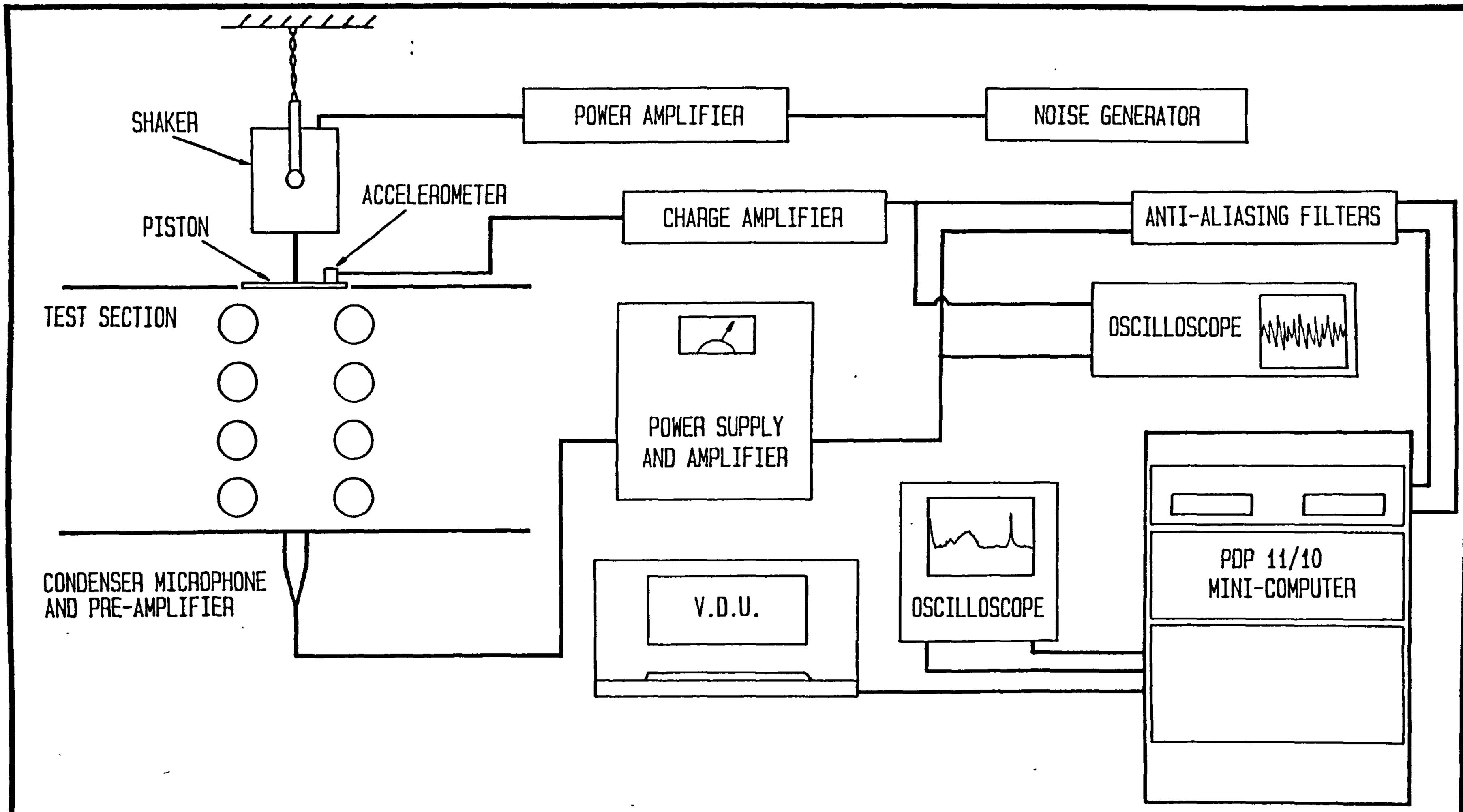

FIGURE 5.8

THE EXPERIMENTAL SET-UP USED FOR THE MEASUREMENT OF ACOUSTIC DAMPING

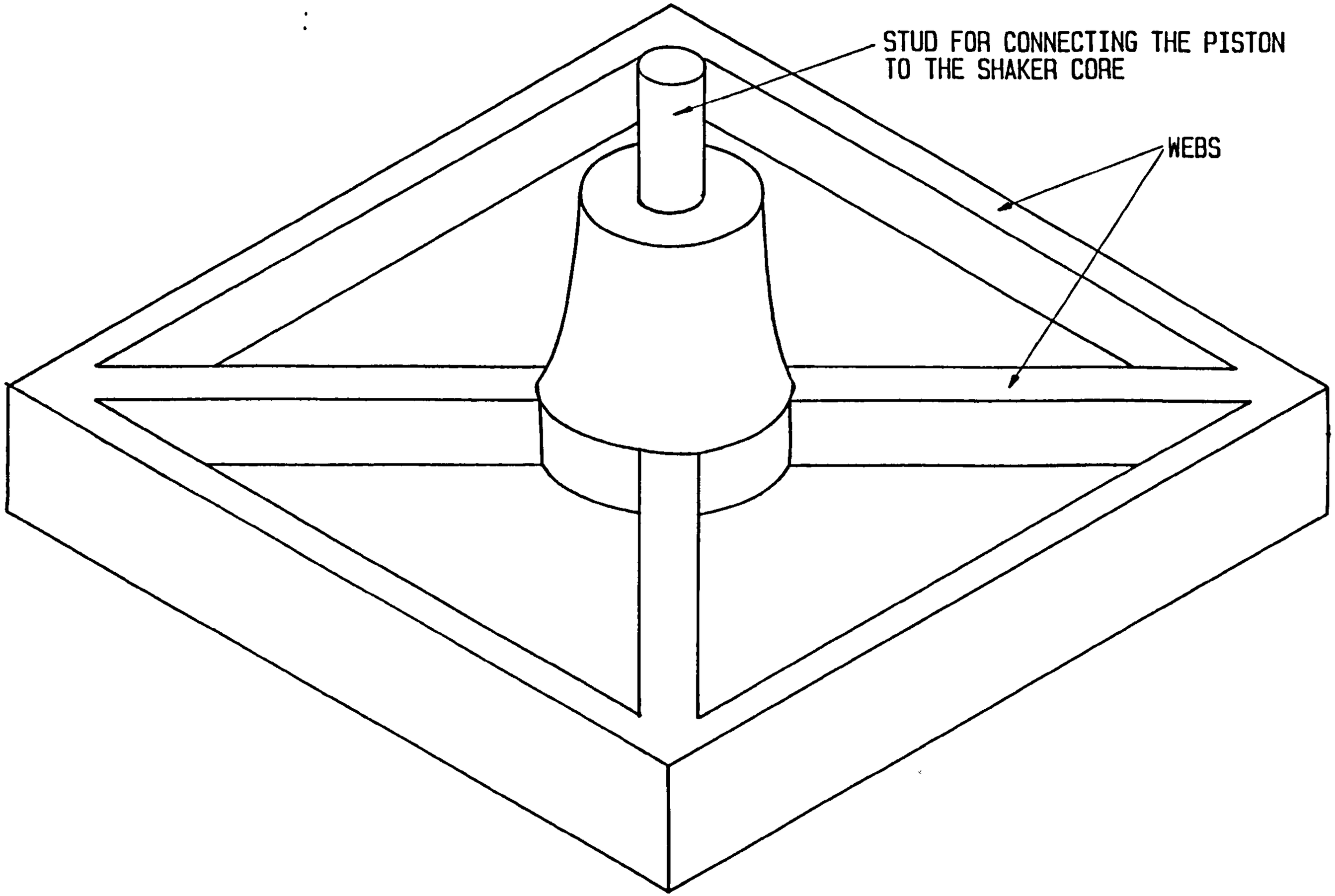

SCHEMATIC DIAGRAM OF PISTON WHICH ILLUSTRATES THE WEB ARRANGEMENT USED TO INCREASE ITS NATURAL FREQUENCY

FIGURE 5.9

5.6 ALTERATION OF ACOUSTIC DAMPING

As mentioned previously one of the objectives of this work was to vary the acoustic damping of the test rig. This would enable the role played by this parameter to be established. It was thought that this would be best achieved by constructing the test section so that the acoustic damping would be low. The damping could then be increased by allowing a greater percentage of the acoustic energy to be radiated from the test section. Figure 5.10 (a) and (b) show the test section lid configurations which were used to achieve this. The inside of the lid was covered with a light polyester sheeting. This allowed acoustic energy to be radiated out of the cut outs and still maintain an air tight seal. The large cut out in the lid provided access for the piston which was used in the measurement of the acoustic damping. The theory behind this method of increasing the acoustic damping is further discussed in chapter 9.1 and Appendix 4.

PHYSICAL DIMENSIONS (INCHES)	NATURAL FREQUENCY f_n
6.0 x 6.0 x 0.25	609 Hz
8.0 x 8.0 x 0.25	237 Hz

TABLE 3

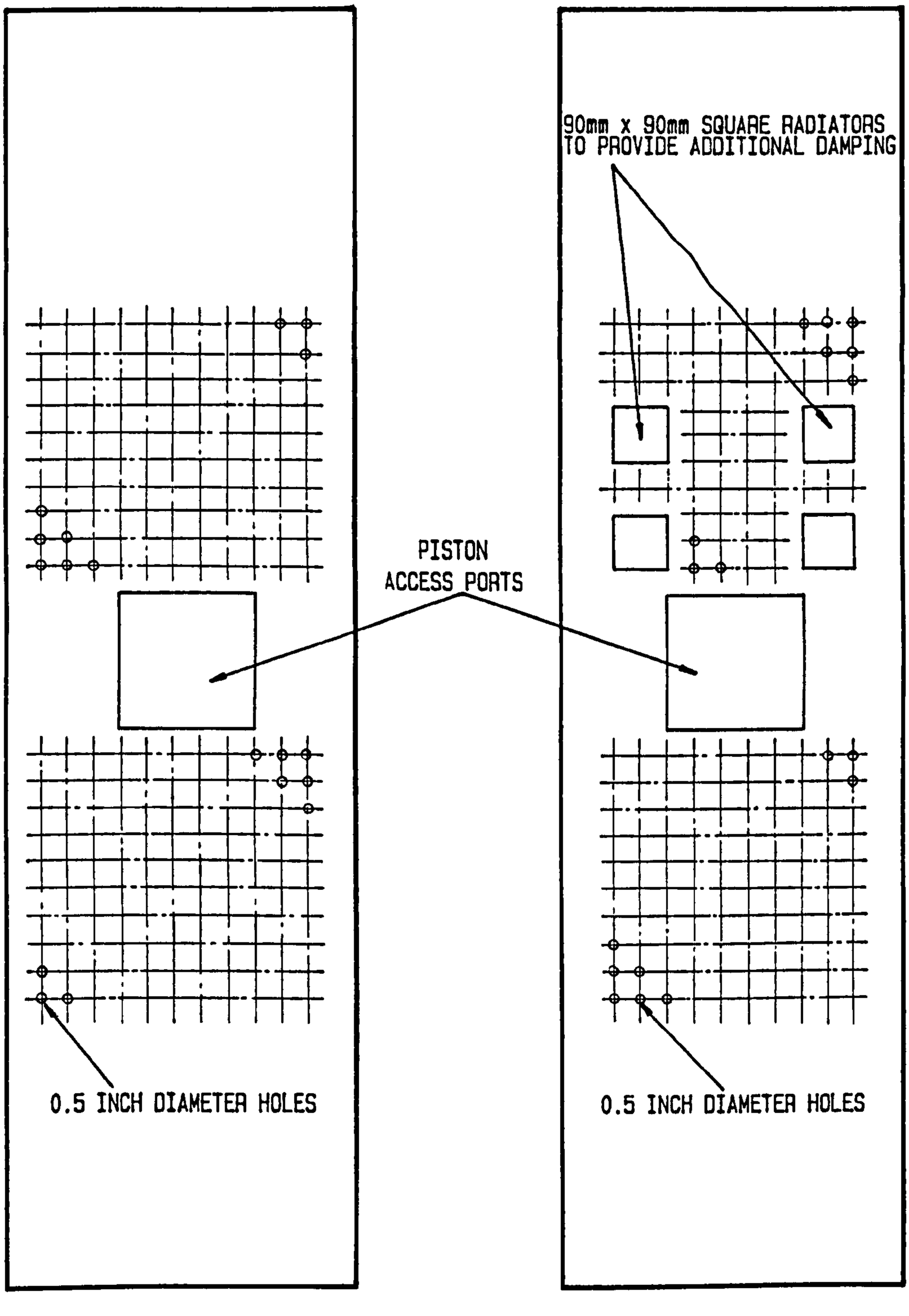

AN ILLUSTRATION OF THE TEST SECTION LIDS WHICH WERE USED TO INCREASE THE ACOUSTIC DAMPING IN THE TEST SECTION

FIGURE 5.10

6.0 SPECTRAL ANALYSIS

6.1 INTRODUCTION

This chapter describes the basic principles and properties of the frequency analysis routines used in this work. This includes a description of some of the different forms of the fourier transform together with the various frequency functions used.

This chapter also contains the various flow charts for the programs developed in this work.

6.2 THE FOURIER TRANSFORM

The concept of frequency analysis by which a complex signal can be broken down into a number (perhaps an infinite number) of co-sinusoidal components at various frequencies is now widely accepted. These frequency components each have a given amplitude and initial phase and are derived as the result of a Fourier analysis. The fourier transform is the mathematical basis of this frequency analysis and takes different forms depending on the type of signal being analysed.

The forward Fourier transform may be written as:

$$F_X(f) = \int_{-\infty}^{\infty} X(t)\ e^{-j2\pi ft}\ dt$$

and/

and the reverse fourier transform is written as:

$$X(t) = \int_{-\infty}^{\infty} F_x(f) e^{j2\pi ft}\, df$$

where X(t) and $F_x(f)$ are continuous functions of time and frequency respectively. In the case of many modern digital processing instruments however, the time function is represented as a finite sequence of discrete values (equi-spaced in time). This representation is known as the "Time Series". The time function is no longer continuous and therefore does not fulfill the requirements of the above integral. In this situation another form of the Fourier transform must be used, this is known as the discrete fourier transform. The forward discrete Fourier transform may be written as:

$$F_x(k) = \frac{1}{N} \sum_{n=0}^{N-1} X(n)\, e^{-\frac{j\,2\pi kn}{N}}$$

and the reverse discrete Fourier transform is given by:

$$X(n) = \sum_{k=0}^{N-1} F_x(k)\, e^{\frac{j\,2\pi kn}{N}}$$

Here the infinite continuous integrals have been replaced by finite sums which are much better adapted to digital computations. Even so, it can be seen that in order to obtain N frequency components from N time samples (or vica versa) it requires N^2 complex multiplications. This is therefore a very slow process due/

due to the large amount of complex multiplications.

In 1965 a paper was published in which a calculation procedure known as the fast fourier transform (FFT) was described. This procedure gives the same result as the discrete Fourier transform but the number of multiplications is reduced to N $\log_2$ N. This gives a reduction in computation time equal to N/$\log_2$ N, which for a typical case of N = 1024 is more than 100. Since its introduction the FFT has revolutionized signal analysis and is now an extensively used procedure.

At this point it is useful to discuss some of the properties of the discrete Fourier transform. As stated previously the "Time Series" is a finite digitized representation of the time function. The sampling of a continuous signal can lead to the misinterpretation of high frequencies as lower frequencies (A high frequency being defined as a frequency above half the sampling frequency). This is termed as aliasing and this effect is illustrated in figure 6.1. Figure 6.1(a) shows the digital form of a continuous d.c. signal (f = 0) and figure 6.1(b) illustrates the digital form of a sine wave of frequency f_s. (i.e. f = sampling frequency). Similarily in figure 6.1(c) the digital form of a sine wave of frequency f_s/N is shown and a sine wave of frequency $(N + 1)f_s/N$ is illustrated in figure 6.1(d). These illustrations clearly show the aliasing effect and how high frequencies may be misinterpreted. The graph in figure 6.2 illustrates the relationship between/

between the actual frequency of the signal and the apparent frequency indicated by the digital representation. This is obviously one of the pitfalls of digitizing a continuous signal. This problem may however be overcome by using a low pass filter to filter out all the frequency information above half the sampling frequency. It is desirable that this filter have a sharp roll-off so that most of the frequency points may be utilised

The continuous Fourier transform gives a spectrum which is a continuous function of frequency. The components of this spectrum have units of spectral density (typically Volts/Hz). The most common way of displaying such a spectrum however, is as an amplitude squared spectrum. This is termed as the "power spectral density" (P.S.D.) and has typical units of $Volts^2/Hz$. Therefore the P.S.D. must be integrated over a finite bandwidth to give a finite power. This can be applied to stationary random functions whose spectrum is continuous but, has a finite and statistically constant power. To apply this concept to stationary deterministic signals with discrete spectra involves the use of delta functions. In this situation it is more common to represent the spectrum as "Power spectrum" scaled directly in power units (typically $Volts^2$). Similarily when considering the discrete Fourier transform, because the frequency spectrum is represented /

represented by a discrete series of components the spectrum is usually displayed as a "Power spectrum".

The result of a Fourier analysis is given as a double sided spectrum centred about the zero frequency axis. It is however usual to display the resulting spectrum as a single sided spectrum, therefore the original must be modified. The d.c. component can be taken directly from the original spectrum. However all the other frequency components are complex and have a corresponding component in the negative frequency domain. A spectral component of frequency f_k may be represented as:

$$F_x\ (f_k) = a_k + jb_k$$

$F_{xx}\ (f_k) = a_k^2 + b_k^2$ double sided power spectrum

This ccmponent has a corresponding component at a frequency of $-f_k$ which may be represented thus:

$$F_x\ (-f_k) = a_k - jb_k$$

$F_{xx}\ (-f_k) = a_k^2 + b_k^2$ double sided power spectrum

now adding these two components together to give a single sided spectrum:

$F_{xx}(f_k) = 2(a_k^2 + b_k^2)$ single sided power spectrum

$$F_{xx\ r.m.s.}(f_k) = \sqrt{2(a_k^2 + b_k^2)}$$

The concept of bandwidth shall now be considered with particular application to the discrete fourier /

Fourier transform. The classical method of obtaining the frequency spectrum of an electrical signal is to pass the signal through a number of analogue bandpass filters. Each filter has a different centre frequency and the spectral components are obtained by measuring the transmitted power from the filter. The bandwidth of the filter can be interpreted as being the degree of frequency uncertainty associated with a measurement. In other words the frequency of a transmitted component can only be said to be somewhere in the filters bandwidth. The bandwidth associated with a measurement is not necessarily determined by the bandwidth of a filter, especially where none is used. This is the situation in digital calculations. The continuous fourier integral gives a result which has an infinitely narrow bandwidth (df). This however is never possible in practice, so the concept of bandwidth must be introduced. In practice a continuous signal is divided into short sections called "time windows". The simplest way of applying such a window is to cut the signal off at each end. This can be considered as a multiplication by a rectangular weighting function of length T, which gives uniform weighting along the selected sample. In this situation it is the effective length of the window that determines the bandwidth. In the case of a time window of length T seconds the bandwidth is limited to a minimum /

minimum value of 1/T. Figure 6.3 shows the effective filter characteristics for the rectangular time window described previously. Figure 6.4 illustrates the power transmission characteristics for the same window. As can be seen from these diagrams the filter characteristics have large side lobes which cause spectral leakage. This effect is illustrated in figures 6.5 (a) - (d). Figure 6.5 (a) represents an endless sinusoidal function in both time and frequency domain. The corresponding power spectrum for this function is shown in figure 6.5 (b). Figure 6.5 (c) however illustrates a similar sinusoidal function which has been multiplied by a rectangular time window. Its corresponding power spectrum is shown in figure 6.5 (d) and as can be seen the result is the filter characteristics centred on $\pm f_o$. These side lobes, caused by the rectangular window, may be reduced by using a different shape of time window. Many different shapes of time window can be used to alter the effective filter characteristics. It must be noted however that all these windows trade off between side lobe level and main lobe bandwidth, and the main lobe bandwidth for any window cannot be less than the bandwidth of the rectangular window. This is illustrated in figure 6.6 where a sinusoidal function has been multiplied by a $\cos^2$ time window. As can be seen the $\cos^2$ window (or Hanning window) has considerably reduced the side lobes but the bandwidth of /

of the main lobe has been increased. It must also be noted that the used of such a time window will reduce the energy content of a sample. This may be compensated for by calibrating the system with a reference signal. Alternatively, the factor by which the energy is reduced may be calculated. In the case of a rectangular window the sample is uniformly weighted (by a factor of unity) over its complete length, so no compensation is required. Any other shape of window will however require some compensation and the factor can be calculated as follows:

$$C_F = \frac{1}{T} \int_{-T/2}^{T/2} \{W(t)\}^2 dt$$

where W(t) is the weighting function with a maximum value of unity. The corresponding attenuation factor in dB is given by $10 \log_{10}$ (CF).

For a discrete weighting funciton:

$$C_F = \frac{\sum_{n=0}^{N-1} |W(n)|^2}{N}$$

It may be shown that the accuracy of a spectral measurement is dependant on the effective bandwidth of the measurement B(Hz) and the record length T(s). This relationship is as follows:

$$\frac{\sigma}{M} \cong \frac{1}{\sqrt{BT}}$$

where/

where σ = standard deviation

m = mean value

In order to successfully apply this relationship the effective bandwidth of the time window must be determined. It has however been shown (ref. B18) that for most practical calculations the B.T. product may be taken as being equal to unity, irrespective of which time window is used. This is because a change in bandwidth obtained by using a shaped time window, is accompanied by a change if effective record length, and an approximately constant B.T. product. So from the above equation $\frac{\sigma}{m} = 1$. This means that the standard deviation of the measurement is equal to the mean value, so the accuracy is very poor. It is interesting to note that increasing the record length T so that more data is analysed will not improve the accuracy of the measurement. This is because as the record length T becomes greater the spectral bandwidth decreases and the B.T. product remains the same ($B = \frac{1}{T}$). So increasing the record length will only increase the frequency resolution. There are two common methods for increasing the B.T. product of a measurement. The first method is to increase B by averaging over a number of adjacent frequency components. The B.T. product is now given by the number of original bandwidths in the integrated bandwidth. This method has the advantage of improving the effective filter characteristics of the /

the window. It does however have the disadvantage of a trade-off between frequency resolution and measurement accuracy. The other method for improving measurement accuracy is to increase the value of T by averaging over several records. This will give a B.T. product equal to the number of individual records over which the average is made. This method was used in this work to improve measurement accuracy.

Many different spectral functions may be calculated using the fourier transform, In this work four different spectral functions were frequently used and these shall now be described.

6.3 THE POWER SPECTRUM

As mentioned previously the power spectrum is defined as follows:

$$F_x(f) = \mathcal{F}\{X(t)\} = \int X(t)\ e^{-j2\pi ft}$$

$$F_x(f) = |Sx| \angle\phi$$

$$F_{xx}(f) = F_x(f).F_x^*(f)$$

* denotes complex conjugate.

F_x results from a fourier transform of X(t). The magnitude | Sx | defines the instantaneous spectral content at frequency f and the phase angle ϕ describes the relative phasing of the components. These angles are not meaningful unless the analysis window is synchronized /

sychronized to a periodic harmonic in the data. F_{xx} represents the average of the squared spectrum magnitude. It is a real spectrum defining the average power (variance) at each frequency.

6.4 THE CROSS SPECTRUM

The cross spectrum is defined as follows:

$$F_x(f) = \int X(t)e^{-j2\pi ft}$$

$$F_y(f) = \int Y(t)e^{-j2\pi ft}$$

$$F_{xy}(f) = F_x^*(f).F_y(f)$$

This is the average complex product of the spectrum of signal Y and the complex conjugate of the spectrum of signal X. This product indicates those frequencies where both X(t) and Y(t) have content. The phase angle indicates the average phase difference between the signals at each frequency.

6.5 THE TRANSFER FUNCTION

A transfer function describes the cause effect relationship between two measured signals, and is defined as the complex ratio of the output to the input of a system.

$$F_x(f) = \int X(t)e^{-j2\pi ft}$$

$$F_y(f) = \int Y(t)e^{-j2\pi ft}$$

$$H_{xy}(f) = \frac{F_y(f)}{F_x(f)}$$

where/

where $H_{xy}(f)$ is the transfer function from X to Y

$F_y(f)$ is the fourier spectrum of the output signal

$F_x(f)$ is the fourier spectrum of the input signal

This equation may be used directly however it can be made easier to compute if the following development is made:

$$H_{xy}(f) = \frac{F_y(f)}{F_x(f)}$$

$$H_{xy}(f) = \frac{F_y(f)}{F_x(f)} \cdot \frac{F_x^*(f)}{F_x^*(f)}$$

$$= \frac{F_{xy}(f)}{F_{xx}(f)}$$

The transfer function is now equal to the ratio of cross spectrum, between the output and input, and the power spectrum of the input. This makes computation easier because the calculation no longer requires division by a complex number. Six transfer functions have become classics in the study of mechanical structures. These are:-

1. Compliance (displacement/force)
2. Apparent Stiffness (force/displacement)
3. Mobility (velocity/force)
4. Impedance (force/velocity)
5. Inertance (acceleration/force)
6. Apparent Mass (force/acceleration)

The/

The compliance, mobility and inertance functions are all ratios of response motion to input force excitation. These functions all identify resonant frequencies by exhibiting a peak in the frequency domain. The apparent stiffness, impedance and apparent mass are the reciprocal relationships of compliance, mobility and inertance respectively. These functions denote a resonant frequency as a valley or minimum value. All six of these transfer fuctions are interrelated by simple algebraic operations and having knowledge of one transfer function is equivalent to knowledge of all six. The nature of available instrumentation and the specific problem usually dictates the transfer function for measurement.

The main reason for calculating the transfer function was to obtain a measure of the acoustic damping in the tunnel. The damping properties of a resonance are descirbed by an amplification factor Q. The amplification factor is related to the damping factor by the relationship $Q = 1/2\zeta$. Three of the most popular methods for calculating the damping from the transfer function are:

Method 1

$$Q = \frac{|X/F|\,(f_n)}{|X/F|\,(o)}$$

where/

where $|X/F|(f_n)$ = Compliance magnitude at the natural frequency

$|X/F|(o)$ = Static Compliance

Method 2

$$Q = fn/\Delta f$$

where f_n = natural frequency

Δf = frequency bandwidth at the point 3dB below the Mobility magnitude at frequency f_n.

Method 3

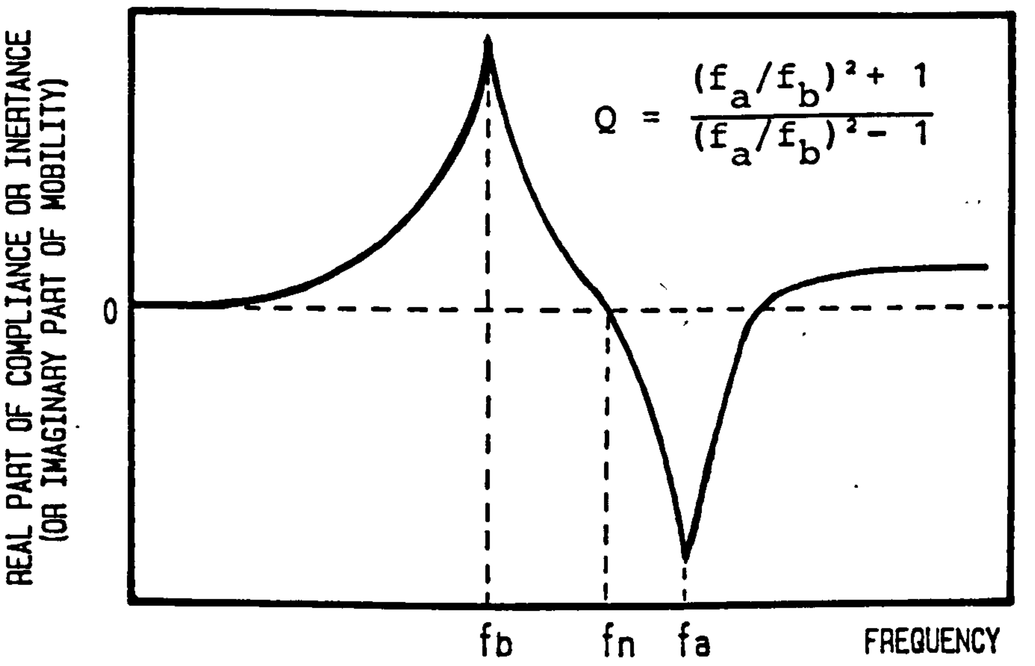

where f_a = frequency above resonance where the real part of compliance or inertance (imag. part of mobility) reaches a peak.

f_b = frequency below resonance where the real part of compliance or inertance (imag. part of mobility) reaches a peak of opposite sign.

The /

The third method was used in this work because it is the most precise for practical implementation. It also has the advantage of being directly applicable to the compliance, mobility or inertance function.

6.6 THE COHERENCE FUNCTIONS

In the case of cross spectrum and transfer function calculations it is not known to what extent $F_y(f)$ results from $F_x(f)$. In this situation it is wise to check the coherence function. The coherence function gives a measure of what proportion of the output power is caused by the input. This can be useful in determining the contributions of a number of independant sources to a given response. Likewise if the signal contains noise then it gives an indication of the signal-to-noise ratio. Hence the coherence function is a useful check on the validity of cross spectrum and transfer function data. The coherence is defined as:

$$\gamma_{xy}^2(f) = \frac{|F_{xy}(f)|^2}{F_{xx}(f).F_{yy}(f)}$$

Where $F_{xy}(f)$ is a cross spectrum obtained by averaging over a number of records.

$F_{xx}(f)$) are power spectra, also averaged over a
)
$F_{yy}(f)$) number of data records.

It is useful to note that the first estimate of $\gamma_{xy}^2(f)$ from one record of X(t) and Y(t) will always be unity./

unity. This follows from:

$$F_{xy}(f) = F_x^*(f)F_y(f) = |F_x(f)||F_y(f)|\underline{\lfloor \phi_y - \phi_x}$$

$$|F_{xy}(f)|^2 = |F_x(f)|^2 . |F_y(f)|^2$$

while $F_{xx}(f) = |F_x(f)|^2$

and $F_{yy}(f) = |F_y(f)|^2$

$$|F_{xy}(f)|^2 = F_{xx}(f)\ F_{yy}(f)$$

However, on averaging over several records it is only when there is no extraneous noise (i.e. the signal Y(t) stems entirely from X(t)) that the individual estimates of cross spectrum have exactly the same phase angles. This effect is illustrated in figure 6.7 and shows that only when the individual cross spectra have the same phase angle can the coherence be equal to 1.

6.7 COMPUTATION OF SPECTRAL FUNCTIONS

A PDP-11 mini computer was used for calculating the various spectral functions. A custom built FFT program was purchased and additional software was written around this program so that the desired frequency functions could be obtained. This FFT program had the advantage of being written in machine language and was therefore very fast compared to its equivalent written in a higher level language. The additional software was constructed in two main parts. The first part /

part sampled the data, stored it on diskette and then calculated the relevant spectral functions. Once these spectral functions have been calculated the results are stored on diskette. This procedure was adopted in order to reduce the running time of the fan, etc. The flow diagram for this program is shown in figure 6.8. The second part of the software reads the results from the diskette, and allows them to be rescaled, expanded or displayed on one of the output devices. The flow diagram for this part of the software is shown in figure 6.9.

[A]

f=0

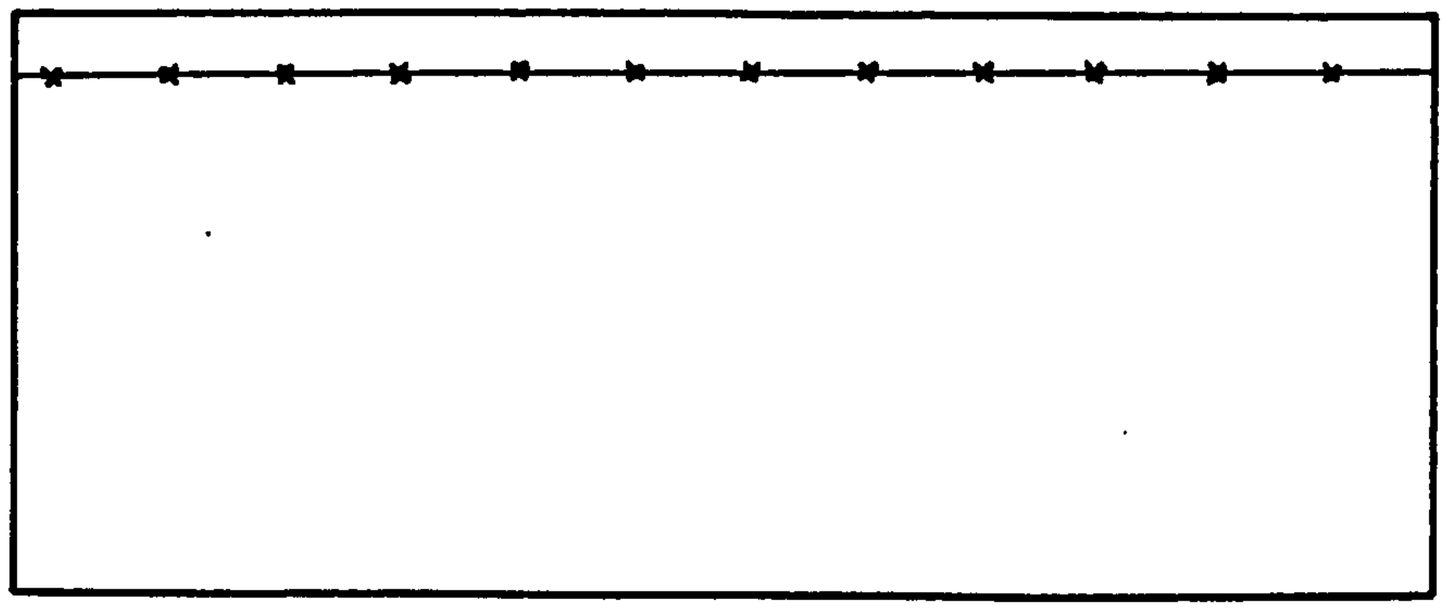

D.C. COMPONENT

[B]

f=fs

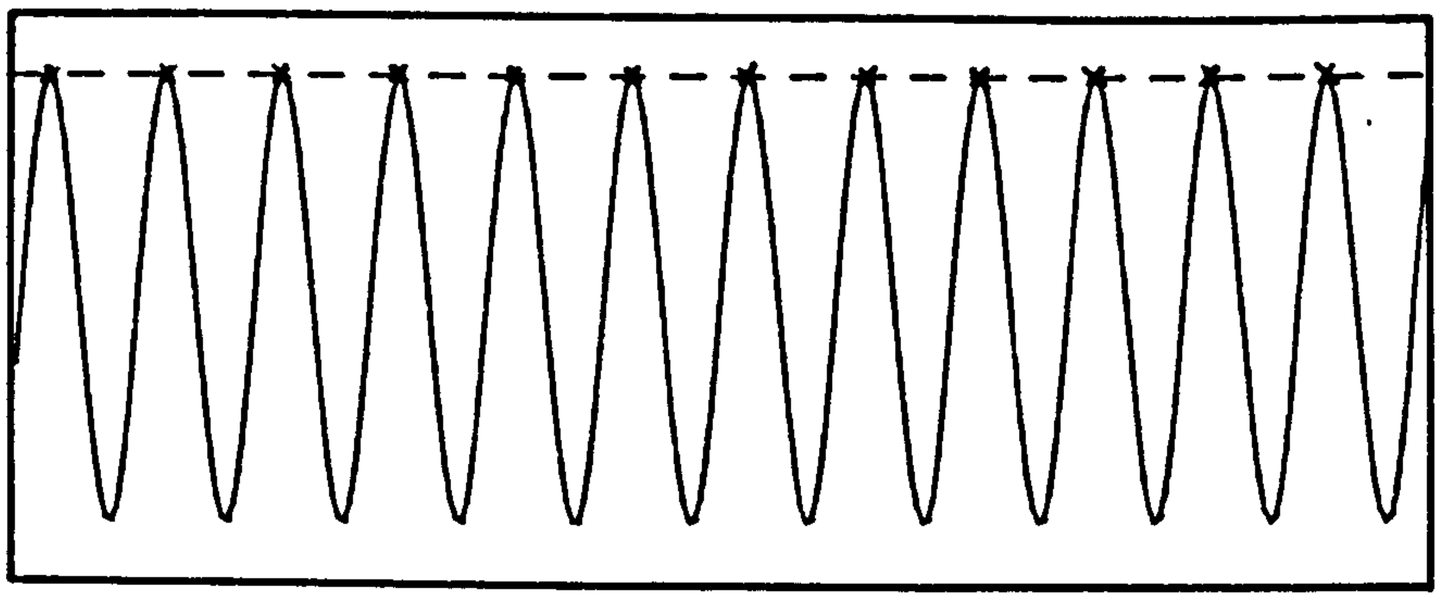

COMPONENT AT SAMPLING FREQUENCY fs INTERPRETED AS D.C.

[C]

f=(1/N) fs

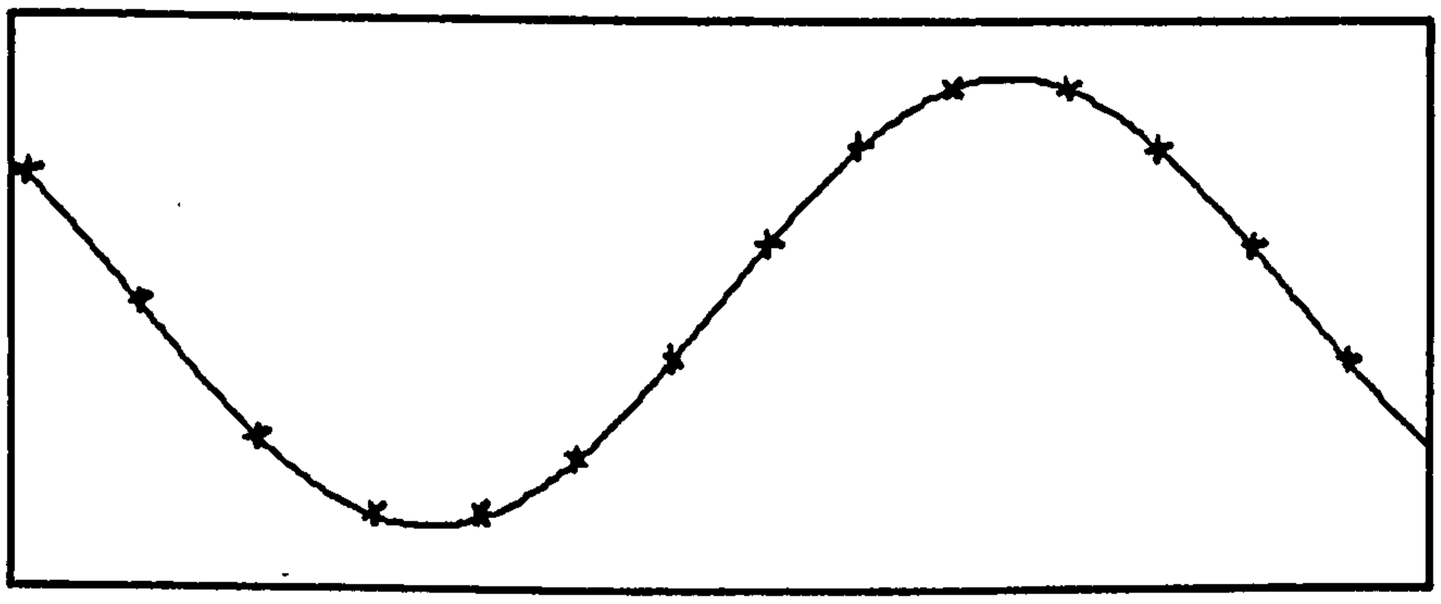

FREQUENCY COMPONENT AT (1/N) fs

[D]

f=((N+1/N)) fs

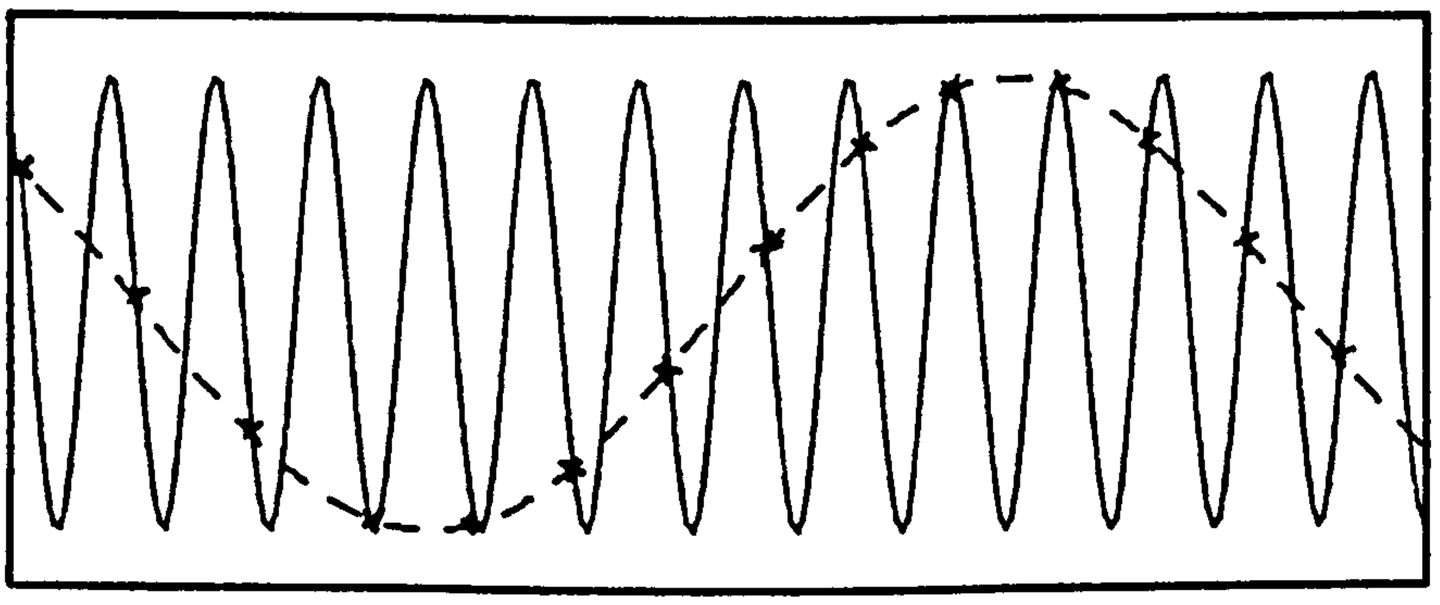

FREQUENCY COMPONENT AT ((N+1/N)) fs INTERPRETED AS (1/N) fs

AN ILLUSTRATION OF ALIASING

FIGURE 6.1

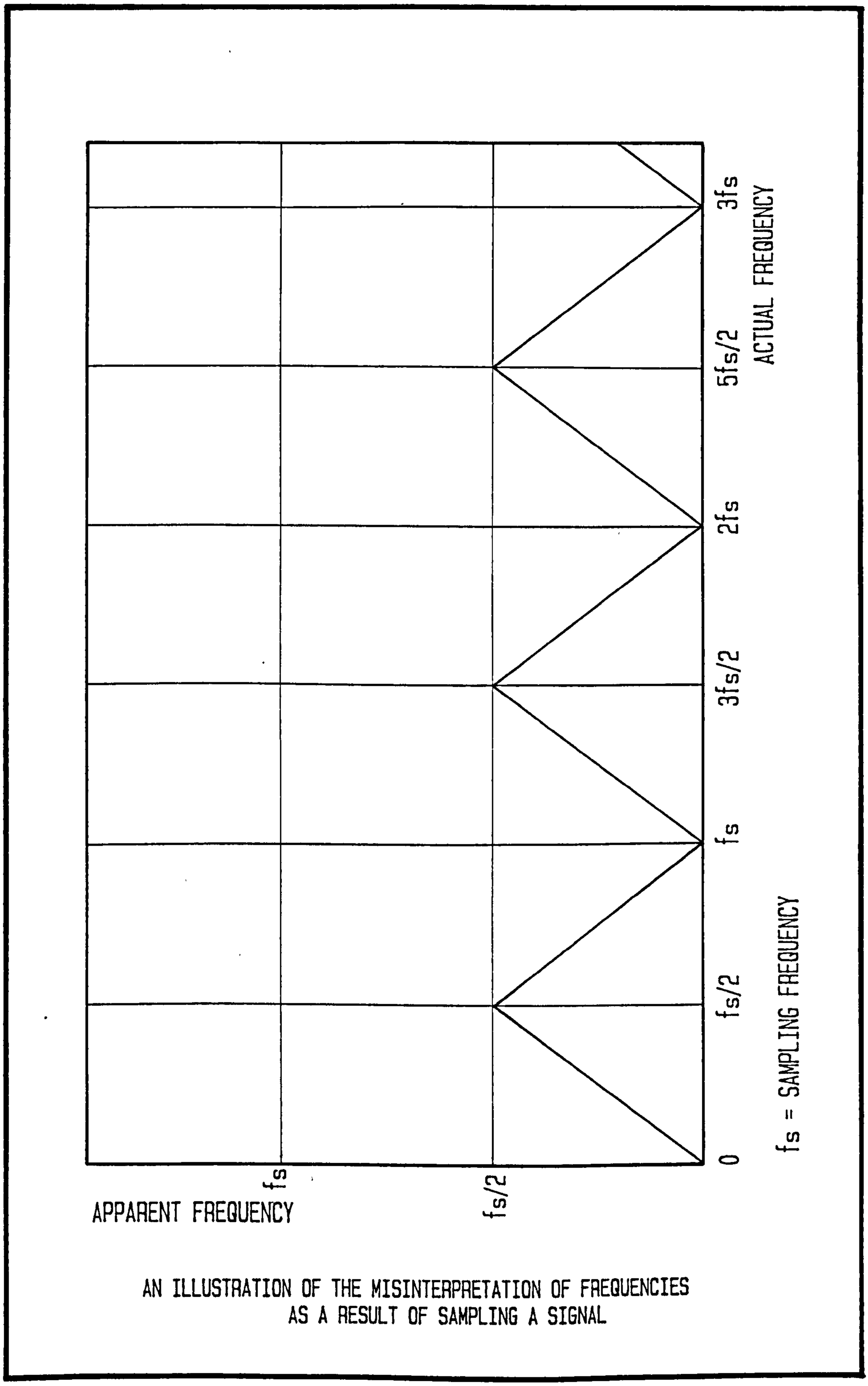

AN ILLUSTRATION OF THE MISINTERPRETATION OF FREQUENCIES
AS A RESULT OF SAMPLING A SIGNAL

FIGURE 6.2

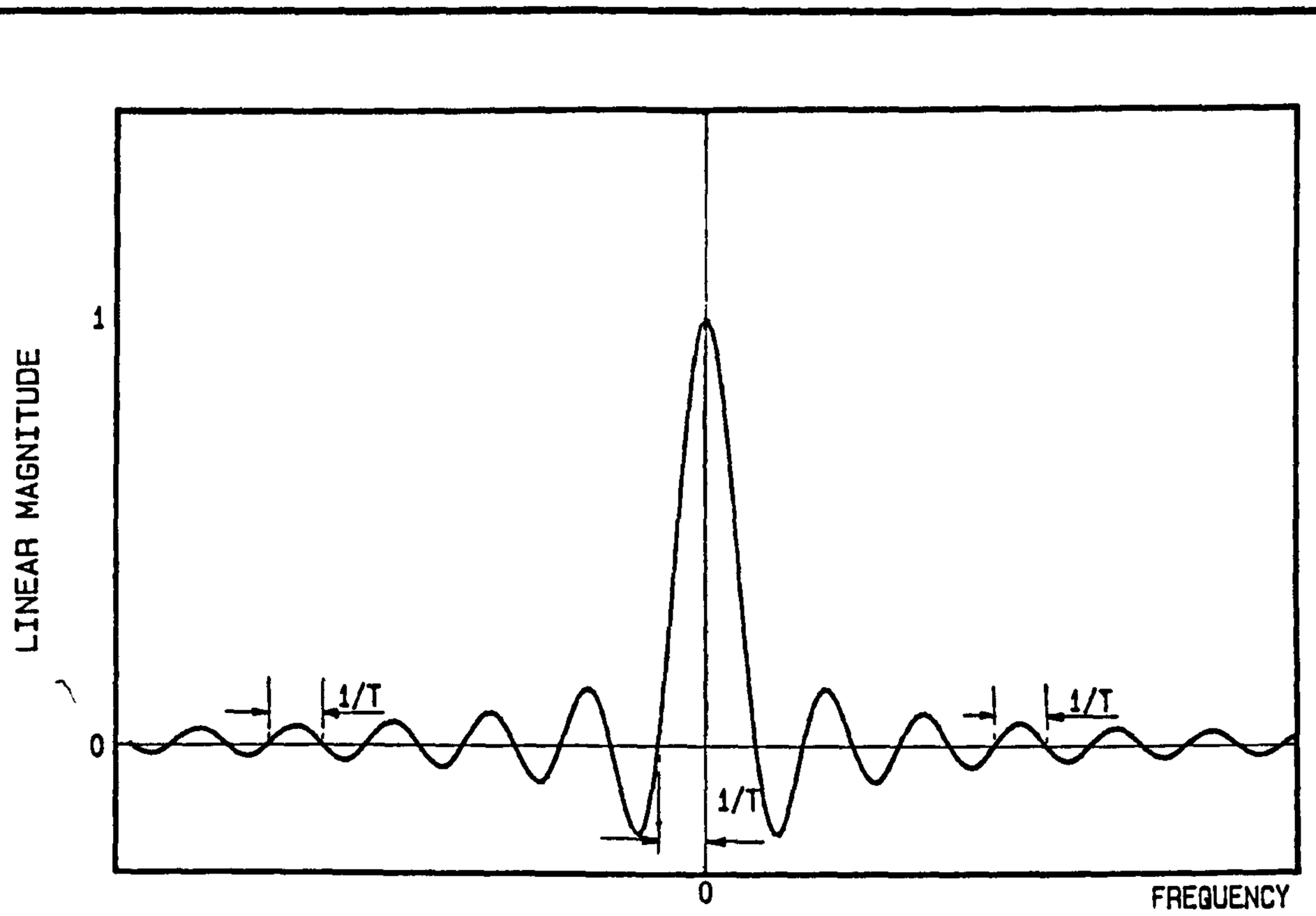

THE EFFECTIVE FILTER CHARACTERISTICS (MAGNITUDE) OF A RECTANGULAR WINDOW OF LENGTH T

FIGURE 6.3

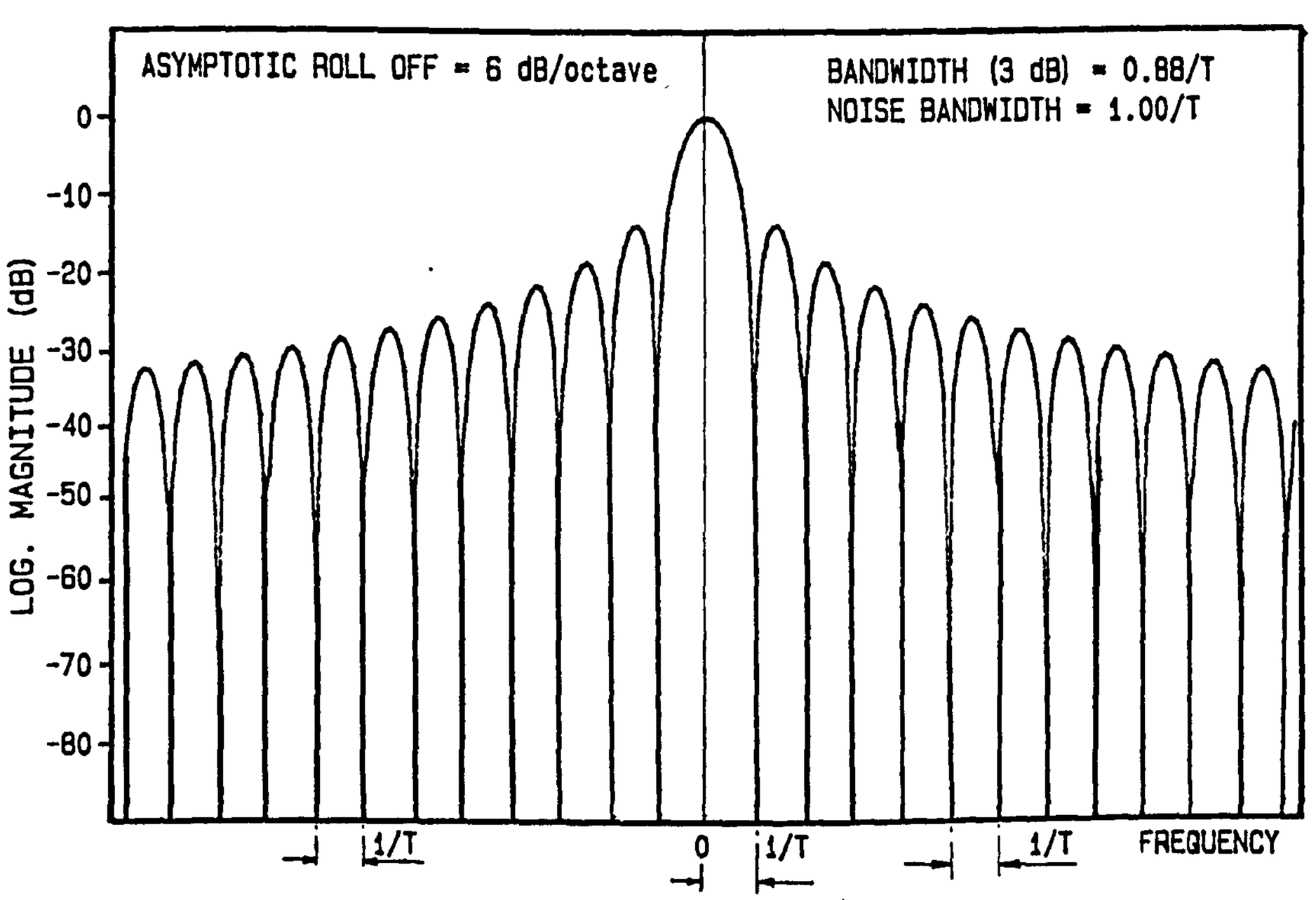

THE EFFECTIVE FILTER CHARACTERISTICS (POWER TRANS.) OF A RECTANGULAR WINDOW OF LENGTH T

FIGURE 6.4

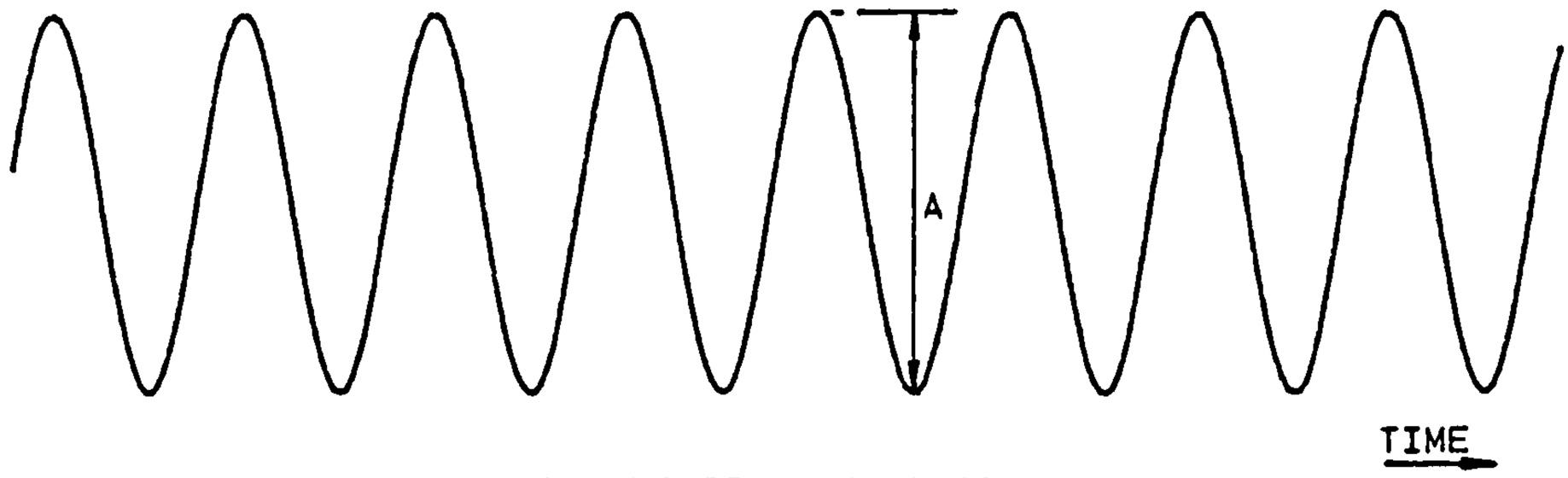

[A]

CONTINUOUS SINUSOIDAL FUNCTION

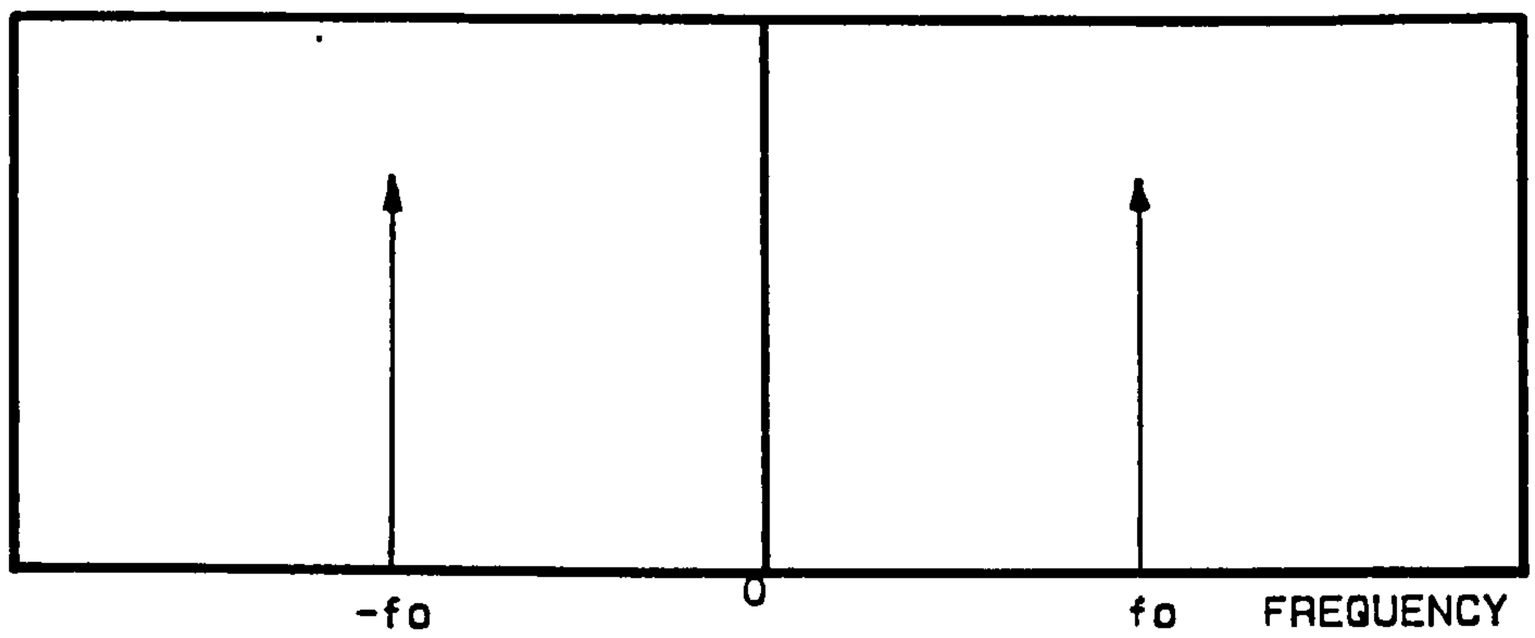

[B]

POWER SPECTRUM

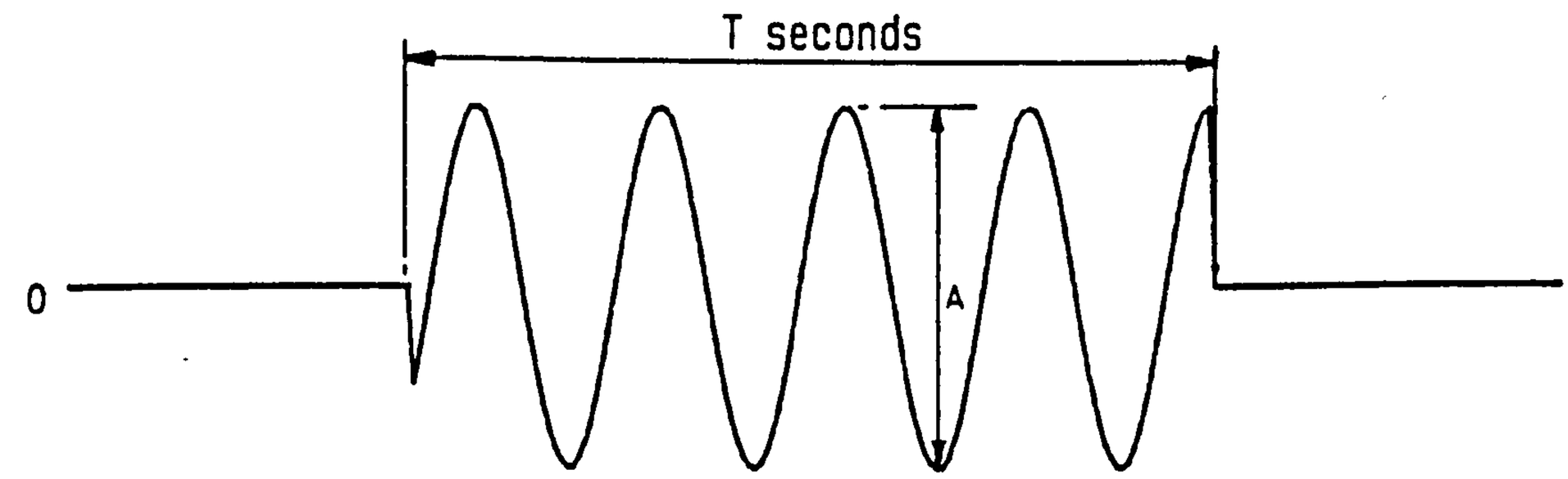

[C]

SINUSOIDAL FUNCTION WITH RECTANGULAR WEIGHTING

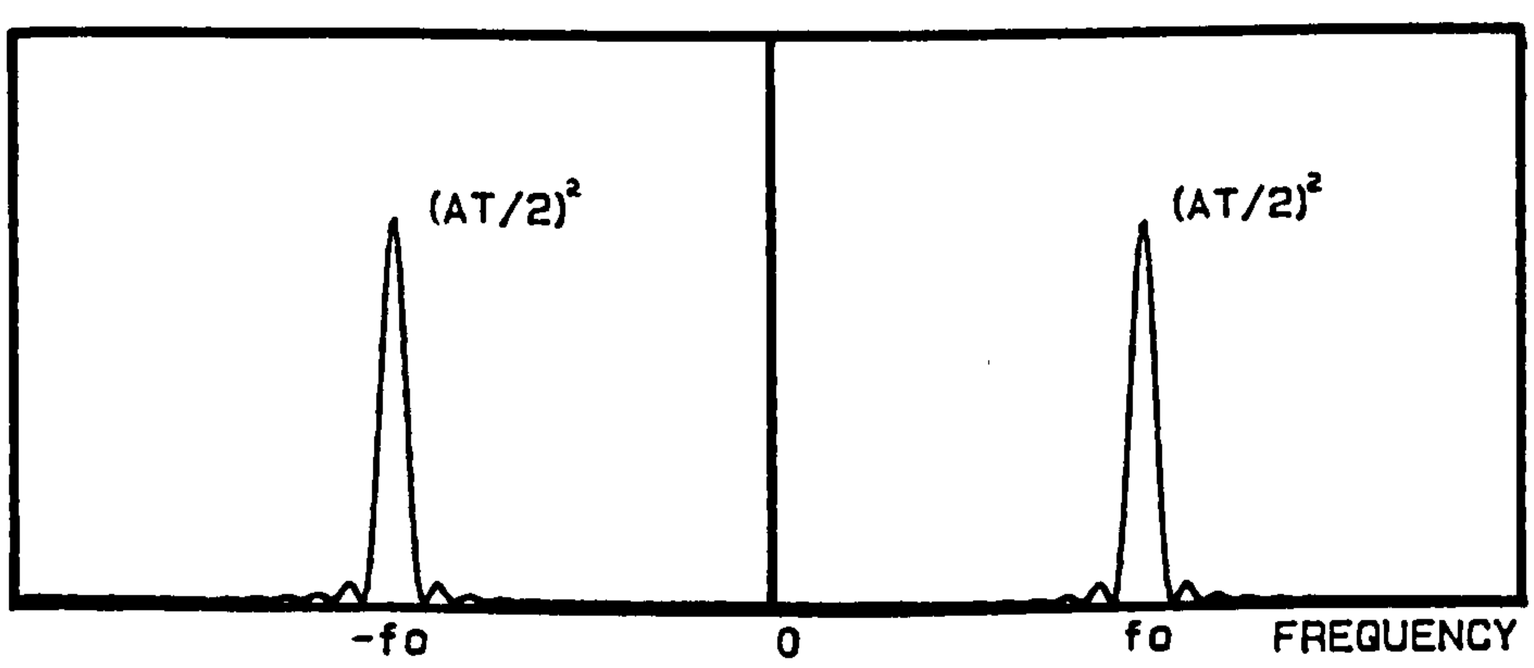

[D]

POWER SPECTRUM

THE EFFECT OF RESTRICTING A SINUSOIDAL SIGNAL TO A LENGTH T

FIGURE 6.5

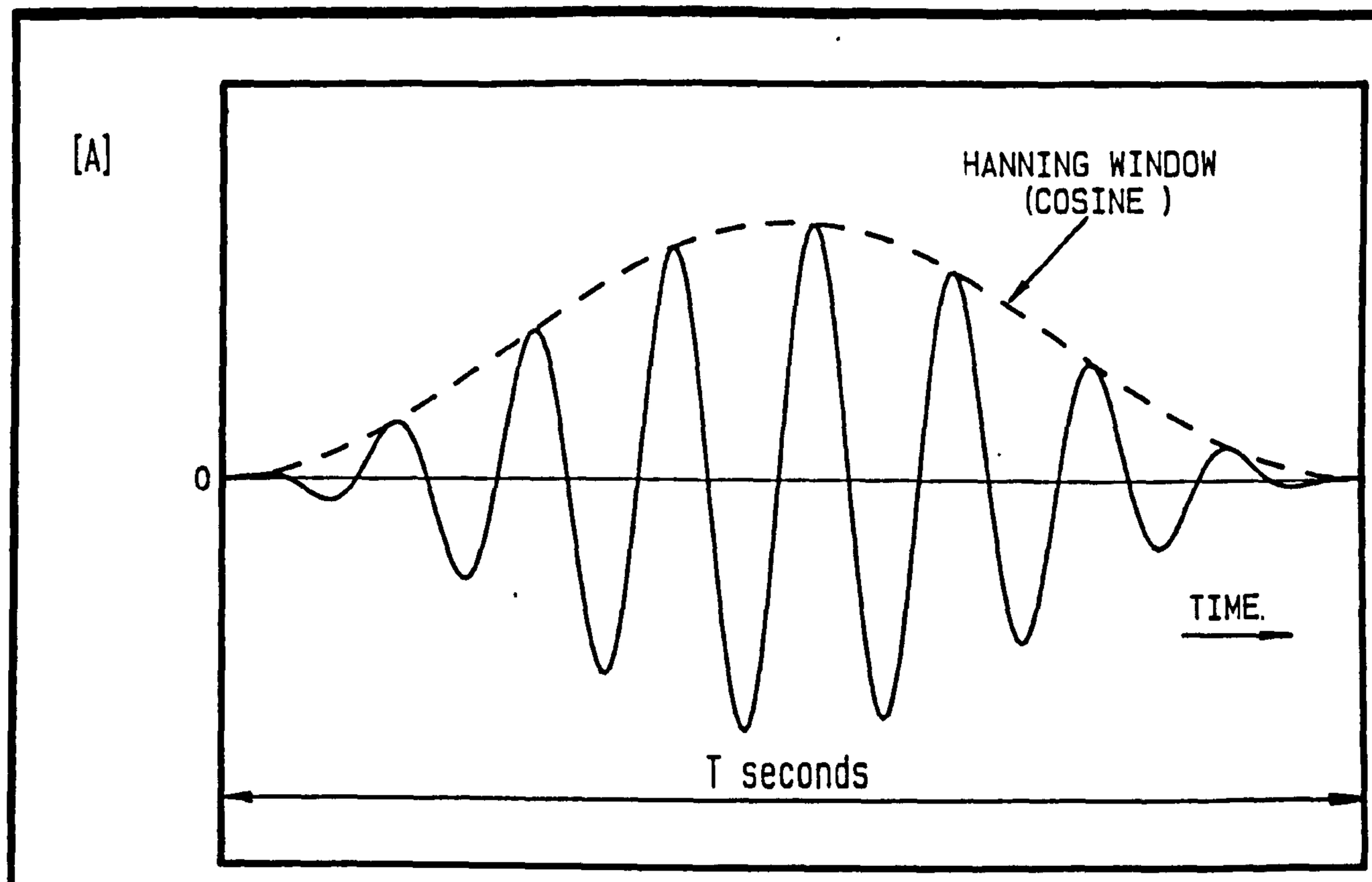

A CONTINUOUS SINUSOIDAL SIGNAL MULTIPLIED BY A HANNING WINDOW

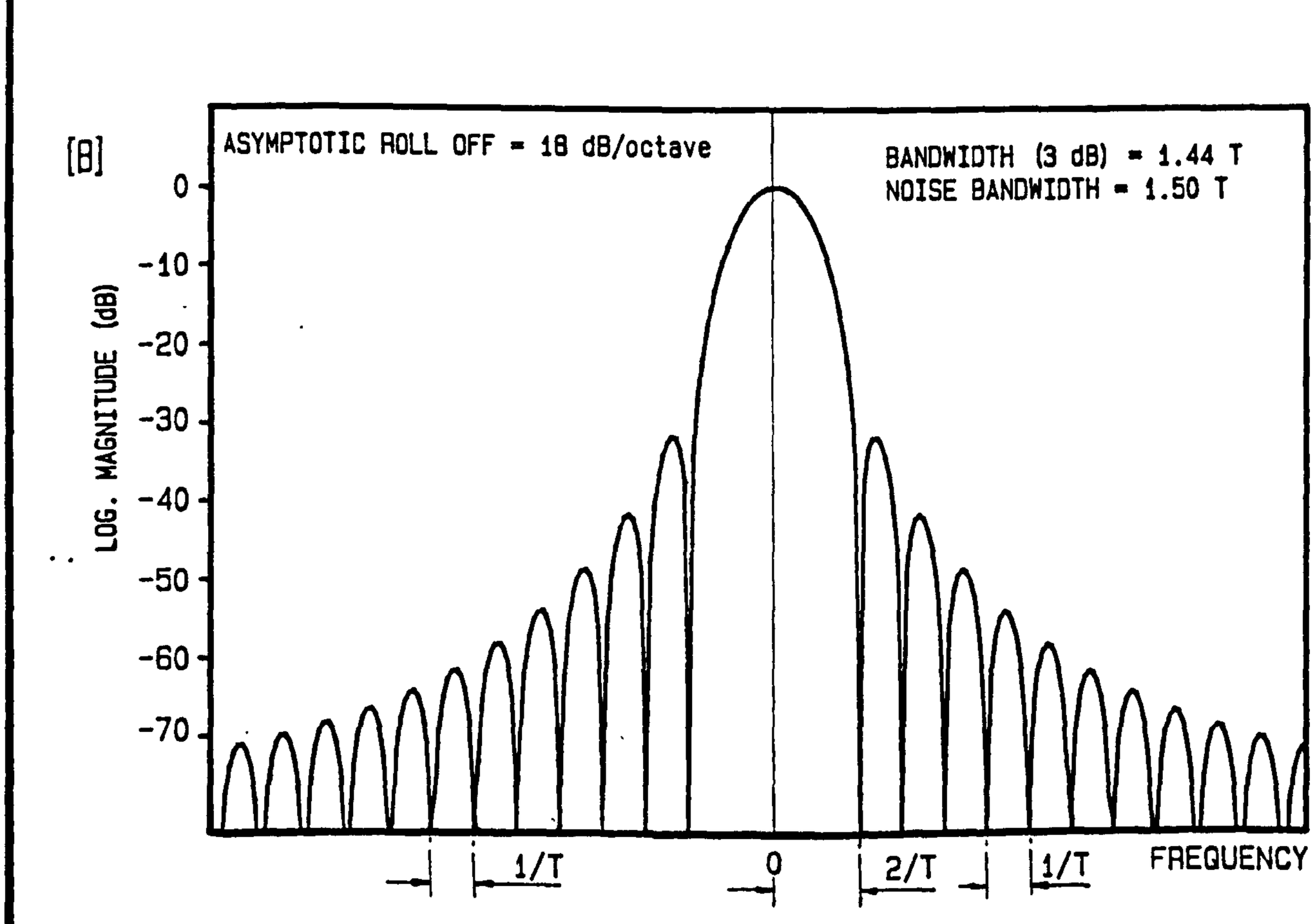

THE EFFECTIVE FILTER CHARACTERISTICS FOR A HANNING WINDOW OF LENGTH T

THE CHARACTERISTICS OF THE HANNING WINDOW

FIGURE 6.6

[A] WITHOUT NOISE

$$\left|\sum_{i} F_{XYi}\right| = \sum_{i} \left|F_{XYi}\right|$$

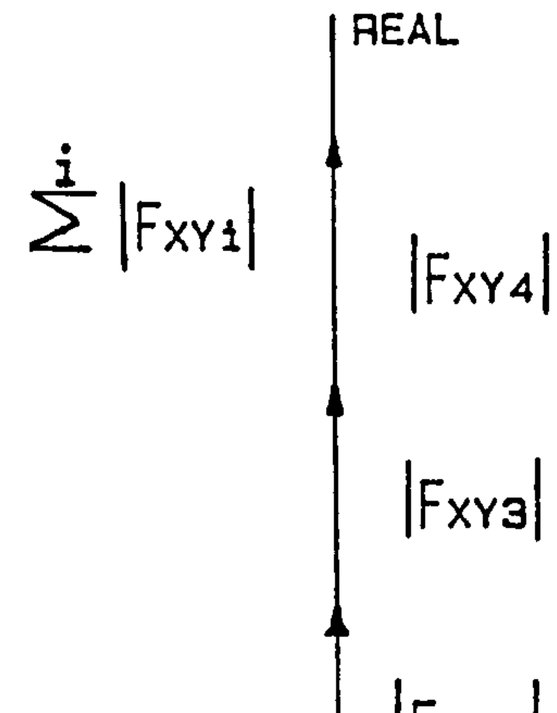

THEREFORE COHERENCE = 1.0

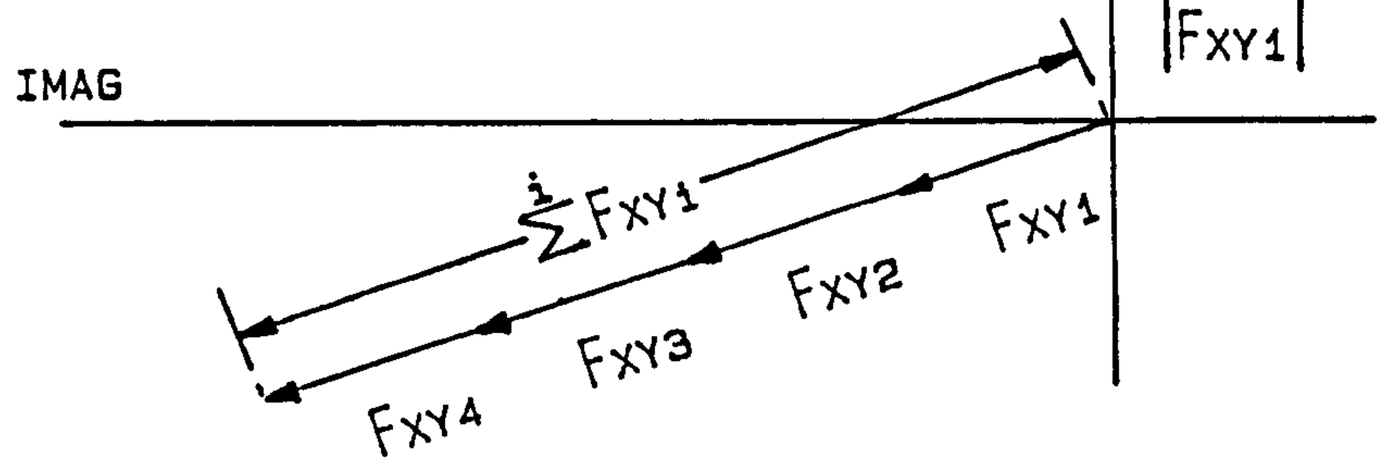

[B] WITH NOISE

$$\left|\sum_{i} F_{XYi}\right| < \sum_{i} \left|F_{XYi}\right|$$

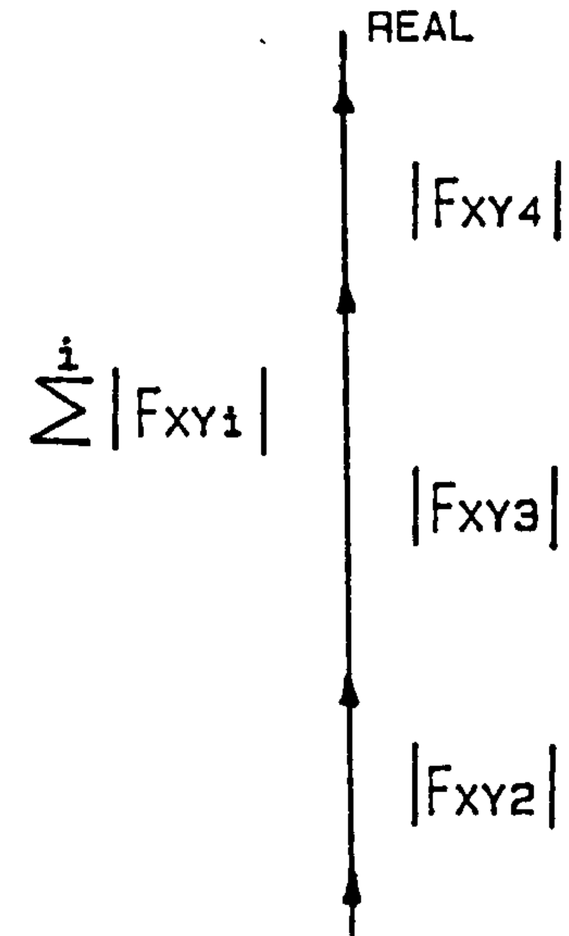

THEREFORE COHERENCE < 1.0

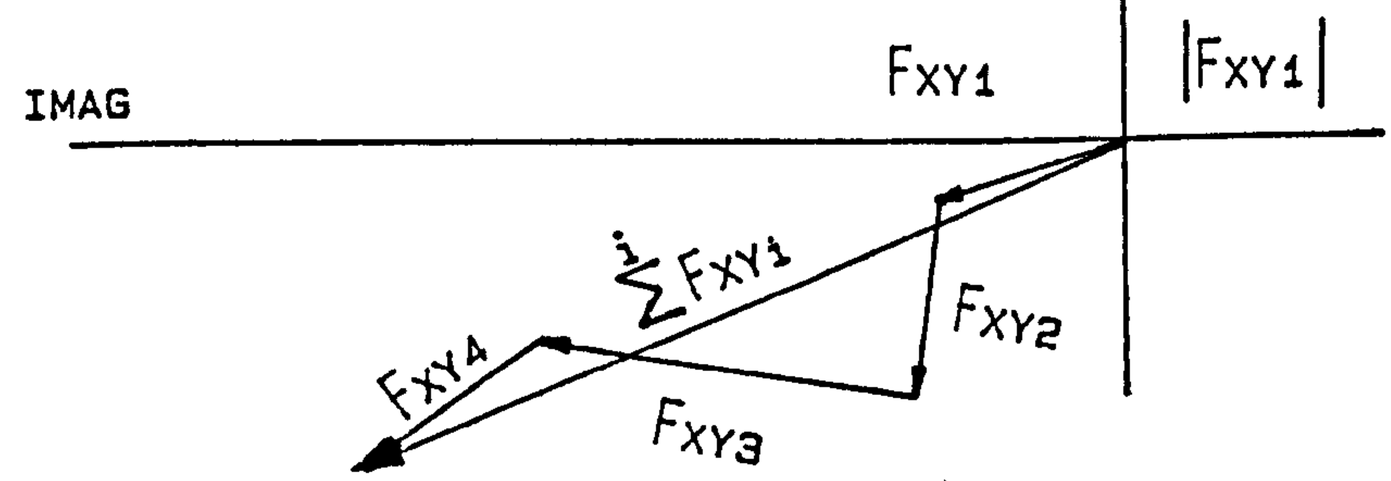

EFFECT OF NOISE ON MODULUS OF AVERAGED CROSS SPECTRUM

FIGURE 6.7

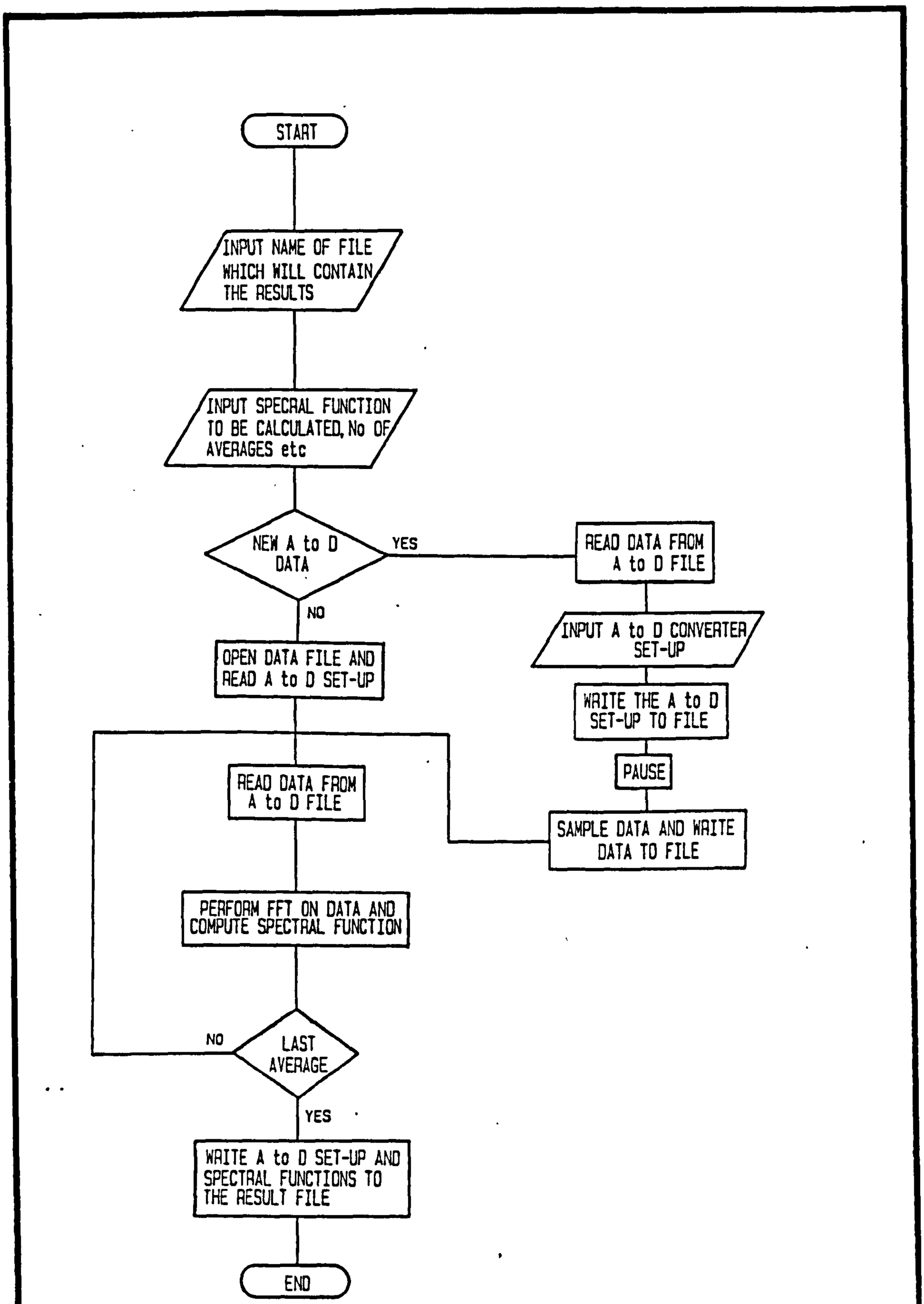

FLOW DIAGRAM FOR THE DATA ACQUISITION AND ANALYSIS PROGRAM

FIGURE 6.8

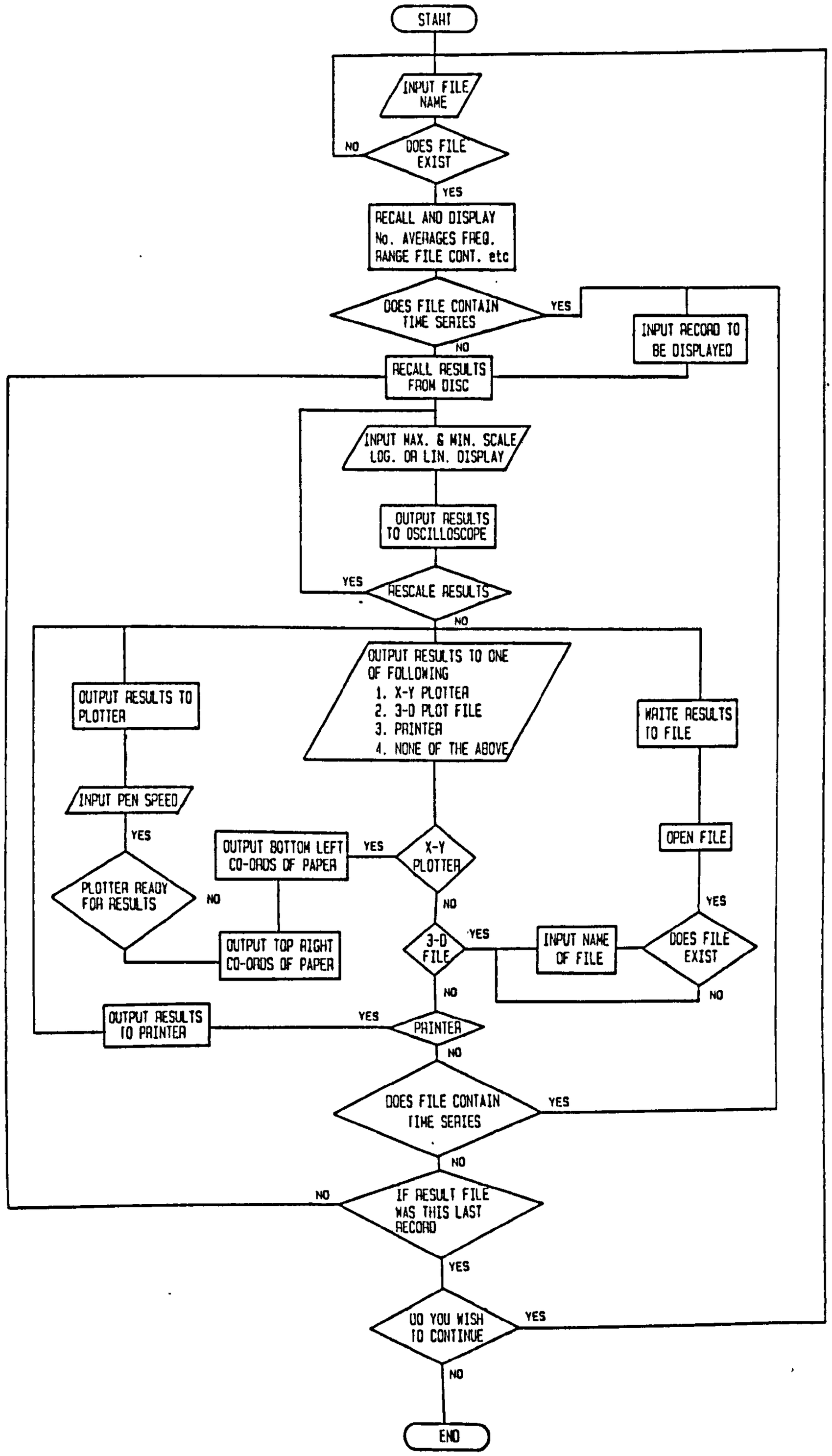

FLOW DIAGRAM FOR THE DISPLAY PROGRAM

FIGURE 6.9

7.0 RESULTS

7.1 INTRODUCTION

The first section of results describes the tests which were conducted during the commissioning of the rig. These results reveal the basic characteristics of the wind tunnel. This is followed by a section on the results from the investigation into the influence of row depth and geometry on the resonance characteristics.

The resonance is characterised by an Acoustic Strouhal Number based on the frequency of the acoustic resonance, the tube diameter and the velocity at onset of the resonance. This velocity is referred to the point of minimum cross sectional area between the tubes. The Acoustic Strouhal Number may be written as:

$$S_A = \frac{f \quad d}{U_m}$$

Although there would be some merit in the use of a Reduced Velocity to describe the resonance, the Strouhal number presentation was chosen to maintain consistency with other work and, aid in its comparison.

The third section of results lists some general observations made during the previous tests, together with the measured mode shapes of the resonance. The final section contains the results obtained by measuring and varying the acoustic damping.

The sound pressure level in the bank was monitored /

monitored using the arrangement illustrated in figure 5.4. For each bank tested the power spectrum was computed over the velocity range attainable in the tunnel. In most of the cases investigated the amplitude of the acoustic resonance rose sharply from the background noise, as illustrated in figure 7.1 (a). In such a situation the velocity at which this resonance occurs is easily identified. In some tube banks however the resonance grew less sharply, as illustrated by figure 7.1 (b). This S.P.L./velocity characteristic makes the Acoustic Strouhal number difficult to evaluate accurately. For this reason a sound pressure level was chosen to define the velocity for calculating the Acoustic Strouhal Number. A S.P.L. of 120 dB was chosen for this purpose because at this level the resonance became audible to the operator.

7.2 TUNNEL CHARACTERISTICS

The wind tunnel was initially tested when the test section was empty. The power spectrum was then recorded for various velocities and the results are illustrated in figure 7.2. This diagram is in the form of a three dimensional plot of S.P.L./frequency/velocity. This diagram reveals two sharp peaks in the spectra at frequencies of 452 Hz and 906Hz. These peaks seem quite large at low velocities but disappear at higher velocities when the background noise /

noise increases. These peaks can be identified as the 1st and 2nd harmonics of the fan blade passing frequency which is:

Fan Speed	=	3390 r.p.m.
	=	56.5 r.p.s
No. of blades on fan	=	8
Blade passing frequency	=	8 x 56.5
	=	452 Hz

This diagram also shows a high S.P.L. at low frequencies. This is due to flow instability and turbulence which is generated in the inlet region of the tunnel. Nevertheless this is of such a low frequency that it will not cause concern in this investigation.

The turbulence intensity in the section upstream of the test section was measured using the apparatus illustrated in figure 5.7. These measurements were made when the test section was empty and then repeated when the test section contained a 12 row bank (X_T = 2.0, X_L = 1.67). The results obtained are illustrated in figure 7.3. This shows a graph of turbulent intensity (t) against approach velocity (U) for both arrangements. The turbulent intensity can be seen to be around 11% (in both cases) when the velocity is low. This level falls off as the velocity is increased and levels out to a value of around 4%. The high level of turbulent intensity /

intensity experienced at low velocities is probably due to the level of low frequency pressure fluctuations illustrated in the power spectra of figure 7.2.

7.3 THE EFFECT OF ROW DEPTH AND GEOMETRY ON THE ONSET OF ACOUSTIC RESONANCE

Each bank was individually tested using the instrumentation described in chapter 5, and the power spectrum was computed for various velocities throughout the range available. In each geometry the banks were built up progressively from 1 to 50 rows, and the Acoustic Strouhal number was derived for each case. These results are summerized in tabular form in Appendix 1.

7.3.1 BANK I $X_T = 2.0$ $X_L = 1.67$

The results for this geometry are shown in figure 7.4 in the form of a plot of Acoustic Strouhal number against bank depth. This shows that as row depth is increased the Acoustic Strouhal number of the main resonance (lower line) varies from a value of around 0.16 in shallow banks to a value of around 0.23 at a row depth of 12. Further increase in row depth can be seen to have little further effect on the Acoustic Strouhal number. This diagram shows a second line, corresponding to an Acoustic Strouhal number of approximately 0.4.This describes a resonance which was experienced /

experienced in a few of the row depths investigated. This diagram also shows that an acoustic resonance was excited when only one row of tubes was present. With the one row bank, the S.P.L. rose slowly as the velocity was increased, reaching 120dB at a velocity of 17m/s. The resonance was stable in amplitude and further increase in velocity, up to a maximum velocity (u) of 23 m/s, resulted in a higher S.P.L. being produced. When the row depth was increased to two rows however, it was found that the first and second harmonics were supressed. Figure 7.5 shows a three dimensional plot of S.P.L. / frequency / velocity for this bank. As can be seen the third harmonic is excited at an approach velocity of approx. 12.5 m/s. Further increase in velocity causes this peak to disappear and no other acoustic resonance is excited. The results obtained with three rows of tubes present are similar to that for the one row bank. This time however the S.P.L. rose more sharply with increasing velocity. In the five row bank, it was observed that as the velocity was increased the third harmonic was the first resonance to be excited. This occurred at an approach velocity of 16.8 m/s. However further increase in velocity led to this resonance disappearing and the first mode being excited. The excitation of the first mode occurred at an approach velocity of 17.2 m/s: Increasing the velocity further led to the S.P.L. of the first mode becoming larger.

In /

In the 12 row configuration a similar result to that of the 5 row bank was obtained. In this bank however it was the second harmonic which was excited prior to the onset of the first. In the case of the 28 row bank the first mode was excited twice, once at a velocity of 5.8 m/s and again at a velocity of 11.4 m/s. A three dimensional plot of S.P.L. / frequency / velocity for this bank is shown in figure 7.6. As can be seen the first mode is excited at a velocity of 5.8 m/s. This peak is relatively small (i.e. 124 dB) and disappears as the velocity is increased. When the velocity reached 11.4 m/s this mode was found to be excited again, in this case however, further increase in velocity resulted in an increase in the S.P.L. This diagram also shows a broad peak in the power spectra which increases in frequency as the velocity is increased. This velocity dependent peak has all the characteristics of vortex shedding, and can be seen to be well removed from the acoustic frequency when the resonance is excited. The excitation of the first mode at around half the velocity of the main resonance was only experienced in the 28 row bank. An increase in S.P.L., for the first mode, was however experienced at this velocity in several other deep banks in this configuration. This is demonstrated in the 43 row bank which exhibited a similar peak, however the maximum S.P.L. in this case was 102 dB. It was only in the 28 row /

row bank that this peak became audible. Figure 7.7. shows a three dimensional plot for the 49 row bank. Again this plot shows the vortex shedding and acoustic frequencies to be unrelated. The vortex peak produced in this bank is however, far more pronounced than before.

7.3.2 BANK II $X_T = 2.0$ $X_L = 2.0$

The results of the investigation into the effect of row depth for this geometry are shown in figure 7.8. This is a graph of Acoustic Strouhal number against row depth. With this geometry the first mode was the only mode excited. Figure 7.8 shows the Acoustic Strouhal number to vary slightly in shallow banks, and settle down to a constant value, of approximately 0.21, as the bank becomes deeper.

The three dimensional diagrams in figures 7.9, 7.10 and 7.11 show the S.P.L. / frequency / velocity plots for the 2, 10 and 24 row banks respectively. These plots all show a very sharp peak corresponding to the acoustic resonance (practically a pure tone). In figures 7.10 and 7.11 the vortex shedding peaks are also evident and can be seen to bear no simple relationship to the acoustic frequency. These diagrams also show the vortex shedding peak to become far more pronounced as the row depth is increased.

7.3.3./

7.3.3. BANK III X_T = 2.0, X_L = 2.34

The results for this configuration are shown in figure 7.12 in the form of a plot of Acoustic Strouhal number against row depth. This diagram also shows the Acoustic Strouhal number to vary slightly in shallow banks, and level out to a constant value as the bank becomes deeper. In some of the banks (N = 2 and 5) the amplitude of the acoustic resonance, at onset, was found to be unstable. That is, the amplitude of the resonance would remain constant for some time then reduce considerably. The amplitude would remain at this reduced value for a time before returning again to the previous level. Further increase in velocity tended to stabilise the amplitude.

Figure 7.13 is a three dimensional plot of S.P.L. / frequency / velocity for the 42 row bank. Once again this plot shows the vortex shedding frequency to be well removed from the acoustic frequency at the onset of the resonance.

In the following series of banks several modes were excited with frequencies which were close to the same transverse mode. For reasons that will be explained later in this chapter these modes were associated with the transverse mode which they lie closest to.

7.3.4. BANK IV X_T= 1.34, X_L = 1.34

Figure /

Figure 7.14 illustrates the Acoustic Strouhal number /row depth relationship for this configuration. As can be seen from this graph the Acoustic Strouhal number for this configuration remains around 0.4 for all the banks tested. This configuration was found to resonate with only 1 row of tubes, and an approach velocity of 10 m/s. This resonance was stable in amplitude and further increase in velocity caused this mode to disappear and the 2nd harmonic to be exicted. The second harmonic was excited at an approach velocity of 19 m/s. When two rows of tubes were placed in the bank the 1st, 2nd and 3rd harmonics of vibration were suppressed and the 4th and 5th harmonics were the only modes excited. The Acoustic Strouhal number remained around 0.4 for all the banks tested except the 5 row bank which produced additional responses around 0.635. These resonances had frequencies of 300 Hz and 1580 Hz and were excited at an approach velocity of 10 and 12 m/s respectively. It should be noted from this diagram that as the row depth is increased the minimum mode number tends to decrease.

Figure 7.15 → 7.17 illustrate three dimensional plots of S.P.L. / frequency / velocity for the 25, 30 and 42 row banks in this geometry. In all the row depths (except N = 5) in this geometry, the resonances were excited in a regular sequence. The hot wire anemometer was again used in this geometry to establish the vortex shedding /

shedding frequency. As with the three dimensional S.P.L. plots there was no evidence of vortex shedding in the hot wire spectra.

7.3.5. BANK V X_T = 1.34, X_L = 1.67

Figure 7.18 illustrates the Acoustic Strouhal number / row depth relationships for this bank. When two rows of tubes were placed in the test section the 1st, 2nd and 9th harmonics were excited. As the velocity through this bank was increased it led to the excitation of the first mode. Increasing the velocity led to this mode disappearing and the 9th harmonic being excited. Further increase in velocity led to the 9th harmonic disappearing and the 2nd harmonic taking its place. In the case of the five row bank however the only mode of vibration excited was that corresponding to the 9th harmonic. Increasing the row depth to 10 rows resulted in no resonance being excited. There was however a small peak corresponding to the 3rd harmonic. Although it did not become audible it was clearly identifiable in the spectrum.

The behaviour of these banks could be explored no further, because of the high velocities associated with the modes of vibration involved. Several banks were however tested in this geometry and as can be seen from figure 7.18 the 15, 19 , 25, 30 and 35 row banks produced/

produced no resonance. Figure 7.19 shows the three dimensional plot for the 25 row bank. This is typical of the results obtained from this range of geometry. When the bank depth was increased to 40 rows however the second mode was excited. This occurred at an approach velocity of 8.4 m/s and is illustrated by the three dimensional plot in figure 7.20.

Similarily in this configuration the hot wire anemometer was used to detect vortex shedding. The results of this investigation were similar to those of the previous bank in that no vortex shedding was detected by this method of measurement.

7.3.6 BANK VI X_T = 1.34 X_L = 2.0

Figure 7.21 illustrates the Acoustic Strouhal number/row depth relationship for this geometry. In the two row bank three modes were excited with frequencies at 290Hz, 318Hz, and 350Hz. This occurred at approach velocities of 9.6 m/s, 13.5 m/s and 13.4 m/s respectively. These modes all have a frequency which is close to that of the first harmonic. When the row depth was increased to three rows the first three modes were excited at a similar Acoustic Strouhal number as before. Further increase in velocity resulted in the excitation of the 8th and 9th harmonics at around twice the velocity of the first mode. Increasing the row depth to 4 rows resulted in only one of the first modes being /

being excited. Increasing the velocity led to this mode disappearing and two frequencies corresponding to the 7th harmonic being excited. Further increase in velocity caused these modes to fall off just prior to the onset of the 2nd harmonic. When the row depth was increased to 10 and 15 rows no acoustic resonance was observed. This is illustrated in figure 7.22 in the form of a S.P.L. / frequency / velocity plot for the 15 row bank. When the bank depth was increased to 20 row two distinct resonances were excited both of which were close to the third harmonic of acoustic vibration. In this situation the lower of the frequencies was excited first closely followed by the excitation of the higher frequency. This result is illustrated by the three dimensional plot in figure 7.23. In the case, of all the other bank depths investigated the modes were excited in a regular sequence (ie 570Hz then 610Hz then 680Hz etc). Some of the results for the other banks tested in this geometry are shown in figures 7.24 → 7.27. These are all three dimensional plots of S.P.L. / frequency / velocity for the 25, 30, 35 and 40 row banks respectively. In this configuration neither the hot wire anemometer or microphone detected vortex shedding. The three dimensional plots shown in this chapter do not always have the z-axis at the same angle. Also in some of these plots the full velocity range is not shown.

7.4 GENERAL OBSERVATIONS

In banks I, II and III it was found, that the magnitude of the main resonance increased continually with velocity up to the maximum velocity attainable in the rig, which was roughly 20 m/s. This respresented an increase of up to 90% of the onset velocity. It would be expected (following the theories presented previously) that such velocities would have caused the first mode to diminish prior to the onset of the second harmonic. The maximum S.P.L. produced by these banks is not known because the microphone output became severly distorted due to the S.P.L. being greater than the microphones dynamic range. Hence it can only be said that the S.P.L. was greater than 160 dB. A second effect was noticed when the velocity was increased beyond the onset point of the main resonance. The frequency of the resonance was seen to increase as the velcoity was increased. This increase in frequency was small but detectable. Two typical examples, for different banks, are shown below.

28 Row X_T = 2.0, X_L = 1.67 U = 12.2 - 16.9 ms^{-1}, f = 265 - 275 Hz

42 Row = X_T = 2.0, X_L = 2.34 U = 12.8 - 14.5 ms^{-1}, f = 250 - 260 Hz

This increase in frequency was detected while the microphone was still within its normal operating range.

It /

It was observed that the frequency of the resonance varied from 295Hz to 248 Hz as the bank depth was varied between 1 and 49 rows. The mode shape of the resonance was therefore measured in several banks to determine if these changes were due solely to changes in the acoustic system, or if different modes were being excited. This was carried out for three different bank depths with a geometry of X_T = 2.0, X_L = 1.67 and the results are illustrated in figures 7.28 - 7.30. The measurements illustrated in figures 7.28 and 7.29 were carried out when the resonance had been excited and the magnitude and phase were measured by two B & K microphones and a B & K phase meter. Each of these diagrams show the tunnel layout with the position of the tube bank and flow direction indicated. The measured magnitude and phase of the acoustic mode is illustrated directly below and this shows the mode of acoustic vibration to be in phase across the length of the bank. Hence the excited mode is a pure transverse mode and has no longitudinal nodes. These diagrams also show the amplitude of the mode to decrease exponentially outside the tube bank. This implies that there is no transmission of acoustic energy along the duct, which is consistant with the work of ref. P1. In figure 7.30 the results were obtained just prior to the onset of resonance. In this occasion the signals from the microphones were fed to the PDP-11 computer where the cross spectrum was calculated. Figure 7.30 shows that three modes were detected with the same transverse mode shape but having different longitudinal mode /

mode shapes, and the mode which was excited was mode number 1. This result is consistant with that observed previously in that the first transverse mode (ie a mode with no longitudinal nodes) was excited. Hence this indicates that the change in frequency observed in these banks was caused solely by changes in the acoustic system, brought about by the increase in bank depth, which in turn increased the area with a lower speed of sound.

In banks IV, V and VI it was found that several modes were excited with frequencies which lay close to that of the same harmonic. It was not possible to conduct a full microphone traverse of the wind tunnel in these geometries because of the close proximity of the tubes. It was however felt reasonable to assume that these frequencies, corresponded to modes of the same transverse mode, but with different longitudinal mode shapes. Hence the frequencies of response were associated with the transverse mode which they lay closest to.

Using the information obtained by the microphone and hot wire anemometer the Strouhal number for each bank was estimated. These results are shown below:-

GEOMETRY		STROUHAL NUMBER
X_T	X_L	
1.34	1.34	----
1.34	1.67	----
1.34	2.00	----
2.00	1.67	0.13
2.00	2.00	0.13
2.00	2.34	0.13

These values show good correlation with the Strouhal number map presented by ref. M4.

In some instances in banks IV, V and VI the time series of the resonance was seen to be modulated. However on inspection of the power spectrum of these signals several very sharp peaks were found to lie in close proximity to each other. Therefore it was the spectral interference between these peaks that caused the modulation of the time series.

7.5 DETERMINATION OF THE ROLE PLAYED BY DAMPING

The next stage of this work required the measurement of acoustic damping, under flow conditions. The results of this work are summerized in tabular form, in Appendix 2. This work will reveal the acoustic damping/velocity relationship, and therefore determine the validity of the feed-back type model. A bank of geometry $X_T = 2.0$, $X_L = 1.67$ and having 38 rows of tubes was placed in the test section. The unaltered lid was placed on the test section and the velocity for the onset of acoustic resonance was determined. This was found to occur at U = 10.62 m/s. The test section lid was then removed and replaced by the lid which had a 6 in square piston inset in it.The shaker, etc. was then connected to the piston as shown in figure 5.8. Once again the velocity required to initiate the acoustic resonance was determined. This time /

time it was found to be U = 10.75 m/s. This shows that the pistons presence has little effect on the acoustic system.

The random noise generator was then set to produce noise between 0 - 500 Hz, and the experiments were commenced. As can be seen from figure 5.8 the shaker is suspended such that the weight of the piston is carried by the shaker. This meant that the signal being fed to the shaker had to be limited in order to prevent the core striking its end stops. It was found with this configuration that the coherence dropped to an unacceptable level at velocities in excess of 17 m/s. The results obtained from this investigation are shown in figure 7.31.

The 38 row bank was replaced by an eighteen row bank of the same geometry. The results obtained from this bank are shown in figure 7.32. This diagram is a Q factor / velocity plot. As can be seen from this diagram the Q factor at no flow is higher than that for the 38 row bank. (Lower damping.) The initial results obtained were however similar to the previous bank in that as the velocity was increased the coherence still fell to an unacceptable level. This problem was overcome by using band limited random noise to give the maximum possible excitation level in the required frequency range. The filter pass band was set to 200-500Hz. This greatly improved the performance of the system /

system and allowed the damping to be measured at much higher velocities. Figure 7.32 shows that the measured Q-factor of the acoustic system increases sharply as the onset of resonance is approached. The 18 row bank was then replaced by an eight row bank of the same geometry. This bank depth was not tested in the original row depth investigation, however the Acoustic Strouhal number was calculated and recorded on figure 7.4. Figure 7.33 illustrates the Q factor /velocity relationship for this bank. However due to the high velocity associated with the resonance, the coherence was found to drop to an unacceptable level before the onset of the resonance. In this bank the second harmonic of acoustic vibration was excited prior to the first mode.

Figure 7.34 illustrates the Q factor / velocity relationship of the 43 row bank. The data from this bank however was not analysed in the usual manner. In this case the data was recorded on a SE 8/4 tape recorded and analysed at BABCOCK POWER RESEARCH CENTRE using a HP 5420 analyser. This analyser was capable of making higher resolution measurements than the PDP-11 computer. The results of the analysis can be seen to be similar to that obtained in the eighteen row bank. Figure 7.35 shows the Q factor / velocity relationship obtained for a 12 row bank of the same geometry. The points marked by circles of this graph are the results of/

of the invesitagation with minimal damping. In this case the data was analysed by the PDP-11 computer. These results can be seen to be of a similar nature to that of the 43 and 18 row banks. The test section lid was now replaced by an alternative lid as described in chapter 5.6. This new lid incorporated an eight inch square piston and a large number of half inch diameter holes. This is illustrated in chapter 5.6 by figure 5.10 (a). Originally the whole lid was covered by a thin polyestor sheeting, including the hole for the piston. The lid was then placed on the test section, which still contained the 12 row bank. Using the usual procedure the S.P.L./ frequency / velocity relationship was determined. The results of this experiment are shown in figure 7.36.

This shows that the acoustic resonance is suppressed, and no resonance became audible in the velocity range available. Figure 7.36 does reveal the exsistance of a peak (115dB in magnitude) corresponding to the first acoustic mode. This occurs at an approach velocity of 18 m/s. It was however impossible to make any damping measurements with this configuration as the piston was not fitted. The next step was to removed the polyestor sheeting, from the piston hole and fit the eight inch square piston. When the tunnel was retested with the piston in place the first mode of acoustic vibration was excited at virtually the same velocity /

velocity as it had been prior to this lid being fitted. The lid was therefore removed and altered to that illustrated by figure 5.10 (b) in chapter 5.6. This diagram shows the lid to contain some larger holes which, were situated directly above the twelve row bank. This lid was placed on the tunnel and the Q factor / velocity relationship was determined. The results of this investigation are also illustrated in figure 7.35. These points are identified by small squares on this diagram. With this modification the onset velocity for the acoustic resonance (Um) was found to be moved from 13.1m/s to a velocity of 14.9 m/s. This means the Acoustic Strouhal number is reduced from 0.207 to 0.187. A three dimensional plot of S.P.L. / frequency / velocity for this configuration is shown in figure 7.37. Some typical plots of Transfer function, Real part of Transfer Function, Phase and Coherence are shown in figures 7.38 - 7.42. These were taken at various velocities (velocity indicated on the diagrams) in the 12 row banks.

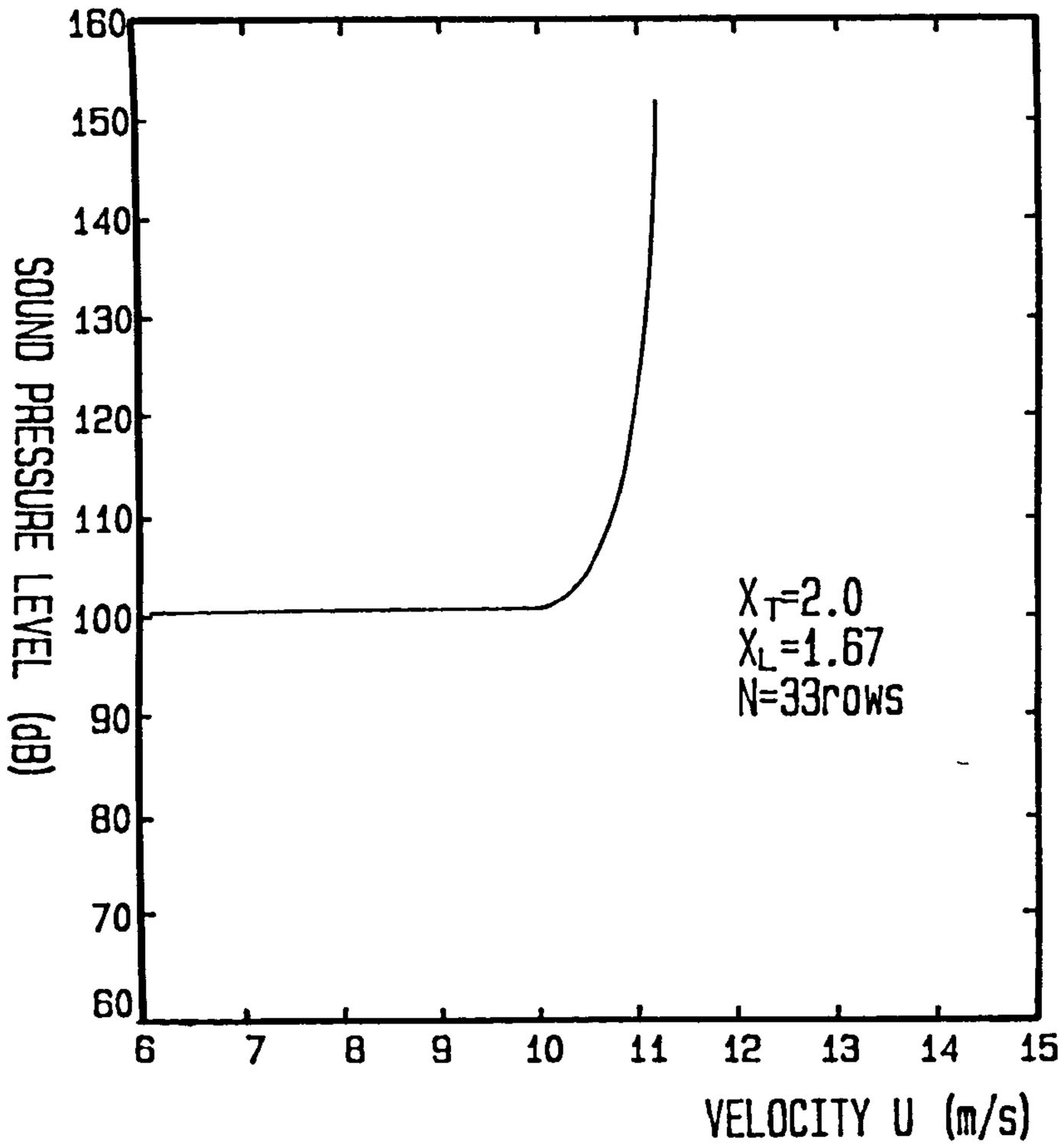

[a]

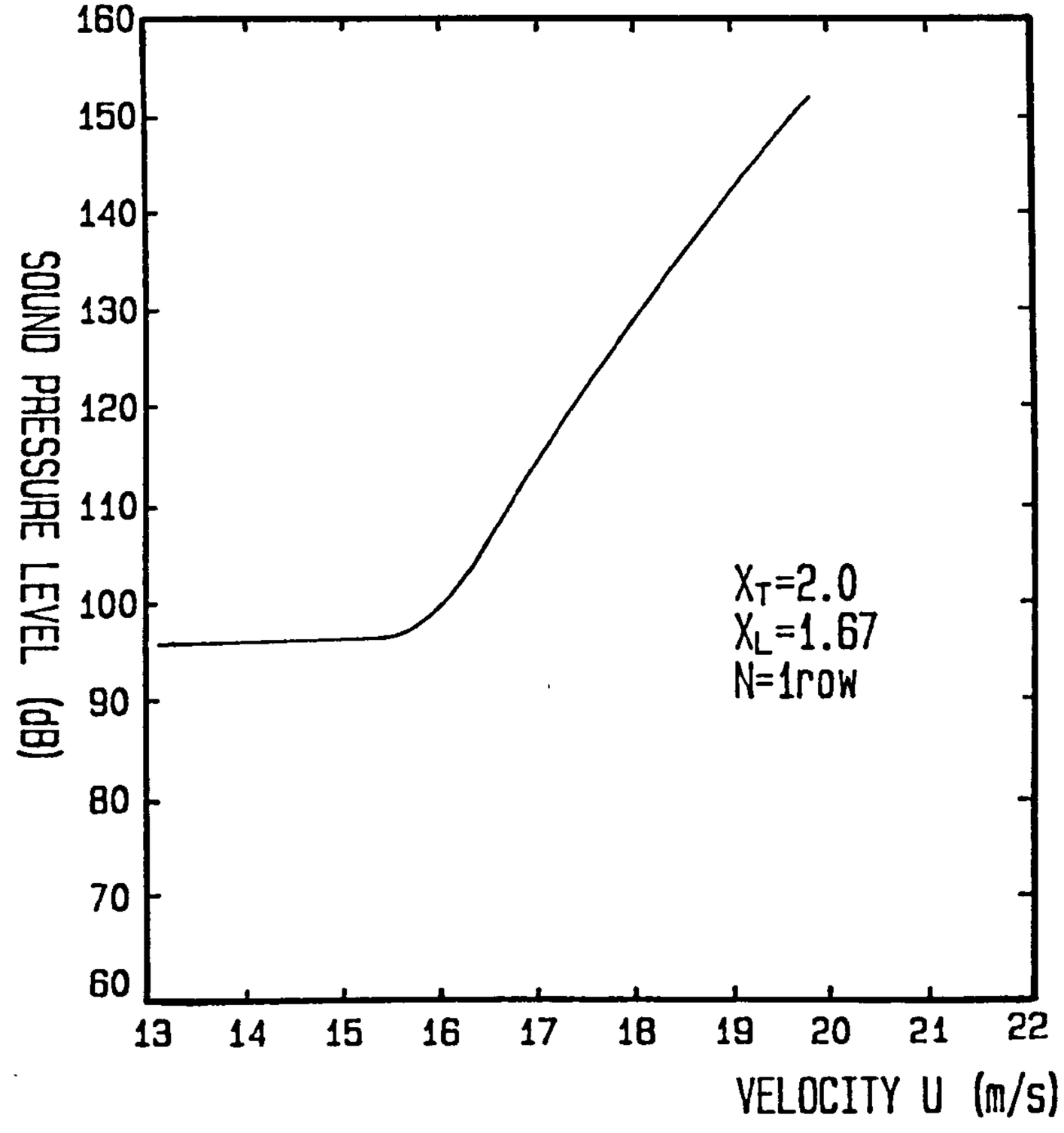

[b]

IN-BANK SOUND PRESSURE LEVELS AT THE ONSET OF ACOUSTIC VIBRATION

FIGURE 7.1

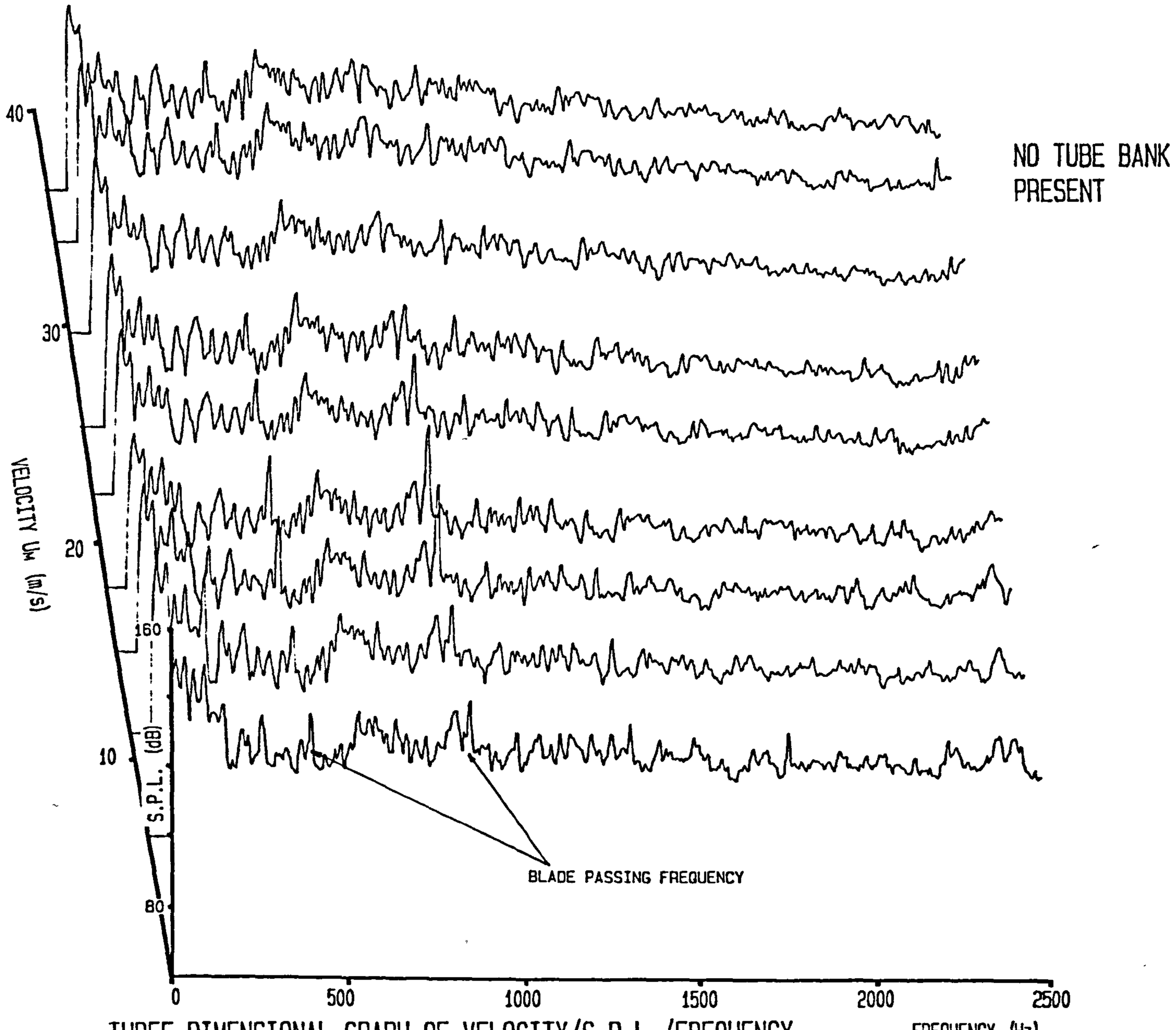

THREE DIMENSIONAL GRAPH OF VELOCITY/S.P.L./FREQUENCY

FIGURE 7.2

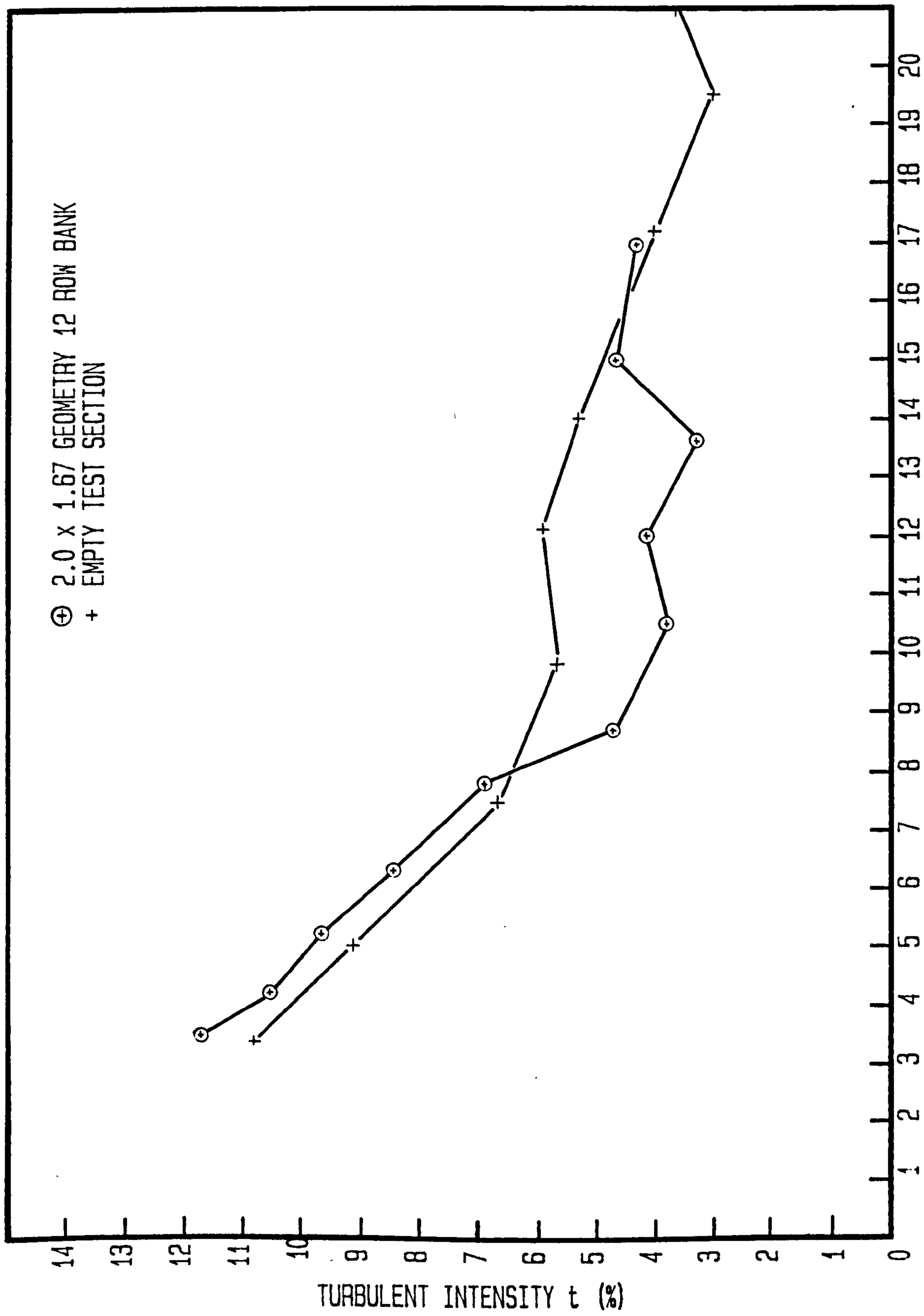

GRAPH OF TURBULENT INTENSITY AGAINST VELOCITY

FIGURE 7.3

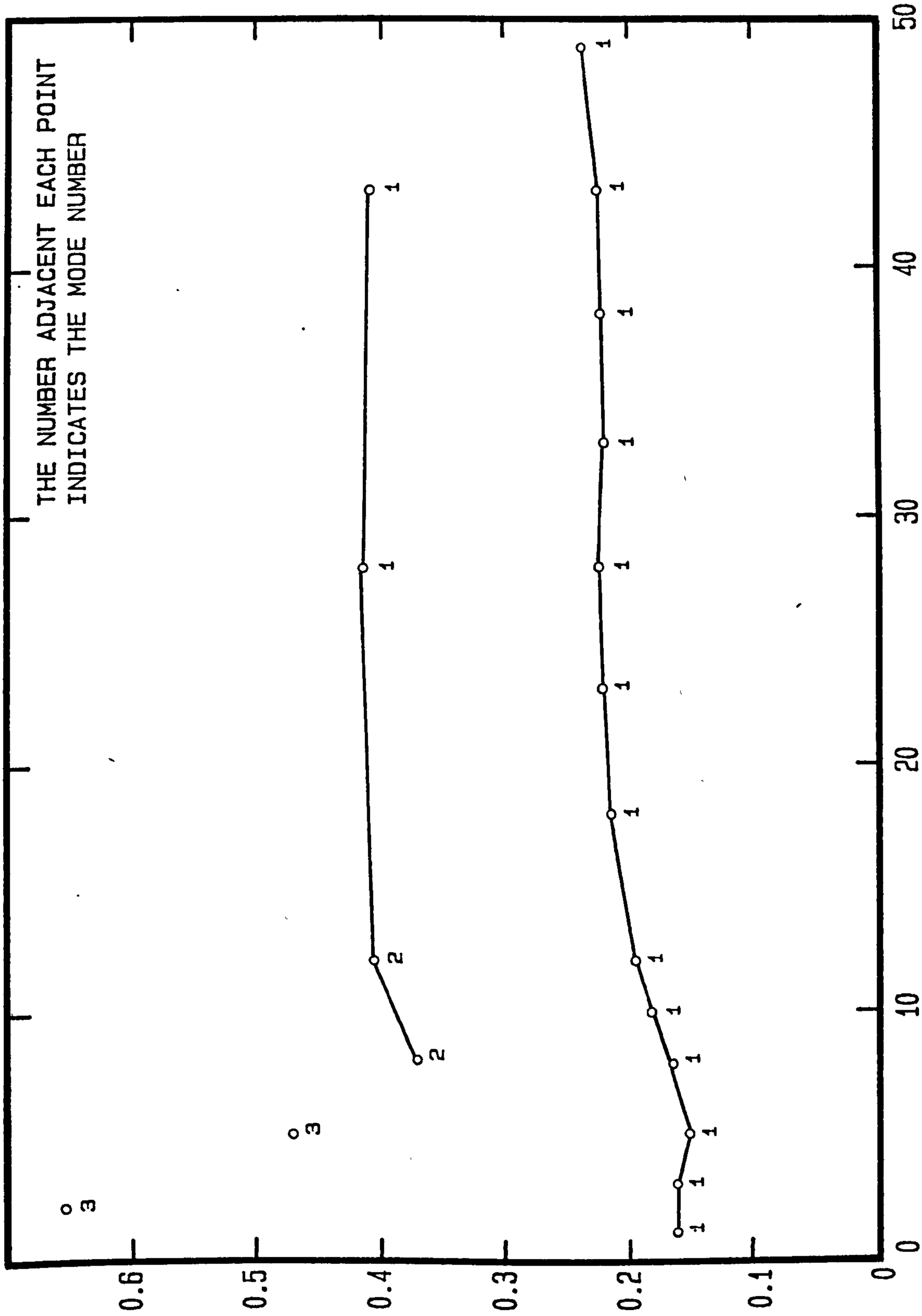

GRAPH OF ACOUSTIC STROUHAL NUMBER AGAINST BANK DEPTH FOR X_T=2.00, X_L=1.67

FIGURE 7.4

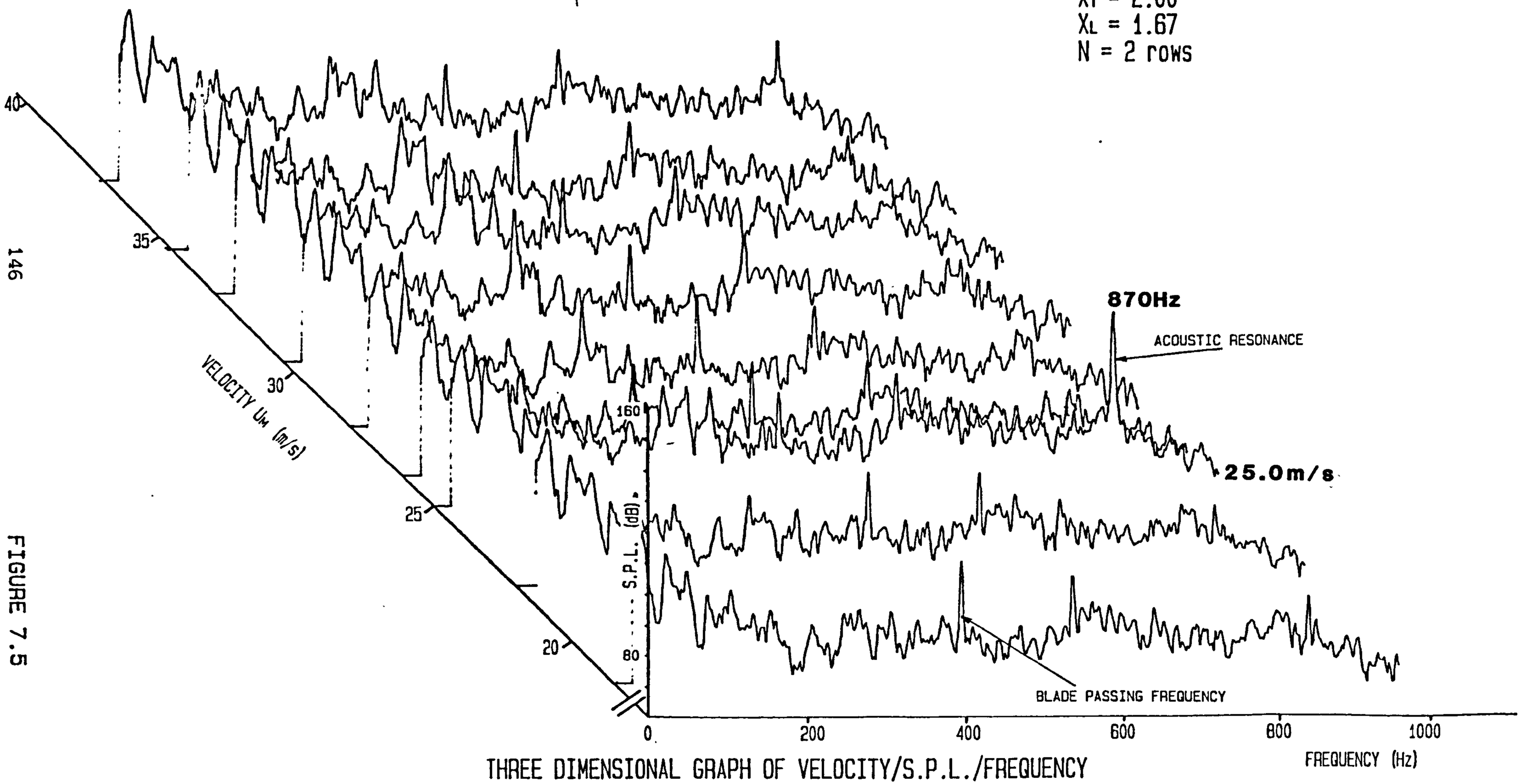

THREE DIMENSIONAL GRAPH OF VELOCITY/S.P.L./FREQUENCY

FIGURE 7.5

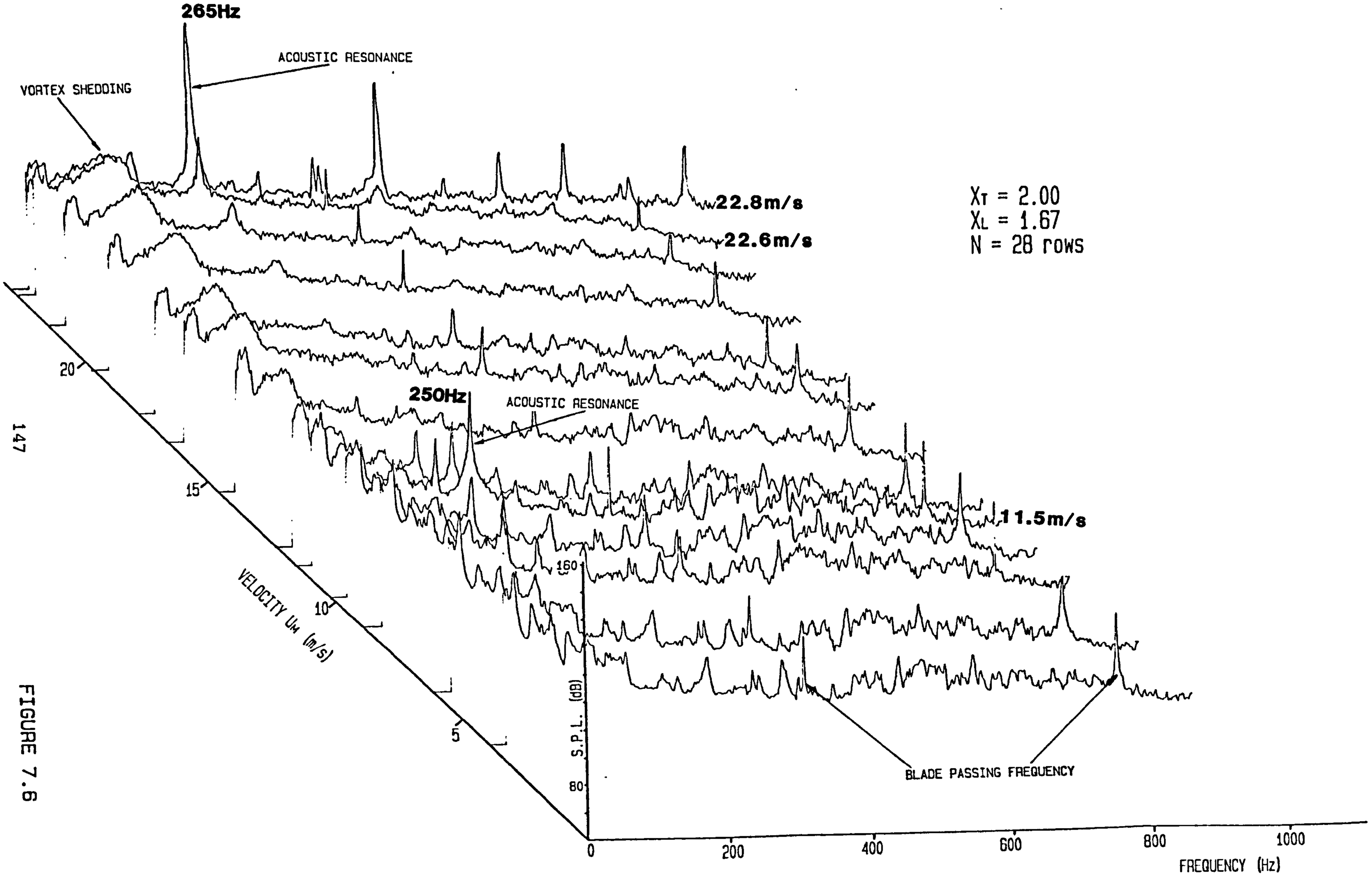

$X_T = 2.00$
$X_L = 1.67$
N = 28 rows

THREE DIMENSIONAL GRAPH OF VELOCITY/S.P.L./FREQUENCY

FIGURE 7.6

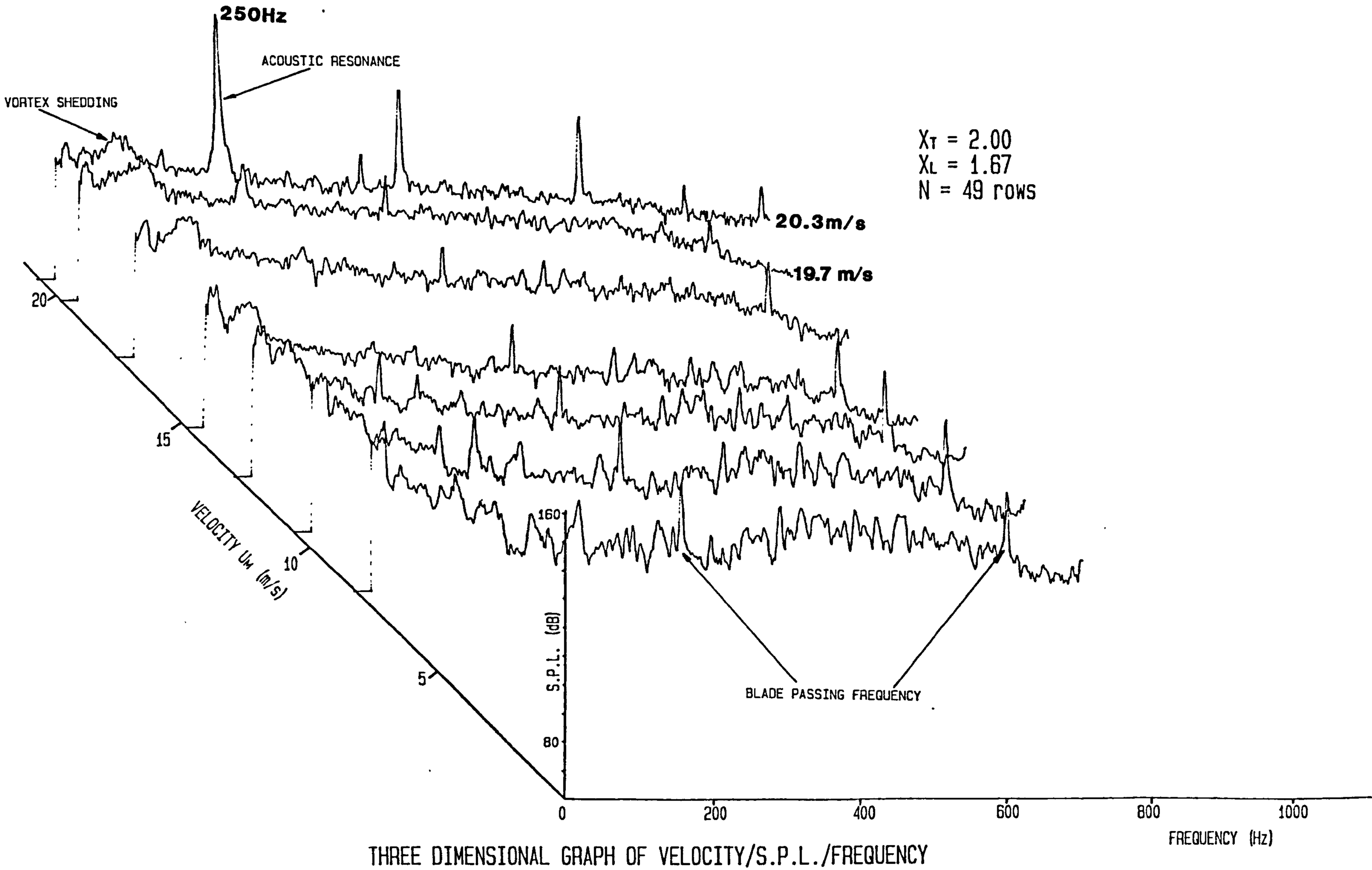

$X_T = 2.00$
$X_L = 1.67$
N = 49 rows

THREE DIMENSIONAL GRAPH OF VELOCITY/S.P.L./FREQUENCY

FIGURE 7.7

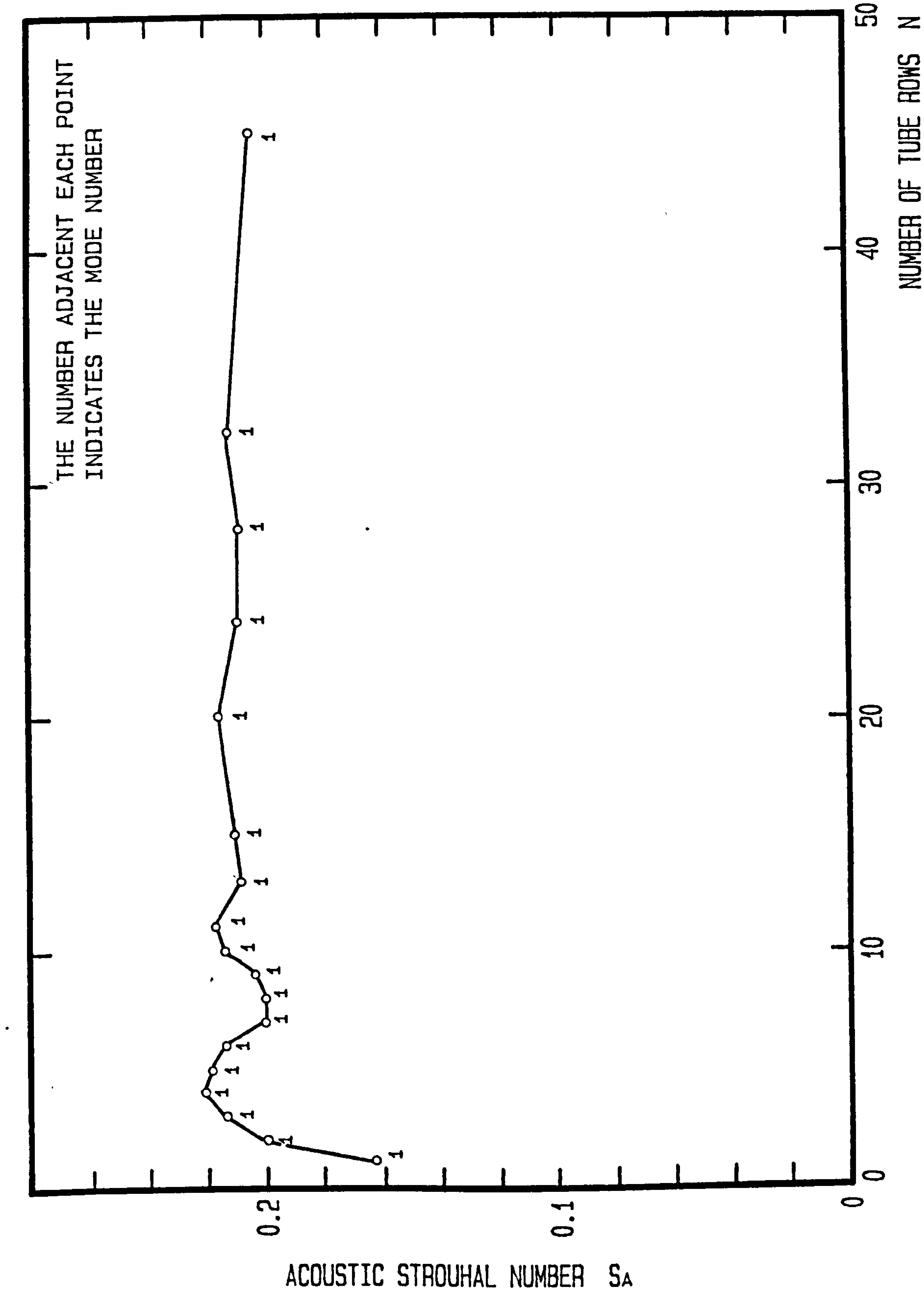

GRAPH OF ACOUSTIC STROUHAL NUMBER AGAINST BANK DEPTH FOR X_T=2.00, X_L=2.00

FIGURE 7.8

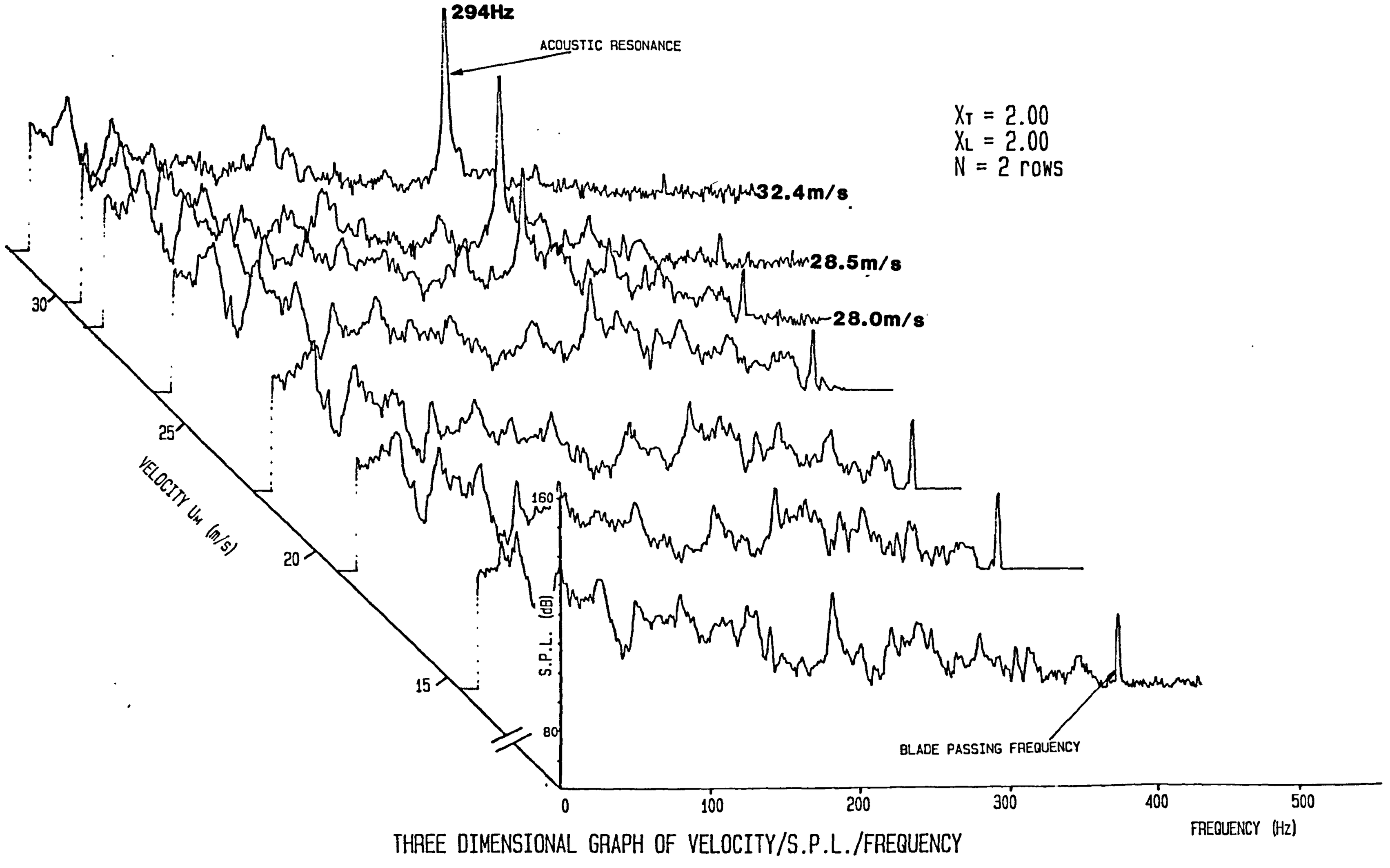

FIGURE 7.9 THREE DIMENSIONAL GRAPH OF VELOCITY/S.P.L./FREQUENCY

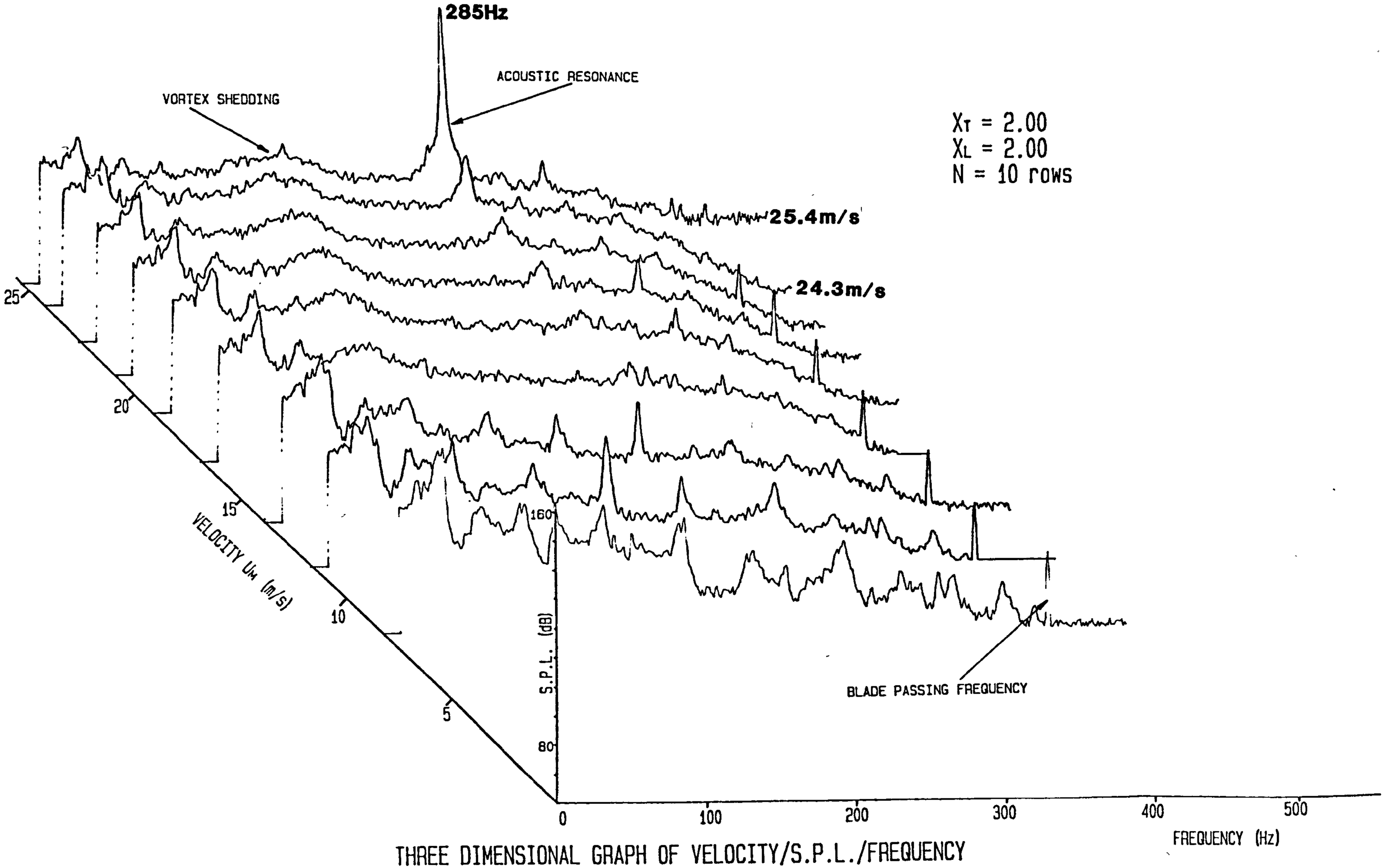

THREE DIMENSIONAL GRAPH OF VELOCITY/S.P.L./FREQUENCY

FIGURE 7.10

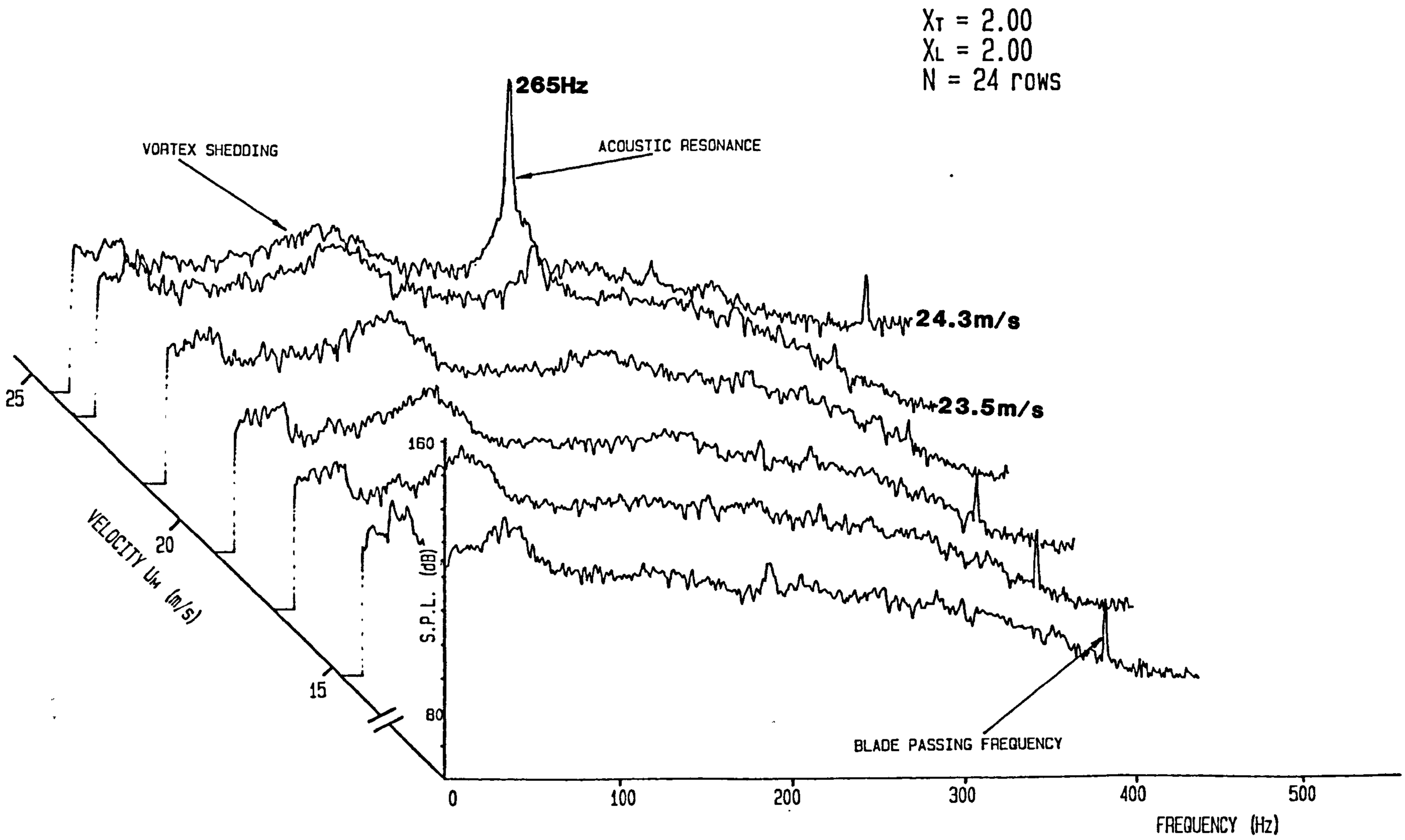

FIGURE 7.11

THREE DIMENSIONAL GRAPH OF VELOCITY/S.P.L./FREQUENCY

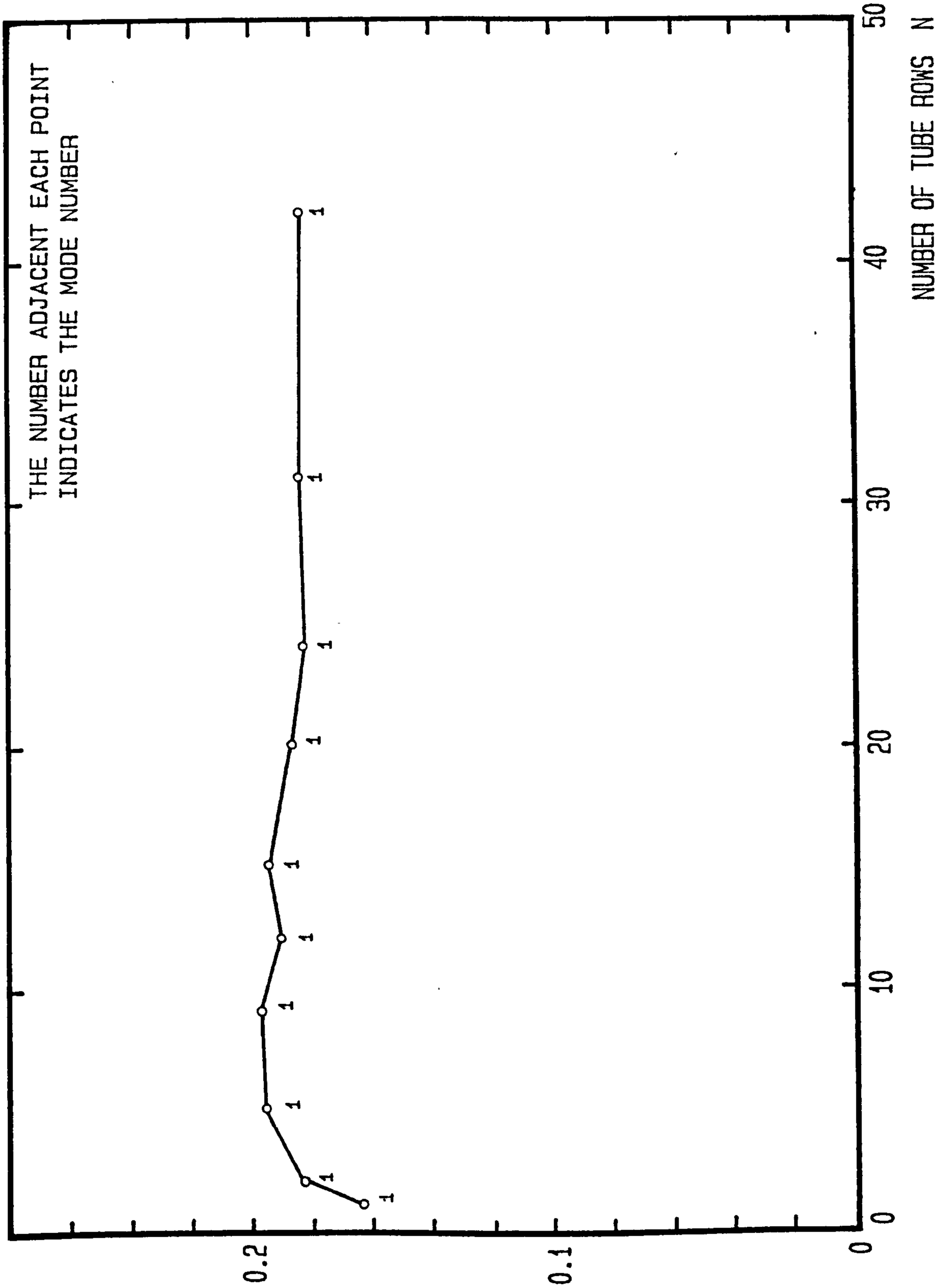

GRAPH OF ACOUSTIC STROUHAL NUMBER AGAINST BANK DEPTH FOR X_T=2.00, X_L=2.34

FIGURE 7.12

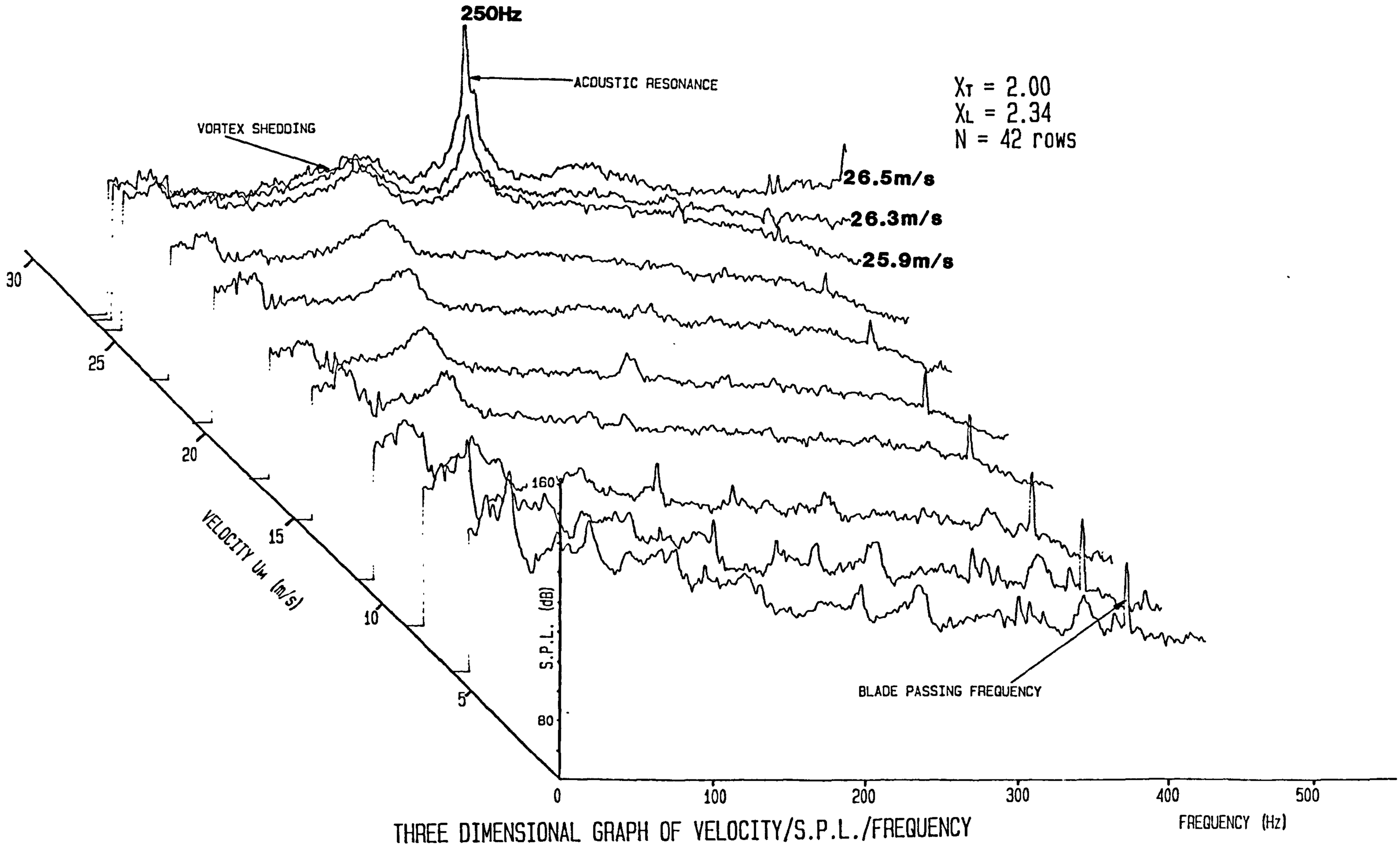

THREE DIMENSIONAL GRAPH OF VELOCITY/S.P.L./FREQUENCY

FIGURE 7.13

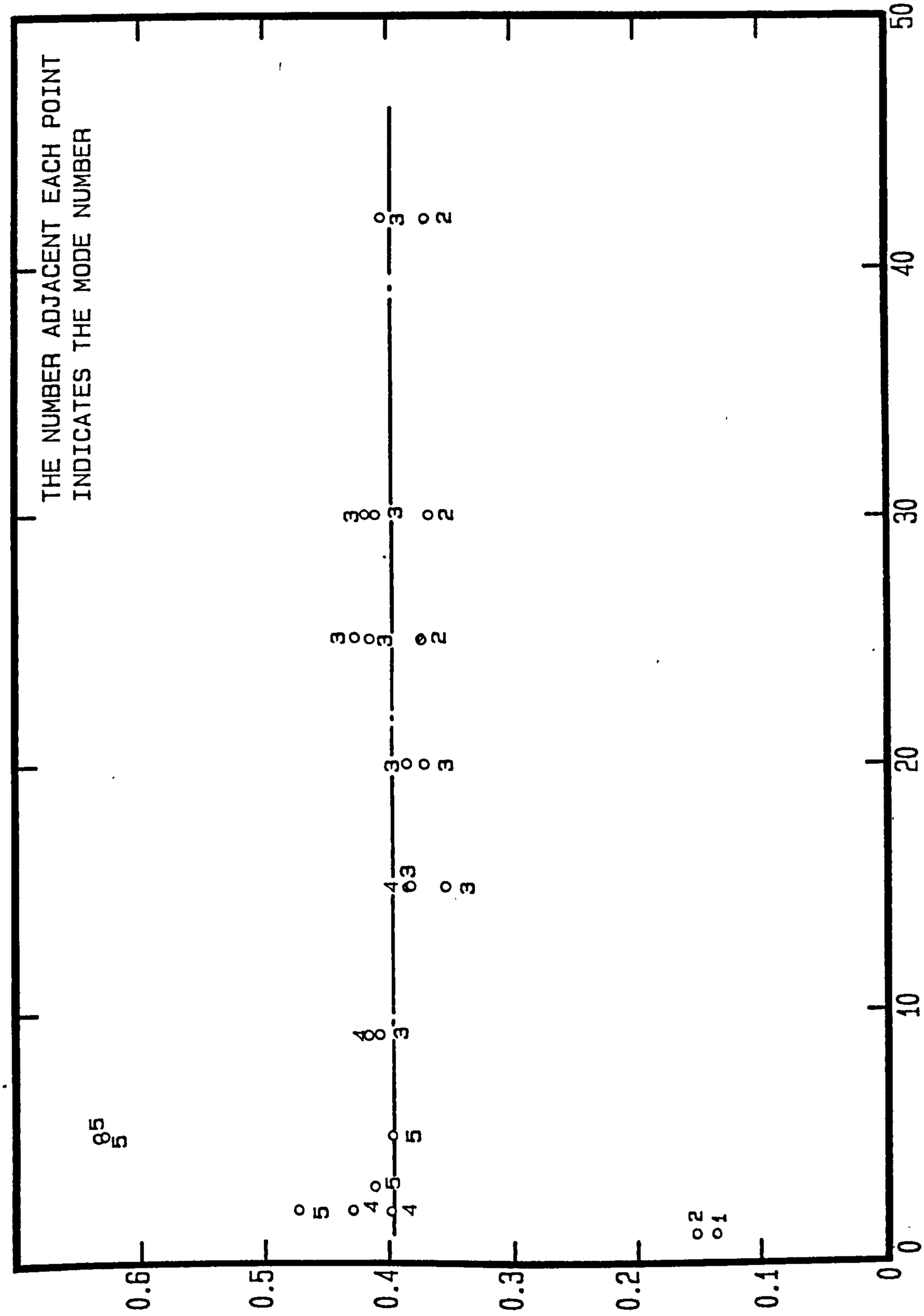

GRAPH OF ACOUSTIC STROUHAL NUMBER AGAINST BANK DEPTH FOR X_T=1.34, X_L=1.34

FIGURE 7.14

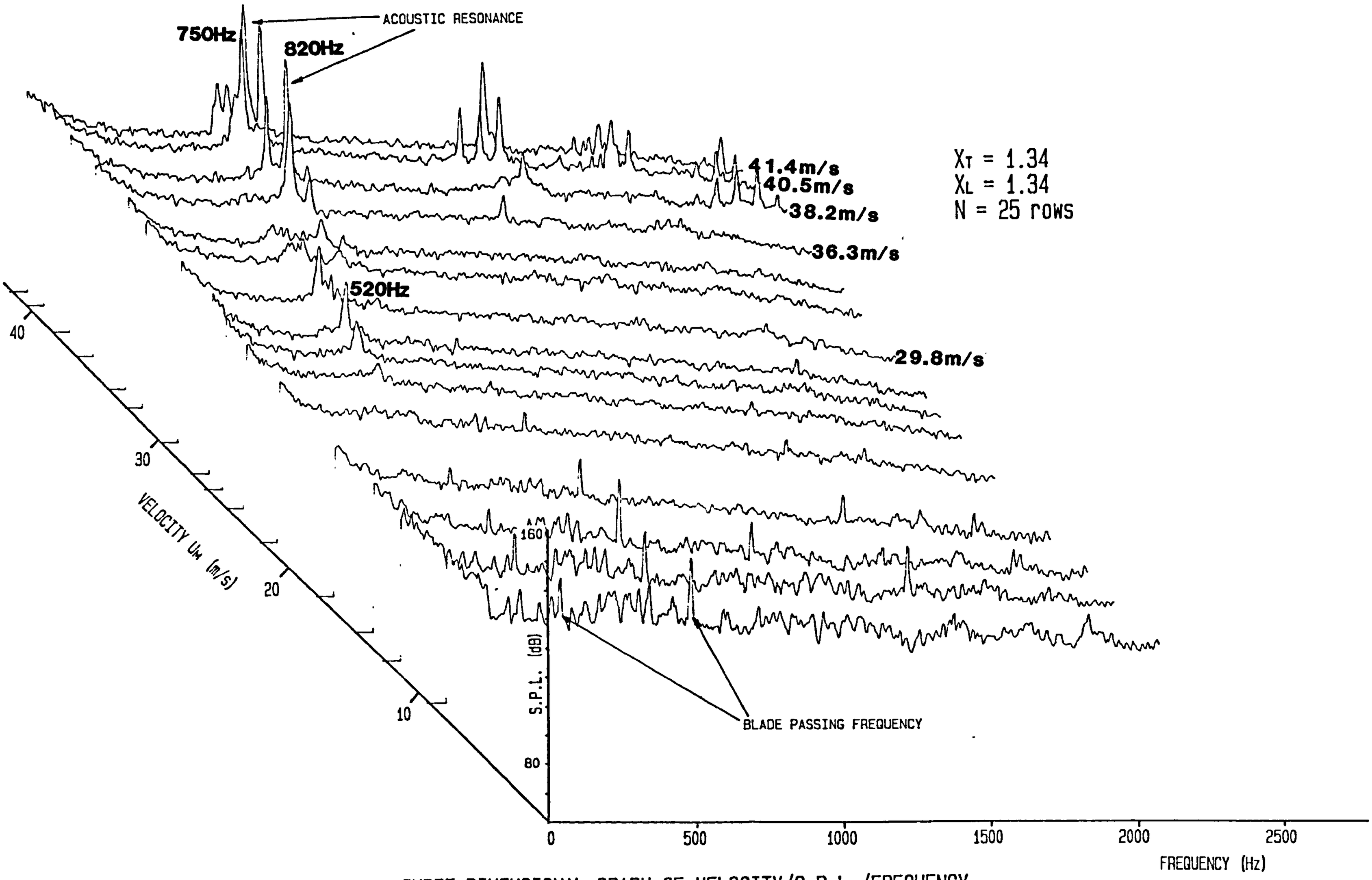

THREE DIMENSIONAL GRAPH OF VELOCITY/S.P.L./FREQUENCY

FIGURE 7.15

730Hz

ACOUSTIC RESONANCE

520Hz

X_T = 1.34
X_L = 1.34
N = 30 rows

35.3m/s

33.2m/s

28.5m/s

40

30

20

10

VELOCITY U_M (m/s)

160

80

S.P.L. (dB)

BLADE PASSING FREQUENCY

0

500

1000

1500

2000

2500

FREQUENCY (Hz)

THREE DIMENSIONAL GRAPH OF VELOCITY/S.P.L./FREQUENCY

FIGURE 7.16

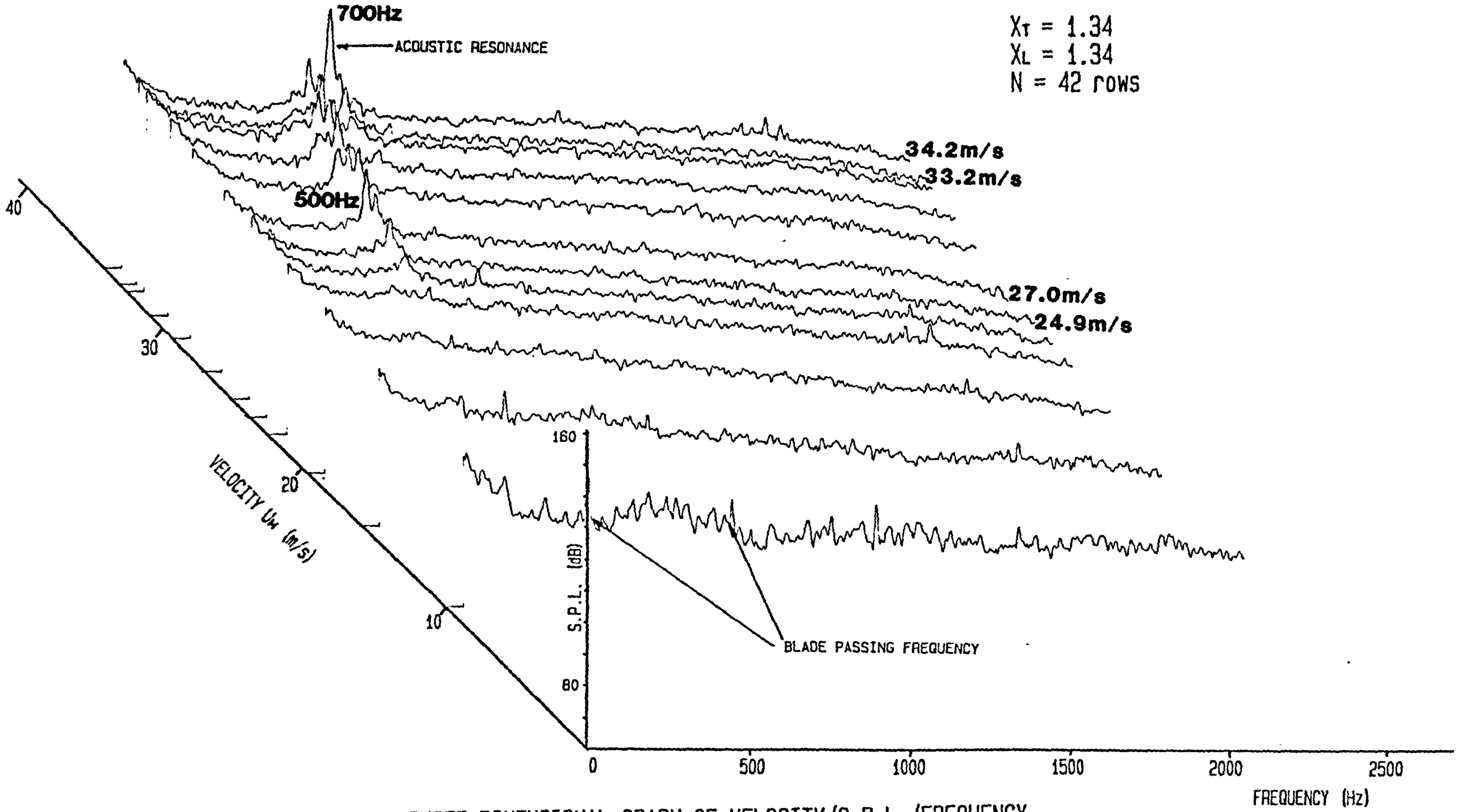

THREE DIMENSIONAL GRAPH OF VELOCITY/S.P.L./FREQUENCY

FIGURE 7.17

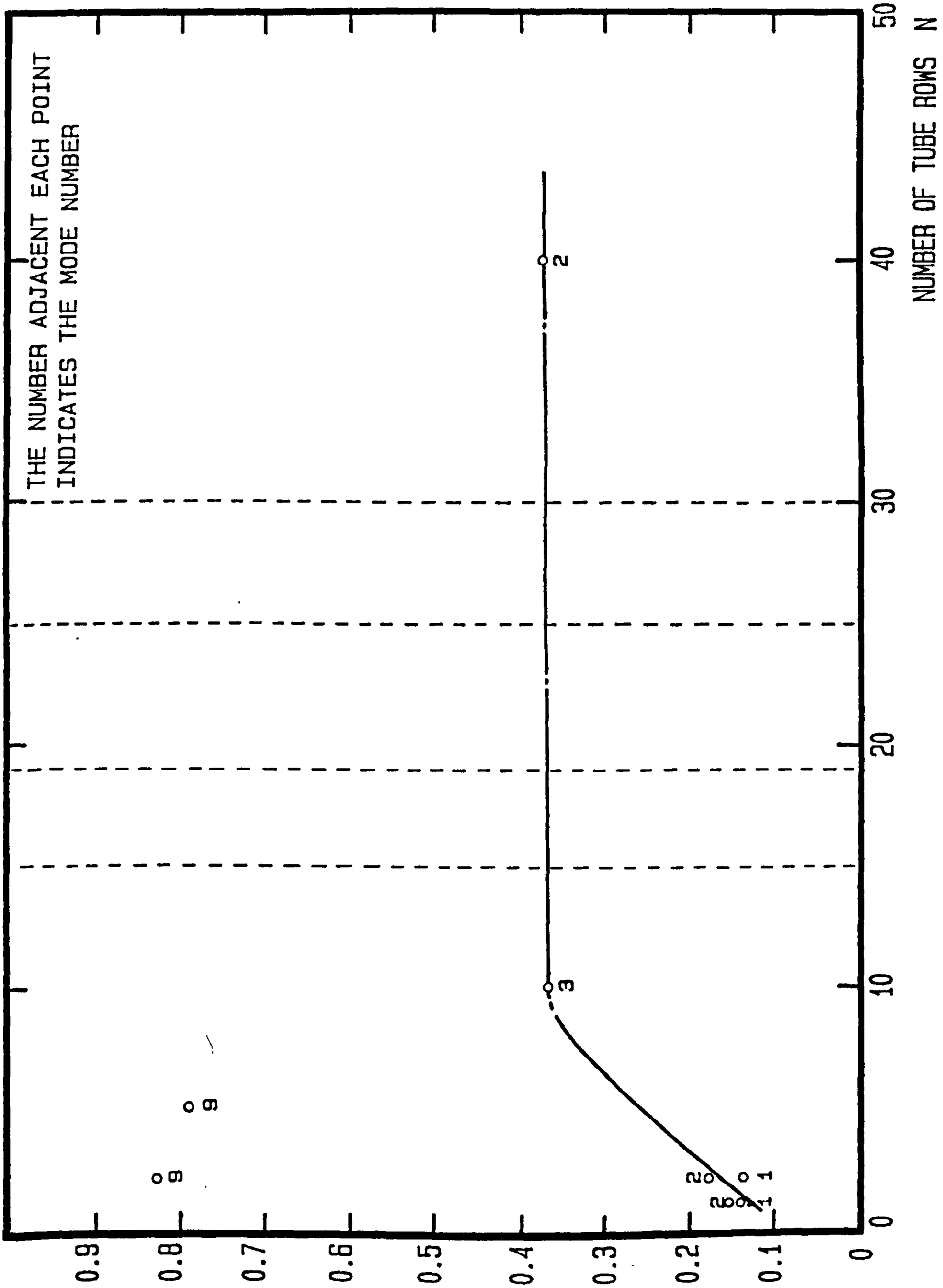

GRAPH OF ACOUSTIC STROUHAL NUMBER AGAINST BANK DEPTH FOR X_T=1.34, X_L=1.67

FIGURE 7.18

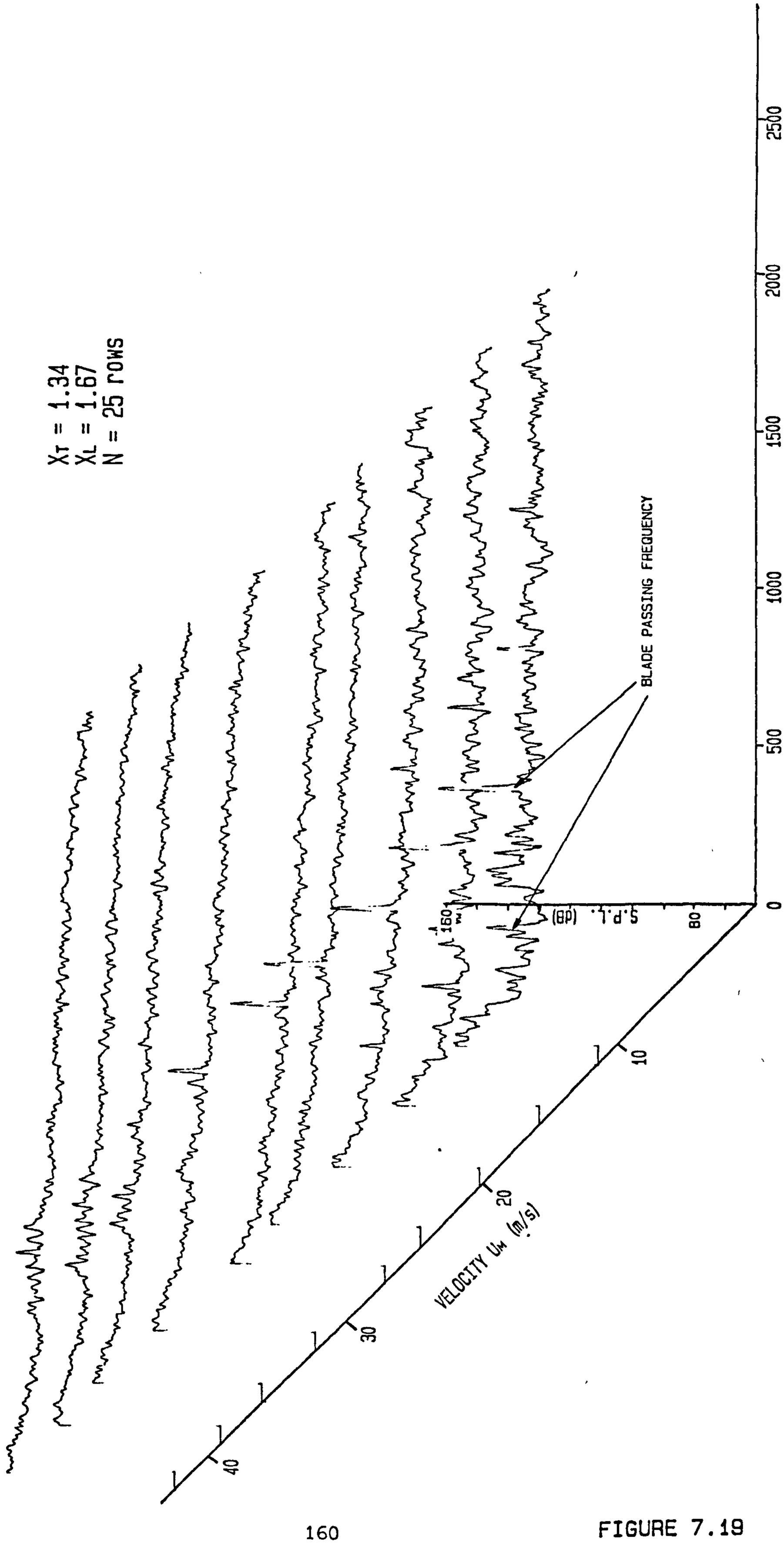
THREE DIMENSIONAL GRAPH OF VELOCITY/S.P.L./FREQUENCY
FREQUENCY (Hz)
2500
2000
1500
1000
500
0
BLADE PASSING FREQUENCY
S.P.L. (dB)
160
80
0
10
20
30
40
VELOCITY Um (m/s)
Xr = 1.34
XL = 1.67
N = 25 rows

FIGURE 7.19

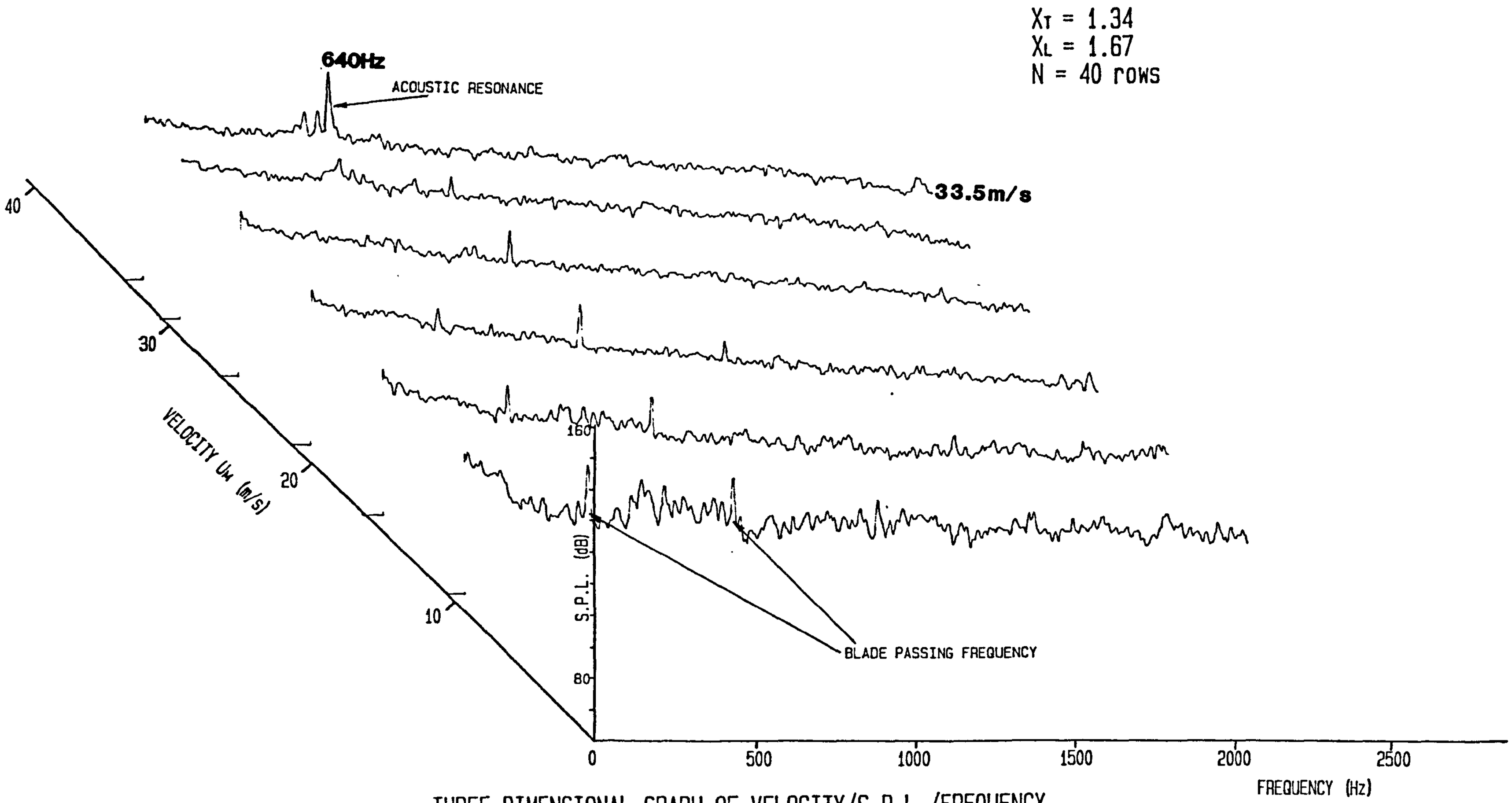

THREE DIMENSIONAL GRAPH OF VELOCITY/S.P.L./FREQUENCY

FIGURE 7.20

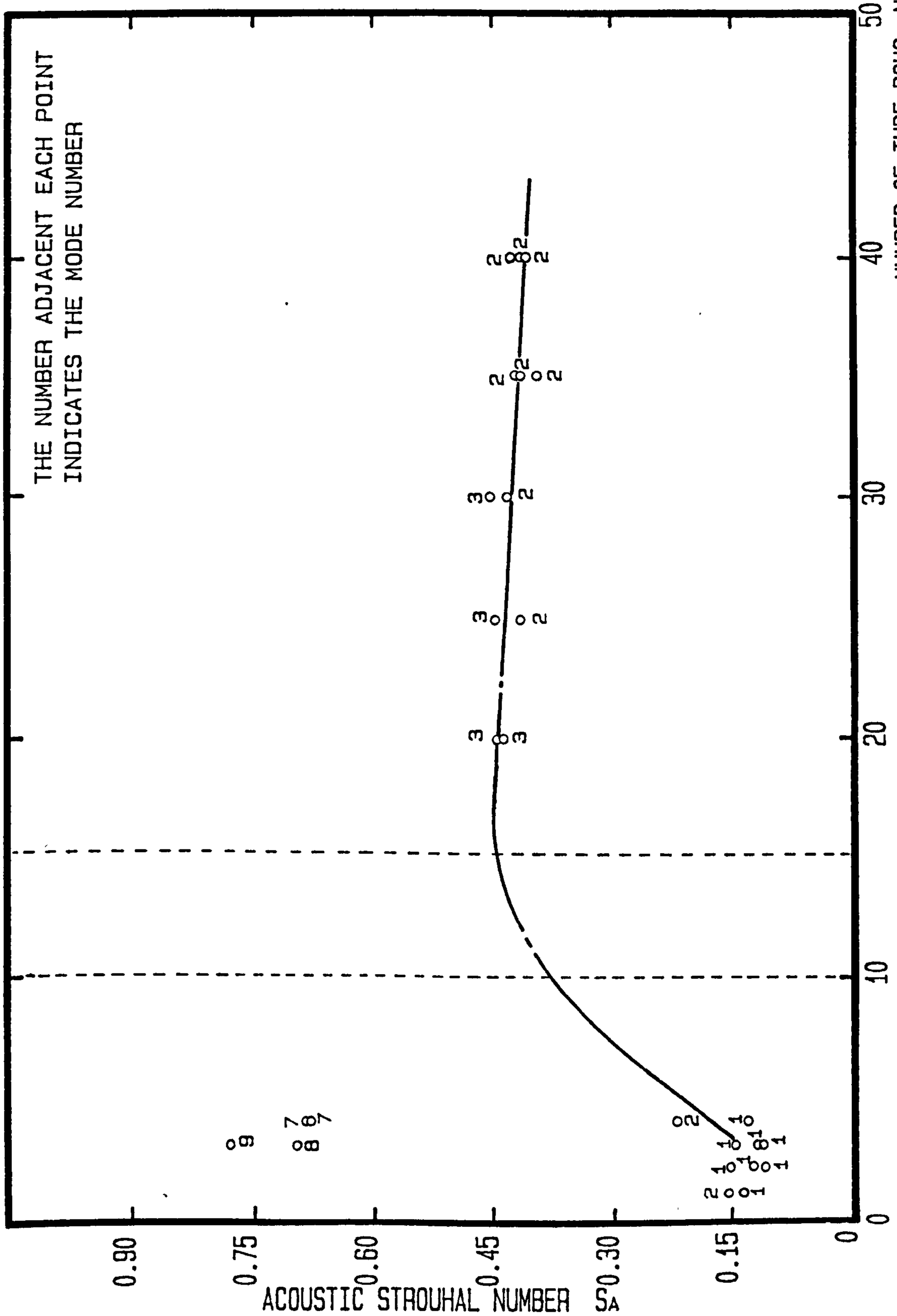

GRAPH OF ACOUSTIC STROUHAL NUMBER AGAINST BANK DEPTH FOR X_T=1.34, X_L=2.00

FIGURE 7.21

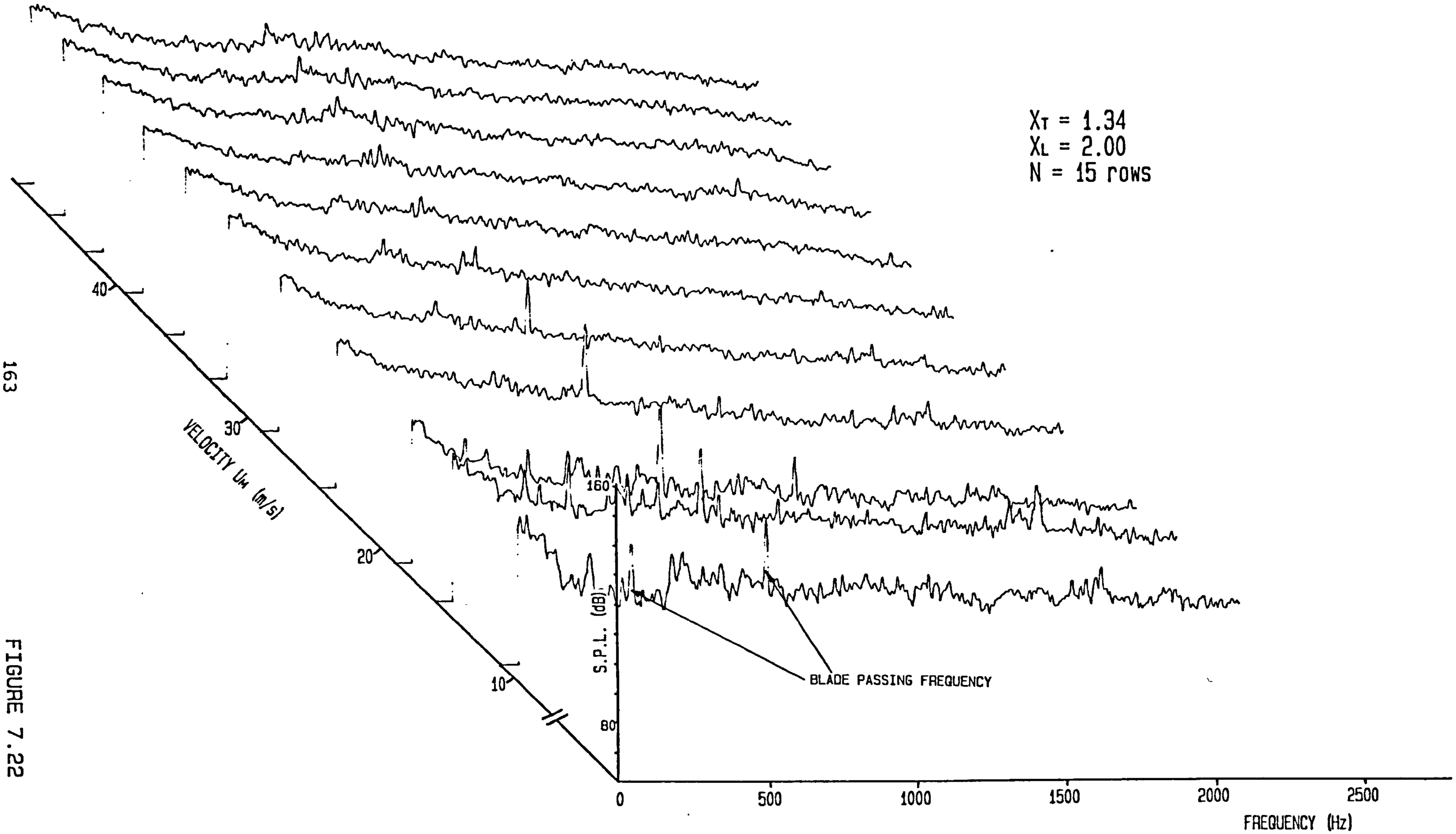

FIGURE 7.22

THREE DIMENSIONAL GRAPH OF VELOCITY/S.P.L./FREQUENCY

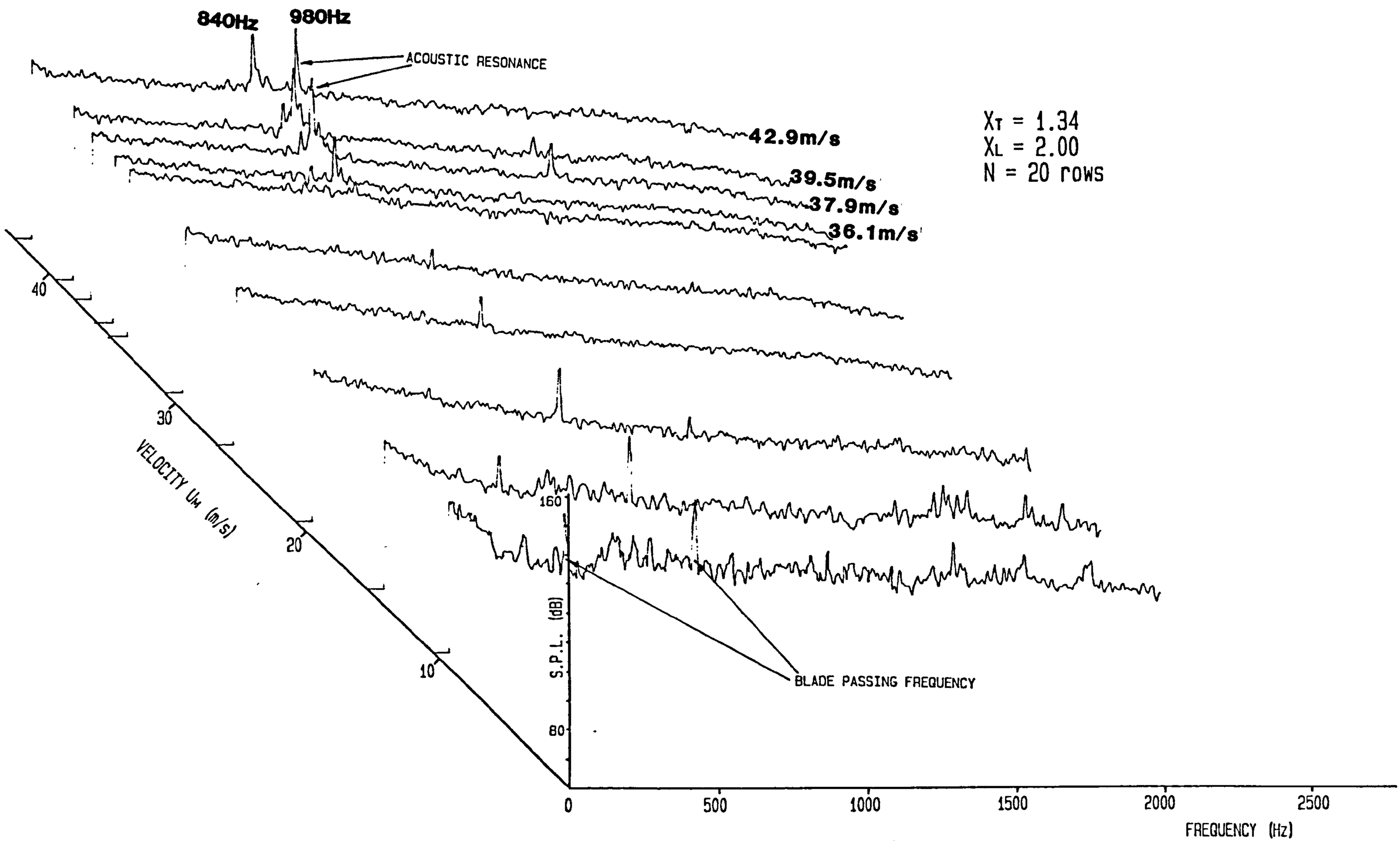

THREE DIMENSIONAL GRAPH OF VELOCITY/S.P.L./FREQUENCY

FIGURE 7.23

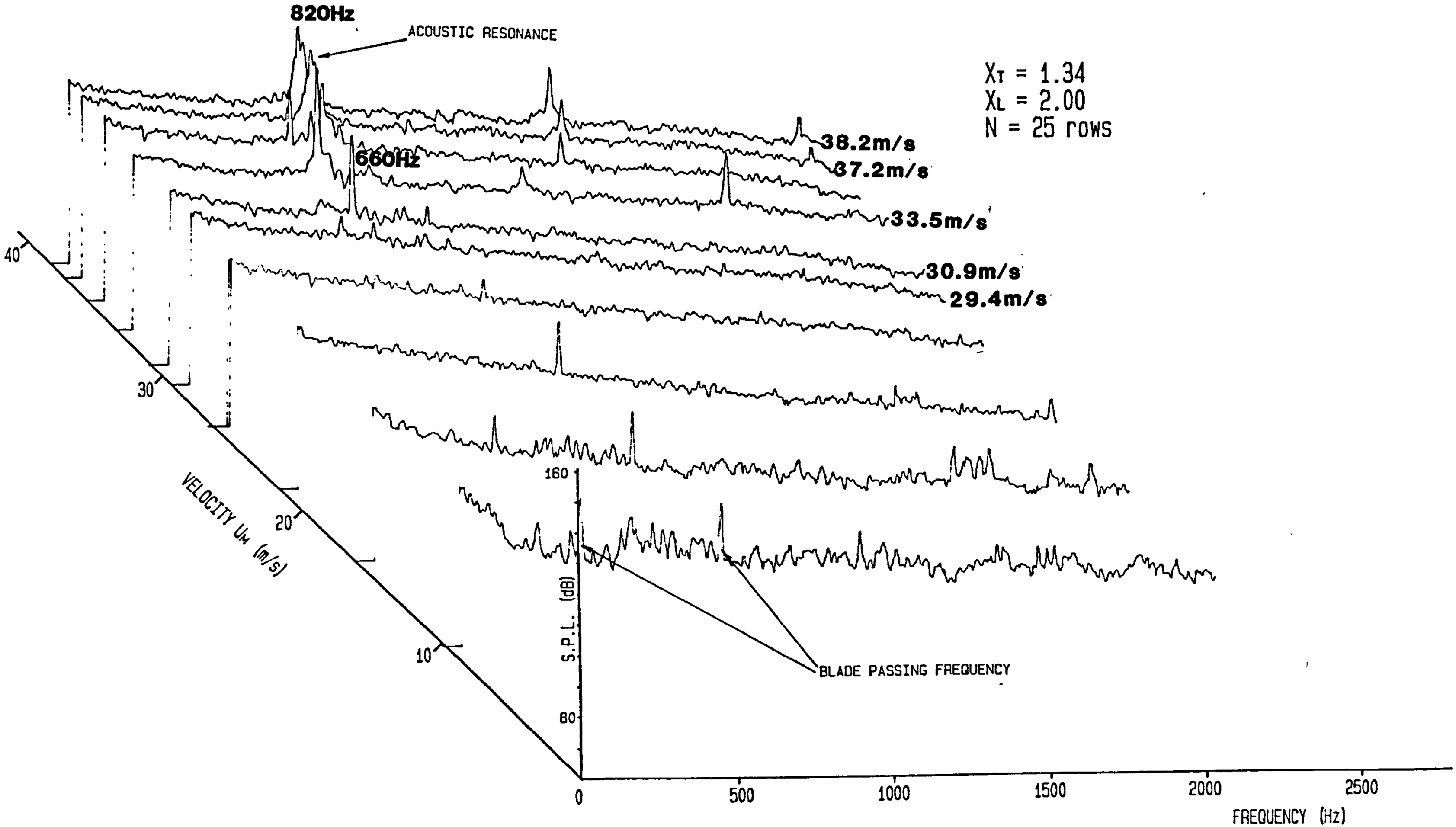

FIGURE 7.24

THREE DIMENSIONAL GRAPH OF VELOCITY/S.P.L./FREQUENCY

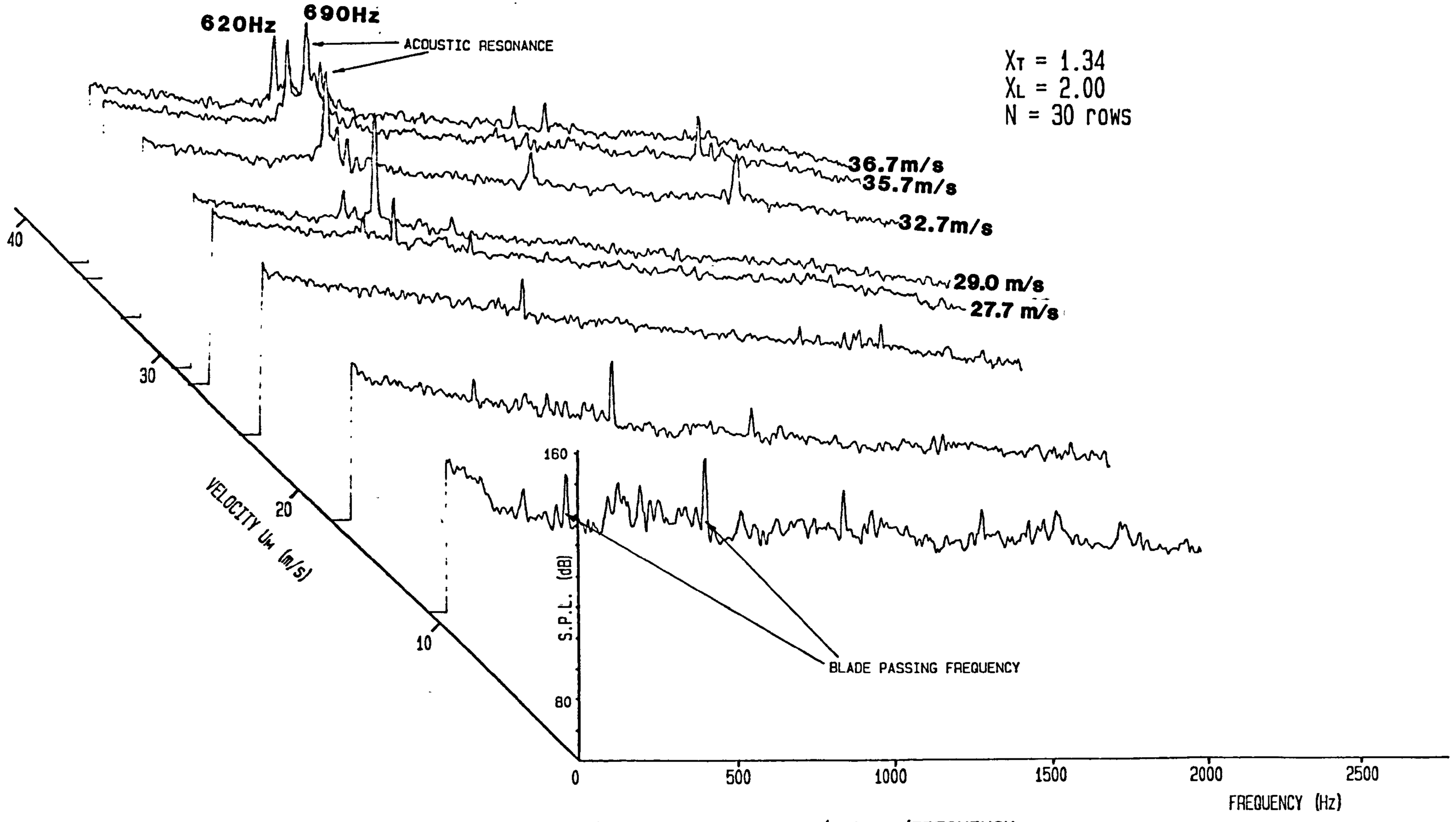

FIGURE 7.25

THREE DIMENSIONAL GRAPH OF VELOCITY/S.P.L./FREQUENCY

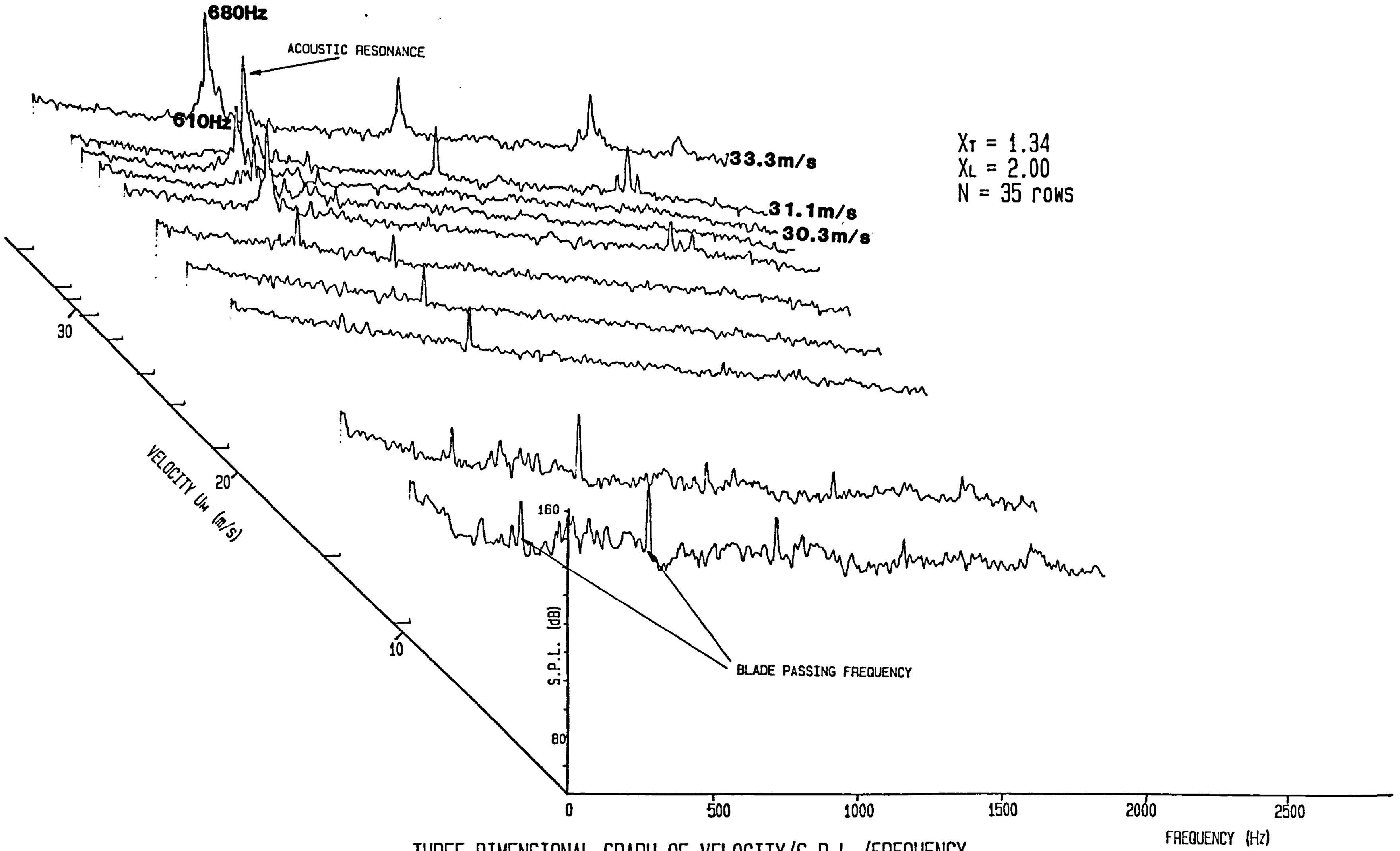

X_T = 1.34
X_L = 2.00
N = 35 rows

FIGURE 7.26

THREE DIMENSIONAL GRAPH OF VELOCITY/S.P.L./FREQUENCY

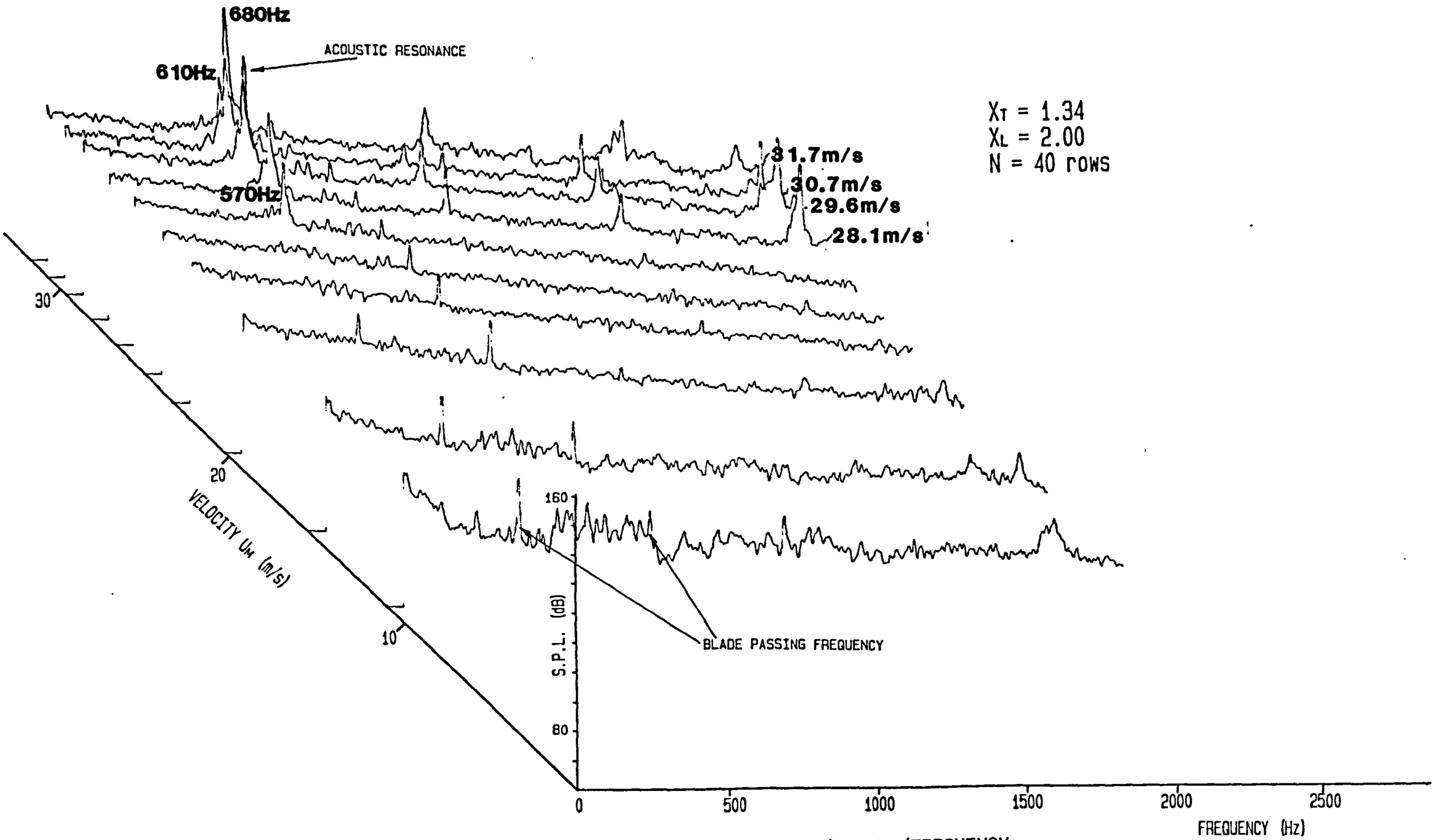

FIGURE 7.27

THREE DIMENSIONAL GRAPH OF VELOCITY/S.P.L./FREQUENCY

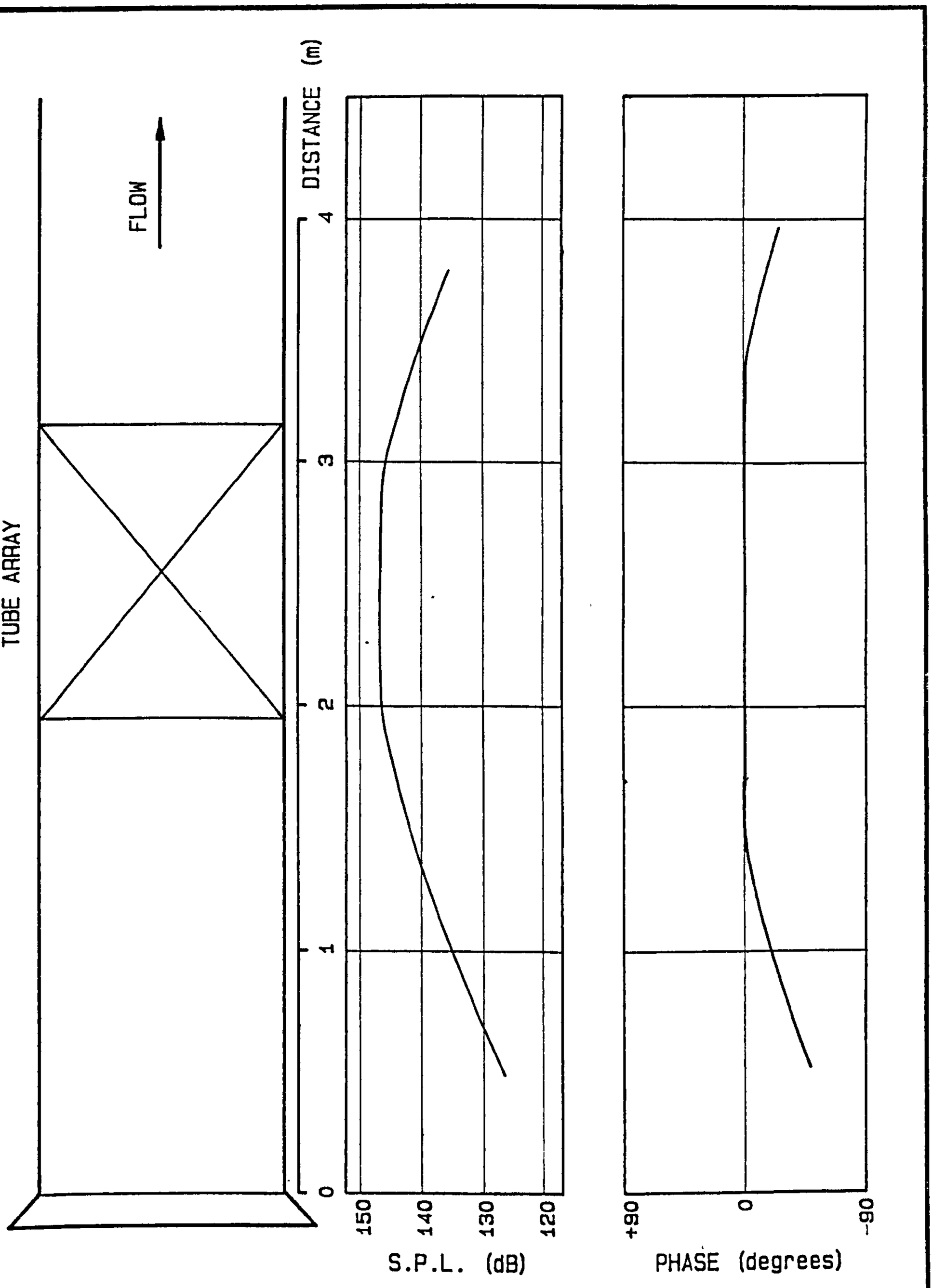

MAGNITUDE AND PHASE DIAGRAMS FOR THE EXCITED MODE OF ACOUSTIC VIBRATION FOR THE 38 row BANK OF TUBES WITH X_T = 2.0 X_L = 1.67
f = 252 Hz

FIGURE 7.28

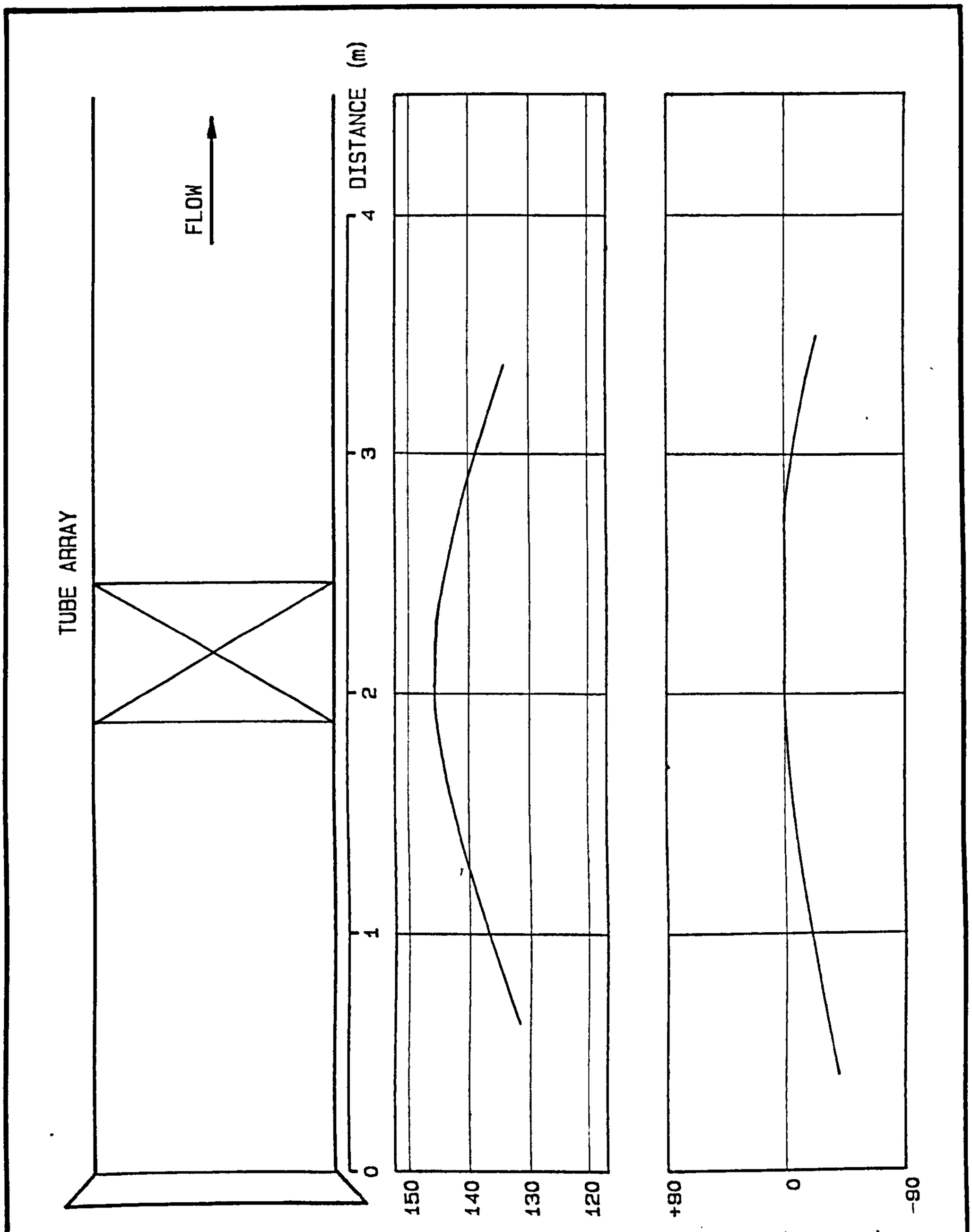

MAGNITUDE AND PHASE DIAGRAMS FOR THE EXCITED MODE OF ACOUSTIC VIBRATION FOR THE 18 row BANK OF TUBES WITH $X_T = 2.0$ $X_L = 1.67$
f = 272 Hz

FIGURE 7.29

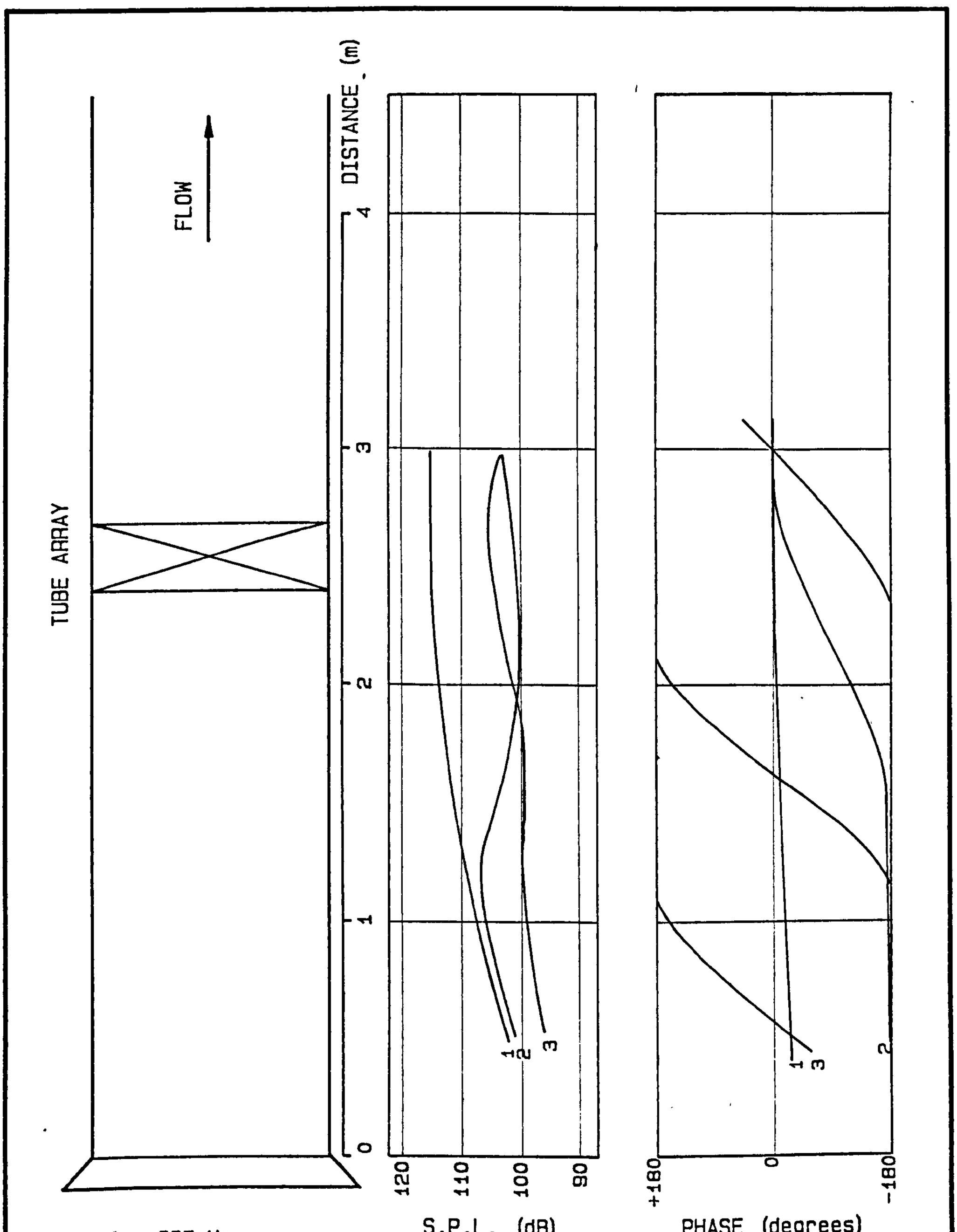

1. f = 295 Hz
2. f = 303 Hz
3. f = 313 Hz

MAGNITUDE AND PHASE DIAGRAMS FOR THREE ACOUSTIC MODES OF THE WIND TUNNEL WITH AN 8 row BANK OF TUBES WITH $X_T = 2.0$ $X_L = 1.67$. THE FREQUENCY OF THE EXCITED MODE f = 295Hz

FIGURE 7.30

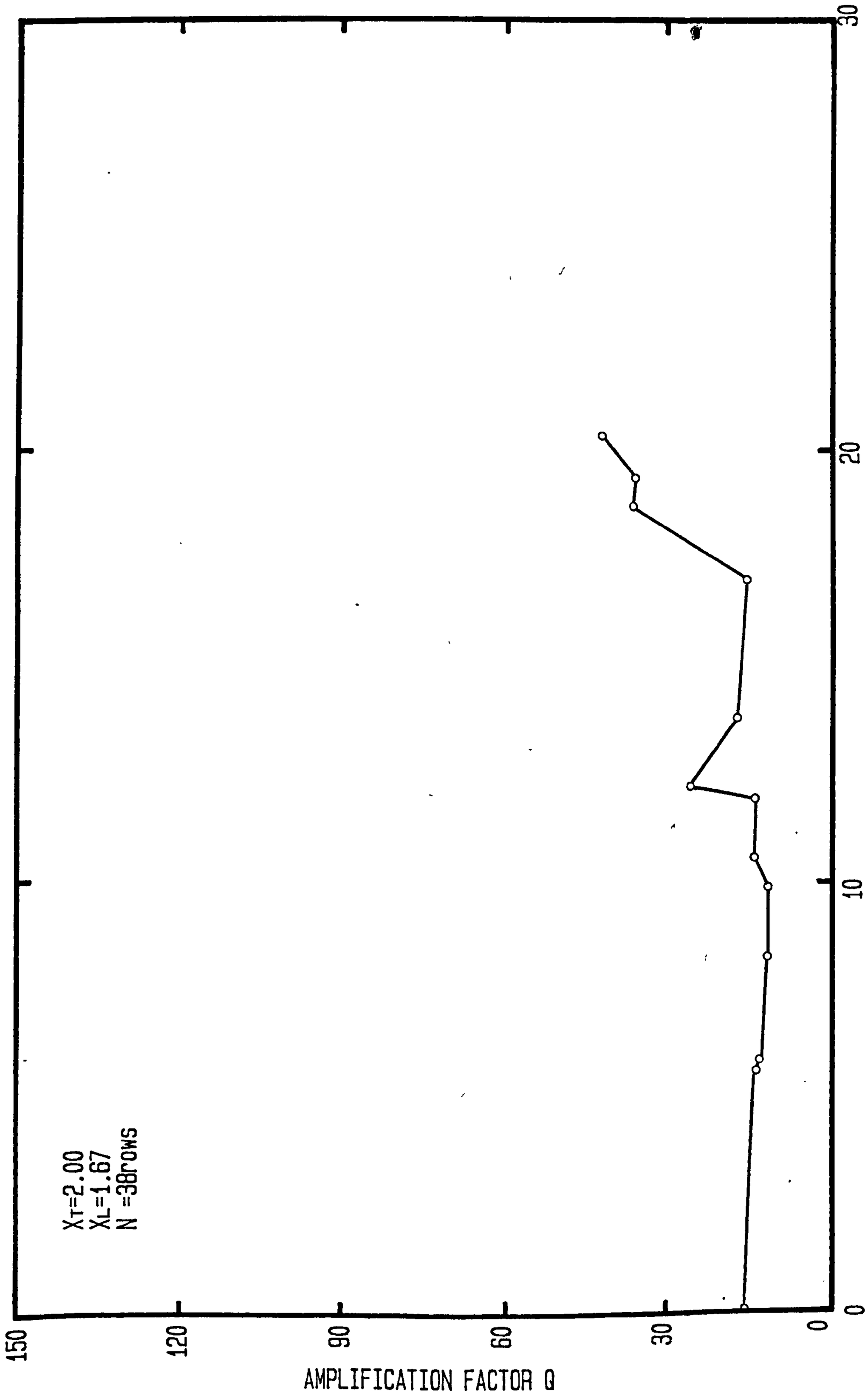

GRAPH OF AMPLIFICATION FACTOR AGAINST VELOCITY FOR THE 38row BANK

FIGURE 7.31

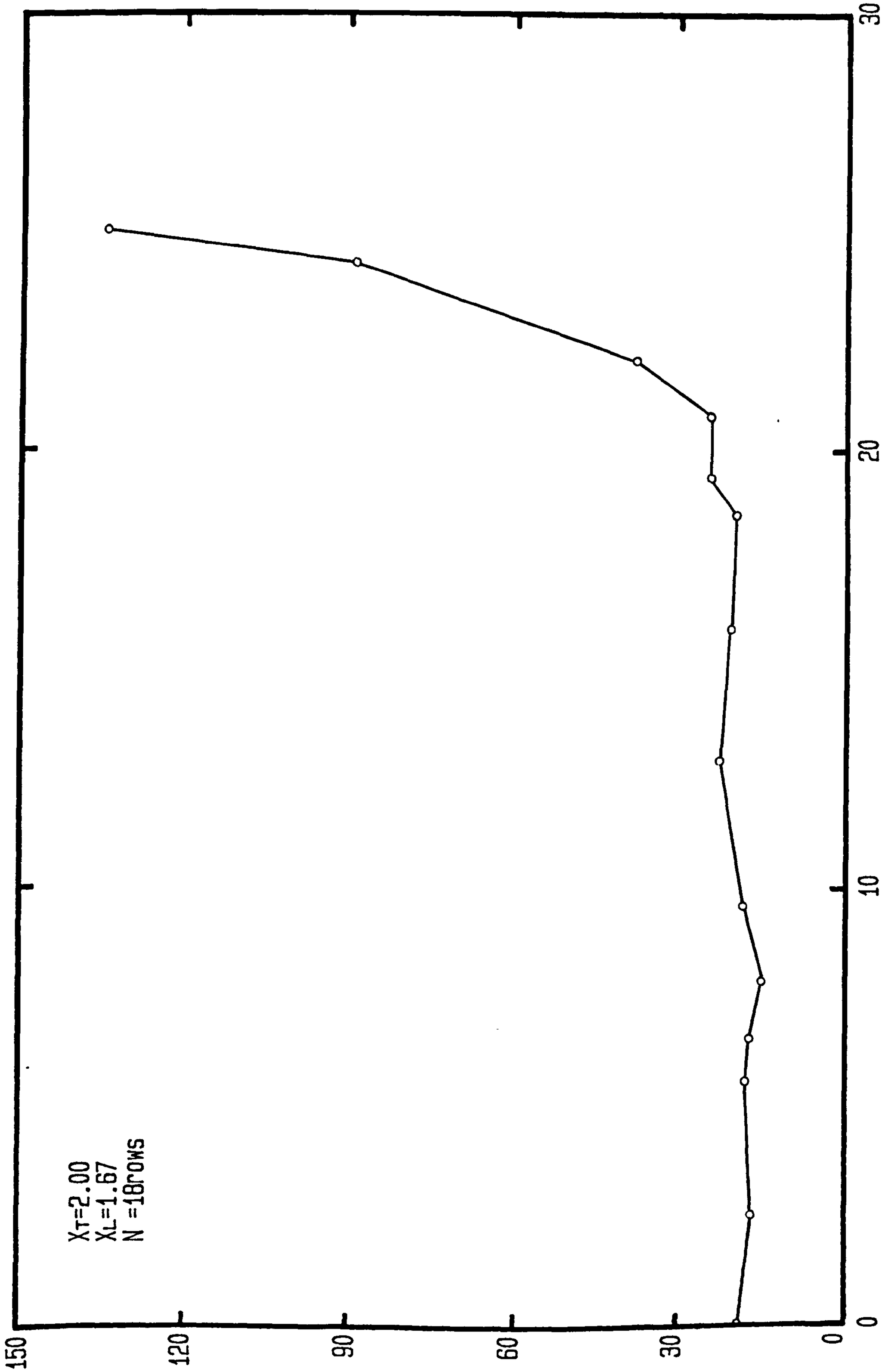

GRAPH OF AMPLIFICATION FACTOR AGAINST VELOCITY FOR THE 18row BANK

FIGURE 7.32

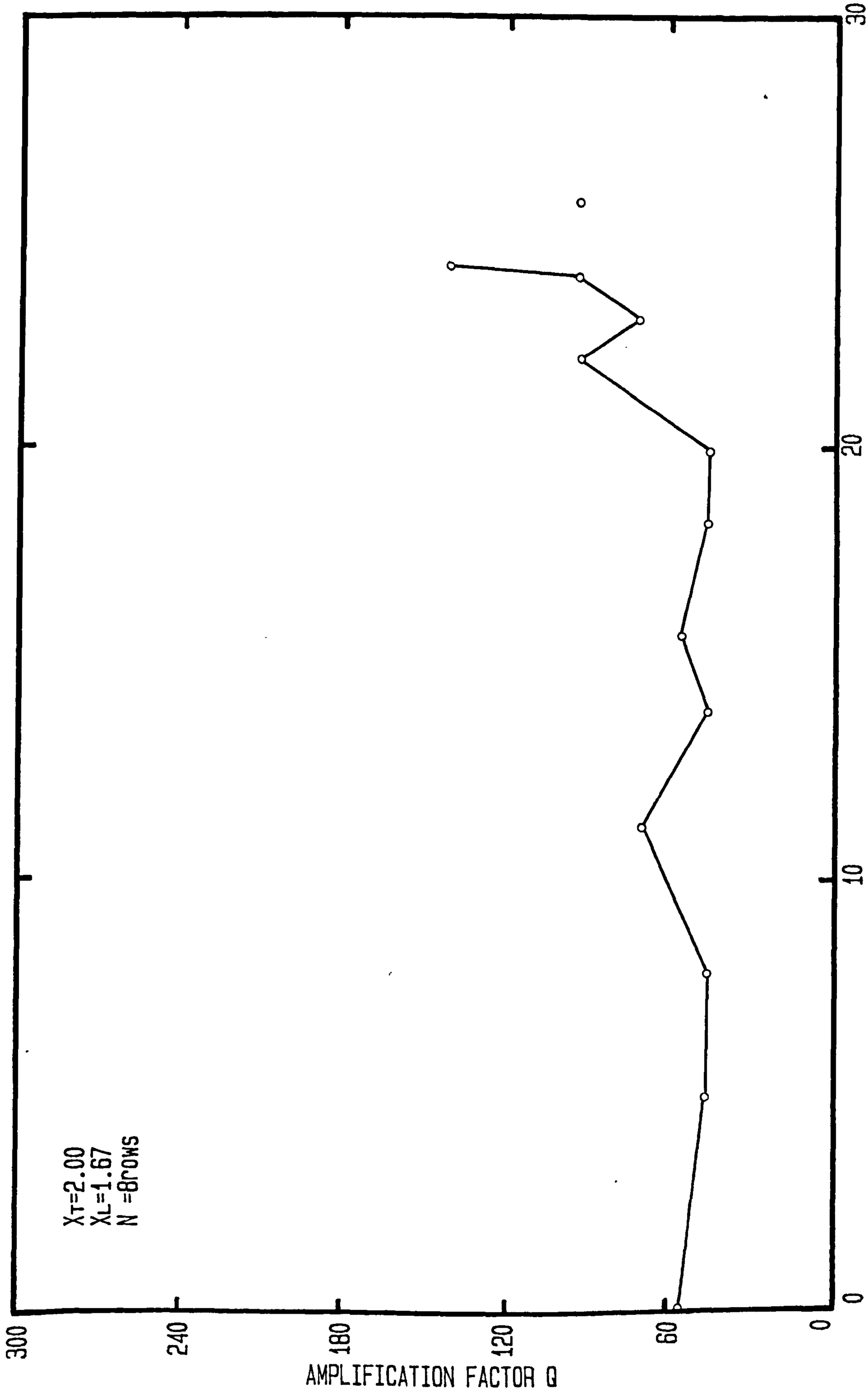

GRAPH OF AMPLIFICATION FACTOR AGAINST VELOCITY FOR THE 8row BANK

FIGURE 7.33

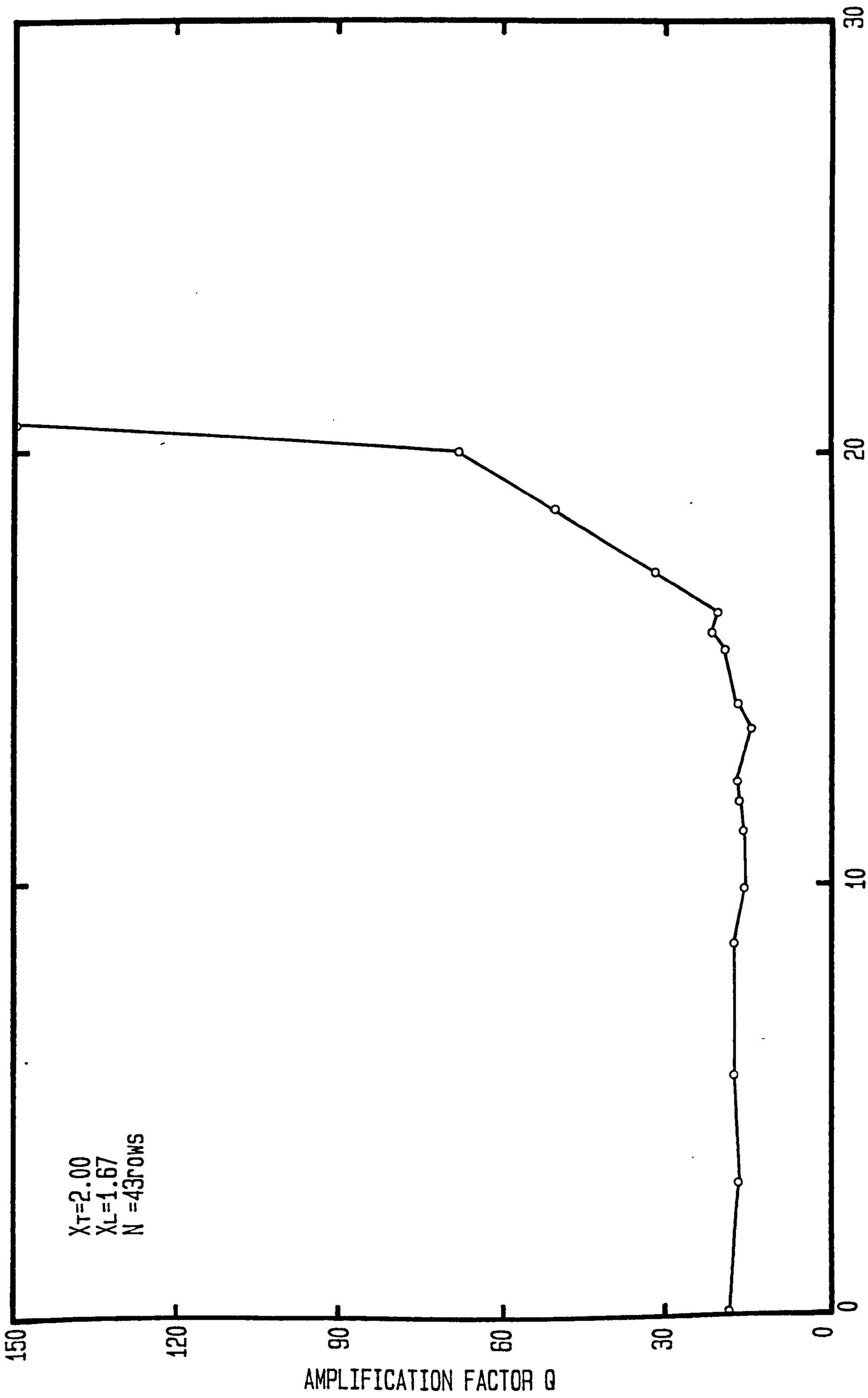

GRAPH OF AMPLIFICATION FACTOR AGAINST VELOCITY FOR THE 43row BANK

FIGURE 7.34

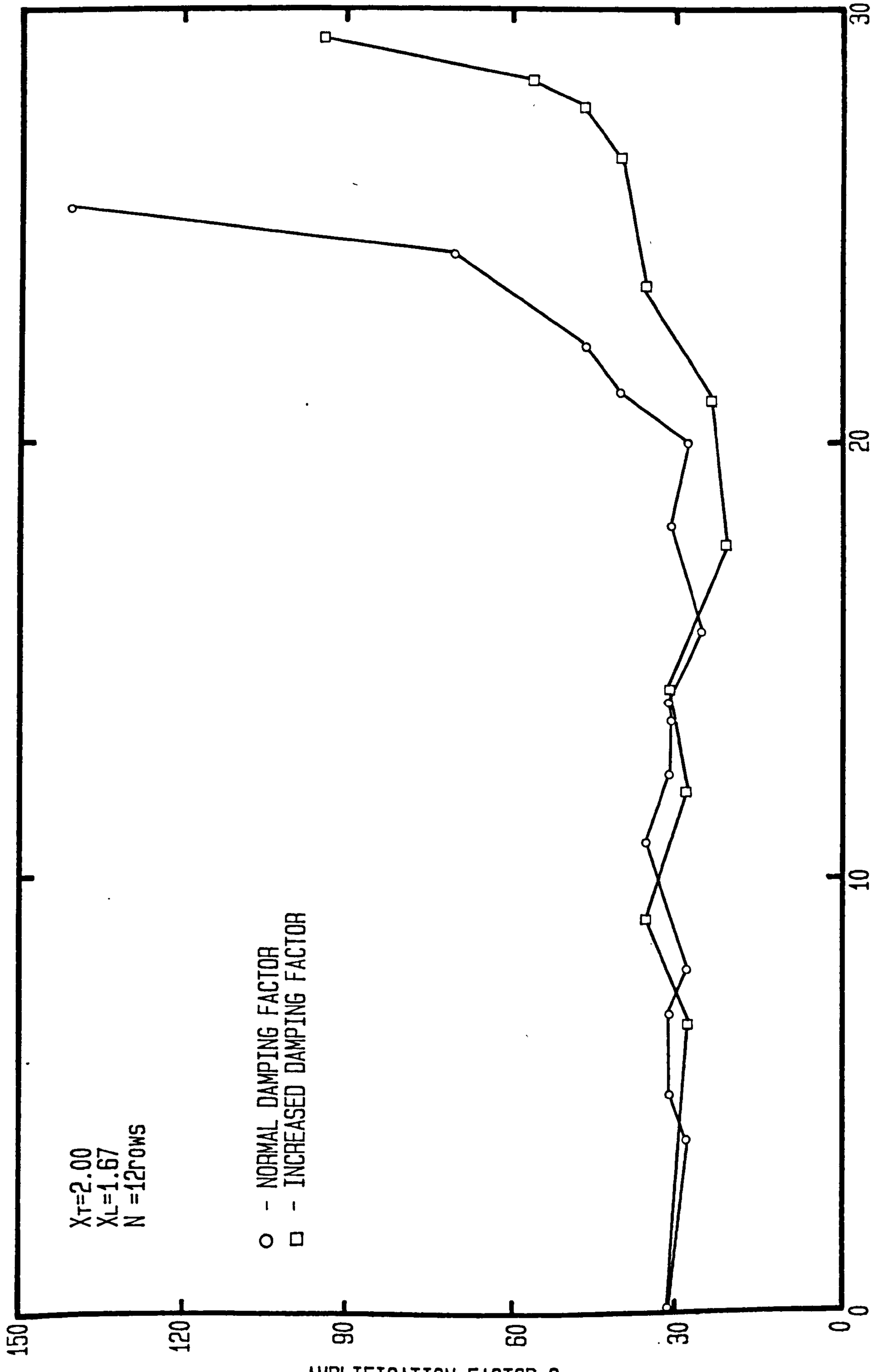

GRAPH OF AMPLIFICATION FACTOR AGAINST VELOCITY FOR THE 12row BANK

FIGURE 7.35

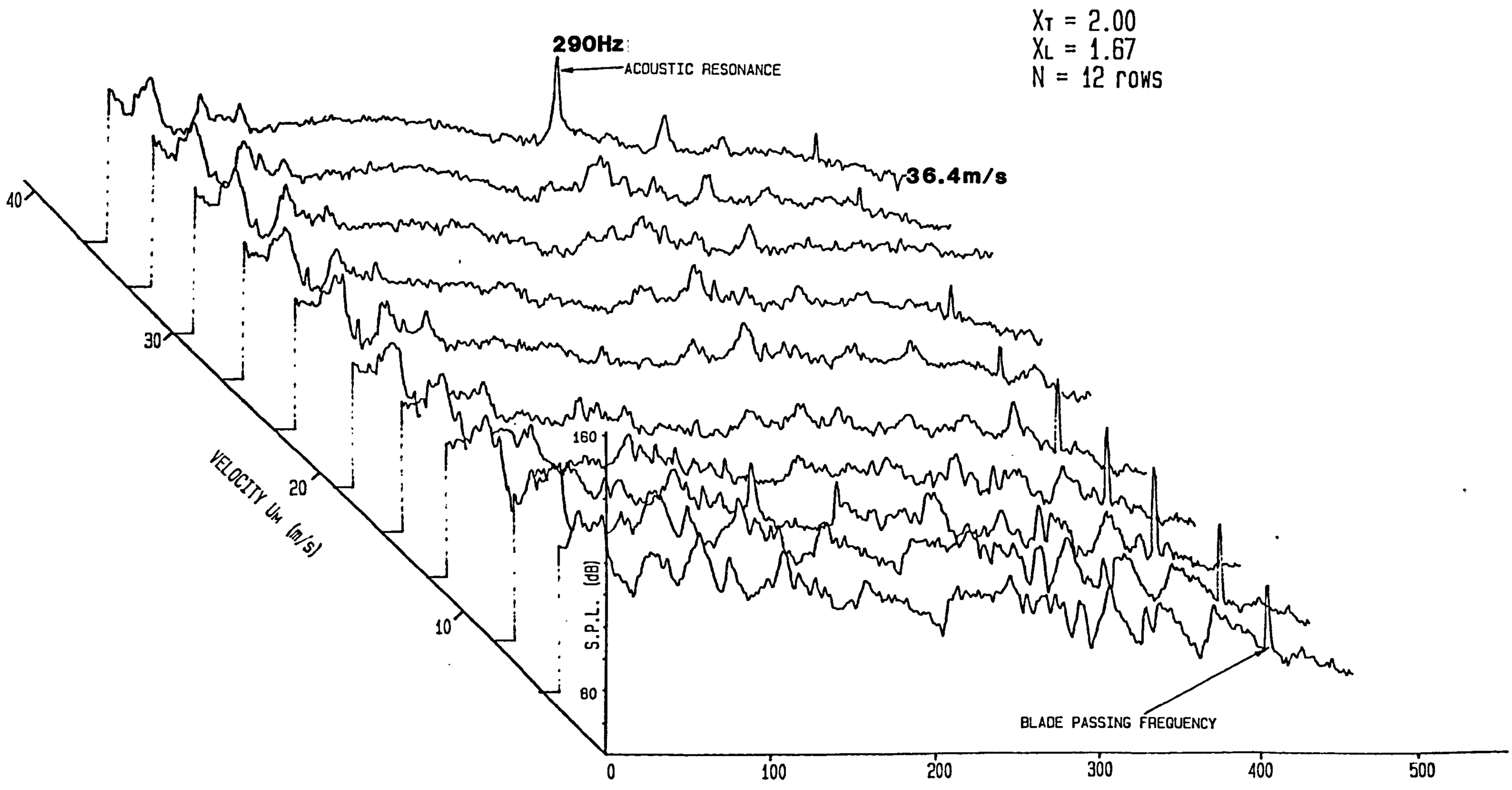

$X_T = 2.00$
$X_L = 1.67$
N = 12 rows

FIGURE 7.36

THREE DIMENSIONAL GRAPH OF VELOCITY/S.P.L./FREQUENCY

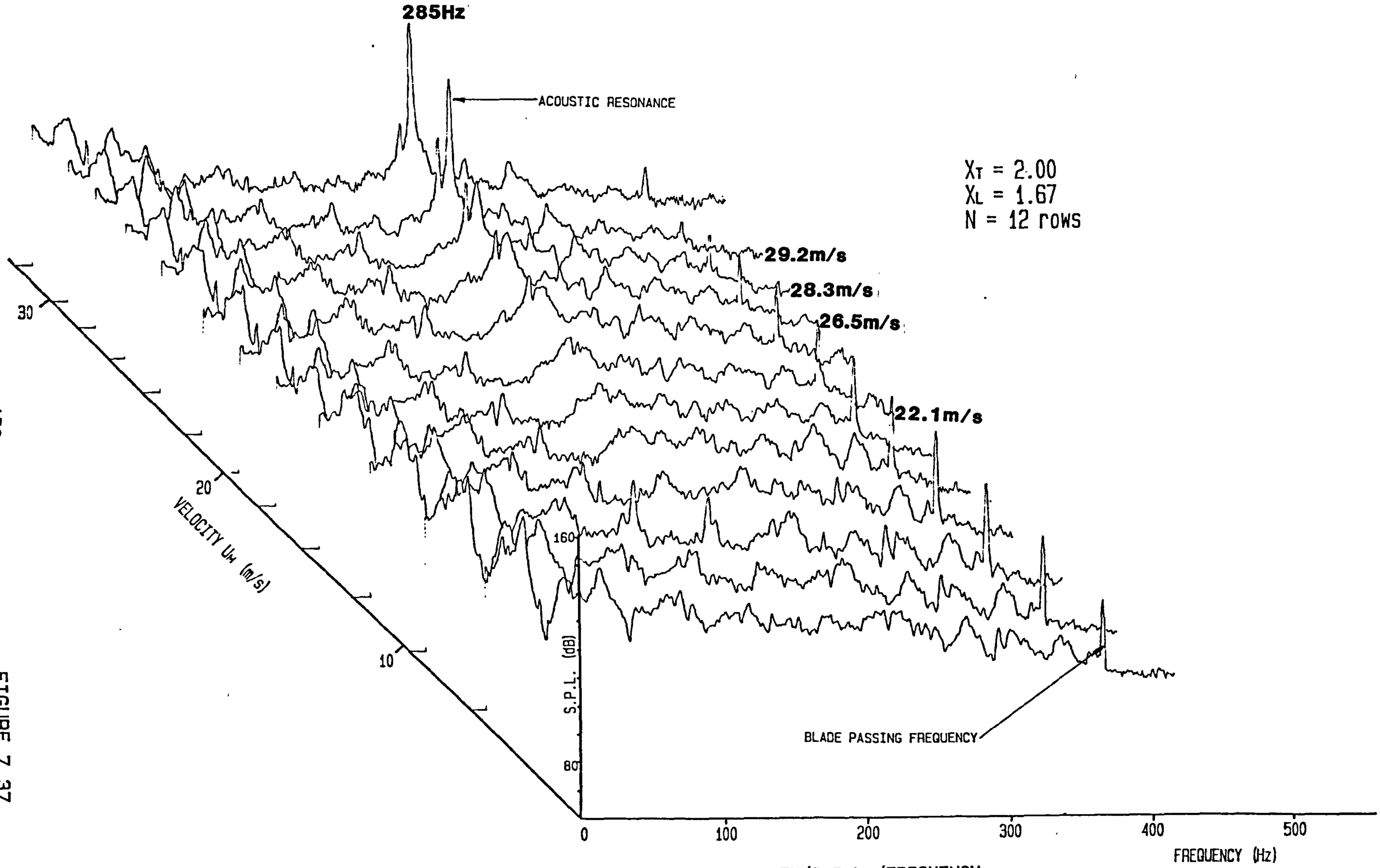

FIGURE 7.37 THREE DIMENSIONAL GRAPH OF VELOCITY/S.P.L./FREQUENCY

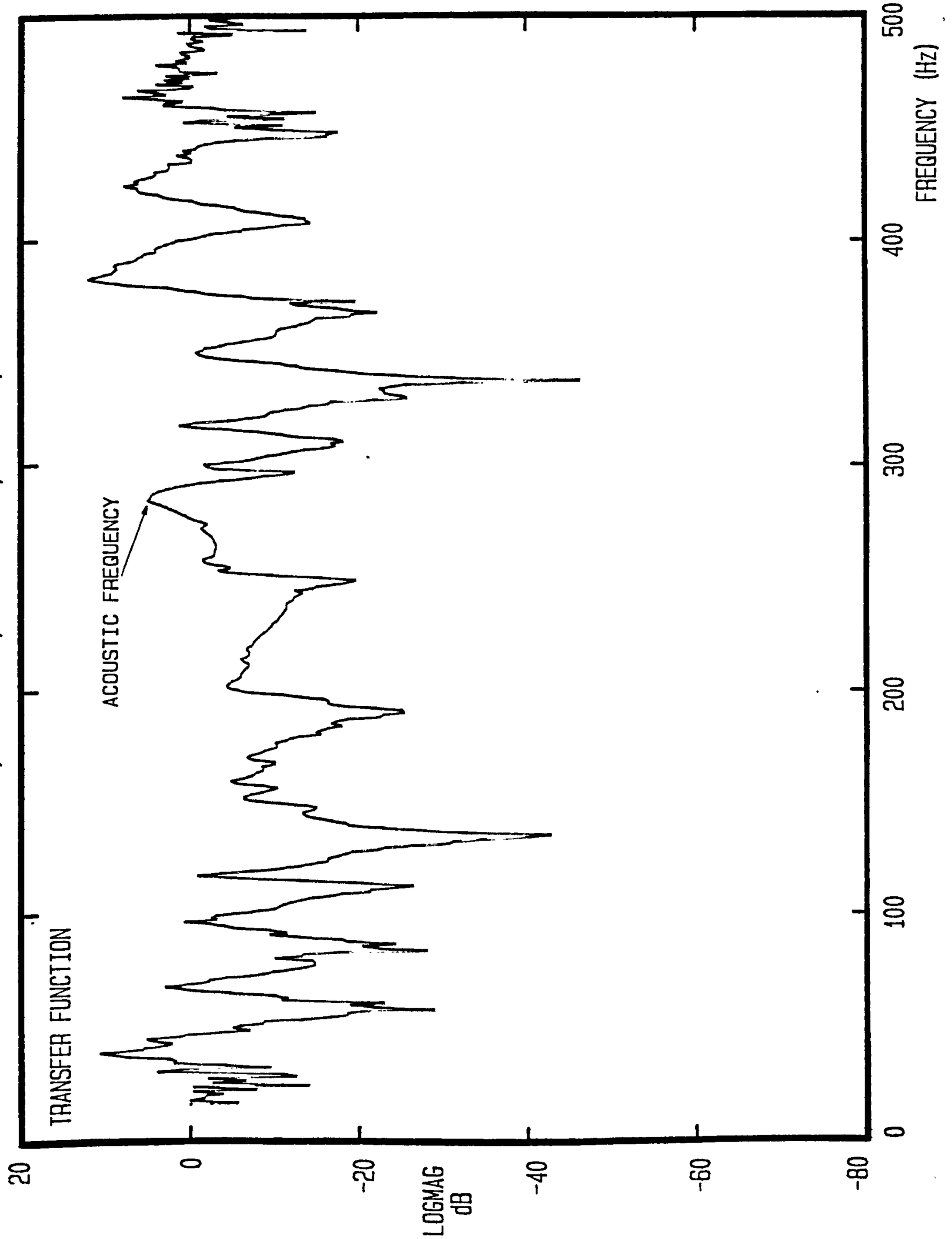
X_T = 2.0, X_L = 1.67, N = 12 rows, U = 0 m/s
TRANSFER FUNCTION
ACOUSTIC FREQUENCY
20
0
-20
-40
-60
-80
LOGMAG
dB
0
100
200
300
400
500
FREQUENCY (Hz)

FIGURE 7.38 [A]

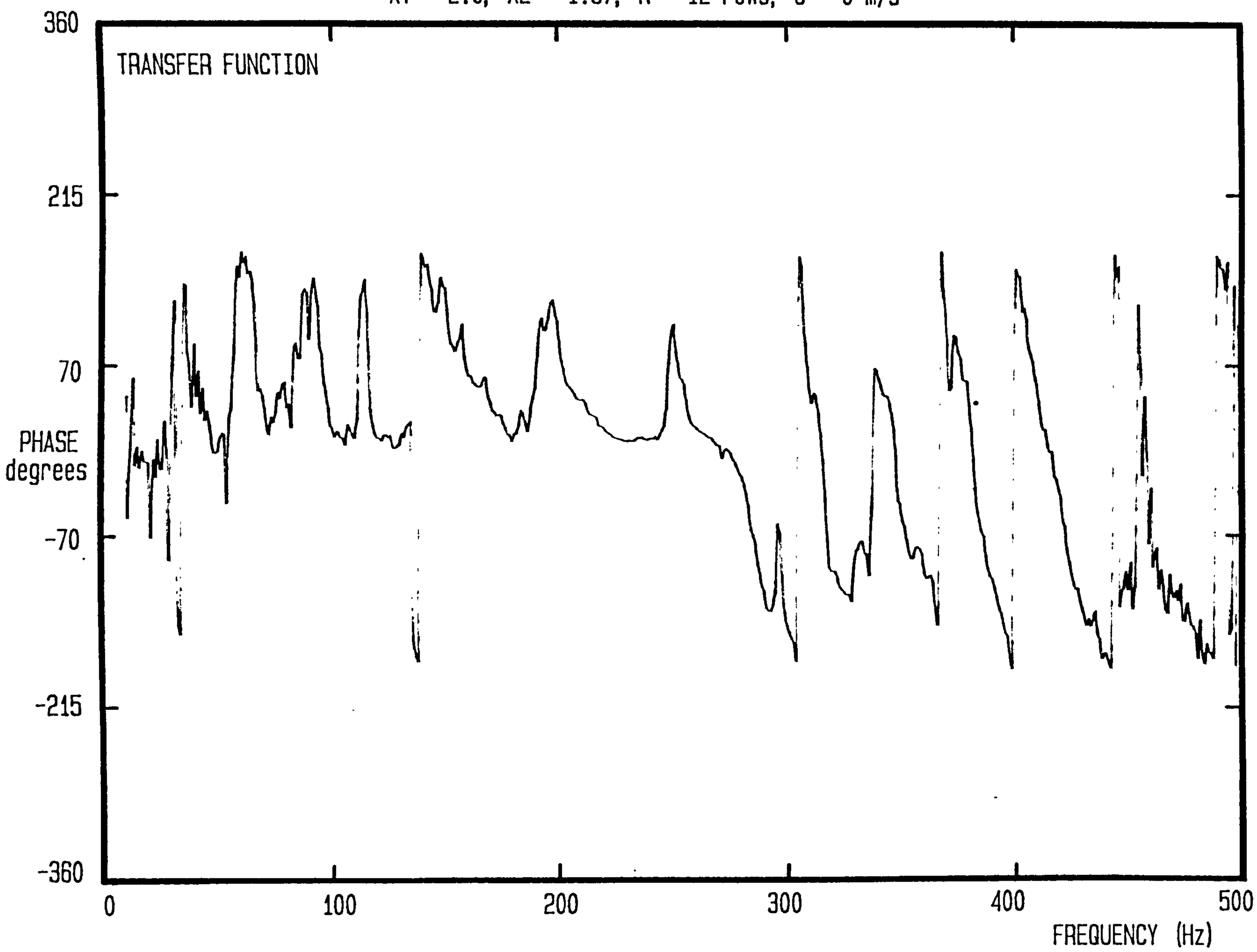
X_T = 2.0, X_L = 1.67, N = 12 rows, U = 0 m/s
TRANSFER FUNCTION
360
215
70
-70
-215
-360
PHASE
degrees
0
100
200
300
400
500
FREQUENCY (Hz)

FIGURE 7.38 [B]

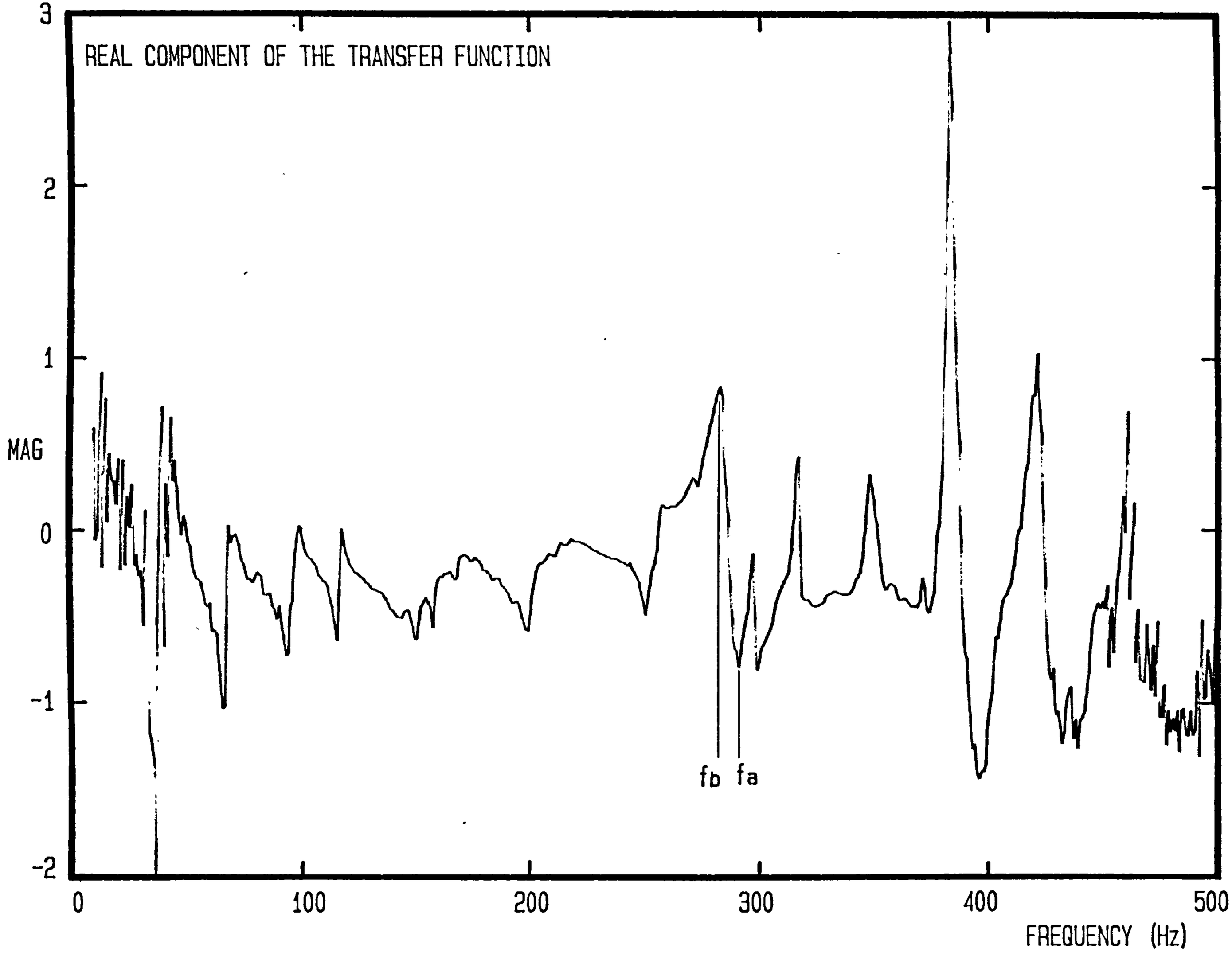
X_T = 2.0, X_L = 1.67, N = 12 rows, U = 0 m/s
REAL COMPONENT OF THE TRANSFER FUNCTION
MAG
3
2
1
0
-1
-2
0
100
200
300
400
500
FREQUENCY (Hz)
fb
fa

FIGURE 7.38 [C]

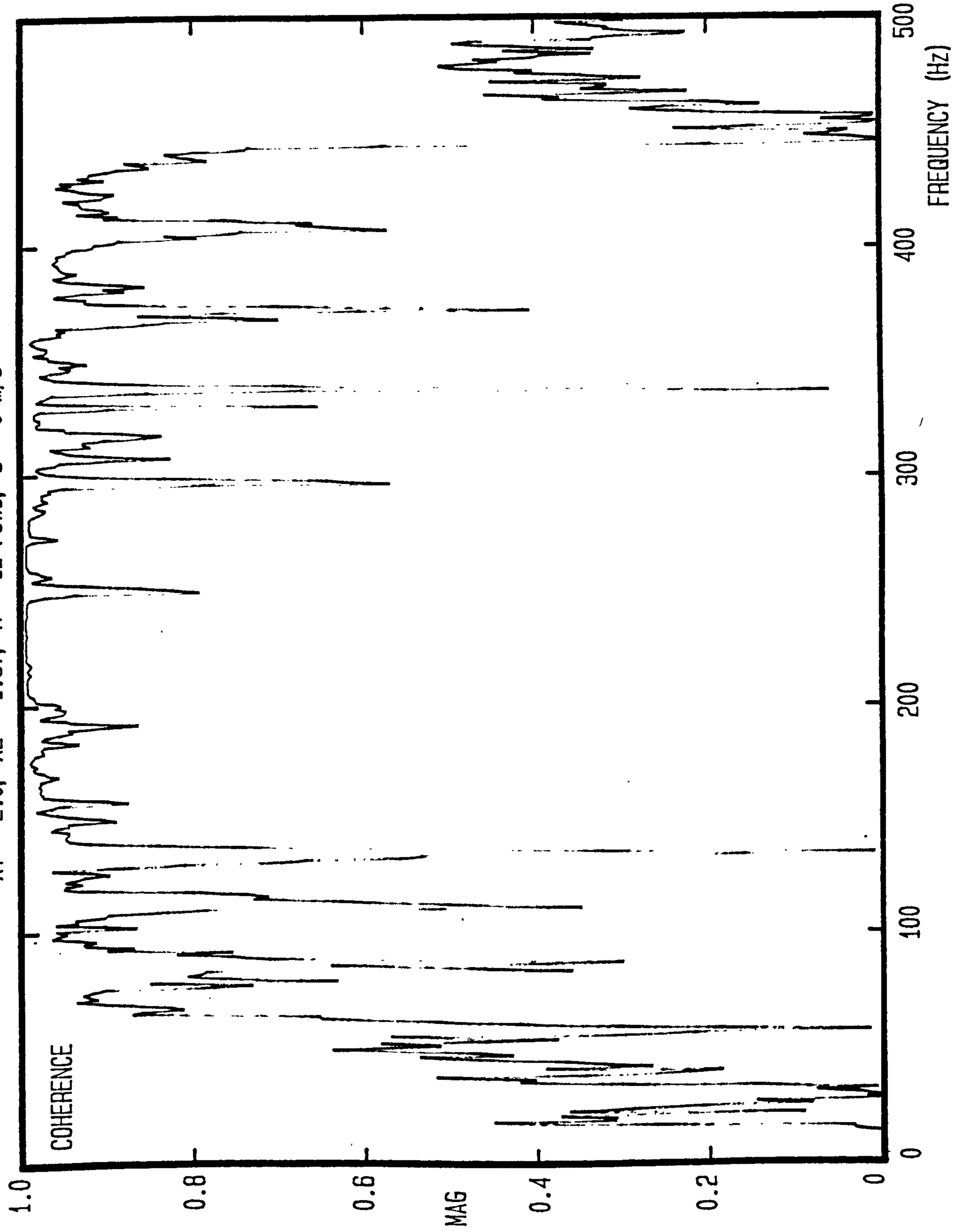
X_T = 2.0, X_L = 1.67, N = 12 rows, U = 0 m/s
COHERENCE
1.0
0.8
0.6
0.4
0.2
0
MAG
0
100
200
300
400
500
FREQUENCY (Hz)

FIGURE 7.38 [D]

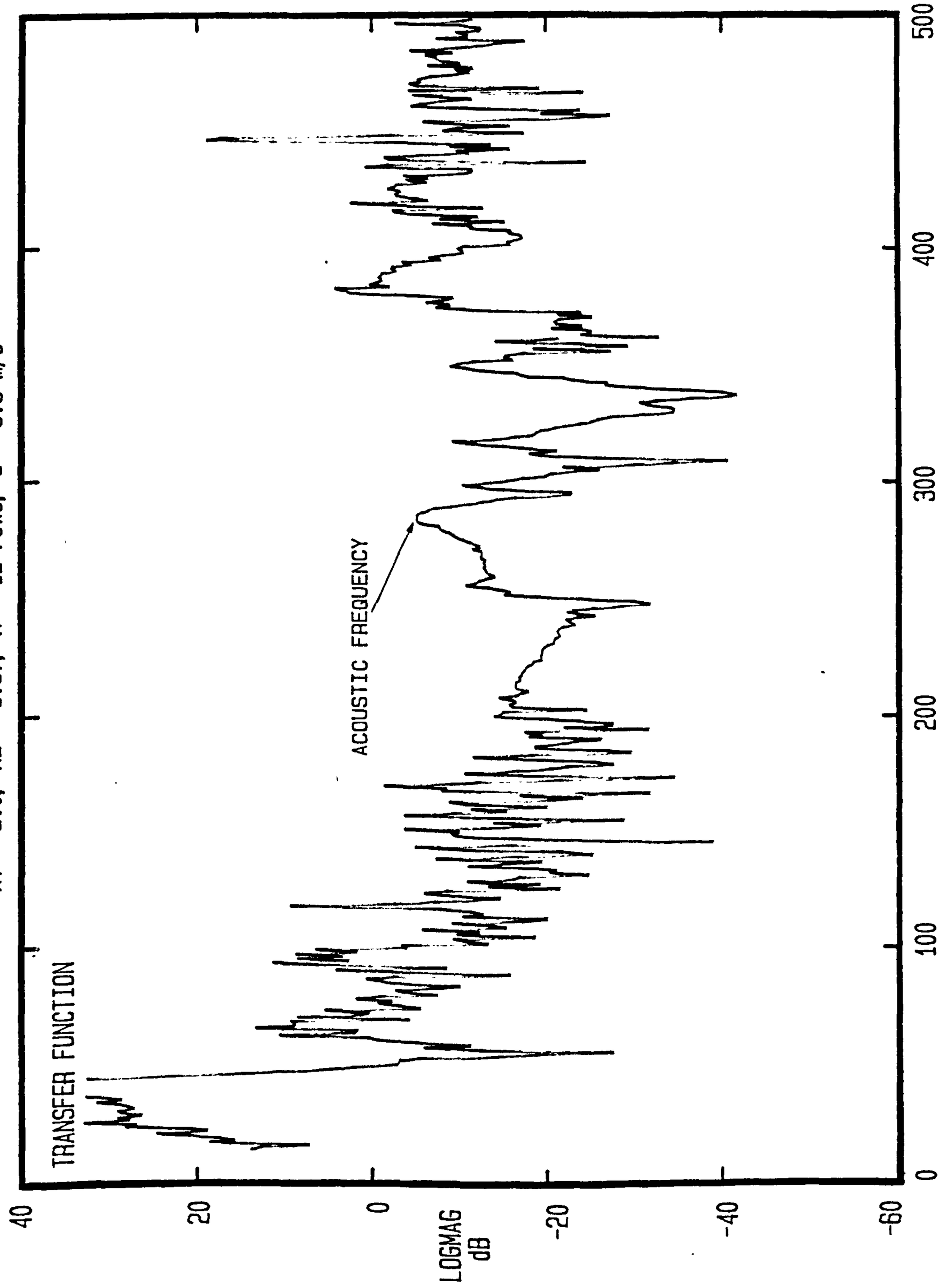
X_T = 2.0, X_L = 1.67, N = 12 rows, U = 3.9 m/s
TRANSFER FUNCTION
ACOUSTIC FREQUENCY
FREQUENCY (Hz)
LOGMAG dB
40
20
0
-20
-40
-60
500
400
300
200
100
0

FIGURE 7.39 [A]

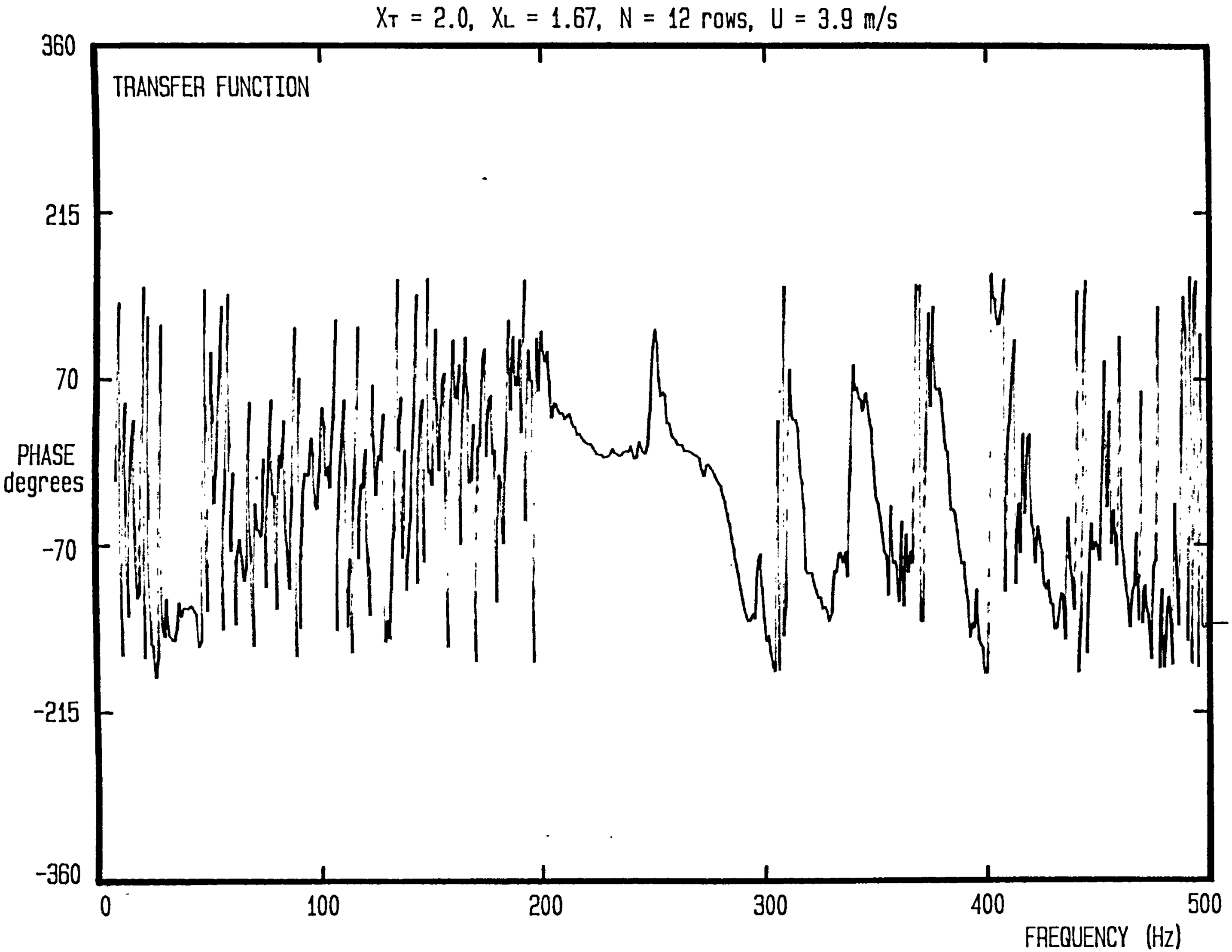
X_T = 2.0, X_L = 1.67, N = 12 rows, U = 3.9 m/s
TRANSFER FUNCTION
360
215
70
-70
-215
-360
PHASE
degrees
0
100
200
300
400
500
FREQUENCY (Hz)

FIGURE 7.39 [B]

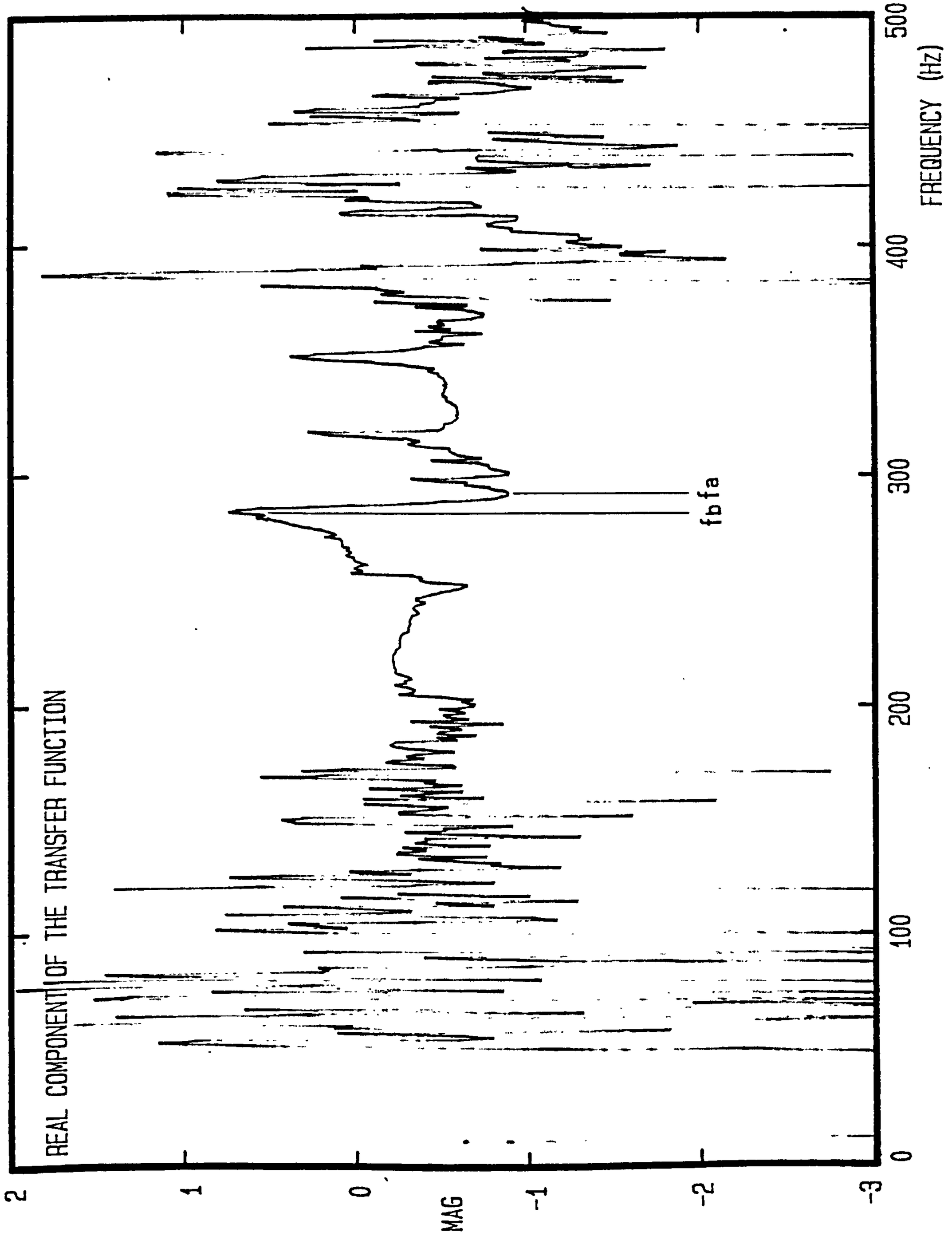
REAL COMPONENT OF THE TRANSFER FUNCTION
MAG
2
1
0
-1
-2
-3
0
100
200
300
400
500
FREQUENCY (Hz)
fb
fa
X_T = 2.0, X_L = 1.67, N = 12 rows, U = 3.9 m/s

FIGURE 7.39 [C]

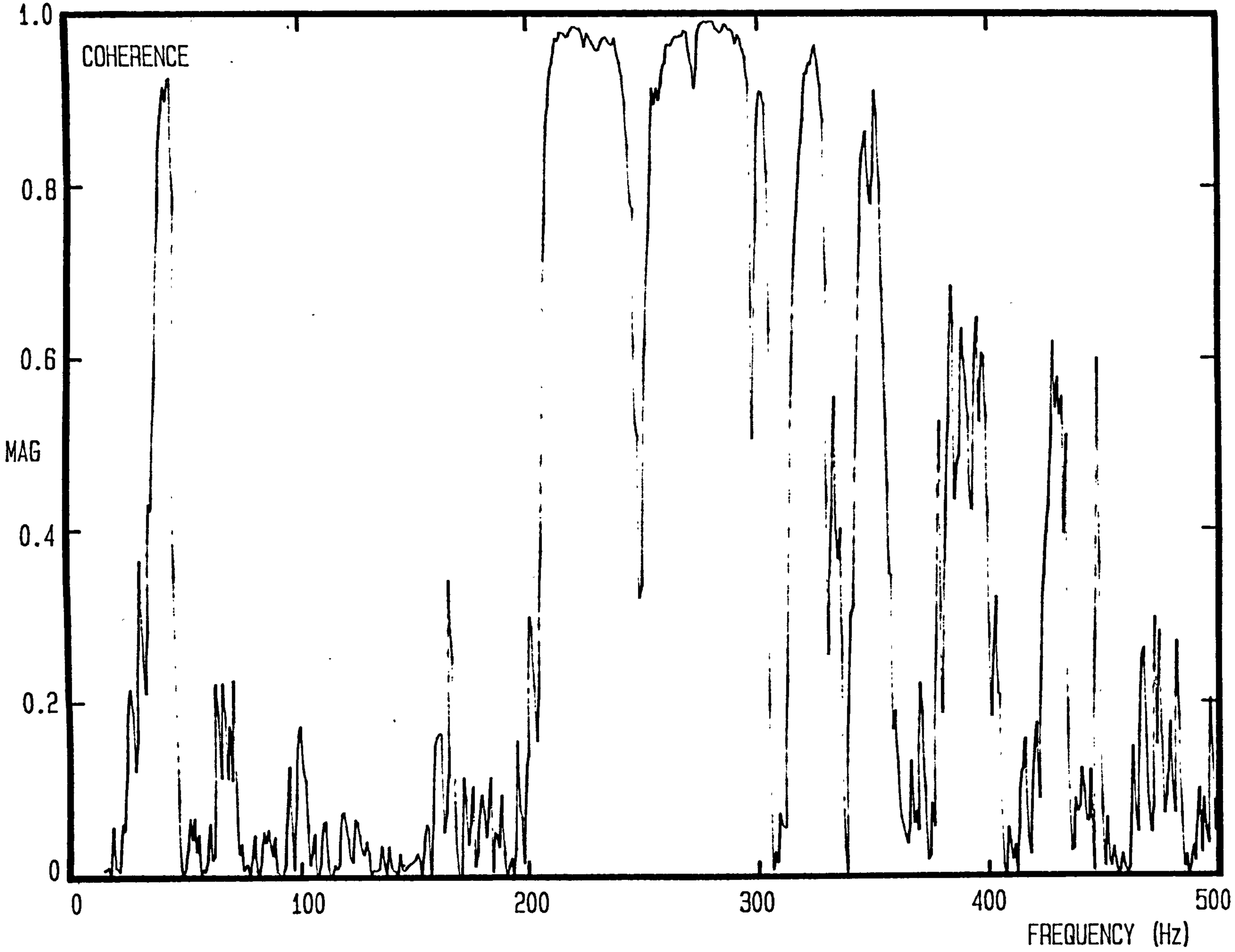
X_T = 2.0, X_L = 1.67, N = 12 rows, U = 3.9 m/s
COHERENCE
MAG
1.0
0.8
0.6
0.4
0.2
0
0
100
200
300
400
500
FREQUENCY (Hz)

FIGURE 7.39 [D]

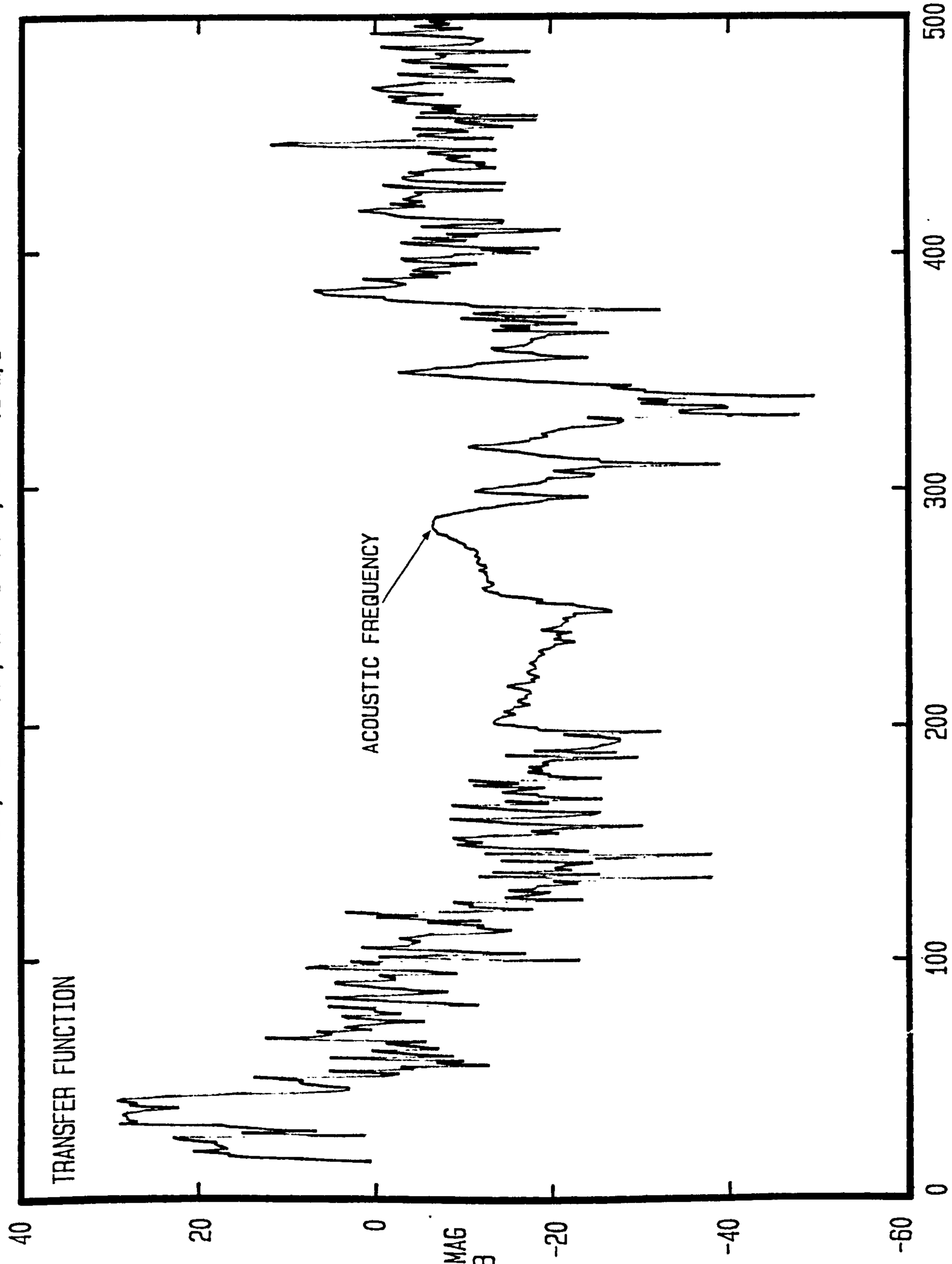
TRANSFER FUNCTION
ACOUSTIC FREQUENCY
X_T = 2.0, X_L = 1.67, N = 12 rows, U = 7.9 m/s
LOGMAG dB
40
20
0
-20
-40
-60
0
100
200
300
400
500
FREQUENCY (Hz)

FIGURE 7.40 [A]

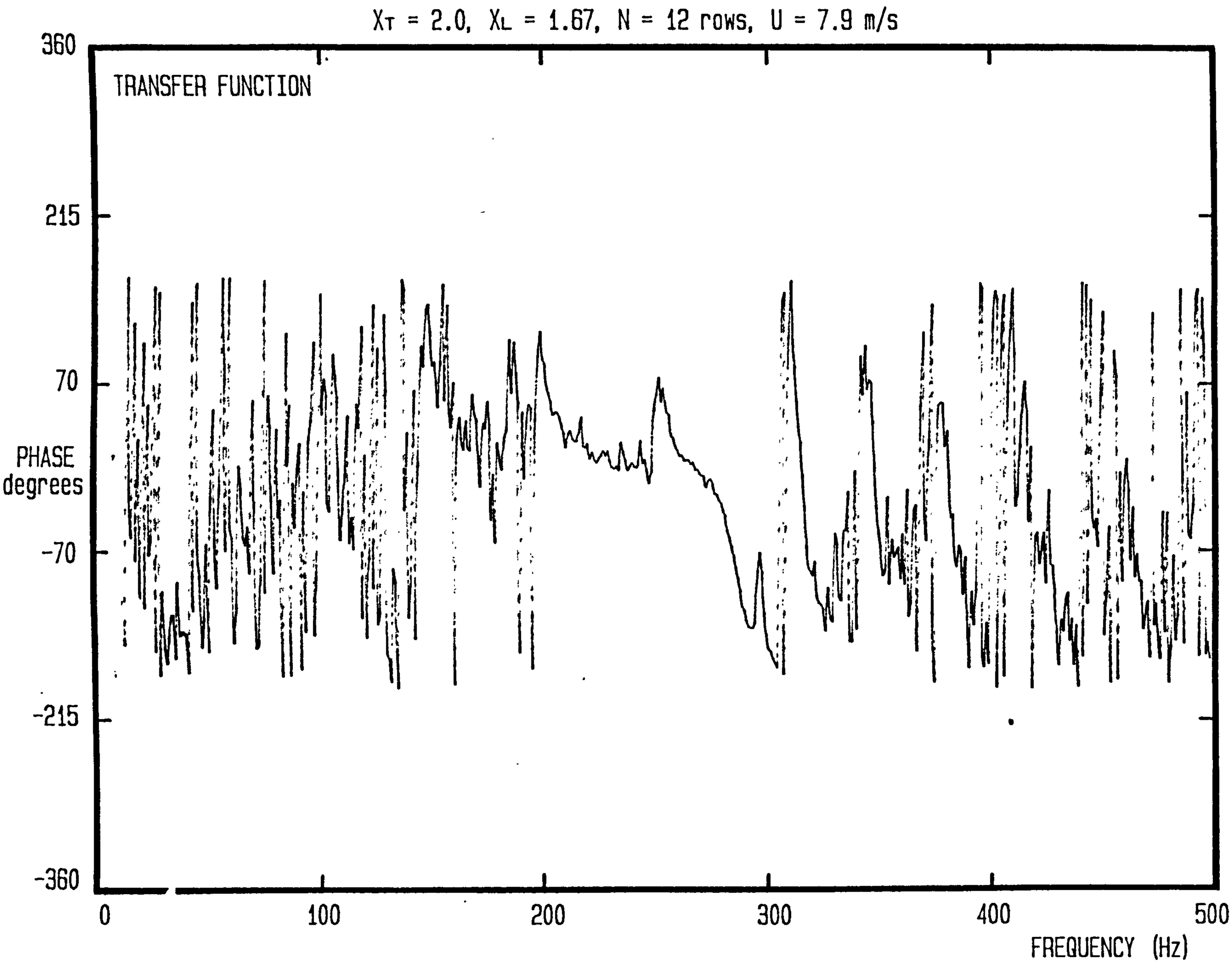
X_T = 2.0, X_L = 1.67, N = 12 rows, U = 7.9 m/s
TRANSFER FUNCTION
360
215
70
PHASE
degrees
-70
-215
-360
0
100
200
300
400
500
FREQUENCY (Hz)

FIGURE 7.40 [B]

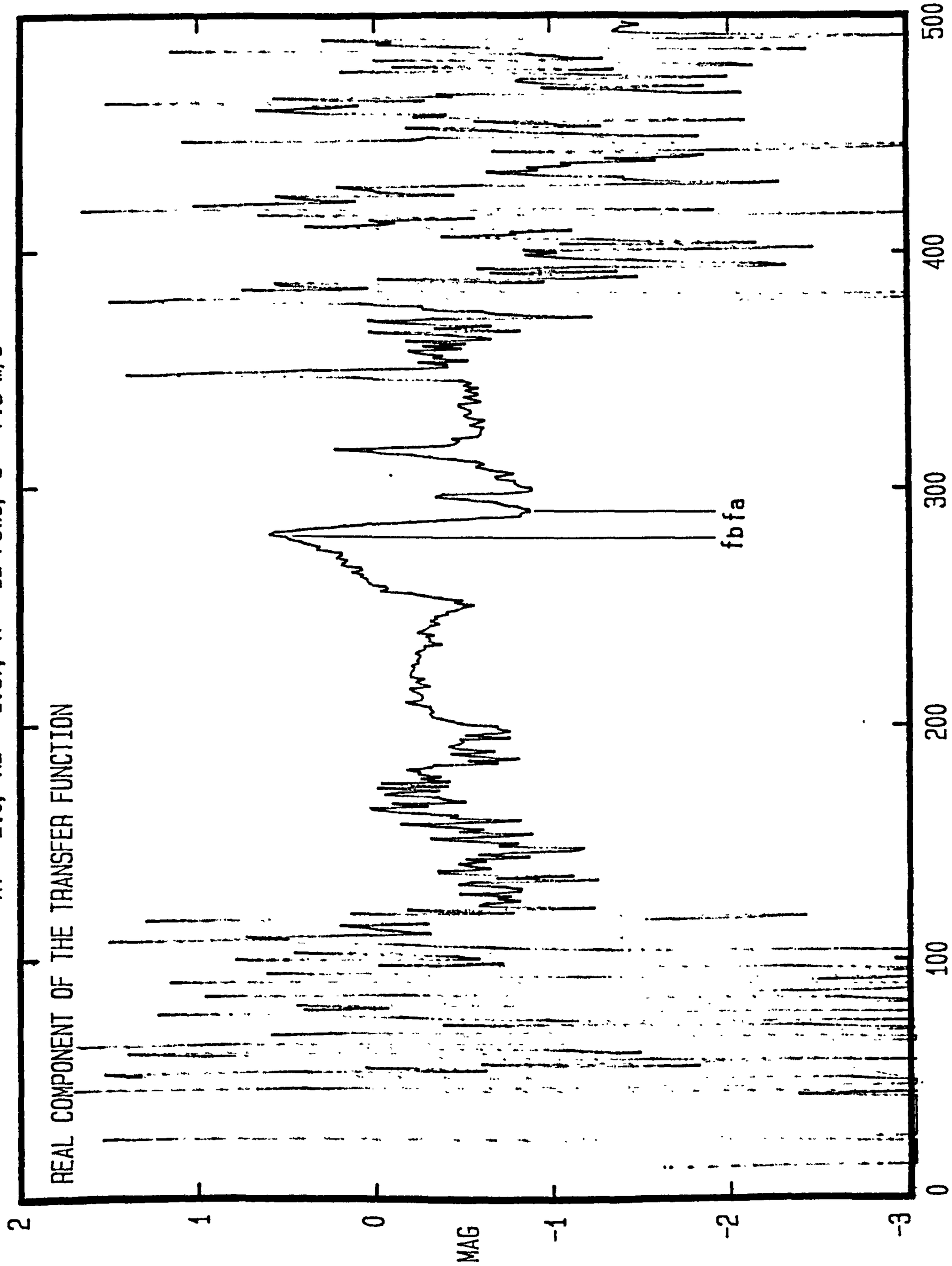
N = 12 rows, U = 7.9 m/s
X_T = 2.0, X_L = 1.67, N
REAL COMPONENT OF THE TRANSFER FUNCTION
2
1
0
MAG
-1
-2
-3
0
100
200
300
400
500
FREQUENCY (Hz)
fbfa

FIGURE 7.40 [C]

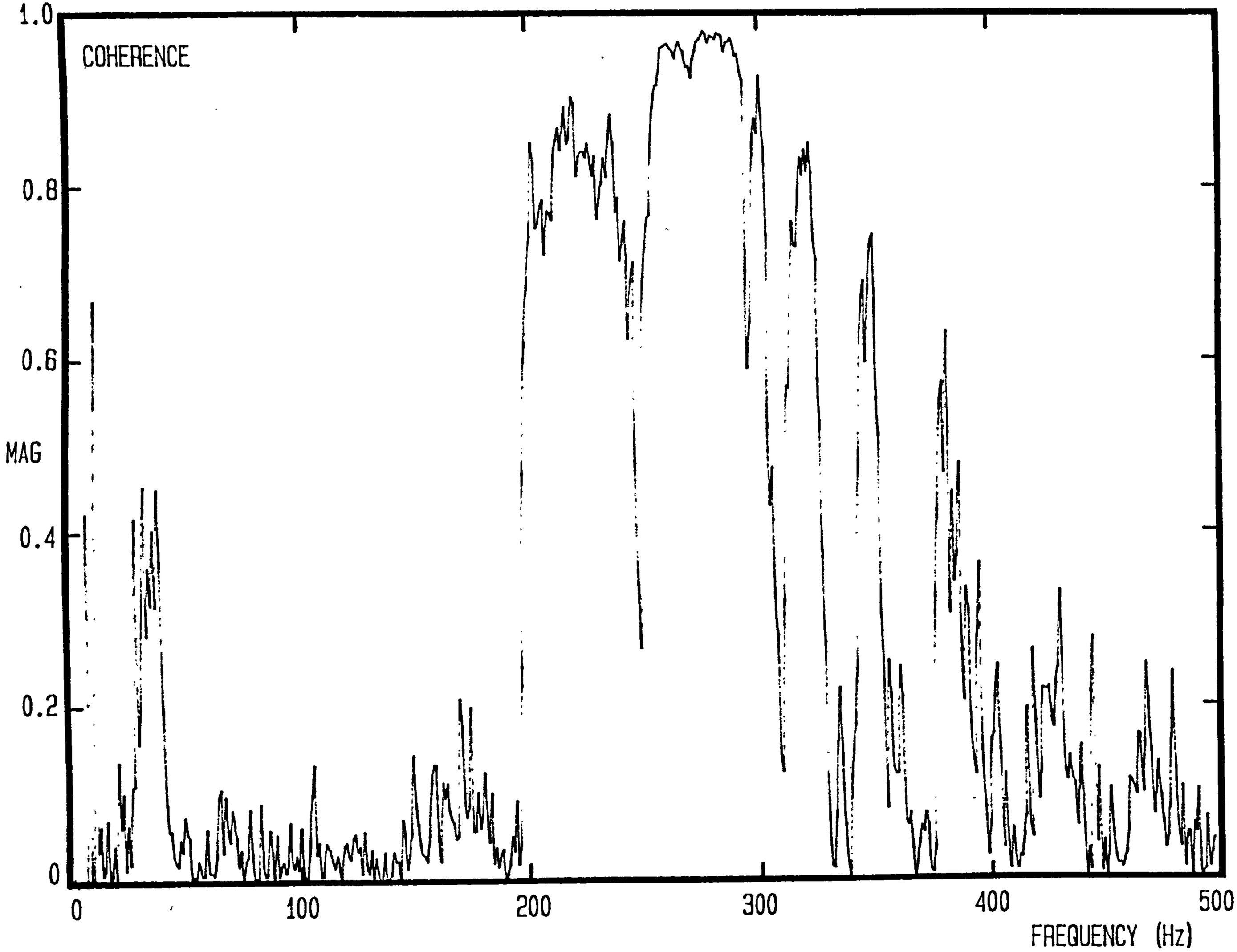
X_T = 2.0, X_L = 1.67, N = 12 rows, U = 7.9 m/s
COHERENCE
MAG
1.0
0.8
0.6
0.4
0.2
0
0
100
200
300
400
500
FREQUENCY (Hz)

FIGURE 7.40 [D]

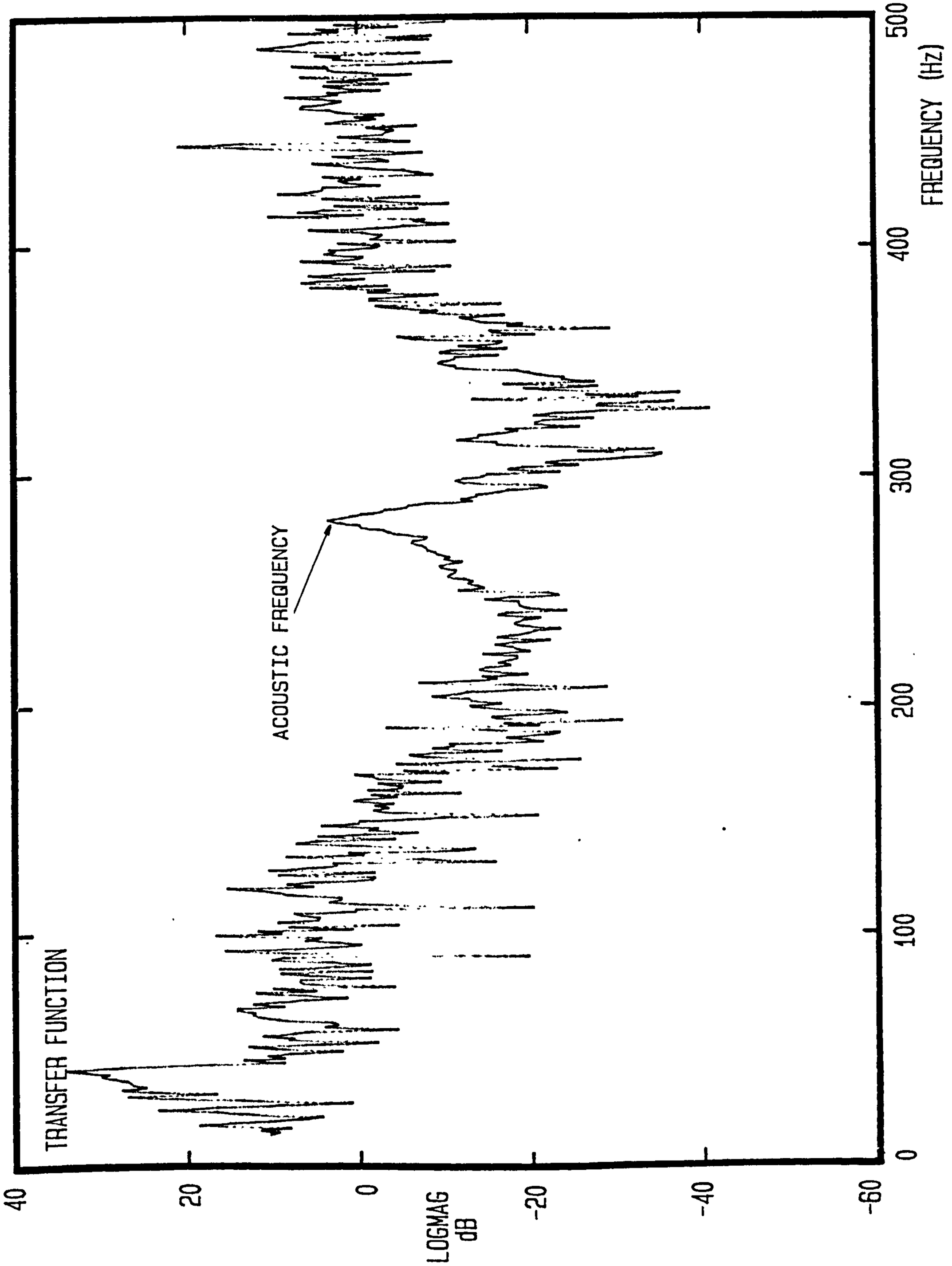
TRANSFER FUNCTION
LOGMAG dB
40
20
0
-20
-40
-60
0
100
200
300
400
500
FREQUENCY (Hz)
ACOUSTIC FREQUENCY
XT = 2.0, XL = 1.67, N = 12 ROWS, U = 11.1 m/S

FIGURE 7.41 [A]

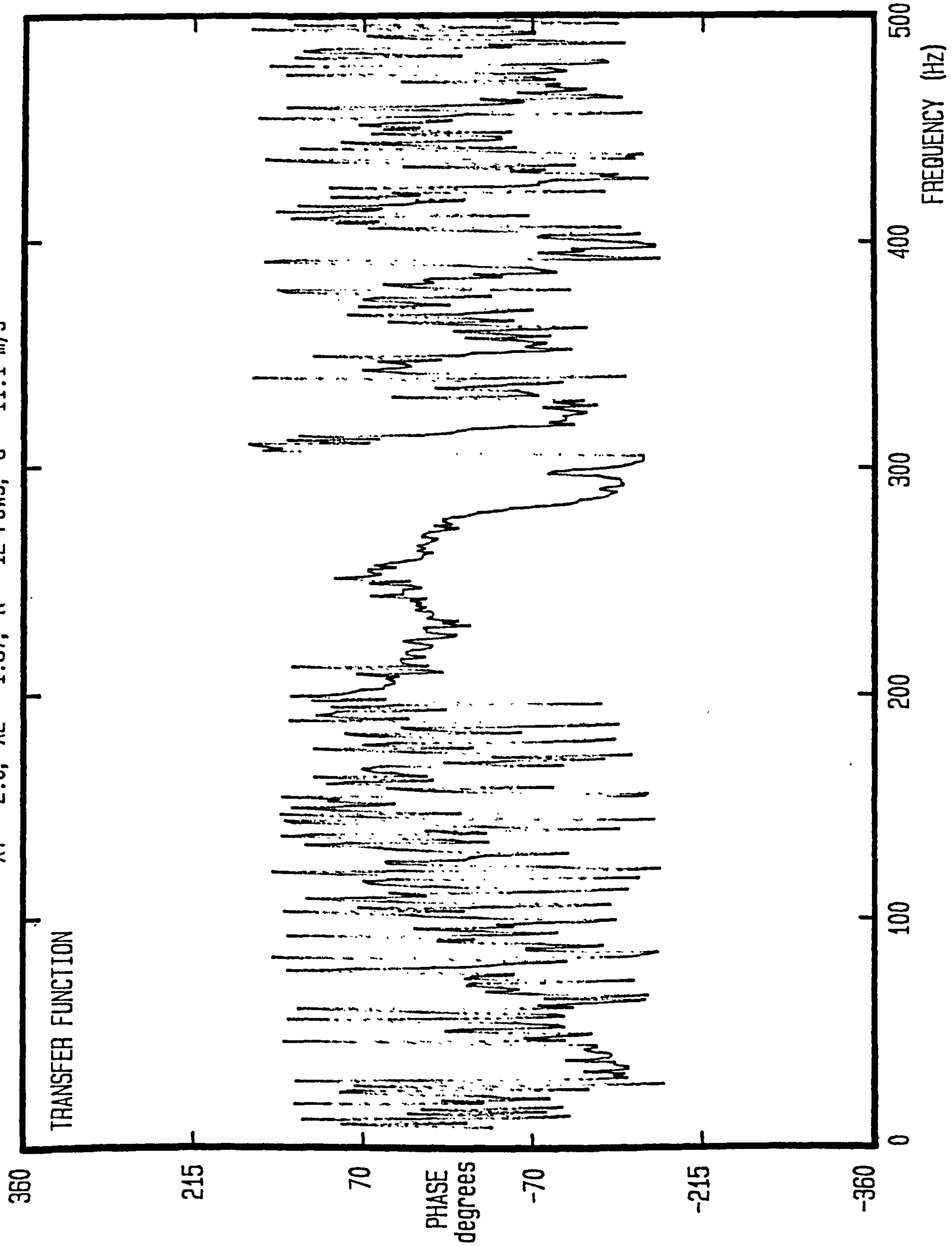
TRANSFER FUNCTION
X_T = 2.0, X_L = 1.67, N = 12 rows, U = 11.1 m/s
360
215
70
PHASE degrees
-70
-215
-360
0
100
200
300
400
500
FREQUENCY (Hz)

FIGURE 7.41 [B]

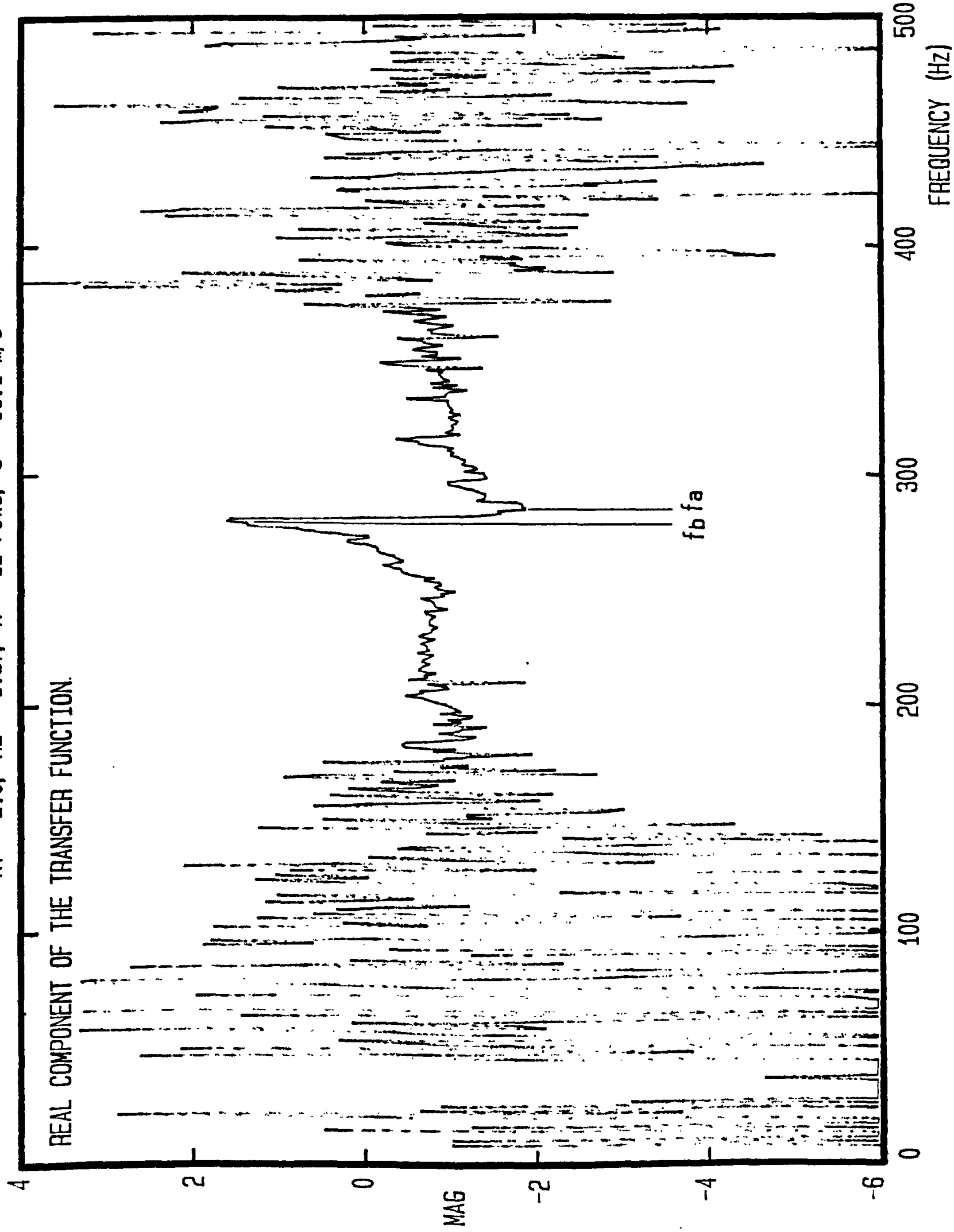
X_T = 2.0, X_L = 1.67, N = 12 rows, U = 11.1 m/S
REAL COMPONENT OF THE TRANSFER FUNCTION.
MAG
FREQUENCY (Hz)
fb fa
4
2
0
-2
-4
-6
500
400
300
200
100
0

FIGURE 7.41 [C]

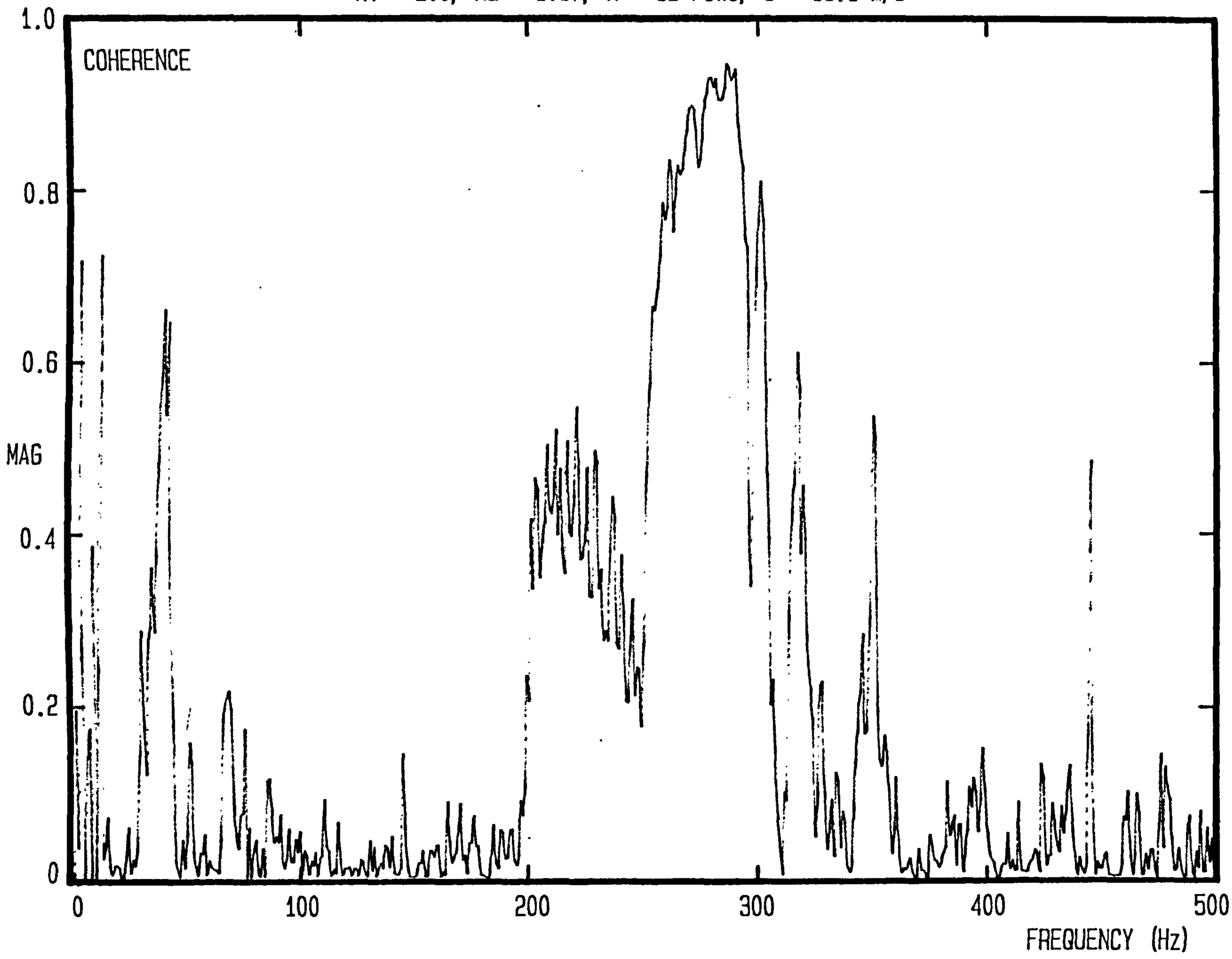
X_T = 2.0, X_L = 1.67, N = 12 rows, U = 11.1 m/s
COHERENCE
MAG
1.0
0.8
0.6
0.4
0.2
0
0
100
200
300
400
500
FREQUENCY (Hz)

FIGURE 7.41 [D]

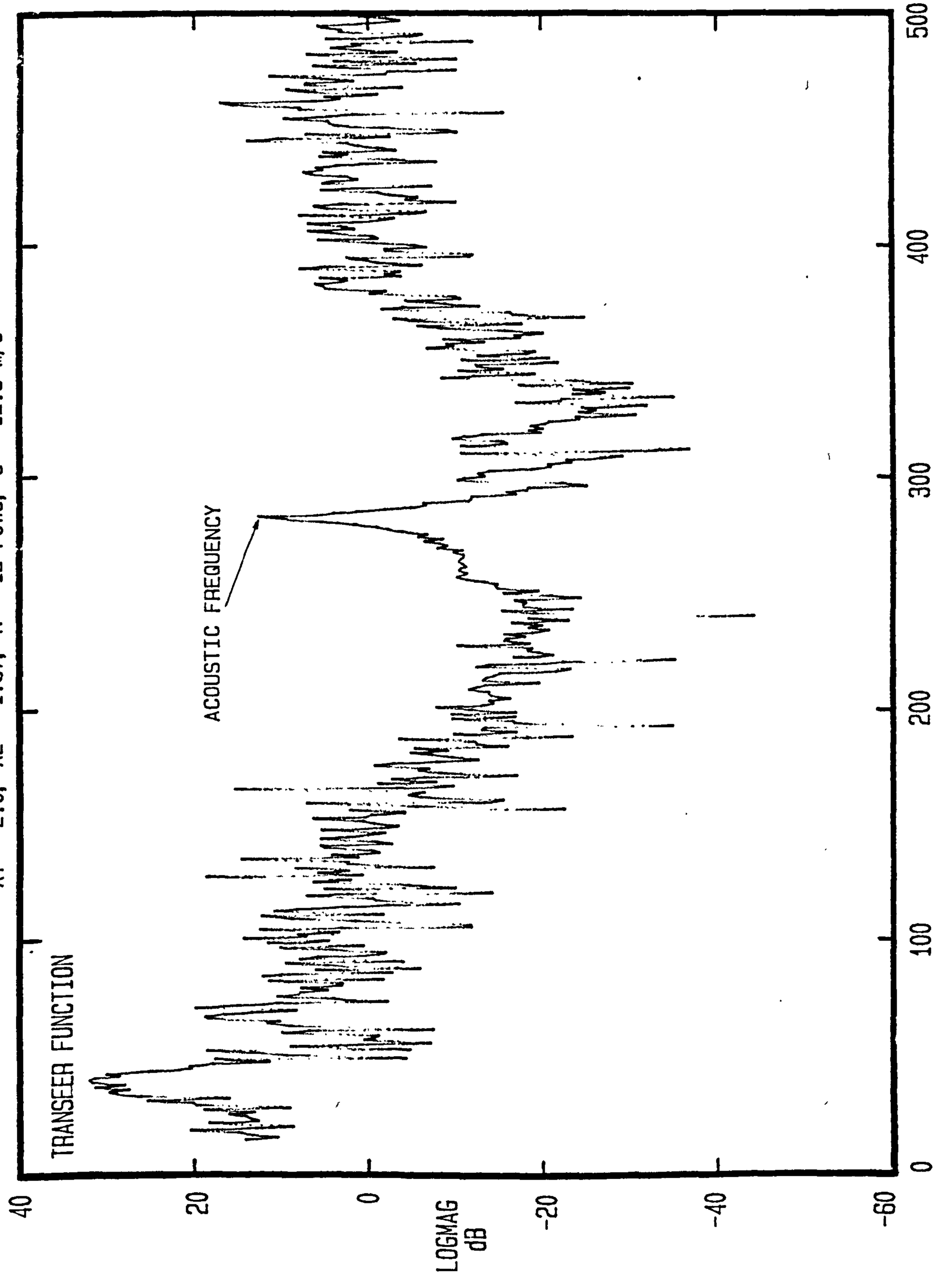
TRANSFER FUNCTION
ACOUSTIC FREQUENCY
X_T = 2.0, X_L = 1.67, N = 12 rows, U = 12.6 m/s
LOGMAG dB
40
20
0
-20
-40
-60
0
100
200
300
400
500
FREQUENCY (Hz)

FIGURE 7.42 [A]

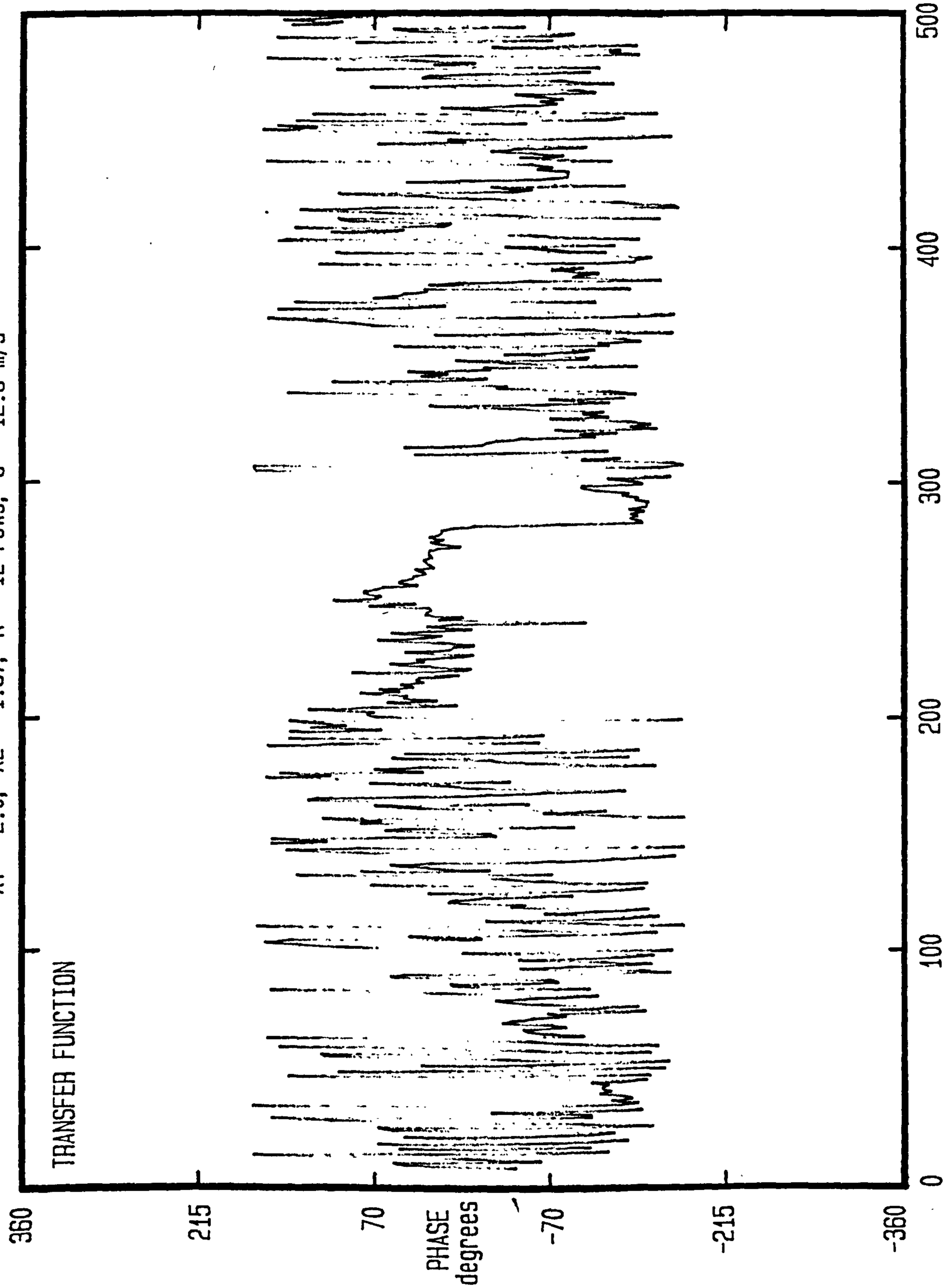
X_T = 2.0, X_L = 1.67, N = 12 rows, U = 12.6 m/s
TRANSFER FUNCTION
500
400
300
200
100
0
FREQUENCY (Hz)
360
215
70
PHASE degrees
-70
-215
-360

FIGURE 7.42 [B]

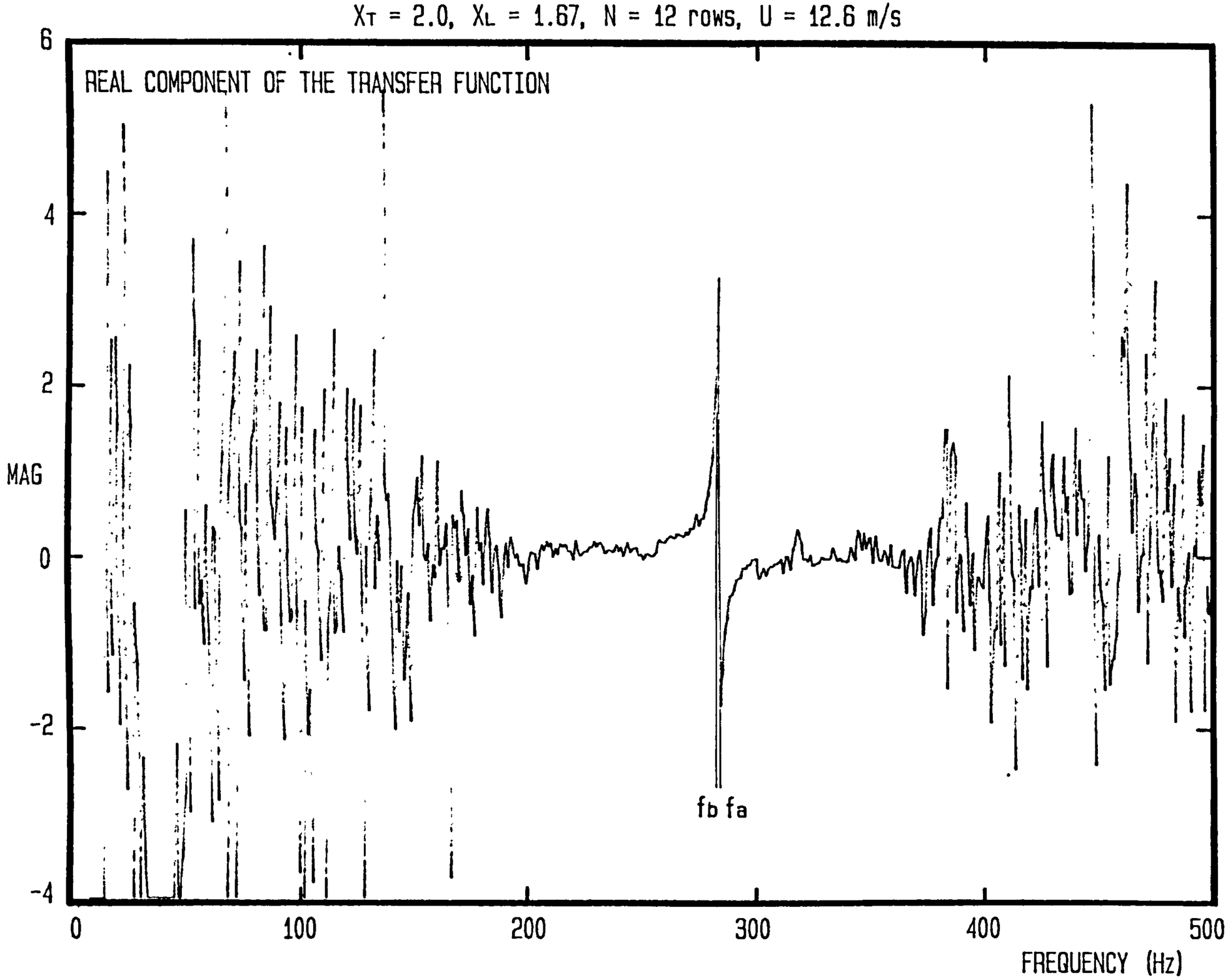
X_T = 2.0, X_L = 1.67, N = 12 rows, U = 12.6 m/s
REAL COMPONENT OF THE TRANSFER FUNCTION
MAG
6
4
2
0
-2
-4
0
100
200
300
400
500
FREQUENCY (Hz)
fb fa

FIGURE 7.42 [C]

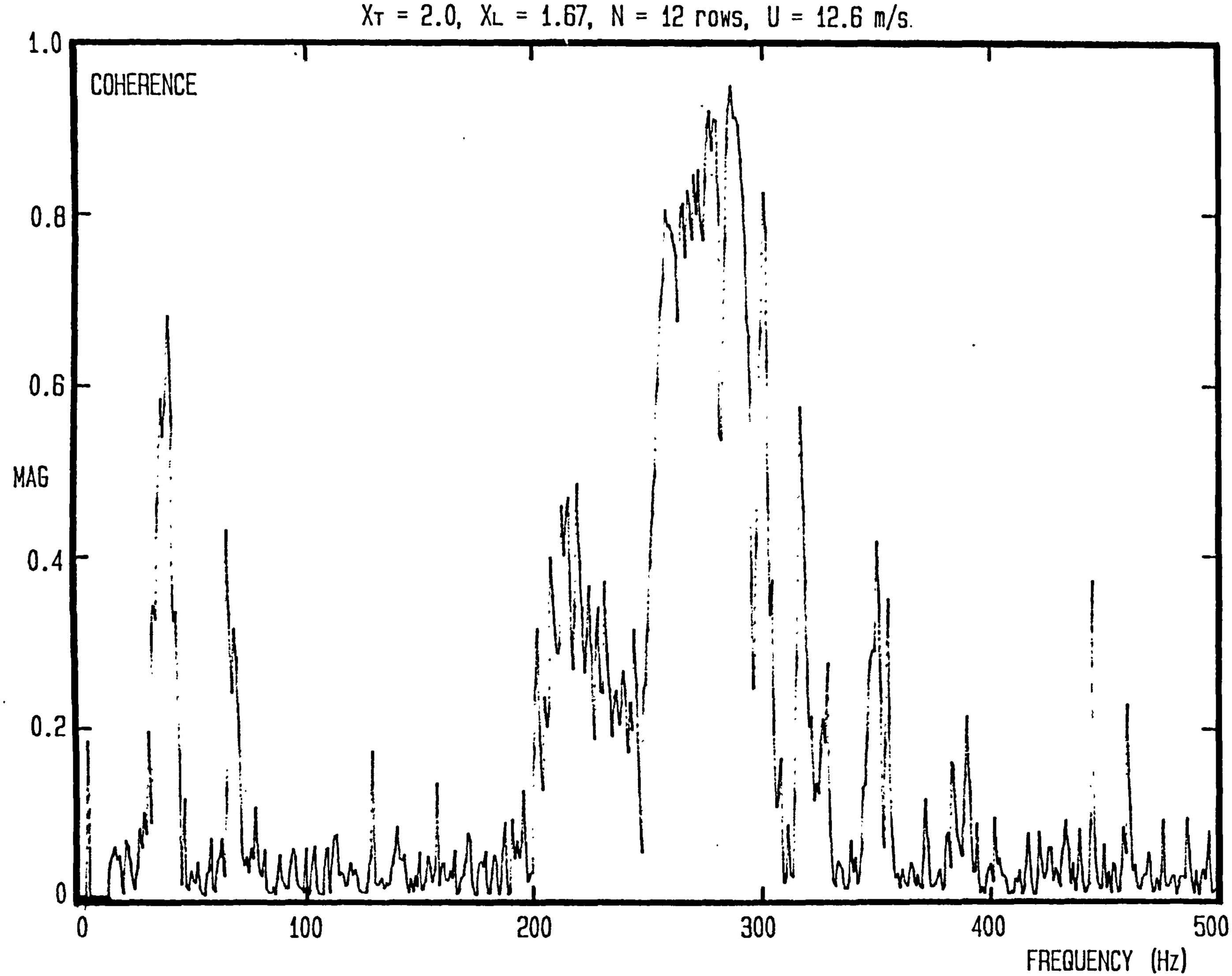
X_T = 2.0, X_L = 1.67, N = 12 rows, U = 12.6 m/s.
COHERENCE
MAG
1.0
0.8
0.6
0.4
0.2
0
0
100
200
300
400
500
FREQUENCY (Hz)

FIGURE 7.42 [D]

8.0 MODEL OF THE ACOUSTIC RESONANCE PHENOMENA IN IN-LINE TUBE ARRAYS

8.1 INTRODUCTION

In the literature survey, the experimental findings from various authors concerning the acoustic phenomena, were described. Using this information it was shown that the existing theories are inadequate in accounting for the observed behaviour. The following chapter describes the application of a more promising model which was originally outlined in ref. (B15).

8.2 PHYSICAL MODEL

Consider the situation illustrated in figure 8.1. In its undisturbed state the flow through an in-line tube bank may be supposed to separate in a uniform manner from the downstream side of each tube. However in the presence of an acoustic standing wave some interaction of the acoustic wave with the separation process may be reasonably expected. A possible instantaneous picture is shown in figure 8.1. The nature of this interaction is likely to be complex and therefore cannot be fully analysed within the scope of the present study. As a starting point, suppose that the separation point is rotated upstream and downstream on opposite sides of the tube by the acoustic pressure gradient/

gradient transverse to the flow. This will, in effect, deflect the flow leaving the tube by an angle θ.This angle θ may be supposed, by dimensional analysis, to be a function of the following:

$$\theta = f(\rho,\ d,\ U_m,\ \mu,\ f,\ l_t,\ \frac{\delta P}{\delta y},\ P)$$

therefore $f(\rho,\ d,\ U_m,\ \mu,\ f,\ l_t,\ \frac{\delta P}{\delta y},\ P,\ \theta) = 0$

using the Buckingham Pi Method of dimensional analysis:

Number of parameters = 9

Primary dimensions = 3

which are M = mass (kg)

L = length (m)

T = time (s)

therefore there are 9-3 = 6 Pi terms.

Shall select ρ, d and U as the three variables which between them contain M, L and T.

$\pi = \rho^a\ d^b\ U_m^c\ \mu$

i.e. $M^\circ L^\circ T^\circ = (\frac{M}{L^3})^a (L)^b (\frac{L}{T})^c \frac{M}{LT}$

M $0 = a + 1$ $\quad a = -1$

T $0 = -C - 1$ $\quad C = -1$

L $0 = -3a + b + c - 1$ $\quad B = -1$

$$\pi = \frac{\mu}{\rho d U_m}$$

$\pi_2 = \rho^a\ d^b\ U_m^c\ f$

i.e. $M^\circ L^\circ T^\circ = (\frac{M}{L^3})^a (L)^b (\frac{L}{T})^c \frac{1}{T}$

M $0 = a$

T $0 = -C - 1$ $\quad c = -1$

L $0 = -3a + b + c$

$b = 1$

$$\pi_2 = \frac{fd}{U_m}$$

$\pi_3 = \rho^a\ d^b\ U_m^c\ l_t$

i.e. $M^\circ L^\circ T^\circ = (\frac{M}{L^3})^a (L)^b\ (\frac{L}{T})^c\ L$

M $\quad 0 = a$

T $\quad 0 = -C$

L $\quad 0 = -3a + b + C + 1$

$b = -1$

$\pi_3 = \frac{l_t}{d}$

$\pi_4 = \rho^a\ d^b\ U_m^c\ \frac{\delta P}{\delta y}$

i.e. $M^\circ L^\circ T^\circ = (\frac{M}{L^3})^a (L)^b\ (\frac{L}{T})^c\ \frac{M}{L^2 T^2}$

M $\quad 0 = a + 1 \quad a = -1$

T $\quad 0 = -c - 2 \quad C = -2$

L $\quad 0 = -3a + b + C - 2$

$b = 1$

$\pi_4 = \frac{d}{\rho U_m^2}\ \frac{\delta P}{\delta y}$

$\pi_5 = \rho^a\ d^b\ U_m^c\ P$

i.e. $M^\circ L^\circ T^\circ = (\frac{M}{L^3})^a (L)^b\ (\frac{L}{T})^c\ \frac{M}{LT^2}$

M $\quad 0 = a + 1 \quad a = -1$

T $\quad 0 = -C - 2 \quad C = -2$

L $\quad 0 = -3a + b + C - 1$

$b = 0$

$\pi_5 = \frac{P}{\rho U_m^2}$

$\pi_6 = \rho^a\ d^b\ U_m^c\ \theta$

i.e. $M^\circ L^\circ T^\circ = (\frac{M}{L^3})^a (L)^b\ (\frac{L}{T})^c$

M $\quad 0 = a$

T $\quad 0 = -C$

L $\quad 0 = -3a + b + C$

$b = 0$

$\pi_6 = \theta$

$\pi_1 = \frac{\mu}{\rho d U_m} = \frac{1}{Re}$

$\pi_2 = \frac{fd}{U_m} = S = \frac{1}{V_R}$

$\pi_3 = \frac{l_t}{d} = X_T$

$\pi_4 = \frac{d}{\rho U_m^2}\ \frac{\delta P}{\delta y}$

$\pi_5 = \frac{P}{\rho U_m^2}$ if introduce the ratio of specific heats γ

$\frac{\gamma P}{\rho U^2} = \frac{1}{M_N^2}$

$$\pi_6 = \theta$$

$$\theta = f(Re,\ M_N,\ \frac{fd}{U_m},\ X_T,\ \frac{d}{\rho U_m^2}\ \ \frac{\delta P}{\delta y})$$

The flow within a tube bank can be considered as being fully turbulent, so, to a first approximation, the Reynolds number effect can be neglected. Also since the work was carried out at low Mach numbers, this effect may also be neglected. Hence

$$\theta = \alpha^1\ \ \frac{d}{\rho U_m^2}\ \ \frac{\delta P}{\delta y} \qquad 8.1$$

where $\alpha' = f(X_T,\ \frac{fd}{U_m})$

Note that the angle θ need not be in phase with the acoustic pressure gradient $\frac{\delta P}{\delta y}$. It is however convenient at this stage to include the phase shift in the α^1 term.

The effect of the interaction of the acoustic pressure field with the tube is to produce a transverse velocity component Vs, which is given by:

$$Vs = U_m \sin\theta$$

This can be written as:

$$Vs = U_m\ \theta$$

for small angles of θ

$$\text{i.e. } Vs = \alpha^1\ \frac{d}{\rho U_m}\ \frac{\delta P}{\delta y} \qquad 8.2$$

For brevity in later discussions, this will be written as: /

as:

$$Vs = \alpha \frac{\delta P}{\delta y}$$

where $\alpha = \frac{\alpha^1 d}{\rho U_m}$

One further result is required. The transverse velocity fluctuations Vs, are carried across the cavity, between adjacent tubes, by the mean flow. Therefore the value of Vs at some distance x downstream of the separation point corresponds to that which left this point a time $\frac{x}{U_x}$ ago. The flow issuing between the tubes will form jets. Therefore the value of the mean velocity across the cavity might be expected to be close to U_m (typically $0.9U_m$ (F2)). For the purposes of this investigation it will be taken as being equal to U_m. Thus:

$$Vs\ (x,t) = Vs\ (O,\ t - \frac{x}{U_m})$$

it follows that.

$$Vs\ (x,t) = \alpha \frac{\delta P}{\delta y}\ (t - \frac{x}{U_m}) \qquad 8.3$$

8.3 ANALYSIS

In the following analysis the above relationship is included in the governing differential equation and a solution obtained. It is convenient to first consider the wave equation and its derivation. Following the procedure of many acoustics text books (e.g. ref (M2)) this may be derived for a one dimensional situation. This /

This is done by combining the continuity and momentum equations.

The continuity equation may be written as follows:

$$\frac{\delta U}{\delta y} = - \frac{1}{P_o} \frac{\delta P}{\delta t} \qquad 8.4$$

The momentum equation in one dimension may be written as:

$$\frac{\delta U}{\delta t} + U_y \frac{\delta U}{\delta y} + \frac{1}{\rho} \frac{\delta P}{\delta y} = 0 \qquad 8.5$$

since U_y is small Uy $\frac{\delta U}{\delta y}$ may be neglected to obtain

$$\frac{\delta U}{\delta t} = - \frac{1}{\rho} \frac{\delta P}{\delta y} \qquad 8.6$$

Thus, combining 8.4 and 8.6

$$\frac{1}{C^2} \frac{\delta^2 P}{\delta t^2} = \frac{\delta^2 P}{\delta y^2} \qquad 8.7$$

where $C = \sqrt{\frac{\gamma P}{\rho}}$ = speed of sound

The solutions of this equation are well known. Consider now the situation in a tube bank. The presence of the tubes may, to a first approximation, be ignored, apart from the production of a transverse velocity Vs, which will be superimposed on the acoustic system. The effect of the transverse velocity fluctuation being carried across the cavity by the mean flow, requires the inclusion of the X-direction convective term in the momentum equation, to give

$\frac{\delta U}{\delta t}$ /

$$\frac{\delta U}{\delta t} + U_m \frac{\delta U}{\delta x} + U_y \frac{\delta U}{\delta y} = - \frac{1}{\rho} \frac{\delta P}{\delta y} \qquad 8.8$$

U_m being the mean bank velocity as before. Now, provided that the cavity width is short compared with the acoustic wave length, the acoustic velocity across the cavity must be constant. Thus the only contribution to the convective term $U_m \frac{\delta U}{\delta x}$ will come from the velocity fluctuation Vs. Thus:

$$\frac{\delta U}{\delta t} + U_m \frac{\delta Vs}{\delta x} + U_y \frac{\delta U}{\delta y} = - \frac{1}{\rho} \frac{\delta P}{\delta y} \qquad 8.9$$

and as before $U_y \frac{\delta U}{\delta Y}$ is negligible.

Invoking equation 8.3 gives.

$$\frac{\delta Vs}{\delta x} = \frac{\delta}{\delta x}(\alpha \frac{\delta P}{\delta y} (t - \frac{x}{U_m})) \qquad 8.10$$

Thus equation 8.9 becomes

$$\frac{\delta U}{\delta t} + U_m \frac{\delta^2}{\delta x \delta y} (P(t - \frac{x}{U_m})) = - \frac{1}{\rho} \frac{\delta P}{\delta y} \qquad 8.11$$

Substituting from the continuity equation as before

$$\frac{\delta^2 U}{\delta t \delta y} + U_m \frac{\delta^3}{\delta x \delta y^2} (P(t - \frac{x}{U_m})) + \frac{1}{\rho} \frac{\delta^2 P}{\delta y^2} = 0$$

$$-\frac{1}{P_o} \frac{\delta^2 P}{\delta t^2} + U_m \frac{\delta^3}{\delta x \delta y^2} (P(t - \frac{x}{U_m})) + \frac{1}{\rho} \frac{\delta^2 P}{\delta y^2} = 0$$

$$\frac{\delta^2 P}{\delta t^2} - C^2 U_m \rho \frac{\delta^3}{\delta x \delta y^2} (P(t - \frac{x}{U_m})) - C^2 \frac{\delta^2 P}{\delta y^2} = 0 \qquad 8.12$$

On this basis, the acoustic resonance in a tube bank is charaterised by equation 8.12. If the solution of this equation is of the form $P_o e^{\beta t} \sin \omega t$, then with positive β the system may be regarded as unstable. Thus /

Thus the system will spontaneously resonate at its natural frequency, with an amplitude limited only by the system non-linearities. If β is negative the system is stable and an initial disturbance will decay to zero. As mentioned in Chapter 1, it has generally been observed that the mode excited in a bank of tubes is one of the transverse modes (ref. B6). For the purposes of this analysis it shall be assumed that this is the excited mode. The equation for the transverse modes of the bank may be written as:

$$P = P_o e^{(i\omega + \beta)t} \cos \frac{2\pi y}{\lambda}$$

now substituting for P in equation 8.12

$$(\beta + i\omega)^2 + \frac{4\pi^2 C^2 \rho U_m \alpha}{\lambda^2} \frac{\delta e^{-(i\omega + \beta)\, x/U_m}}{\delta x} + (\frac{2\pi C}{\lambda})^2 = 0 \qquad 8.13$$

It is convenient at this stage to eliminate x by integrating each term of the equation with respect to x across the cavity between limits of 0 and a. A fuller discussion of the value of "a" will be given later. Thus

$$(\beta + i\omega)^2 + \frac{\rho U_m \alpha}{a} (\frac{2\pi C}{\lambda})^2 (e^{-(i\omega + \beta)\, a/U_m} - 1) + (\frac{2\pi C}{\lambda})^2 = 0 \qquad 8.14$$

Now separating this equation into its real and imaginary parts. To accomplish this the real and imaginary terms which describe the phase difference between θ and $\frac{\delta P}{\delta y}$ must be extracted from α. This will be described by a $(g + ih)$ term. Thus.

$$(\beta + i\omega)^2 + (\frac{2\pi C}{\lambda})^2 \frac{\alpha^1 d}{a} (g + ih) ((\cos \frac{\omega a}{U_m} - j \sin \frac{\omega a}{U_m})\, e^{-\beta a/U_m} - 1) + (\frac{2\pi C}{\lambda})^2 = 0$$

$$\text{Re: } \beta^2-\omega^2 + \left(\frac{2\pi C}{\lambda}\right)^2 \frac{\alpha^1 d}{a}\left(\left(g\cos\frac{\omega a}{U_m} + h\sin\frac{\omega a}{U_m}\right) e^{-\beta a/U_m} - g\right) + \left(\frac{2\pi C}{\lambda}\right)^2 \qquad 8.15$$

As a bank approaches instability β will tend towards zero. Therefore, for a bank on the point of resonance β^2 may be neglected when compared with ω^2. Hence we obtain:

$$\omega^2 = \left(\frac{2\pi C}{\lambda}\right)^2 \left(1 + \frac{\alpha^1 d}{a}\left(\left(g\cos\frac{\omega a}{U_m} + h\sin\frac{\omega a}{U_m}\right) - g\right)\right) \qquad 8.16$$

The imaginary part of 8.14 gives

$$\text{Im: } 2\omega\beta + \frac{\omega^2\alpha^1 d}{a}\left(\left(h\cos\frac{\omega a}{U_m} - g\sin\frac{\omega a}{U_m}\right) e^{-\beta a/U_m} - h\right) = 0$$

$$2\omega\beta = \frac{\omega^2\alpha^1 d}{a}\left(\left(g\sin\frac{\omega a}{U_m} - h\cos\frac{\omega a}{U_m}\right) e^{-\beta a/U_m} + h\right)$$

$$\beta = \frac{\pi f d\alpha^1}{a}\left(\left(g\sin\frac{\omega a}{U_m} - h\cos\frac{\omega a}{U_m}\right) e^{-\beta a/U_m} + h\right) \qquad 8.17$$

In the case of the geometries examined in this study the instability occurred at low values of acoustic Strouhal number (typ. 0.19 - 0.4) . This implies that the acoustic pressure gradient is varying slowly when compared to the time taken for a particle to travel a distance of one tube diameter. As it is the effect on the separation process that is of interest, there would be some merit in considering the distance over which the separation point is deflected instead of the tube diameter. This would have the effect of further reducing the frequency ratio S_A since $d\theta/2 << d$. Hence as $S_A \rightarrow 0$ the acoustic pressure gradient can almost be considered stationary when compared to the flow at the separation points. Therefore for these values of S the velocity component Vs can be assumed to be in phase with the pressure gradient $\frac{\delta P}{\delta y}$. This gives:

$$g = 1 \qquad h = 0$$

$$\beta = \frac{\pi f d\alpha^1}{a}\sin\frac{\omega a}{U_m} e^{-\beta a/U_m}$$

which can be written as

$$\beta = \frac{\pi f d\alpha^1}{a}\sin\frac{\omega a}{U_m} \qquad 8.18$$

as $\beta \rightarrow 0$

This is the principal result of the analysis. Clearly from this equation β is positive implying large amplitude vibration for $\frac{\omega a}{U_m}$ less than π. (assuming α^1 positive).

i.e. for $\frac{fa}{U_m}$ less than $\frac{1}{2}$

It remains to define the effective depth of the cavity between the tubes. It may be supposed that this is less than the longitudinal pitch of the bank, X_L, but greater than the width of the gap between the tubes $X_L - d$. However from the results of figure 8.2 it would appear that the experimental data is well described by

$$\frac{a}{d} = X_L - 0.5$$

According to equation 8.18 the bank will resonate for all values of :-

$$\frac{U_m}{fd} > 2\ (X_L - 0.5)$$

This result does however ignore damping.

8.4 DAMPING

It is not possible to include the effect of damping in a rigorous way in the basic differential equation. However, it may be shown that if a general damping loss term $D\ \frac{\delta P}{\delta t}$ is added to equation 8.12 to give:

$$\frac{\delta^2 P}{\delta t^2} \quad /$$

$$\frac{\delta^2 P}{\delta t^2} - \rho C^2 \alpha \frac{\delta^3}{\delta x \delta y^2} (P(t-x/U_m)) + D \frac{\delta P}{\delta t} = C^2 \frac{\delta^2 P}{\delta Y^2} \qquad 8.19$$

the effect is simply to add another term in equation 8.18 to give:

$$\beta = \frac{\pi f d \alpha^1}{a} \sin \frac{\omega a}{U_m} - D/2 \qquad 8.20$$

Therefore resonance will occur if:

$$\frac{\pi f d \alpha^1}{a} \sin \frac{\omega a}{U_m} - \frac{D}{2} > 0 \qquad 8.21$$

$$\text{i.e. } \frac{2\pi f d \alpha^1}{a} \sin \frac{\omega a}{U_m} > D$$

The damping parameter D includes the effect of viscous damping and radiation losses.

Let us now consider the stability diagram illustrated in figure 8.3. This diagram shows the variation in the value of β as V_r is increased. An acoustic resonance will occur at all values of V_r for which a positive value of β exists. For the values of V_r that β is negative then any disturbance will decay to zero. This diagram shows that the theory predicts the existence of additional resonant zones corresponding to $\frac{\omega a}{U_m}$ equal to $\pi + 2n\pi$.

The effect of introducing damping to this diagram would be to offset the whole β curve by a value of $\beta = -D/2$. Thus as the value of D is increased a higher value of V is required to initiate the resonance. This trend will continue until $D > 2\pi f d \alpha^1/a$ at which point there is no value of U_m which will satisfy the inequality /

inequality 8.21. Thus for each mode there exists a value of damping which, if exceeded, will cause that mode to be missed. In figure 8.4 the stability diagrams for the first three harmonics of acoustic vibration are shown. A few points should be made about this diagram. Firstly the theory only applies for small values of θ. Also the theory initially assumes the existence of an acoustic pressure gradient which interacts with the separation process. Therefore equation 8.12 was solved for a constant amplitude of acoustic disturbance P_o. This implies that as the velocity, U_m, becomes small θ will become very large, and the theory will no longer apply. In the practical situation however such an acoustic disturbance would not be present. A better representation would be obtained if equation 8.12 had been solved for a constant amplitude of θ.This would illustrate more clearly how a disturbance at the tube would effect the acoustic system. This effect can be shown by the existing equations if α^1 is made proportional to V_R^2. This is illustrated in figure 8.5 by a graph of β against mean velocity U_m. Also shown on this diagram is the experimental results obtained from the 43 row bank with a geometry of $X_T = 2.0$ and $X_L = 1.67$. This geomety was also used for the theoretical calculations. As can be seen from the theoretical curve the energy input to the acoustic system is much smaller at low velocities. This is due to two factors. Firstly /

Firstly the value of 'Vs' will be smaller and secondly, the effect of the local velocity fluctuations 'Vs' at low velocities, will be largely self cancelling due to the large phase shift across the cavity. At large values of U_m however the velocity fluctuations will be roughly in phase and will therefore reinforce one another.

Figure 8.4 illustrates the possibility of the second and third harmonics being excited at a slightly lower velocity than the first harmonic. The second and third harmonics are excited when $\frac{\omega a}{U} = 3\pi$ while $\frac{\omega a}{U} = \pi$ for the first harmonic. This situation is repeated for other values of $\frac{\omega a}{U}$ however this condition is of most interest in a practical situation. This is because as $\frac{\omega a}{U}$ is increased the likelyhood of a resonant zone causing acoustic vibration is decreased, as shown by figure 8.5.

The theoretical model will be further discussed in chapter 9.8, where it will be compared more fully with the experimental findings of this investigation.

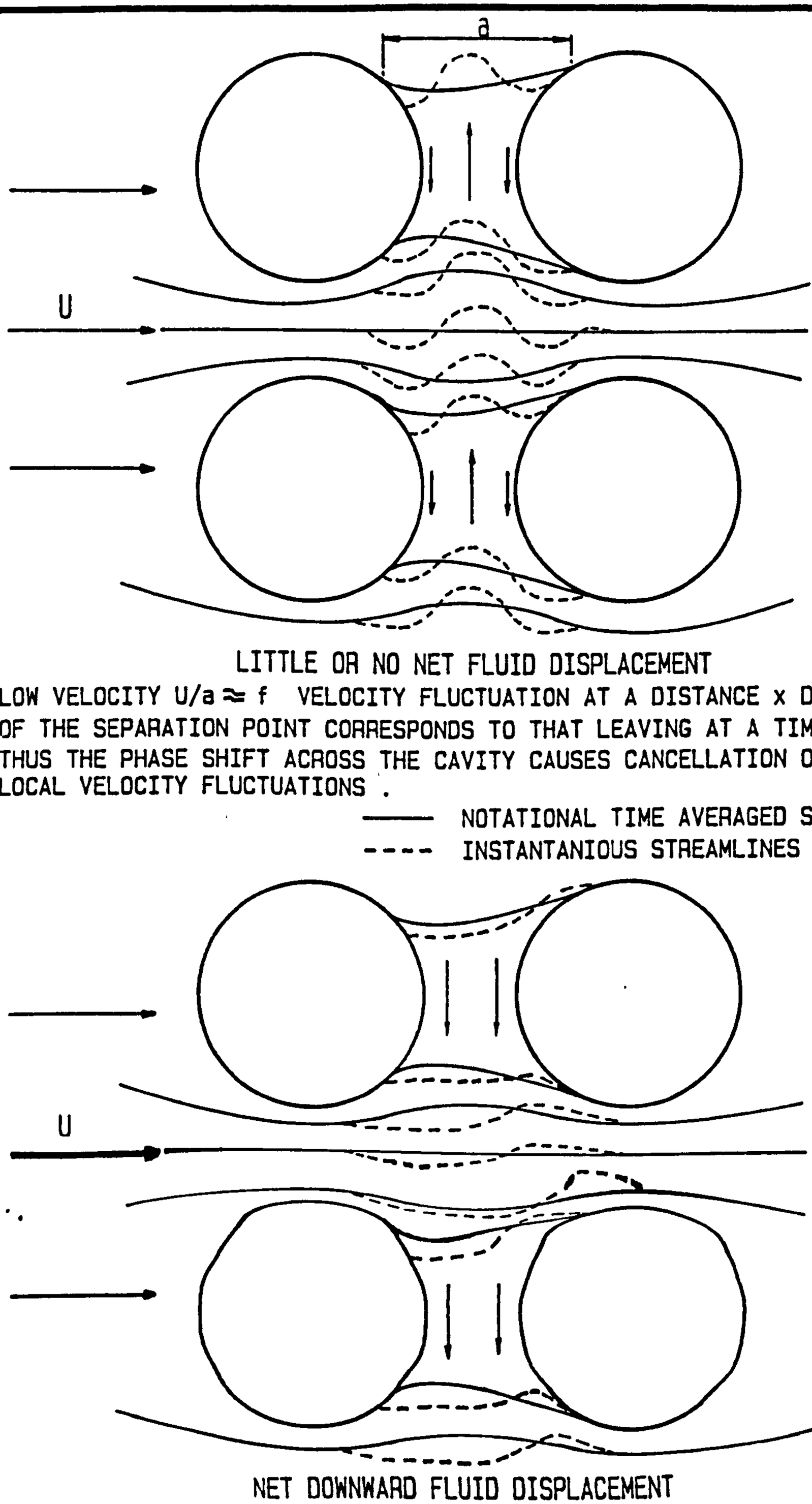

LITTLE OR NO NET FLUID DISPLACEMENT

LOW VELOCITY $U/a \approx f$ VELOCITY FLUCTUATION AT A DISTANCE x DOWNSTREAM OF THE SEPARATION POINT CORRESPONDS TO THAT LEAVING AT A TIME x/U AGO. THUS THE PHASE SHIFT ACROSS THE CAVITY CAUSES CANCELLATION OF THE LOCAL VELOCITY FLUCTUATIONS .

——— NOTATIONAL TIME AVERAGED STREAMLINES

- - - - INSTANTANIOUS STREAMLINES

NET DOWNWARD FLUID DISPLACEMENT

HIGH VELOCITY $U/a >> f$ TRANSVERSE VELOCITY FLUCTUATIONS ARE IN PHASE ACROSS THE CAVITY WIDTH

NOTIONAL FLOW PATTERNS WITHIN A TUBE BANK

FIGURE 8.1

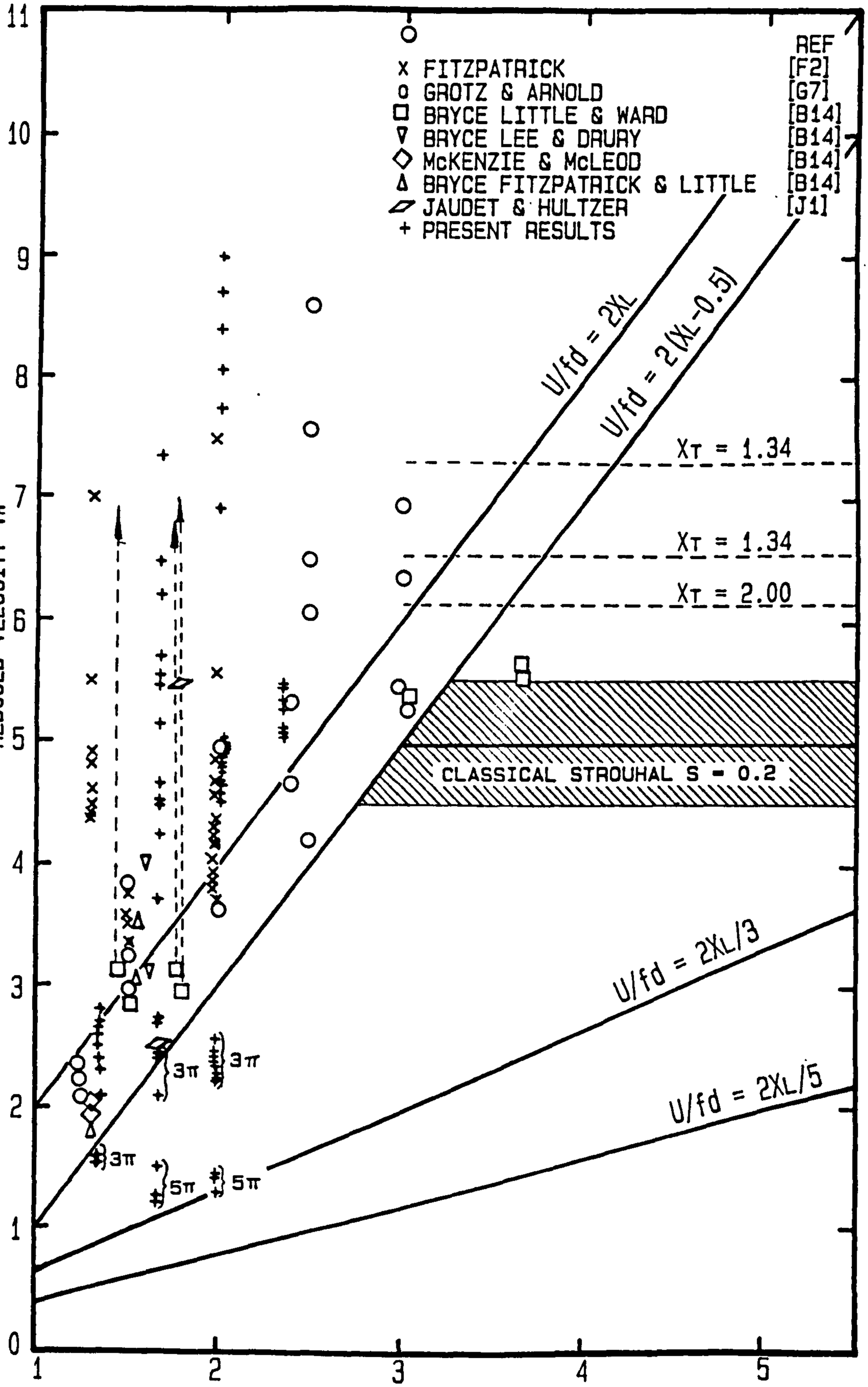

GRAPH OF REDUCED VELOCITY AGAINST LONGITUDINAL PITCH RATIO

FIGURE 8.2

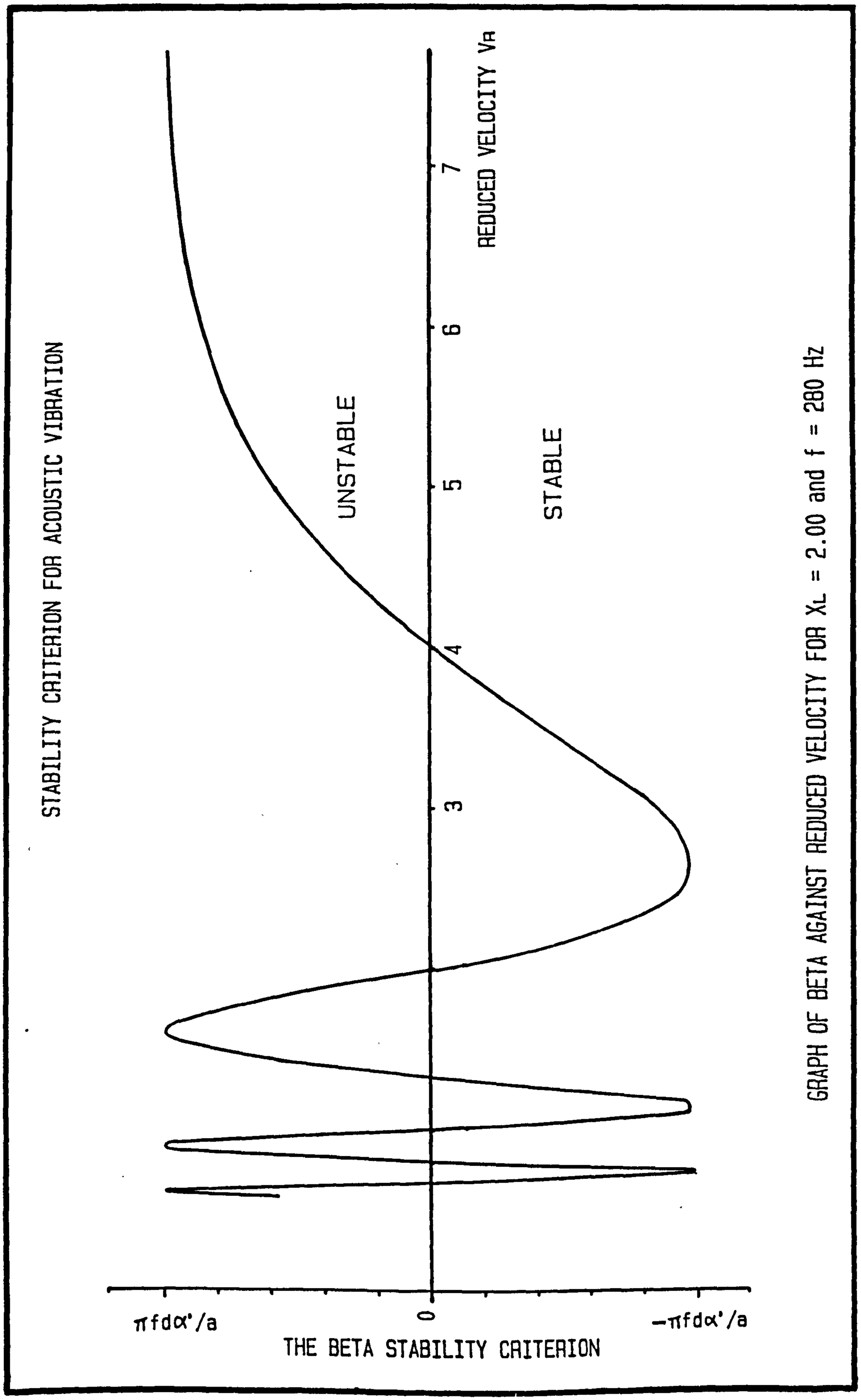
STABILITY CRITERION FOR ACOUSTIC VIBRATION
UNSTABLE
STABLE
REDUCED VELOCITY VR
3
4
5
6
7
GRAPH OF BETA AGAINST REDUCED VELOCITY FOR XL = 2.00 and f = 280 Hz
πfdα'/a
0
-πfdα'/a
THE BETA STABILITY CRITERION

FIGURE 8.3

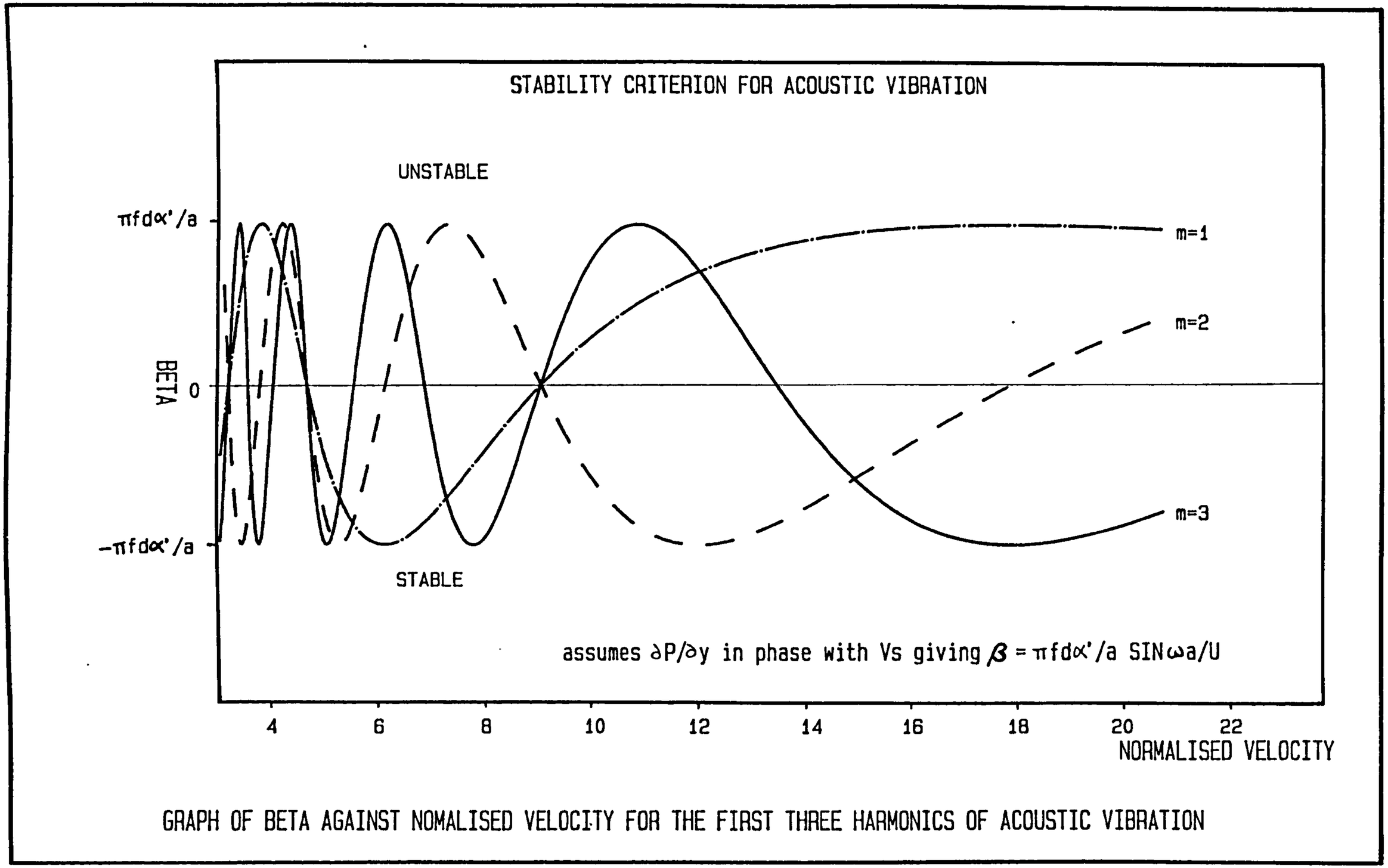

GRAPH OF BETA AGAINST NOMALISED VELOCITY FOR THE FIRST THREE HARMONICS OF ACOUSTIC VIBRATION

FIGURE 8.4

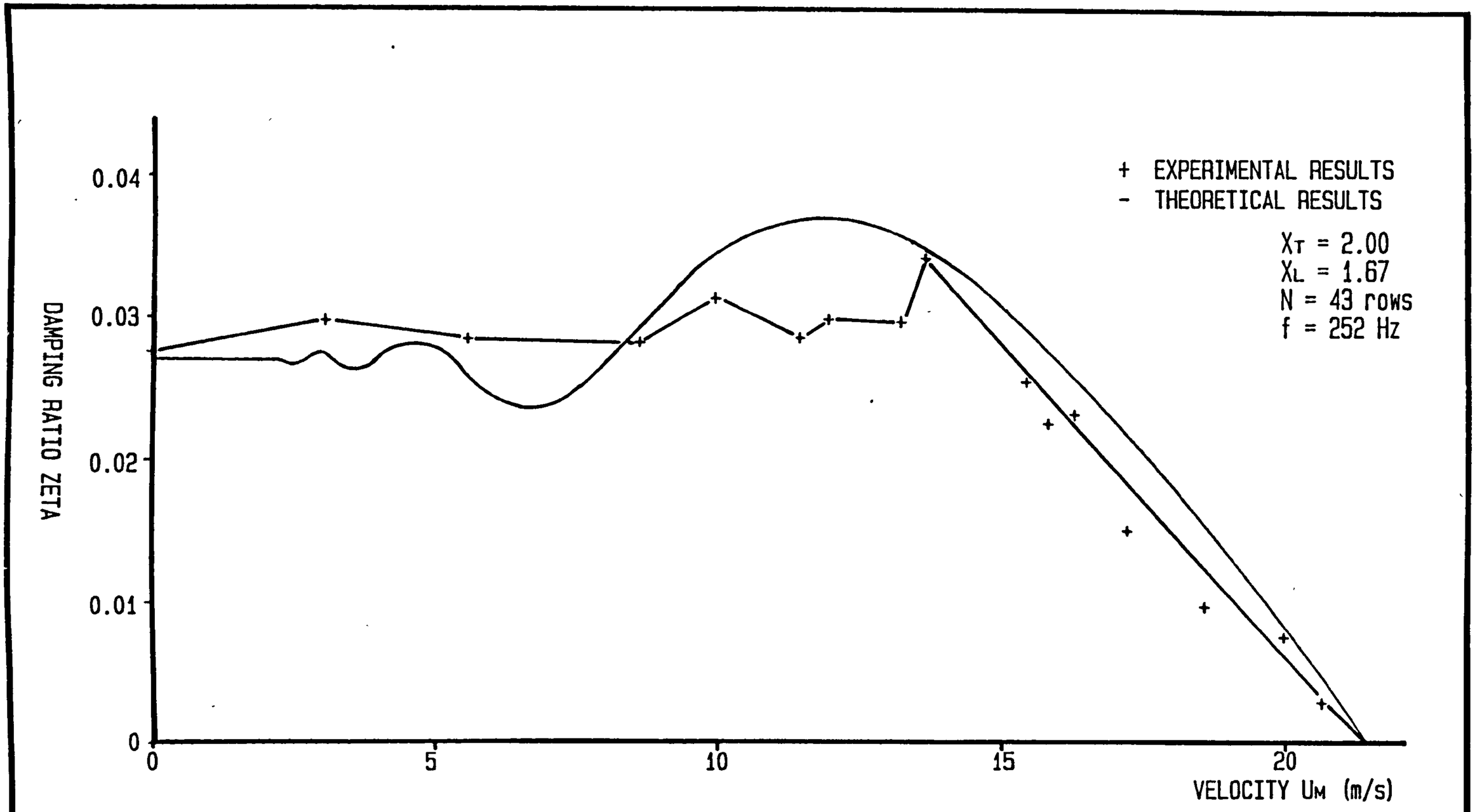

GRAPH OF ZETA AGAINST VELOCITY FOR THEORETICAL AND EXPERIMENTAL RESULTS

FIGURE 8.5

9.0 DISCUSSION

9.1 INTRODUCTION

The following discussion will be split into 7 parts. The first 6 parts will deal with the behaviour of each individual geometry tested. This will be followed by a general discussion on the effect of row depth and acoustic damping. Before proceeding with the first geometry it would be useful to consider the damping offered to the acoustic mode within a tube bank. Clearly several different factors will determine the energy dissipated from the acoustic mode during vibration. These will include the effects of the inherent damping, viscous damping and radiation losses.

In any vibrating medium one might expect a certain degree of energy dissipation due to the frictional forces between the vibrating particles. The inherent damping will vary according to the medium involved, however for a column of air this component will be negligible in comparison with the others.

As the vibrating medium passes over the walls and tubes of the bank it will be subjected to some degree of viscous damping. This component will vary in direct proportion to the surface area over which the vibrating medium travels. Therefore this damping factor will decrease as the scale of a given geometry is increased. Likewise if the row depth is increased then this damping/

damping factor will also increase.

The energy lost by the standing wave as acoustic radiation is also a form of damping. Although a full analysis is complex, it is clear that as the ratio of the open area of the bank to its volume increases, then a greater fraction of the stored energy will be radiated during one cycle of vibration. Therefore the corresponding damping factor will increase as the area/volume ratio is increased. If the scaling factor of a bank is increased, then this will cause a greater reduction in volume than open area , hence the area/volume ratio will increase resulting in an increase in damping factor. Similarily if the row depth is increased this will result in an increase of the banks volume, which will decrease the damping factor.

Let us now consider the net effect of increasing the row depth. This will result in an increase in the surface area and volume of the bank which in turn will increase the viscous damping factor and decrease the radiation term. Likewise as the row depth is increased the number of disturbance sources (i.e. tubes) within the bank will increase. This will result in a much stronger feedback effect in the acoustic resonance model. Therefore the net effect would perhaps be more easily visualized if considered on a per row basis i.e. a constant magnitude of feed back effect. Hence increasing the row depth will cause a reduction in the radiation/

radiation damping term with the viscous damping term remaining fairly constant.

A summary of all the results obtained in the row depth investigation, together with data from other compatible sources, are shown on figure 8.2. This is a graph of Reduced Velocity against longitudinal pitch to diameter ratio. As can be seen from this diagram many of the points fall either side of the $U/fd = 2\ X_L$ stability criterion. However if we consider the $U/fd = 2(X_L - 0.5)$ stability criterion, as proposed in chapter 8, then it can be seen that all the points are encased within its boundary.

9.2 BANK I $X_T = 2.0$ $X_L = 1.67$

The Acoustic Strouhal number / row depth relationship for this geometry is illustrated by figure 7.4. The lower line on this diagram describes the relationship for the main resonance. That is the instability region corresponding to $\frac{\omega a}{U} = \pi$. This line shows the Acoustic Strouhal number to increase with row depth and level out to a constant value for row depths greater than 20 (approximately). Such an effect can be explained by the damping / row depth relationship, as described in chapter 9.1. Consider the diagram in figure 8.3. This curve will be displaced downward by a value corresponding to D/2.* The value of D/

** see equation 8.20*

D will be relatively large for small row depths, so the curve will be displaced by a large amount. As the row depth is increased, and the value of D is reduced, the curve will move upwards hence reducing the velocity at which the acoustic resonance is excited. This will have the effect of increasing the Acoustic Strouhal Number. This trend will continue until a saturation value is reached, where upon the reduction in damping with increasing row depth becomes negligable.

Several other unusual effects were also observed in this geometry. An acoustic resonance was excited when only 1 row of tubes was present. To obtain a resonance with such a bank is very rare, and presumably was only observed in this instance because the test section had a low value of acoustic damping. However this situations is not representative of any of the longitudinal pitches investigated, and is more akin to a bank with an infinite longitudinal pitch. Therefore the 1 row bank shall not be considered when assessing the effect of the row depth. In the case of the twenty eight row bank the first harmonic was initially excited at a velocity of 5.8 ms^{-1}. This resonance only existed for a small velocity range then completely disappeared. Further increase in velocity caused the first harmonic to be excited again, this time at a velocity of 11.4ms^{-1}, see figure 7.6. This behaviour is unusual, but can be explained by the theoretical model./

model. Consider again the stability diagram shown in figure 8.3. This diagram reveals the existance of additional areas of instability corresponding to $\omega a/U = 3\pi$, 5π, etc. The region of instability experienced at $5.8ms^{-1}$ would correspond to the 3π region on figure 8.3. As explained previously this region of instability corresponds to a 360° phase shift between Vs and $\frac{\delta P}{\delta y}$, as Vs travels across the cavity. Although this bank was the only one in which this phenomenon occurred, several other banks exhibited an increase in magnitude of response for the first harmonic at this region. An example of this is shown in figure 7.7.

For the case of the two row bank the first and second harmonics were not excited, and the third harmonic was the first mode to be excited. This could be explained by the large value of damping factor which exists in shallow banks and resulted in the first two modes remaining stable. When the row depth was further increased the first harmonic was excited. However in the 5, 8 and 12 row banks the second and third harmonic was found to be excited prior to the onset of the first. This phenomenon can again be explained by the theory. Consider figure 8.4, this diagram shows the stability curves for the first three harmonics of acoustic vibration. Now imagine these diagrams are displaced downwards by varying amounts which represents the damping for each mode. For the case of the/

the five row bank the instability curve for the third harmonic is in such a position that it allows the 3π region to become excited. This is not the case for the second harmonic and it remains stable. In the case of the first harmonic it is displaced downwards, by an amount sufficient to allow the third harmonic to be excited separately. Therefore when the velocity is increased the third harmonic is the first mode to be excited, closely followed by the establishment of the first harmonic. It should be remembered that this diagram only illustrates the relative positions of the instability regions and that the magnitude of the peaks have been normalized. In the case of the 8 and 12 row banks the increase in row depth has produced a corresponding reduction in the acoustic damping for each mode. This has allowed the second harmonic to become excited in its 3π instability region. Therefore it becomes the first mode to be excited.

When the row depth is increased beyond 12 rows the first harmonic becomes the first mode to be excited. This can be explained by the reduction in acoustic damping which now allows the onset velocity for the first harmonic to become lower than the second. This observation will be discussed more fully in chapter 9.8. As can be seen from figure 7.7 contributions from the second and third harmonics do exist once the first harmonic has been excited.

The three dimensional diagrams in figures 7.5 - 7.7 clearly shows the existance of vortex shedding within these banks. It also shows the acoustic resonance to occur at a frequency well removed from that of vortex shedding.

9.3 BANK II $X_T = 2.0$ $X_L = 2.0$

In these banks the longitudinal pitch to diameter ratio was increased which has resulted in a reduction in the tube packing density. This will result in a decrease in the area/volume ratio, and as explained in chapter 9.1 this will lower the value of acoustic damping. It is for this reason that the Acoustic Strouhal number/row depth effect shown in figure 7.8 is less pronounced than that observed previously. In a study by Fitzpatrick (ref. F2) the Acoustic Strouhal number/row depth relationship was investigated for a similar geometry. The rig in which these experiments were conducted was of a much lighter construction, with the test section being made from aluminium and perspex. This test section housed a bank of 6.25mm diameter tubes which was at least 12 columns wide and up to 40 rows deep. Following the arguements of chapter 5 and 9.1 one might expect a larger value of acoustic damping in this rig, as compared to the one used in this study. Also since the tube diameter was smaller in Fitzpatrick's /

Fitzpatrick's rig, one could expect a much larger value of area/volume ratio in shallow banks. However this difference would be marginal for very deep banks. Therefore following the arguements in chapter 9.1 one might expect Fitzpatrick's rig to exhibit a much greater variation in acoustic damping as row depth is increased. This will result in a more pronounced effect on the Acoustic Strouhal Number. (especially in shallow banks). Figure 2.8 shows this to be consistant with the results obtained.

As predicted by the theory the increase in longitudinal pitch has caused a decrease in the Acoustic Strouhal number. The three dimensional diagrams in figures 7.9 - 7.11 distinctly show the existance of vortex shedding. These diagrams also show the acoustic resonance to become established at a frequency well removed from that of vortex shedding.

9.4 BANK III $X_T = 2.0$ $X_L = 2.34$

Figure 7.12 illustrates the Acoustic Strouhal number/row depth relationship for this geometry. Once again the only difference between this geometry and that previously tested is an increase in the longitudinal pitch to diameter ratio. As predicted by the theory this increase in pitch has resulted in a lower value of Acoustic Strouhal number, as explained in /

in Chapter 9.1 this increase in pitch will also cause a reduction in the acoustic damping. It is for this reason that a very small variation in Acoustic Strouhal number was observed over the row depths investigated.

The geometry also produced areas of increased response at velocities corresponding to the 3π instability region, an example of which is shown in figure 7.13. Nevertheless none of the banks investigated became unstable in this region. As with the previous geometry neither the second or third harmonics were excited prior to the onset of the first. This could be explained by the lower value of acoustic damping experienced in these banks, which prevented this phenomenon from occuring.

Figure 7.13 shows a typical three dimensional plot for this geometry. This again shows the frequency of vortex shedding to be well removed from that of the acoustic mode at resonance.

9.5 BANK IV $X_T = 1.34$ $X_L = 1.34$

In this geometry both the longitudinal and transverse pitch to diameter ratio have been reduced. It is difficult to predict what the effect on the acoustic damping will be because the area and volume of the bank have been reduced. Similarily the surface area of the bank has increased considerably, due to the tube /

tube packing density, which will increase the viscous damping term.

Figure 7.14 illustrates the Acoustic Strouhal number/row depth relationship for this geometry. Once again this geometry produced a resonance when only one row of tubes was present. As before this results will be ignored when assessing the overall row depth effect.

In this geometrical configuration the 1st, 2nd and 3rd harmonics remained stable in the shallow banks. However, it can be seen from figure 7.14 that as the row depth increases, and the acoustic damping of each mode is reduced, the mode number for the first mode excited is reduced. This continues up to the maximum row depth tested at which point the second mode is the first to be excited. Had the row depth been increased sufficiently, then the first mode may have been excited. As can be seen from this diagram the higher order modes fail to appear in the deeper banks. This is because the velocities required to excite these modes could no longer be attained by the test rig.

The five row bank was the only bank in which the 3π instability region was excited. In this bank both the 1300Hz and 1580Hz mode were excited in this region. In all the other banks the π region of instability was the only region excited, and all the modes were excited in a regular sequence.

In this geometry no evidence of vortex shedding was /

was detected by the measurement techniques used.

9.6 BANK V $X_T = 1.34$ $X_L = 1.67$

The main difference between this geometry and the previous one is that the longitudinal pitch to diameter ratio has been increased. As described in Chapter 9.1 this will result in a reduction in the acoustic damping term. Figure 7.18 illustrates the Acoustic Strouhal number / row depth effect for this geometry. As can be seen from this diagram there are very few points where an acoustic resonance was established. In the case of the two row bank the 1st, 2nd and 9th harmonics were all excited. The first harmonic was excited at a velocity of $10.2ms^{-1}$, remained for $2 \rightarrow 3ms^{-1}$ and disappeared. This was followed by the excitation of the 9th harmonic at a velocity of $15.9ms^{-1}$ and the 2nd at $16ms^{-1}$. Increasing the row depth to 5 rows changed the response of the bank considerably, and only the 9th harmonic was excited.

Further increase in the row depth meant that the rig could no longer achieve the velocity required to excite the 9th harmonic. With a row depth of ten rows a small peak in the spectra was observed at 870Hz (which corresponds to the 3rd harmonic). Although this resonance did not become audible, it was /

was clearly identifiable in the spectra and was therefore recorded. No significant peaks were observed in the power spectra until a row depth of 40 was reached. In this bank the second harmonic was excited, however this was achieved at the very limit of the rigs capabilities, see figure 7.20. Once again this behaviour can be explained by the damping / row depth characteristics as described in chapter 9.1.

Although the data for this geometry is very sparse, it can be seen from figure 8.2 that all the points fall well within the stability criterion. As with the previous geometry no evidence of vortex shedding was detected by the measurement techniques used.

9.7 BANK IV X_T = 1.34 X_L = 2.0

Once again the only difference between this bank and that previously investigated was that the longitudinal pitch to diameter ratio had been increased. As explained in chapter 9.1 this will result in a reduction in the value of acoustic damping. Figure 7.21 illustrates the acoustic Strouhal number / row depth relationship for this geometry. As can be seen the acoustic damping of the first mode was low enough to allow it to be excited in the shallow banks. In these banks some high order modes /

were excited at Strouhal numbers which corresponded to the 5π instability region. However when the row depth was increased to 10 rows, the velocity required to excite the modes observed previously was no longer attainable. It was not until the row depth had been increased to 20 rows that the damping became low enough, to allow the third harmonic to be excited in its 3π instability region. Further increase in row depth allowed the second harmonic to become established in the 3π instability region. However when the row depth was increased beyond 35 rows the velocity required to excite the third harmonic could no longer be attained. As can be seen from figure 7.21, the increase in longitudinal pitch has decreased the Acoustic Strouhal number for the π instability region, this is consistent with the behaviour predicted by the theoretical model.

As in the previous banks no evidence of vortex shedding was detected by the measurement techniques adopted.

9.8 GENERAL DISCUSSION

The results from the row depth investigation has revealed the existance of a mechanism, which cannot be readily explained by the existing models. However the feedback model described in the previous chapter /

chapter has the facility to explain all the observations made. As mentioned in chapter 7 the frequency of the resonance was observed to increase with velocity. Similar observations have been made by ref. (D2). From equation 8.16 it can be seen that if the phase difference between Vs and $\frac{\delta P}{\delta y}$ is small, then the theory predicts that the frequency of the resonance will increase with velocity.

The results from geometries with a transverse pitch to diameter ratio of 2.0 proved that vortex shedding could exist within deep banks. On inspection of the three dimensional diagrams for these banks, it may be observed that the vortex shedding peak becomes larger and more pronounced as the row depth is increased. This would suggest that there is some degree of correlation between the vortex shedding of adjacent rows which produces this increase in magnitude. Nevertheless in each bank investigated the acoustic resonance was always excited at some frequency well removed from that of vortex shedding. In addition to this the Strouhal number (vortex shedding) was found to remain constant for all the banks investigated. The Acoustic Strouhal number however was found to decrease with longitudinal pitch and could increase slightly with row depth.

The frequency of the acoustic mode was observed to decrease as the row depth was increased. (f /

(f=295Hz → 248Hz for N=1 → 50, typically) . Hence for three banks with a geometry of X_T=2.0 and X_L=1.67, the mode shape of the acoustic standing wave was measured. These results are shown in figures 7.28 to 7.30 and represent 38, 18 and 8 row banks respectively. As can be seen from these diagrams it was the first transverse mode that was excited in each case. Therefore the change in frequency was caused by changes in the acoustic system brought about by the increase in row depth, as discussed in chapter 7.4.

For the geometries with a transverse pitch to diameter ratio of 1.34 several modes were excited around the same mode number. As explained in chapter 7.4 a full microphone tranverse of these banks could not be conducted, due to the high tube packing density. Although no data was available, it was felt reasonable to assume that these were all modes of the same transverse mode shape, but with different longitudinal mode shape.

In almost all of the banks tested the acoustic resonance, once excited, producted a pure tone of constant amplitude. However in some of the banks with X_T = 1.34 a modulated time series response was produced. On investigation of the power spectrum associated with these conditions it was revealed that, the modulation was caused by spectral interference of two very sharp peaks, closely spaced in the frequency domain./

domain. Further increase in velocity from this point saw a reduction in one of the peaks, and the return to a sinusoidal response of constant amplitude.

The results obtained in this investigation are summarised in figure 8.2, in the form of a graph of Reduced Velocity against longitudinal pitch to diameter ratio. This diagram shows the Reduced Velocity for instability to increase in direct proportion to the longitudinal pitch. However one would not expect the Reduced Velocity to increase indefinetly with longitudinal pitch. Therefore some upper limit must exist. The results obtained with 1 row of tubes is quite representative of a bank with an infinite longitudinal pitch (or at least a very large longitudinal pitch). Therefore these results could be considered as an indication of this limit and is indicated on figure 8.2 by a dotted line.

The results for the 3π and 5π instability regions can be seen to be well within the bounds specified by the theory. However it was observed in the investigation of the $X_T = 2.0$, $X_L = 1.67$ banks, that the π instability region for the first mode could be excited at a lower velocity than the 3π region for the second mode. As can be seen from figure 8.4, this is not consistant with the theoretical prediction. Hence it suggests that either the π region can occur at a lower velocity or the 3π region occurs at a higher velocity /

velocity than theoretically predicted. This discrepancy could be accounted for by some of the assumptions made in the theory. The theory ignored the presence of all the tubes, except for the production of the velocity component Vs. However the tubes, together with the associated pressure gradients around them, will have a definite effect on Vs, and the onset velocity. This is, to some extent, compensated for by the introduction of an effective cavity width in chapter 8.3. As Vs travels across the cavity some degree of decay in its magnitude will occur. This being due to viscous and turbulent shear stresses. This decay will effect all the instability regions, however it will be more pronounced for the higher order instability regions where there is a large phase shift between Vs and $\frac{\delta P}{\delta y}$. In this situation Vs opposes the production of an acoustic vibration at some points across the cavity width. Hence this decay could alter the point at which there is a net energy input to the system. The theory also assumes a constant velocity across the cavity. As shown by ref. F2, this assumption is not perfectly true and the velocity can vary throughout the width of the cavity. This effect should be quite small, however the effect on the higher order instability regions will be more pronounced.It was also assumed that Vs and $\frac{\delta P}{\delta y}$ were in phase, although this should be quite realistic there may be a small phase difference, especially at the higher /

higher reduced velocities. However this would only cause a small increase in the reduced velocity for onset of the π instability region.

In figures 7.31 - 7.35 the acoustic damping/velocity relationships for various row depths of the $X_T = 2.0$, $X_L = 1.67$ geometry are illustrated. The results shown in figure 7.31 were obtained prior to the alteration in measurement technique. Therefore these results are limited to the lower velocities and do not show any clear trends. In the case of figures 7.32 - 7.35 a dramatic decrease in the damping is experienced when the onset velocity is approached. Some typical transfer function phase and coherence results are shown in figures 7.38 - 7.42. These results were obtained from the 12 row bank, (velocity indicated on each diagram) and clearly shows the change in damping illustrated by the previous diagrams. This result verifies the approach taken by the feedback model; that is, the acoustic resonance is self excited. If this had been a resonance condition, then no change in damping would have been indicated. Also when the forcing frequency came close to the natural frequency of the mode, then the coherence (which indicates the signal to noise ratio) would have fallen to a low value because the exciting force would appear as noise. As can be seen from figure 8.5 the theory gives a very close approximation of the acoustic damping behaviour for the

π /

π instability region.

The assumption that the acoustic resonance is a self excited mechanism is further substantiated by the results in figures 7.35 - 7.37. These diagrams illustrate the results obtained when the acoustic damping of the tunnel was increased. In figure 7.35 the damping/velocity relationship in the 12 row bank, is shown for the standard and increased damping values. Unfortunately the increase in damping was not large enough to be detected by the instrumentation when no air flow was present. Nevertheless a 14% increase in the onset velocity was obtained.

The three dimensional plot in figure 7.37, shows the result obtained when the acoustic damping was further increased. This increase was obtained by using the piston cut out as an additional radiator. This of course meant that no damping measurement could be made. Nevertheless the effect is obvious. As shown in this diagram no evidence of a resonance is detected until a velocity of $36ms^{-1}$, at which point the peak had reached 110dB. This peak is very sharp and the onset velocity has increased by a value in excess of 38%.

Resonant systems and self excited systems respond in a very different way to an increase in damping. Where as in a simple resonant system and increase in damping will produce a decrease in amplitude, (and increase in bandwidth) a small increase in damping in a /

a self excited system can eliminate vibration completely. Clearly these results show that the acoustic mechanisms behaviour is consistant with that of a self excited system.

To conclude this chapter a summary of some of the more important points from the previous section shall be presented:

1. It has been clearly shown that vortex shedding is not the mechanism responsible for the excitation of the acoustic resonance.
2. The vortex shedding peak becomes more pronounced as the bank depth is increased.
3. The Stroùhal numbers derived in this investigation show good correlation with the Strouhal number map presented by ref. M4.
4. The mode of acoustic vibration excited in banks I, II and III was the transverse mode of the bank.
5. The frequency of the acoustic resonance,once excited was observed to increase with velocity.
6. The Acoustic Strouhal number was observed to vary in indirect proportion to the longitudinal pitch.
7. The same mode of vibration can be excited in several different velocity regions. This can result in modes being excited several times or the modes being excited in an irregular sequence.
8. The behaviour of the acoustic mechanism has been shown/

shown to be consistant with that of a self excited system.

9. The feedback model, as presented in chapter 8 has been shown to describe the behaviour of the mechanism very accurately. It also has the facility to account for all the observations made in this investigation. As explained previously some of the assumptions made in the theory are over simplifications of the actual situation, nevertheless, the model does give useful insight to the mechanism responsible for this phenomenon.

9.9 DESIGN PROCEDURE

The results from this investigation have clearly shown that tube vibration and the acoustic resonance phenomena must be treated separately. When designing a tube bank to be free from vortex induced tube vibrations, then a Strouhal number correlation where the data has been derived by a non acoustic technique should be used. That is a technique which does not rely on the acoustic response of the bank e.g. tube vibration, vortex peaks in the pressure spectra, hot wire anemometry, etc. An example of such a correlation is shown in figure 2.9. The Strouhal numbers from such a correlation can then be reliably used to predict vortex induced tube vibration.

It is clear from the results presented in this study that the conditions under which damaging acoustic responses /

responses occur are very dependent on the damping offered to the acoustic mode. However the results do indicate that the excitation of the π region of instability will not occur for values of $\frac{U}{fd} < 2(X_L - 0.5)$

As the tube pitch to diameter ratios are increased the frequency of vortex shedding will be allowed to approach that of the acoustic resonance. Therefore one must ensure that these frequencies do not coincide. However due to the Strouhal numbers associated with the two phenomena this should only be possible for longitudinal pitches of 2.5 and greater. Therefore for these tube spacings the value of $\frac{U}{fd}$ should be kept below 4.5 to ensure the absence of any acoustic resonances, see figure 8.2.

It is uncertain what value of acoustic damping will be encountered in a full size heat exchanger. Nevertheless the existence of the higher order regions of instability must be considered. The theory predicts that these regions will occur for $\frac{\omega a}{U} = 3\pi, 5\pi$, etc. For the banks with a transverse pitch to diameter ratio of 2.0, which were investigated in this study, the S.P.L.s, produced in these regions, were not of practical significance. However in the case of the banks with a transverse pitch to diameter ratio of 1.34 the 3π region produced very large S.P.L.s. Hence it would seem from the data available that these regions are /

are of little practical significance for banks with a large transverse tube spacing, however they must be considered in banks with small transverse tube spacings. This could be due to the smaller value of open area in these banks which, as described in chapter 9.1, reduces the value of the radiation damping term. Therefore the higher order instability regions can be excited.

Current design procedures allow for the insertion of baffle plates between the tube columns. The insertion of such a plate reduces the cavity width and therefore increases the acoustic frequency. This will have the effect of moving the operating point vertically downwards on figure 8.2. If these measures can not be used and it is not possible to operate within these bounds, then model tests should be undertaken. However the model should be designed to ensure that the acoustic damping is similar to that of the prototype. This implies that a comparable row depth, scale and wall stiffness should be used.

10.0 CONCLUSIONS

The three dimensional plots of S.P.L. / frequency / velocity for banks I, II and III clearly show the existence of a velocity dependant peak with the characteristics of vortex shedding. These plots also show the vortex shedding peak to be well removed from the frequency of acoustic resonance when the resonance is first initiated. The results have also shown the two mechanisms to respond quite differently to changes in the banks geometry. The Acoustic Strouhal number was found to be inversley proportional to the longitudinal pitch, while the Strouhal number remained constant for banks I, II and III. However when the transverse pitch was reduced in banks IV, V and VI no evidence of vortex shedding was detected. In banks I, II and III it was found that the Acoustic Strouhal number was reduced in shallow banks and stabilised to a constant value as the row depth was increased. The only row depth effect noticed for the Strouhal number was that the vortex shedding peak was seen to become more pronounced as the row depth was increased. On this basis it is concluded that vortex shedding is not the mechanism which is responsible for exciting the acoustic resonance in tightly packed banks. It was also shown that none of the main theories on the acoustic phenomenon could satisfactorily explain the mechanism or its complex nature./

nature.

The results obtained by measuring the acoustic damping under flow conditions shows that the acoustic damping tends towards zero as the onset velocity is approached. This suggests that some sort of feedback mechanism is responsible for the sudden onset of high noise levels. The results have also shown that the velocity at which these high noise levels occur is very sensitive to variations in the acoustic damping. Small increases in this parameter have been seen to cause a mode to disappear. This behaviour supports the idea of a feedback mechanism and is in direct contrast to the behaviour of a resonant system. In the case of a resonant system, a small increase in damping will result in a reduction in the amplitude and frequency of vibration, together with an increase in the bandwidth of the resonant peak. It can be observed from the results that each time a resonance was excited the peak was practically a pure tone. (regardless of the initial damping). The results also demonstrate that if the acoustic damping was sufficiently large it could cause a mode of vibration to be missed completely.

Chapter 8 shows the development of the theortical model. As can be seen this approach has the facility to accommodate all the observations made in this study. For example the theory predicts the existance of additional "resonant" zones at $\frac{\omega a}{U} = 3\pi, 5\pi$ etc. The results /

results from the experiments also revealed the existence of such zones. Likewise the variation of acoustic damping with velocity, as predicted by the theory, gives a good representation of that measured in the tunnel.

Finally when designing an in-line cross flow heat exchanger, with plain tubes, then the guidelines in Chapter 9.9 should be followed to predict the conditions required for acoustic resonances and vortex induced tube vibration.

11.0 FURTHER WORK

Although the work described herein has gone some way in explaining the anomalies in the literature, there are some questions which remain unanswered. It is therefore felt that the following work would be a logical progression of the research in this field:

1) The present work was restricted to in-line arrays. Although, in general, good agreement between Acoustic Strouhal Numbers and Strouhal Numbers have been obtained for staggered arrays, some inconsistancies have been observed (ref. B6 and Z4). A study similar to the present could be carried out to establish if vortex shedding is responsible for the acoustic resonance, or if a similar mechanism to that observed in this study exists for irregular arrays.

2) Many heat exchangers employ the use of finned tubes to improve the heat transfer characteristics of the bank. The effect of using finned tubes on the acoustic system could possibly be accounted for by using an equivalent diameter for the tube. This might be achieved in a similar manner to that used for vortex shedding. Nevertheless this is an area where uncertainty does exist and the effect of various sizes of fin should be investigated.

3) Some further work should also be done to quantify the damping values to be incorporated in the acoustic model./

model. This should include the following areas of work:

a) Gather data from existing plant and establish typical values of acoustic damping in such equipment.

b) To evaluate the acoustic damping required to stabilise a mode of vibration in various different geometries. This would establish how the geometry, particularily the transverse geometry, effects this requirement. This work should include an investigation of the requirements for the higher order stability regions and modes of vibration.

c) Using the information obtained in a) and b) a full design criterion could be formulated. This would indicate the geometries, dampings etc that will cause a region or mode to become unstable.

ACKNOWLEDGEMENTS

The author wishes to express his sincere thanks to Dr B.G. Murray for his supervision, technical guidance and encouragement during the course of this project, and for his patience during the prolonged period of writing.

For making this project possible and for their support and cooperation during the course of this work the author wishes to thank the staff of Robert Gordon's Institute of Technology, with special thanks going to Mr J. Bathgate for his work in the construction of the test facility.

This work would not have been possible without the funding provided by the Science Research Council and Babcock Power Ltd and the author expresses his thanks to the above bodies.

For deciphering the manuscript and her meticulous typing of the work, the author wishes to thank Miss Julia H. Rae.

Finally, but by no means least the author expresses his thanks to his family for the support and encouragement received during the period of the work.

REFERENCES

A1 F.H. Abernathy and R.E. Kronauer - The Formation of Vortex Streets, Journal of Fluid Mechanics Vol. 13 1962 pp1-20.

A2 F.S. Archibald - Self-Excitation of an Acoustic Resonance by Vortex Shedding, Journal of Sound and Vibration Vol 28(1) 1975 pp81-103.

B1 D. Bai - Vortex-Excited Vibration and Acoustic Phenomena in Tube Banks in Cross Flow, Stress and Materials in Reactor Technology Conf. London 1975.

B2 R.C. Baird - Pulsation Induced Vibration in Steam Generating Units, Combustion Vol. 25 April 1954 pp38-44.

B3 E.A. Barrington - Cure Exchanger Acoustic Hydrocarbon Processing Vol. 57 July 1978 pp193-198.

B4 J.P. Batham - Pressure Distributions on In-Line Tube Arrays in Cross Flow, International Symposium on Vibration Problems in Industry, Keswick Session 4 April 1973 paper 411 JKAEA/NPL.

B5 J.P. Batham - Pressure Distributions on Circular Cylinders at Critical Reynolds Numbers, Journal of Fluid Mechanics Vol. 57(2) 1973 pp209-228.

B6 J.A. Baulay - The Generation of Acoustic Vibrations in Tubular Heat Exchangers. A study of the Phenomenon, M.Sc. Thesis, University of Newcastle-upon-Tyne June 1969 Thesis no. H610.

B7 G. Baylac, D. Bai and J.P. Gregoire - Study of Flow and Acoustic Phenomena in a Tube-Bank, International Symposium on Vibration Problems in Industry Keswick Session 2, April 1973 UKAEA/NPL.

B8 G. Baylac and J.P. Gregoire - Acoustic Phenomena in a Steam Generating Unit, Journal of Sound and Vibration Vol 42(1) 1975 pp31-48.

B9 L.L. Bevanek - Noise and Vibration Control.

B10 C. Bingham, M.D. Godfrey and J.W. Tukey - Modern Techniques of Power Spectrum Estimation. I.E.E.E. /

I.E.E.E. Transactions on Audio and Electoacoustics Vol AU-15(2) June 1967 pp56-66.

B11 R.D. Blevins - Flow Induced Vibration, Van Nostrand Reinhold New York 1977.

B12 R.D. Blevins - Acoustic Resonance in Heat Exchanger Tube, Bundles, Proceedings of the the Third International Conference on Vibration in Nuclear Plant (Keswick) May 1982.

B13 A.N. Bolton - Silencing Fans and Blowers, Engineering Designer March 1980 pp20-24.

B14 W.B. Bryce, J.S. Wharmby and J. Fitzpatrick - Duct Acoustic Resonances Induced by Flow Over Coiled and Rectangular Heat Exchanger Test Banks of Plain and Finned Tubes B.N.E.S. Vibration in Nuclear Plant, Keswick Session 3 May 1978 paper 3:5.

B15 W.B. Bryce and B.G. Murray - Design Criteria for Flow Induced Vibration in Heat Exchangers, Symposium on Practical Experiences with Flow Induced Vibrations, Karlsruhe, Germany, Session A Sept. 1979 pp118-128. See pocket at rear

B16 British Standard - Methods of Testing Fans for General Purposes B.S. 848 Part (1) 1980.

B17 T.E. Burton - Letter to the Editor, Sound Speed in a Heat Exchanger Tube Bank, Journal of Sound and Vibration Vol. 71 (1) 1980 pp157-160.

B18 Bruel and Kjaer - Application of B & K Equipment to Frequency Analysis.

B19 Babcock Power Ltd - Personal Communication.

B20 R.E.D. Bishop and A.Y. Hassan - The Lift and Drag Forces on a Circular Cylinder in a Flowing Fluid, Proc. of Royal Soc. London Series A Vol. 277 1964 pp32-75.

C1 S.S. Chen - Cross Flow-Induced Instabilities of Circular Cylinders, Shock and Vibration Digest Vol. 12 May 1980 pp21-34.

C2 Y.N. Chen - Frequency of the Karman Vortex Streets in Tube Banks, Journal of the Royal Aeronautical Society Vol. 71 March 1967 pp211-214.

C3 Y.N. Chen - Flow Induced Vibration and Noise in Tube/

Tube Bank Heat Exchangers Due to Von Karman Streets, Transactions of A.S.M.E. Feb. 1968 pp134-146.

C4 Y.N. Chen and M. Weber - Flow Induced Vibrations in Tube Bundle Heat Exchangers with Cross and Parallel Flow. Winter annual meeting of A.S.M.E. Flow Induced Vibration in Heat Exchangers Dec. 1970 pp57-77.

C5 Y.N. Chen - Fluctuating Lift Forces of the Karman Vortex Streets on Single Circular Cylinders and in Tube Bundles, Journal of Engineering for Industry May 1972 pp603-628.

C6 Y.N. Chen - Karman Vortex Streets and Flow Induced Vibrations in Tube Banks, Journal of Engineering for Industry Feb. 1973 pp410-414.

C7 Y.N. Chen - The Orbital Movement and the Damping of the Fluidelastic Vibration of Tube Banks Due to Vortex Formation, Transactions of the A.S.M.E. Journal of Engineering for Industry (1), (2) and (3) Aug 1974 pp1060-1075.

C8 P. Clasen and R. Gregorig - A Vibration Criterion for a Tube in Transverse Flow, Chemie-Ing-Tech Vol. 43 1971 pp982-985.

C9 P. Clasen - Vibration Criterion for a Tube in Cross Flow, Chemie-Ing-Tech 1972 pp671-679.

C10 L.J. Cohen and W.J. Deane - Elimination of Destructive Self Excited Vibrations in Large Gas and Oil Fired Utility Units, Journal of Engineering for Power Vol. 87 April 1965 pp223-228.

C11 H.J. Connors - Fluidelastic Vibration of Tube Arrays Excited by Cross Flow, Winter annual meeting of A.S.M.E, Flow Induced Vibrations in Heat Exchangers Dec. 1970 pp42-57.

C12 N.A. Cumpsty and D.S. Whitehead - The Excitation of Acoustic Resonances by Vortex Shedding, Journal of Sound and Vibration 1971 pp353-369.

C13 N. Curle - The Influence of Solid Boundaries upon Aerodynamic Sound. Proceedings of Royal Society Series A Vol. 231 1955 pp505-514.

C14 Y.N. Chen - Sulzer Research. 1966 p70.

D1 J.P. Den Hartog - Mechanical Vibrations, Fourth Edition McGraw-Hill Book Company 1965.

D2/

D2 I.S. Donaldson - Turbulence and Acoustic Signals in a Cross-Flow Heat Exchanger Model, Conference Proceedings, Flow Induced Vibrations June 1979 pp123-128.

D3 R.C.F. Dye - Flow Induced Vibration and Noise with Particular Reference to Heat Exchanger Tube Systems. Proceedings of I.Mech.E Vol 180 (3J) Paper 17 1965-66 pp260-267.

D4 R.C.F. Dye - Vortex-Excited Vibration of a Heat Exchanger Tube Row in Cross Flow. International Symposium on Vibration Problems in Industry Keswick Vol 4 (417) 1973 pp1-8.

E1 J.B.Erskine and W. Waddington - A Review of Some Tube Vibration Failures in Shell and Tube Heat Exchangers and Failure Prediction Methods. International Symposium on Vibration Problems in Industry Keswick Session 4 April 1973.

F1 J.S. Fitz-Hugh - Flow Induced Vibration in Heat Exchangers, International Symposium on Vibration Problems in Industry Keswick Session 4 April 1973.

F2 J.A. Fitzpatrick - A Study of Flow and Acoustic Phenomena in Tube Banks. Ph.d. Thesis. Queens Univeristy Belfast 1976.

F3 J.A. Fitzpatrick and I.S. Donaldson - A Preliminary Study of Flow and Acoustic Phenomena in Tube Banks, An A.S.M.E. publication 77-FE-7.

F4 M. Funakawa and R. Umakoshi - The Acoustic Resonance in a Tube Bank. Bullitin Japanese Society of Mechanical Engineers Vol. 13 1970 pp348-355.

F5 M. Funakawa - Vibration of Tube Banks by Wake Force. International Symposium on Vibration Problems in Industry Keswick Session 4 April 1973.

G1 C.R. Gerlach and F.T. Dodge - An Engineering Approach to Tube Flow-Induced Vibrations Winter annual meeting of A.S.M.E. Flow Induced Vibration in Heat Exchangers Dec. 1970.

G2 J.H. Gerrard - An Experimental Investigation of the Oscillating lift and Drag of a Circular Cylinder Shedding Turbulent Vortices, Journal of Fluid Mechanics Vol. 11 pp244-256.

G3/

G3 R.W.F. Gould and P.J. Ponsford - Experiments with Surface Roughness to Enhance the Effective Reynolds Number of Wind Tunnel Tests on Grouped Legs Representing a Concrete Gravity Platform. Department of Industry U.K. Maritime Institute Report R67 June 1982.

G4 R. Gregorig and H.K.M. Andritzky - Vibrational Criterion for a Tube Under Conditions of Transverse Flow Chem-Ing-Tech Vol. 39 Aug. 1967 pp894-900.

G5 R. Gregorig and H.K.M. Andritzky - Vibrational criterion for a pipe under Conditions of Transverse Incident Flow Chemie-Ing-Technik Vol. 40 May 1968 pp483-488.

G6 E.D. Grimison - Correlation and Utilization of New Data on Flow Resistance and Heat Transfer for Cross Flow of Gasses over Tube Banks. Transactions of A.S.M.E. Vol. 59 pp583-594.

G7 B.J. Grotz and F.R. Arnold - Flow Induced Vibrations in Heat Exchangers. Department of Mechanical Engineering, Stanford University Technical Report no. 3 Aug. 1956.

H1 E. Heinecke - Stationary and Instationary Flow Phenomena in and Behind Staggered and In-Line Tube Banks, International Symposium on Vibration Problems in Industry Keswick Session 4 April 1973.

H2 R.J. Hill and C. Armstrong - Aerodynamic Sound in Tube Banks. Proceedings of Phys. Soc. Vol. 79 (1) Jan 1962 pp225-227.

H3 R.T. Hartlen - Recent Field Experience with Flow Induced Vibration of Heat Exchanger Tubes. Vibration Problems in Industry. International Symposium on Vibration Problems in Industry, Keswick, Session 4 April 1973.

I1 S. Ishigai and E. Nishikawa - Experimental Study of Structure of Gas Flow in Tube Banks with Tube Axis Normal to Flow Bullitin of the J.S.M.E. Vol. 18 no. 119 May 1875 pp528-535.

J1 A. Jaudet and D. Hutzler - Acoustic Pulsations and Vibratory Stresses in Heat Exchangers, Heat Exchangers Conference Paris June 1971 pp255-271.

K1 S.C. Kacker, B. Pennington and R.S. Hill - Measurement of /

of the Fluctuating Lift Coefficient and of the Correlation Length for Vortex Shedding from Cylindrical Tubes. International Symposium on Vibration Problems in Industry Keswick 1973 Paper 416 pp1-21.

K2 A Konig and R. Gregorig - Vibrational Criteria for a pipe Under Conditions of Transverse Incident Flow. Chemie-Ing-Technik Vol. 40 1968 pp645-650.

L1 H.C. Lin and S.S. Chen - Acoustically Induced Vibration of Circular Cylinderical Rods, Journal of Sound and Vibration Vol. 51(1) 1977 pp89-96.

L2 J.L. Livesey and C.F. Dye - Vortex Excited Vibration of a Heat Exchanger Tube Row, Journal of Mechanical Engineering Science Vol. 4(4) 1962 pp349-352.

MC1 C. MacKenzie - Flow Induced Vibration at Inlet Region of H.P. Bank of Hartlepool, Babcock Power Internal Report.

MC2 W.H. McAdams - Heat Transmission, Third Edition. McGraw-Hill.

M1 M.V. Morkovin - Flow Around Circular Cylinder - A Kaleidoscope of Challenging Fluid Phenomena. Proceedings of A.S.M.E. Symposium. Philadelphia May 1964 pp102-118.

M2 Morse and Ingard - Theoretical Acoustics, McGraw -Hill.

M3 B.G. Murray - Internal Babcock and Wilcox Report, 1977.

M4 B.G. Murray, G. Rae and W.B. Bryce - Strouhal Numbers in Tube Arrays. Proceedings of the 3rd International Conference on Vibration in Nuclear Plant Session 2 May 1982 (Keswick) pp231-243.

N1 D.E. Newlands - An Introduction to Random Vibrations and Spectral Analysis. Fourth Edition Longman Series.

O1 P.R. Owen - Buffeting Excitation of Boiler Tube Vibrations, Journal of Mechanical Engineering Science Vol. 7 (4) 1965 pp431-439.

P1 R. Parker - Acoustic Resonances in Passages Containing Banks of Heat Exchanger Tubes, Journal/

Journal of Sound and Vibration Vol. 57(2) 1978 pp245-260.

P2 I.S. Pearsall - Calibration of Three Conical Inlet Nozzles, National Engineering Laboratory Report No. 39 . Department of Scientific and Industrial Research June 1962.

P3 A.A. Putnam - Flow Induced Noise and Vibration in Heat Exchangers, An A.S.M.E. Publication 64-WA/HT-21.

P4 A.A. Putnam - Flow Induced Noise in Heat Exchangers, Journal of Engineering for Power Vol.81(4) Oct. 1959 pp417-422.

P5 M.J. Pettigrew and A.O. Campagna - Heat Exchanger Tube Vibration: Comparison Between Operating Experiences and Vibration Analysis, Symposium on Practical Experiences with Flow - Induced Vibrations, Karlsruhe, Germany Session A Sept. 1979 pp72-83.

R1 B.W. Roberts - Low Frequency Aeroelastic Vibrations in a Cascade of Circular Cylinders, Mechanical Engineering Science Monograph No.4 Sept. 1966.

R2 J.D. Rodgers and C.A. Penterson - Predicting Sonic Vibration in Cross Flow Heat Exchangers - Experience and Model Testing, An A.S.M.E. Publication 77-WA/DE-28 1977.

R3 A. Roshko - Experiments on the Flow Past a Circular Cylinder at Very High Reynolds Number, Journal of Fluid Mechanics Vol.10 pp345-356.

S1 S.D. Savkar - A Survey of Flow - Induced Vibrations of Cylinderical Arrays in Cross Flow, An A.S.M.E. Publication 76-WA/FE-21.

T1 G.H. Toebes - The Unsteady Flow and Wake Near an Oscillating Cylinder, Journal of Basic Engineering Series D Vol.91(3) Sept. 1969 pp493-505

W1 W.M. Walker and G.F.S. Reising - Flow Induced Vibrations in Cross Flow Heat Exchangers, Chemical and Process Engineering Nov. 1968 pp95-103.

Z1 M.M. Zdravkovich - Flow Induced Vibrations in Irregular Staggered Tube Bundles and Their Suppression, International Symposium on Vibration Problems in Industry Keswick Session 4 April 1973.

Z2 /

Z2 M.M. Zdravkovich - On the Elimination of Aerodynamic Noise in a Staggered Tube Bank, Journal of Sound and Vibration Vol.34(2) 1974 pp173-177.

Z3 A. Zukauskas and V. Katinas - Flow - Induced Vibration in Heat Exchanger Tube Banks, Symposium on Vibration Problems in Industry Keswick Session 4 April 1973.

Z4 M.M. Zdravkovich and J.A. Nuttal - On the Elimination of Aerodynamic Noise in a Staggered Tube Bank , Journal of Sound and Vibration Vol.32(4) 1974 pp173-177.

APPENDIX 1

ROW DEPTH RESULTS

BANK GEOMETRY X_T= 2.0 X_L=1.67

BANK DEPTH 1 ROWS	
ACOUSTIC FREQUENCY	295 Hz
VELOCITY U (m/s)	S.P.L. (d B)
16.33	105
17.56	124
18.12	130
19.55	148
ACOUSTIC STROUHAL NUMBER S_A= 0.163	

BANK DEPTH 2 ROWS	
ACOUSTIC FREQUENCY	870 Hz
VELOCITY U (m/s)	S.P.L. (dB)
12.35	---
12.54	120
13.08	---
ACOUSTIC STROUHAL NUMBER S_A= 0.659	

BANK DEPTH 3 ROWS	
ACOUSTIC FREQUENCY	288 Hz
VELOCITY U (m/s)	S.P.L. (dB)
15.99	108
16.37	112
16.42	116
16.56	146
ACOUSTIC STROUHAL NUMBER S_A= 0.161	

BANK GEOMETRY $X_T = 2.0$ $X_L = 1.67$

BANK DEPTH	5 ROWS
ACOUSTIC FREQUENCY	280 Hz
VELOCITY U (m/s)	S.P.L. (d B)
16.18	100
16.65	104
17.20	110
17.33	148
ACOUSTIC STROUHAL NUMBER $S_A = 0.154$	

BANK DEPTH	5 ROWS
ACOUSTIC FREQUENCY	840 Hz
VELOCITY U (m/s)	S.P.L. (dB)
15.7	98
16.18	106
16.65	116
17.2	124
17.33	90
ACOUSTIC STROUHAL NUMBER $S_A = 0.471$	

BANK DEPTH	10 ROWS
ACOUSTIC FREQUENCY	285 Hz
VELOCITY U (m/s)	S.P.L. (dB)
13.88	100
14.47	115
14.89	118
14.95	148
ACOUSTIC STROUHAL NUMBER $S_A = 0.182$	

BANK GEOMETRY X_T= 2.0 X_L= 1.67

BANK DEPTH	12 ROWS
ACOUSTIC FREQUENCY	285 Hz
VELOCITY U (m/s)	S.P.L. (d B)
12.75	104
13.25	104
13.93	116
14.10	154
ACOUSTIC STROUHAL NUMBER S_A= 0.194	

BANK DEPTH	12 ROWS
ACOUSTIC FREQUENCY	515 Hz
VELOCITY U (m/s)	S.P.L. (dB)
11.17	83
11.71	92
12.03	116
ACOUSTIC STROUHAL NUMBER S_A= 0.407	

BANK DEPTH	18 ROWS
ACOUSTIC FREQUENCY	272 Hz
VELOCITY U (m/s)	S.P.L. (dB)
11.91	108
12.03	116
12.07	157
ACOUSTIC STROUHAL NUMBER S_A= 0.215	

BANK GEOMETRY X_T= 2.0 X_L= 1.67

BANK DEPTH 23 ROWS	
ACOUSTIC FREQUENCY 268 Hz	
VELOCITY U (m/s)	S.P.L. (d B)
10.6	104
11.07	108
11.44	118
11.48	154
ACOUSTIC STROUHAL NUMBER S_A= 0.222	

BANK DEPTH 28 ROWS	
ACOUSTIC FREQUENCY 250 Hz	
VELOCITY U (m/s)	S.P.L. (dB)
5.04	92
5.55	106
5.76	120
ACOUSTIC STROUHAL NUMBER S_A= 0.413	

BANK DEPTH 28 ROWS	
ACOUSTIC FREQUENCY 265 Hz	
VELOCITY U (m/s)	S.P.L. (dB)
9.81	98
10.71	104
11.31	116
11.41	156
ACOUSTIC STROUHAL NUMBER S_A= 0.223	

BANK GEOMETRY $X_T = 2.0$ $X_L = 1.67$

BANK DEPTH	33 ROWS
ACOUSTIC FREQUENCY	255 Hz
VELOCITY U (m/s)	S.P.L. (d B)
10.00	100
10.78	110
11.00	116
11.07	152
ACOUSTIC STROUHAL NUMBER $S_A = 0.220$	

BANK DEPTH	38 ROWS
ACOUSTIC FREQUENCY	252 Hz
VELOCITY U (m/s)	S.P.L. (dB)
10.00	100
10.71	112
10.82	114
10.86	154
ACOUSTIC STROUHAL NUMBER $S_A = 0.221$	

BANK DEPTH	43 ROWS
ACOUSTIC FREQUENCY	248 Hz
VELOCITY U (m/s)	S.P.L. (dB)
5.67	102
6.85	90
ACOUSTIC STROUHAL NUMBER $S_A = 0.409$	

BANK GEOMETRY X_T= 2.0 X_L=1.67

BANK DEPTH 43 ROWS	
ACOUSTIC FREQUENCY 252 Hz	
VELOCITY U (m/s)	S.P.L. (d B)
9.41	93
10.31	101
10.71	116
10.75	152
ACOUSTIC STROUHAL NUMBER S_A= 0.223	

BANK DEPTH 49 ROWS	
ACOUSTIC FREQUENCY 250 Hz	
VELOCITY U (m/s)	S.P.L. (dB)
9.41	96
10.00	108
10.27	150
ACOUSTIC STROUHAL NUMBER S_A= 0.236	

BANK DEPTH ROWS	
ACOUSTIC FREQUENCY Hz	
VELOCITY U (m/s)	S.P.L. (dB)
ACOUSTIC STROUHAL NUMBER S_A=	

BANK GEOMETRY $X_T = 2.0$ $X_L = 2.0$

BANK DEPTH 2 ROWS	
ACOUSTIC FREQUENCY 294 Hz	
VELOCITY U (m/s)	S.P.L. (d B)
13.65	106
13.99	116
14.26	142
16.18	152
ACOUSTIC STROUHAL NUMBER $S_A = 0.199$	

BANK DEPTH 3 ROWS	
ACOUSTIC FREQUENCY 292 Hz	
VELOCITY U (m/s)	S.P.L. (dB)
12.78	108
13.08	126
13.43	142
13.93	148
ACOUSTIC STROUHAL NUMBER $S_A = 0.214$	

BANK DEPTH 4 ROWS	
ACOUSTIC FREQUENCY 292 Hz	
VELOCITY U (m/s)	S.P.L. (dB)
12.29	---
12.54	114
12.72	142
ACOUSTIC STROUHAL NUMBER $S_A = 0.221$	

BANK GEOMETRY X_T= 2.0 X_L= 2.0

BANK DEPTH	5 ROWS
ACOUSTIC FREQUENCY	292 Hz
VELOCITY U (m/s)	S.P.L. (d B)
12.54	112
12.66	120
12.84	140
13.71	150
ACOUSTIC STROUHAL NUMBER S_A= 0.219	

BANK DEPTH	6 ROWS
ACOUSTIC FREQUENCY	290 Hz
VELOCITY U (m/s)	S.P.L. (dB)
12.9	114
13.02	126
13.14	144
ACOUSTIC STROUHAL NUMBER S_A= 0.214	

BANK DEPTH	7 ROWS
ACOUSTIC FREQUENCY	290 Hz
VELOCITY U (m/s)	S.P.L. (dB)
13.28	---
13.77	122
13.82	150
ACOUSTIC STROUHAL NUMBER S_A= 0.201	

BANK GEOMETRY X_T= 2.0 X_L = 2.0

BANK DEPTH	8 ROWS
ACOUSTIC FREQUENCY	288 Hz
VELOCITY U (m/s)	S.P.L. (d B)
13.19	112
13.71	120
14.37	152
ACOUSTIC STROUHAL NUMBER S_A= 0.200	

BANK DEPTH	9 ROWS
ACOUSTIC FREQUENCY	285 Hz
VELOCITY U (m/s)	S.P.L. (dB)
13.02	112
13.31	124
13.71	147
ACOUSTIC STROUHAL NUMBER S_A= 0.204	

BANK DEPTH	10 ROWS
ACOUSTIC FREQUENCY	285 Hz
VELOCITY U (m/s)	S.P.L. (dB)
12.13	112
12.57	120
12.69	152
ACOUSTIC STROUHAL NUMBER S_A= 0.215	

BANK GEOMETRY X_T=2.0 X_L=2.0

BANK DEPTH	11 ROWS
ACOUSTIC FREQUENCY	282 Hz
VELOCITY U (m/s)	S.P.L. (d B)
12.04	106
12.29	118
12.72	142
ACOUSTIC STROUHAL NUMBER S_A= 0.218	

BANK DEPTH	13 ROWS
ACOUSTIC FREQUENCY	280 Hz
VELOCITY U (m/s)	S.P.L. (dB)
12.41	105
12.90	124
13.02	144
ACOUSTIC STROUHAL NUMBER S_A= 0.208	

BANK DEPTH	15 ROWS
ACOUSTIC FREQUENCY	278 Hz
VELOCITY U (m/s)	S.P.L. (dB)
12.29	112
12.78	125
12.90	150
ACOUSTIC STROUHAL NUMBER S_A= 0.210	

BANK GEOMETRY X_T= 2.0 X_L = 2.0

BANK DEPTH 20 ROWS	
ACOUSTIC FREQUENCY 268 Hz	
VELOCITY U (m/s)	S.P.L. (d B)
11.03	98
11.78	112
12.1	142
ACOUSTIC STROUHAL NUMBER S_A= 0.215	

BANK DEPTH 24 ROWS	
ACOUSTIC FREQUENCY 265 Hz	
VELOCITY U (m/s)	S.P.L. (dB)
11.74	112
12.04	118
12.16	152
ACOUSTIC STROUHAL NUMBER S_A= 0.209	

BANK DEPTH 28 ROWS	
ACOUSTIC FREQUENCY 260 Hz	
VELOCITY U (m/s)	S.P.L. (dB)
11.07	102
11.94	120
11.97	146
ACOUSTIC STROUHAL NUMBER S_A= 0.207	

BANK GEOMETRY X_T= 2.0 X_L= 2.34

BANK DEPTH	24 ROWS
ACOUSTIC FREQUENCY	260 Hz
VELOCITY U (m/s)	S.P.L. (d B)
13.25	110
13.48	122
13.71	150
ACOUSTIC STROUHAL NUMBER S_A=0.183	

BANK DEPTH	31 ROWS
ACOUSTIC FREQUENCY	255 Hz
VELOCITY U (m/s)	S.P.L. (dB)
12.41	---
13.31	114
13.54	150
ACOUSTIC STROUHAL NUMBER S_A=0.182	

BANK DEPTH	42 ROWS
ACOUSTIC FREQUENCY	250 Hz
VELOCITY U (m/s)	S.P.L. (dB)
12.78	112
12.96	119
13.14	128
13.25	154
ACOUSTIC STROUHAL NUMBER S_A= 0.183	

BANK GEOMETRY X_T= 2.0 X_L=2.34

BANK DEPTH	12 ROWS
ACOUSTIC FREQUENCY	278 Hz
VELOCITY U (m/s)	S.P.L. (d B)
13.28	104
13.77	114
13.93	120
14.10	138
ACOUSTIC STROUHAL NUMBER S_A= 0.19	

BANK DEPTH	15 ROWS
ACOUSTIC FREQUENCY	270 Hz
VELOCITY U (m/s)	S.P.L. (dB)
12.41	98
13.02	110
13.31	132
13.54	142
ACOUSTIC STROUHAL NUMBER S_A= 0.195	

BANK DEPTH	20 ROWS
ACOUSTIC FREQUENCY	262 Hz
VELOCITY U (m/s)	S.P.L. (dB)
12.29	98
13.19	110
13.40	136
13.54	138
ACOUSTIC STROUHAL NUMBER S_A= 0.187	

BANK GEOMETRY X_T= 2.0 X_L=2.34

BANK DEPTH	2 ROWS
ACOUSTIC FREQUENCY	290 Hz
VELOCITY U (m/s)	S.P.L. (d B)
14.41	102
14.95	119
15.20	140
16.37	146
ACOUSTIC STROUHAL NUMBER S_A= 0.184	

BANK DEPTH	5 ROWS
ACOUSTIC FREQUENCY	290 Hz
VELOCITY U (m/s)	S.P.L. (dB)
13.60	110
14.04	124
14.42	148
ACOUSTIC STROUHAL NUMBER S_A= 0.196	

BANK DEPTH	9 ROWS
ACOUSTIC FREQUENCY	282 Hz
VELOCITY U (m/s)	S.P.L. (dB)
13.14	102
13.54	114
13.71	128
14.15	138
ACOUSTIC STROUHAL NUMBER S_A= 0.197	

BANK GEOMETRY X_T= 2.0 X_L= 2.0

BANK DEPTH 32 ROWS	
ACOUSTIC FREQUENCY 258 Hz	
VELOCITY U (m/s)	S.P.L. (d B)
10.72	104
11.71	122
11.78	158
ACOUSTIC STROUHAL NUMBER S_A= 0.211	

BANK DEPTH 45 ROWS	
ACOUSTIC FREQUENCY 252 Hz	
VELOCITY U (m/s)	S.P.L. (dB)
11.38	105
11.78	117
11.91	150
ACOUSTIC STROUHAL NUMBER S_A= 0.203	

BANK DEPTH ROWS	
ACOUSTIC FREQUENCY Hz	
VELOCITY U (m/s)	S.P.L. (dB)
ACOUSTIC STROUHAL NUMBER S_A=	

BANK GEOMETRY X_T= 1.34X_L=1.34

BANK DEPTH	1 ROWS
ACOUSTIC FREQUENCY	293 Hz
VELOCITY U (m/s)	S.P.L. (dB)
9.53	90
10.75	138
11.03	140
ACOUSTIC STROUHAL NUMBER S_A= 0.137	

BANK DEPTH	1 ROWS
ACOUSTIC FREQUENCY	590 Hz
VELOCITY U (m/s)	S.P.L. (dB)
17.90	102
18.37	116
19.03	126
19.23	142
ACOUSTIC STROUHAL NUMBER S_A= 0.153	

BANK DEPTH	2 ROWS
ACOUSTIC FREQUENCY	1170 Hz
VELOCITY U (m/s)	S.P.L. (dB)
13.31	108
13.77	118
14.42	122
15.05	116
15.85	116
ACOUSTIC STROUHAL NUMBER S_A= 0.400	

BANK GEOMETRY $X_T = 1.34$ $X_L = 1.34$

BANK DEPTH	2 ROWS
ACOUSTIC FREQUENCY	1240 Hz
VELOCITY U (m/s)	S.P.L. (d B)
13.31	108
13.77	116
14.42	138
15.05	122
15.85	122
ACOUSTIC STROUHAL NUMBER $S_A = 0.431$	

BANK DEPTH	2 ROWS
ACOUSTIC FREQUENCY	1440 Hz
VELOCITY U (m/s)	S.P.L. (dB)
13.77	104
14.42	116
15.05	128
15.85	142
ACOUSTIC STROUHAL NUMBER $S_A = 0.474$	

BANK DEPTH	3 ROWS
ACOUSTIC FREQUENCY	1410 Hz
VELOCITY U (m/s)	S.P.L. (dB)
16.28	110
16.37	114
16.84	140
ACOUSTIC STROUHAL NUMBER $S_A = 0.413$	

BANK GEOMETRY $X_T = 1.34$ $X_L = 1.34$

BANK DEPTH	5 ROWS
ACOUSTIC FREQUENCY	1300 Hz
VELOCITY U (m/s)	S.P.L. (d B)
9.37	94
9.69	118
10.16	122
ACOUSTIC STROUHAL NUMBER $S_A = 0.631$	

BANK DEPTH	5 ROWS
ACOUSTIC FREQUENCY	1360 Hz
VELOCITY U (m/s)	S.P.L. (dB)
15.9	---
16.42	114
16.65	148
ACOUSTIC STROUHAL NUMBER $S_A = 0.398$	

BANK DEPTH	5 ROWS
ACOUSTIC FREQUENCY	1580 Hz
VELOCITY U (m/s)	S.P.L. (dB)
11.24	110
11.58	112
12.03	122
ACOUSTIC STROUHAL NUMBER $S_A = 0.638$	

BANK GEOMETRY $X_T = 1.34 X_L = 1.34$

BANK DEPTH	9 ROWS
ACOUSTIC FREQUENCY	810 Hz
VELOCITY U (m/s)	S.P.L. (d B)
9.12	96
9.85	138
10.89	138
ACOUSTIC STROUHAL NUMBER $S_A = 0.410$	

BANK DEPTH	9 ROWS
ACOUSTIC FREQUENCY	1100 Hz
VELOCITY U (m/s)	S.P.L. (dB)
12.66	100
12.72	138
13.52	136
ACOUSTIC STROUHAL NUMBER $S_A = 0.418$	

BANK DEPTH	15 ROWS
ACOUSTIC FREQUENCY	770 Hz
VELOCITY U (m/s)	S.P.L. (dB)
9.53	110
9.73	120
10.01	130
10.82	132
ACOUSTIC STROUHAL NUMBER $S_A = 0.381$	

BANK GEOMETRY $X_T = 1.34$ $X_L = 1.34$

BANK DEPTH	15 ROWS
ACOUSTIC FREQUENCY	860 Hz
VELOCITY U (m/s)	S.P.L. (d B)
10.01	108
10.82	116
11.51	118
12.10	124
ACOUSTIC STROUHAL NUMBER $S_A = 0.354$	

BANK DEPTH	15 ROWS
ACOUSTIC FREQUENCY	980 Hz
VELOCITY U (m/s)	S.P.L. (dB)
12.10	---
12.35	124
ACOUSTIC STROUHAL NUMBER $S_A = 0.384$	

BANK DEPTH	20 ROWS
ACOUSTIC FREQUENCY	740 Hz
VELOCITY U (m/s)	S.P.L. (dB)
8.95	---
9.25	130
10.35	132
ACOUSTIC STROUHAL NUMBER $S_A = 0.388$	

BANK GEOMETRY $X_T = 1.34 X_L = 1.34$

BANK DEPTH	25 ROWS
ACOUSTIC FREQUENCY	820 Hz
VELOCITY U (m/s)	S.P.L. (d B)
8.60	---
9.20	120
9.69	152
10.53	156
ACOUSTIC STROUHAL NUMBER $S_A = 0.429$	

BANK DEPTH	30 ROWS
ACOUSTIC FREQUENCY	520 Hz
VELOCITY U (m/s)	S.P.L. (dB)
5.55	106
5.95	110
6.39	115
6.68	117
7.24	130
ACOUSTIC STROUHAL NUMBER $S_A = 0.369$	

BANK DEPTH	30 ROWS
ACOUSTIC FREQUENCY	730 Hz
VELOCITY U (m/s)	S.P.L. (dB)
8.19	112
8.42	118
8.69	124
8.95	148
ACOUSTIC STROUHAL NUMBER $S_A = 0.411$	

BANK GEOMETRY $X_T = 1.34$ $X_L = 1.34$

BANK DEPTH	20 ROWS
ACOUSTIC FREQUENCY	850 Hz
VELOCITY U (m/s)	S.P.L. (d B)
10.35	---
10.82	116
11.14	136
ACOUSTIC STROUHAL NUMBER $S_A = 0.376$	

BANK DEPTH	25 ROWS
ACOUSTIC FREQUENCY	520 Hz
VELOCITY U (m/s)	S.P.L. (dB)
6.21	108
6.63	118
6.91	124
7.55	128
ACOUSTIC STROUHAL NUMBER $S_A = 0.375$	

BANK DEPTH	25 ROWS
ACOUSTIC FREQUENCY	750 Hz
VELOCITY U (m/s)	S.P.L. (dB)
8.23	---
8.60	118
9.20	146
ACOUSTIC STROUHAL NUMBER $S_A = 0.416$	

BANK GEOMETRY $X_T = 1.34$ $X_L = 1.34$

BANK DEPTH	30 ROWS
ACOUSTIC FREQUENCY	790 Hz
VELOCITY U (m/s)	S.P.L. (dB)
8.69	---
8.95	116
9.29	126
9.45	138
9.69	148
ACOUSTIC STROUHAL NUMBER $S_A = 0.419$	

BANK DEPTH	42 ROWS
ACOUSTIC FREQUENCY	500 Hz
VELOCITY U (m/s)	S.P.L. (dB)
5.69	---
6.02	112
6.33	118
6.85	124
ACOUSTIC STROUHAL NUMBER $S_A = 0.370$	

BANK DEPTH	42 ROWS
ACOUSTIC FREQUENCY	580 Hz
VELOCITY U (m/s)	S.P.L. (dB)
6.85	---
7.45	118
7.85	124
8.28	122
ACOUSTIC STROUHAL NUMBER $S_A = 0.370$	

BANK GEOMETRY $X_T = 1.34$ $X_L = 1.34$

BANK DEPTH 42 ROWS	
ACOUSTIC FREQUENCY 640 Hz	
VELOCITY U (m/s)	S.P.L. (d B)
7.85	---
8.28	118
8.42	126
8.69	128
ACOUSTIC STROUHAL NUMBER $S_A = 0.370$	

BANK DEPTH 42 ROWS	
ACOUSTIC FREQUENCY 700 Hz	
VELOCITY U (m/s)	S.P.L. (dB)
8.28	116
8.42	122
8.69	142
ACOUSTIC STROUHAL NUMBER $S_A = 0.403$	

BANK DEPTH ROWS	
ACOUSTIC FREQUENCY Hz	
VELOCITY U (m/s)	S.P.L. (dB)
ACOUSTIC STROUHAL NUMBER $S_A =$	

BANK GEOMETRY X_T=1.34 X_L=1.67

BANK DEPTH	2 ROWS
ACOUSTIC FREQUENCY	292 Hz
VELOCITY U (m/s)	S.P.L. (d B)
9.61	106
10.16	112
10.96	140
ACOUSTIC STROUHAL NUMBER S_A=0.136	

BANK DEPTH	2 ROWS
ACOUSTIC FREQUENCY	580 Hz
VELOCITY U (m/s)	S.P.L. (dB)
14.04	104
15.40	110
15.85	118
16.18	154
ACOUSTIC STROUHAL NUMBER S_A=0.176	

BANK DEPTH	2 ROWS
ACOUSTIC FREQUENCY	2650 Hz
VELOCITY U (m/s)	S.P.L. (dB)
14.69	106
15.25	116
15.99	128
ACOUSTIC STROUHAL NUMBER S_A=0.824	

BANK GEOMETRY X_T= 1.34 X_L = 1.67

BANK DEPTH	5 ROWS
ACOUSTIC FREQUENCY	2480 Hz
VELOCITY U (m/s)	S.P.L. (d B)
13.65	102
14.63	108
15.20	120
15.94	114
ACOUSTIC STROUHAL NUMBER S_A= 0.786	

BANK DEPTH	ROWS
ACOUSTIC FREQUENCY	Hz
VELOCITY U (m/s)	S.P.L. (dB)
ACOUSTIC STROUHAL NUMBER S_A=	

BANK DEPTH	ROWS
ACOUSTIC FREQUENCY	Hz
VELOCITY U (m/s)	S.P.L. (dB)
ACOUSTIC STROUHAL NUMBER S_A=	

BANK GEOMETRY $X_T = 1.34$ $X_L = 1.67$

BANK DEPTH	10 ROWS
ACOUSTIC FREQUENCY	870 Hz
VELOCITY U (m/s)	S.P.L. (d B)
11.24	108
11.48	116
11.78	110
ACOUSTIC STROUHAL NUMBER $S_A = 0.365$	

BANK DEPTH	15 ROWS
ACOUSTIC FREQUENCY	Hz
VELOCITY U (m/s)	S.P.L. (dB)
No Resonance	
ACOUSTIC STROUHAL NUMBER $S_A =$	

BANK DEPTH	19 ROWS
ACOUSTIC FREQUENCY	Hz
VELOCITY U (m/s)	S.P.L. (dB)
No Resonance	
ACOUSTIC STROUHAL NUMBER $S_A =$	

BANK GEOMETRY $X_T = 1.34$ $X_L = 1.67$

BANK DEPTH	25 ROWS
ACOUSTIC FREQUENCY	Hz
VELOCITY U (m/s)	S.P.L. (d B)
No Resonance	
ACOUSTIC STROUHAL NUMBER S_A=	

BANK DEPTH	30 ROWS
ACOUSTIC FREQUENCY	Hz
VELOCITY U (m/s)	S.P.L. (dB)
No Resonance	
ACOUSTIC STROUHAL NUMBER S_A=	

BANK DEPTH	40 ROWS
ACOUSTIC FREQUENCY	640 Hz
VELOCITY U (m/s)	S.P.L. (dB)
7.75	---
8.42	126
8.51	118
ACOUSTIC STROUHAL NUMBER S_A=	

BANK GEOMETRY $X_T = 1.34$ $X_L = 2.0$

BANK DEPTH	2 ROWS
ACOUSTIC FREQUENCY	290 Hz
VELOCITY U (m/s)	S.P.L. (d B)
8.42	96
9.45	104
9.69	128
10.16	140
10.82	156
ACOUSTIC STROUHAL NUMBER $S_A = 0.145$	

BANK DEPTH	2 ROWS
ACOUSTIC FREQUENCY	318 Hz
VELOCITY U (m/s)	S.P.L. (dB)
13.02	100
14.04	126
14.53	---
ACOUSTIC STROUHAL NUMBER $S_A = 0.111$	

BANK DEPTH	2 ROWS
ACOUSTIC FREQUENCY	350 Hz
VELOCITY U (m/s)	S.P.L. (dB)
13.02	108
14.04	130
14.53	150
ACOUSTIC STROUHAL NUMBER $S_A = 0.124$	

BANK GEOMETRY X_T= 1.34X_L =2.0

BANK DEPTH	3 ROWS
ACOUSTIC FREQUENCY	295 Hz
VELOCITY U (m/s)	S.P.L. (d B)
9.45	104
9.77	116
9.89	126
10.08	144
ACOUSTIC STROUHAL NUMBER S_A=0.145	

BANK DEPTH	3 ROWS
ACOUSTIC FREQUENCY	318 Hz
VELOCITY U (m/s)	S.P.L. (dB)
12.41	104
13.60	124
14.10	124
ACOUSTIC STROUHAL NUMBER S_A=0.115	

BANK DEPTH	3 ROWS
ACOUSTIC FREQUENCY	350 Hz
VELOCITY U (m/s)	S.P.L. (dB)
12.41	110
14.10	110
14.21	150
ACOUSTIC STROUHAL NUMBER S_A=0.119	

BANK GEOMETRY $X_T = 1.34$ $X_L = 2.0$

BANK DEPTH	3 ROWS
ACOUSTIC FREQUENCY	2200 Hz
VELOCITY U (m/s)	S.P.L. (d B)
14.21	---
15.35	128
16.18	132
ACOUSTIC STROUHAL NUMBER $S_A = 0.693$	

BANK DEPTH	3 ROWS
ACOUSTIC FREQUENCY	2600 Hz
VELOCITY U (m/s)	S.P.L. (dB)
15.35	---
16.18	120
ACOUSTIC STROUHAL NUMBER $S_A = 0.775$	

BANK DEPTH	4 ROWS
ACOUSTIC FREQUENCY	290 Hz
VELOCITY U (m/s)	S.P.L. (dB)
8.91	98
10.75	112
11.03	152
ACOUSTIC STROUHAL NUMBER $S_A = 0.129$	

BANK GEOMETRY $X_T = 1.34$ $X_L = 2.0$

BANK DEPTH	4 ROWS
ACOUSTIC FREQUENCY	680 Hz
VELOCITY U (m/s)	S.P.L. (d B)
14.53	112
14.69	114
15.45	136
15.90	142
ACOUSTIC STROUHAL NUMBER $S_A = 0.22$	

BANK DEPTH	4 ROWS
ACOUSTIC FREQUENCY	1900 Hz
VELOCITY U (m/s)	S.P.L. (dB)
12.44	108
12.96	120
14.15	126
14.42	120
14.53	120
ACOUSTIC STROUHAL NUMBER $S_A = 0.677$	

BANK DEPTH	4 ROWS
ACOUSTIC FREQUENCY	2100 Hz
VELOCITY U (m/s)	S.P.L. (dB)
14.42	---
14.53	118
14.69	120
15.45	122
ACOUSTIC STROUHAL NUMBER $S_A = 0.689$	

BANK GEOMETRY $X_T = 1.34 X_L = 2.0$

BANK DEPTH	10 ROWS
ACOUSTIC FREQUENCY	Hz
VELOCITY U (m/s)	S.P.L. (d B)
No Resonance	
ACOUSTIC STROUHAL NUMBER $S_A =$	

BANK DEPTH	15 ROWS
ACOUSTIC FREQUENCY	Hz
VELOCITY U (m/s)	S.P.L. (dB)
No Resonance	
ACOUSTIC STROUHAL NUMBER $S_A =$	

BANK DEPTH	20 ROWS
ACOUSTIC FREQUENCY	Hz
VELOCITY U (m/s)	S.P.L. (dB)
8.91	112
9.16	124
9.61	136
10.01	132
ACOUSTIC STROUHAL NUMBER $S_A = 0.441$	

BANK GEOMETRY $X_T = 1.34$ $X_L = 2.0$

BANK DEPTH	20 ROWS
ACOUSTIC FREQUENCY	980 Hz
VELOCITY U (m/s)	S.P.L. (d B)
10.01	---
10.46	114
10.89	132
ACOUSTIC STROUHAL NUMBER $S_A = 0.446$	

BANK DEPTH	25 ROWS
ACOUSTIC FREQUENCY	660 Hz
VELOCITY U (m/s)	S.P.L. (dB)
7.34	108
7.45	110
7.85	132
8.51	142
ACOUSTIC STROUHAL NUMBER $S_A = 0.416$	

BANK DEPTH	25 ROWS
ACOUSTIC FREQUENCY	820 Hz
VELOCITY U (m/s)	S.P.L. (dB)
8.51	112
9.04	128
9.45	132
9.69	136
ACOUSTIC STROUHAL NUMBER $S_A = 0.450$	

BANK GEOMETRY X_T=1.34 X_L=2.0

BANK DEPTH	35 ROWS
ACOUSTIC FREQUENCY	610 Hz
VELOCITY U (m/s)	S.P.L. (dB)
7.08	----
7.45	120
7.70	128
ACOUSTIC STROUHAL NUMBER S_A= 0.394	

BANK DEPTH	35 ROWS
ACOUSTIC FREQUENCY	680 Hz
VELOCITY U (m/s)	S.P.L. (dB)
7.70	112
7.90	140
8.46	144
ACOUSTIC STROUHAL NUMBER S_A= 0.423	

BANK DEPTH	40 ROWS
ACOUSTIC FREQUENCY	570 Hz
VELOCITY U (m/s)	S.P.L. (dB)
6.33	---
6.74	122
ACOUSTIC STROUHAL NUMBER S_A= 0.408	

BANK GEOMETRY X_T= 1.34X_L= 2.0

BANK DEPTH	40 ROWS
ACOUSTIC FREQUENCY	610 Hz
VELOCITY U (m/s)	S.P.L. (d B)
6.74	---
7.13	130
7.50	132
ACOUSTIC STROUHAL NUMBER S_A=0.419	

BANK DEPTH	40 ROWS
ACOUSTIC FREQUENCY	680 Hz
VELOCITY U (m/s)	S.P.L. (dB)
7.50	108
7.80	134
8.04	144
ACOUSTIC STROUHAL NUMBER S_A=0.428	

BANK DEPTH	ROWS
ACOUSTIC FREQUENCY	Hz
VELOCITY U (m/s)	S.P.L. (dB)
ACOUSTIC STROUHAL NUMBER S_A=	

APPENDIX 2

DAMPING / VELOCITY RESULTS

X_T = 2.0	X_L = 1.67
N = 38 rows	
VELOCITY U_m m/s	Q-FACTOR
0	14.4
5.6	13.6
5.8	12.9
8.2	11.8
9.9	11.3
10.5	13.6
11.9	13.6
12.2	25.8
13.8	17.3
17.0	15.2
18.7	36.9
19.4	36.9

X_T = 2.0 X_L = 1.67	
N = 18 rows	
VELOCITY U_m m/s	Q-FACTOR
0	19.4
2.5	17.0
5.6	18.2
6.6	17.0
7.9	15.1
9.6	18.2
12.9	22.7
15.9	21.0
18.5	21.0
19.4	24.8
20.8	24.8
22.1	38.8
24.3	90.8
25.0	136.0

X_T = 2.0 X_L = 1.67	
N = 8 rows	
VELOCITY U_m m/s	Q-FACTOR
0	56.9
5.0	47.5
7.9	47.5
11.2	71.3
13.9	47.5
15.7	56.9
18.2	47.5
20.0	47.5
22.1	95.2
22.9	72.9
23.9	95.2
24.1	142.9

X_T = 2.0 X_L = 1.67	
N = 43 rows	
VELOCITY U_m m/s	Q-FACTOR
0	18.1
3.0	16.8
5.6	17.5
8.6	17.6
9.9	15.9
11.2	16.2
11.9	16.7
12.4	17.5
13.6	14.6
14.2	16.8
15.4	19.6
15.8	22.1
16.3	21.5
17.2	32.9
18.7	51.3
20.0	64.2
20.7	164.7

X_T = 2.0 X_L = 1.67	
N = 12 rows	
VELOCITY m/s	Q-FACTOR
0	31.6
3.9	28.5
5.0	31.6
6.8	31.6
7.9	28.5
10.8	35.6
12.4	31.6
13.6	31.6
14.0	31.6
15.7	26.0
18.1	31.6
20.1	28.5
21.1	40.8
22.2	47.5
24.2	71.3
25.3	142.5

NORMAL DAMPING FACTOR

X_T = 2.0	X_L = 1.67
N = 12 rows	
VELOCITY U_m m/s	Q-FACTOR
0	31.6
6.6	28.5
9.0	35.6
11.9	28.5
14.2	31.6
17.6	22.0
20.9	23.8
23.6	35.6
26.5	40.8
27.6	47.5
28.3	56.9
29.2	94.8

INCREASED DAMPING FACTOR

APPENDIX 3

EXTRACTION FROM DEN HARTOG ON GALLOPING OF ELECTRIC TRANSMISSION LINES

APPENDIX 3

The following is an extract from "Mechanical Vibrations" by Den Hartog (ref. D1) on the subject of self excited vibrations.

GALLOPING OF ELECTRIC TRANSMISSION LINES

In aerodynamic work it is customary to resolve the total air force on an object into two components:

a. In the direction of the wind (the drag or resistance D).

b. Perpendicular to the wind (the lift L).

These forces can be measured easily with the standard windtunnel apparatus.

Let the diagram illustrated below represent a section moving downward in its vibrational motion so that the wind appears to come from below at an angle $\alpha = \tan^{-1} v/V$.

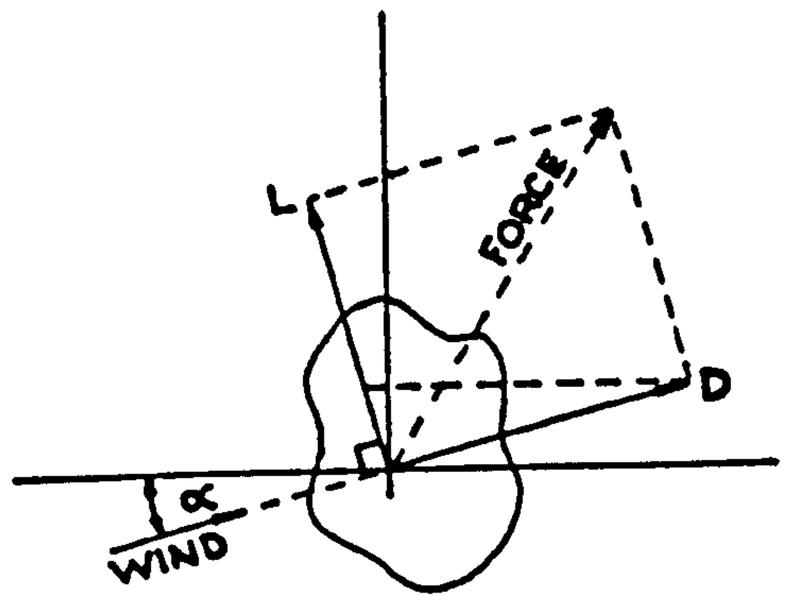

The lift and drag forces L and D have vertical upward components (i.e. components opposite to the direction of the motion) of L cos α and D sin α. The total upward damping force F of the wind is

$$F = L \cos \alpha + D \sin \alpha \qquad (3.1)$$

We are not interested in the force F itself but rather in $dF/d\alpha$, i.e. in the variation of the upward force with a variation in α or in v/V. Assume that F has a large value and that $dF/d\alpha$ is zero. The result would be that part of the weight of the line would not be carried by the towers but by the wind directly. Any vibration or galloping of the line would not change the wind-carried weight ($dF/d\alpha = 0$) so that the vibration would not be affected. On the other hand, assume that $dF/d\alpha$ is negative, which means that the upward wind force increases for negative α and decreases for positive α.Then clearly we have the case of an encouraging alternating force as already explained. The criterion for dynamic stability is

$$\frac{dF}{d\alpha} < 0 \quad \text{(unstable)}$$

and

$$\frac{dF}{d\alpha} > 0 \quad \text{(stable)}$$

In performing the differentiation on (3.1), it is to be noted that, for small vibrations, v is small with respect to V, so that α is a small angle of which the /

the cosine equals unity and the sine is negligible with respect to unity:

$$\frac{dF}{d\alpha} = \frac{dL}{d\alpha}.\cos\ \alpha - L\ \sin\ \alpha\ + \frac{dD}{d\alpha}\ \sin\alpha\ + D\ \cos\alpha$$

$$= \sin\ \alpha\ (-L + \frac{dD}{d\alpha})\ + \cos\ \alpha\ (\frac{dL}{d\alpha} + D)$$

$$\approx \frac{dL}{d\alpha}\ +\ D$$

Thus the system is unstable when

$$\frac{dL}{d\alpha} + D < 0 \qquad (3.2)$$

The values of the lift and drag of an arbitrary cross section cannot be calculated from theory but can be found from a wind-tunnel test. The results of such tests are usually plotted in the form of a diagram such as Fig. 1. In words, (3.2) states that.

A section is dynamically unstable if the negative slope of the lift curve is greater than the ordinate of the drag curve.

In Fig. 1 it is seen that an elongated section is always stable when held "along" the wind ($\alpha = 0$), whereas it is usually unstable when held "across" the wind ($\alpha = 90$ deg.). A transmission line which is being coated with sleet at approximately freezing temperature has the tendency to form icicles that are more or less elongated in a vertical direction, corresponing to $\alpha = 90$ deg. in the diagram.

At this angle, for small amplitudes of vibration (say /

(say varying between 89 and 91 deg.), there is energy input during a cycle. This will increase the amplitude, and the increase will continue so long as there is an excess of energy furnished by the wind. At some large amplitude this excess of energy will become zero so that we have energy balance and reach the final amplitude. In Fig. 1 this will take place presumably at α varying between 30 and 150 deg., say. Near the ends

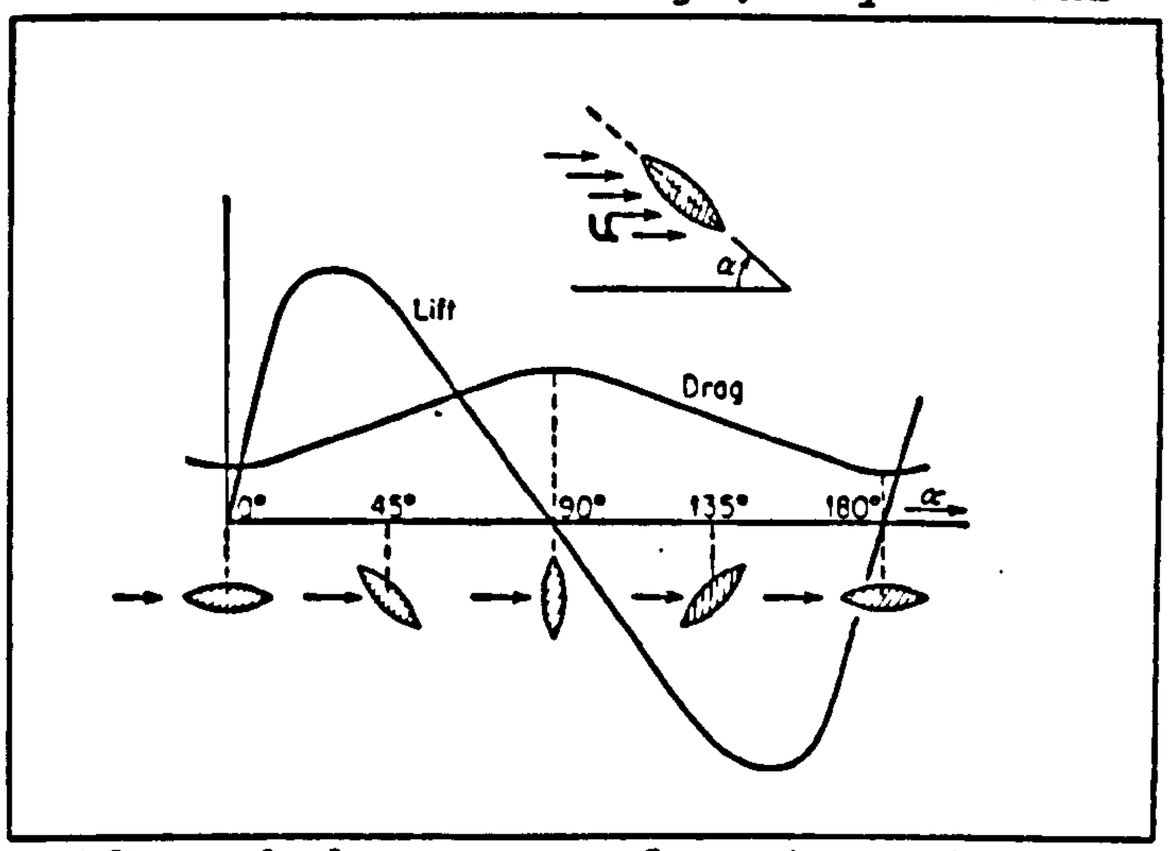

Figure 1 Lift and drag as a function of the angle of attack for an elongated, symmetrical cross section.

of each stroke, energy is put in; but in the middle of the stroke, energy is destroyed by damping, since $\frac{dL}{d\alpha}$ + D is larger than zero at these places (see also Fig. 2). The final amplitude can be found by a process of graphical or numerical integration over the known curve of the diagram, in the manner already indicated.

Thus far in the discussion the system has been assumed to be one of a single degree of freedom, which certainly is not the case with a span of transmission line, of which each point vibrates with a different amplitude /

amplitude (large in the center of the span and small near the towers). Since the wind force is small in comparison to the elastic and inertia forces of the vibration, the form of the motion is the same as if the wind force were absent; in other words, the line vibrates in its first natural mode. The final amplitude can be determined by finding the energy input for the whole span. If for a certain assumed amplitude this energy comes out positive, the amplitude assumed was too small; whereas, if the energy comes out negative (damping), the assumed amplitude was too great. The determination of the energy involves a double graphical integration, first with respect to α for each point of the line and then with respect to the position x along the line. This process is straightforward and involves no difficulties, though it may require much time.

The phenomenon discussed so far is one of very low frequency and large amplitude in the transmission line. It has been observed but rarely, where the weather conditions brought together sleet deposits as well as a lateral wind of considerable strength. There is another case of vibration of transmission lines characterized by high frequency and small amplitude which is much more common and for the occurrence of which only a lateral wind is necessary. The explanation of this phenomenon is found in the so-called "Kármán vortex trail".

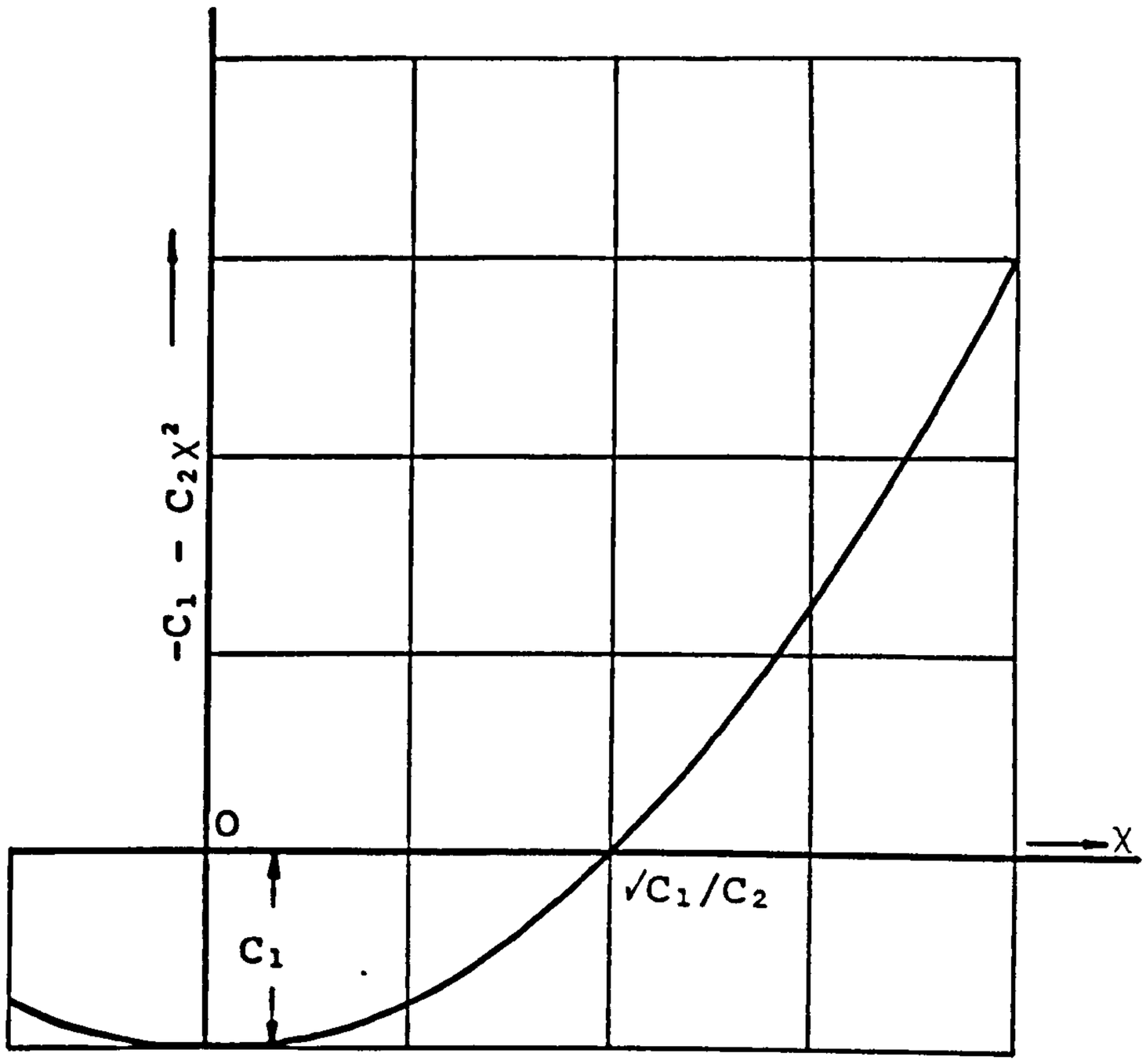

FIGURE 2

A linear vibratory system with negative damping builds up oscillations of infinite amplitude. Of course, this is physically impossible and in all actual systems the damping becomes positive again for sufficiently large amplitudes, thus limiting the motion. The actual relation between the damping coefficient and the amplitude varies from case to case, but for a general understanding it is useful to write down the simplest possible mathematical expression that will make the damping force negative for small amplitudes χ and positive again for larger ones. Such an expression is

$$\text{Damping force} = -(C_1 - C_2\chi^2)$$

The damping coefficient as a function of χ is shown in the diagram above. It is seen that zero damping occurs at an amplitude $\chi = \sqrt{C_1/C_2}$.

APPENDIX 4

THEORY OF THE METHOD FOR INCREASING THE ACOUSTIC DAMPING

APPENDIX 4

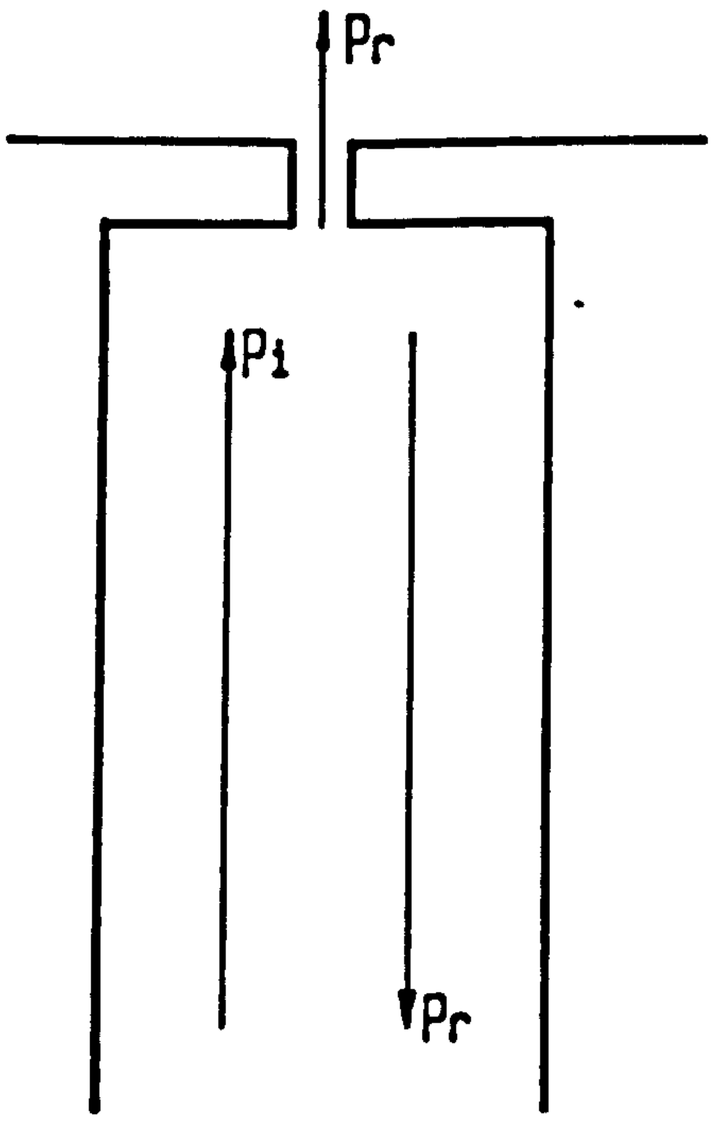

Holes will be bored at each cavity of the bank: so, to simplify the model, we will consider on one cavity only.

S_1 = XSA of wall

S_2 = XSA of hole

c = speed of sound

ρ_o = fluid density

$P_i = Ae^{j(wt - kx)}$

$P_r = Be^{j(wt + kx)}$

$$\text{Volume velocity } Ui = \frac{P_i}{\rho_o\, c/s}$$

$$Ur = \frac{P_r}{\rho_o\, c/s}$$

at any point x, the acoustic impedance $Z = \frac{P}{U}$

$$\text{With both waves present } Zx = \frac{Pi + Pr}{Ui + Ur}$$

$$= \frac{\rho_o\, c}{S_1} \quad \frac{Pi + Pr}{Pi - Pr}$$

$$= \frac{\rho_o c}{S_1} \quad \frac{Ae^{-jkx} + Be^{jkx}}{Ae^{-jkx} - Be^{jkx}}$$

Due to requirements of continuity of pressure and volume velocity, there must be continuity of acoustic impedance at x = 0 acoustic impedance.

Z_o = /

$$Z_o = \frac{\rho_o c}{S} \frac{A + B}{A - B}$$

$$\frac{B}{A} = \frac{Z_o - \rho_o c/s}{Z_o + \rho_o c/s}$$

If we ignore for the moment any wave which may be reflected from what is to be placed on the holes and assume only the single wave Pt exists in the hole. Therefore the acoustic impedance at the origin is $_oc/s_2$

So, since we have continuity of acoustic impedance, we may write:

$$\frac{B}{A} = \frac{\rho_o c/s_2 - \rho_o c/s_1}{\rho_o c/s_2 + \rho_o c/s_1} = \frac{S_1 - S_2}{S_1 + S_2}$$

which is the ratio of magnitudes between the reflected and transmitted wave.

Consider a 10:1 area ratio.

$$\frac{B}{A} = \frac{10 - 1}{10 + 1} = 0.82 \qquad B = 0.82A$$

$$\delta = \frac{1}{n - 1} \log_e \frac{X_I}{X_I + n}$$

$$\delta = \log_e \frac{100}{672}$$

$$\delta = 0.395$$

$$\zeta = \frac{\delta}{2\pi}$$

$$\zeta = 0.063$$

DESIGN CRITERIA FOR FLOW INDUCED VIBRATION IN HEAT EXCHANGERS.

W.B. BRYCE
Research Mechanical Engineering Manager,

B.G. Murray*
Vibration Group Leader,

Babcock and Wilcox (Ops) Ltd.,
Research Division, Renfrew, Scotland.

* Present Address: Robert Gordon's Institute of Technology,
Schoolhill, Aberdeen.

SUMMARY.

This paper describes our practical experiences in the development of design procedures for the avoidance of vortex induced tube vibration and acoustic resonances in heat exchangers. It has become clear that published Strouhal number data forms an inadequate basis for design with results from various sources being quite contradictory. Work carried out recently by the Authors' Company has shown that:

(i) acoustic resonances can occur in heat exchangers at gas velocities well removed from that predicted by the measured Strouhal number.

(ii) the velocity for acoustic resonance appears to depend on the degree of acoustic damping present in the system.

(iii) an alternative explanation offers more promise than vortex shedding to predict the occurrence of acoustic resonance in closely packed heat exchanger banks.

(iv) conversely, tube vibration data appears to correlate well on the basis of a Strouhal number..

On this basis separate correlations are proposed for tube vibration and acoustic phenomena. The acoustic resonance correlation appears to be quite consistent with published data. While most of the published tube vibration data appears fairly consistent, there remains a need for further work to build up a reliable set of Strouhal numbers based directly on tube vibration measurements.

1. INTRODUCTION.

The possibility of damaging flow induced vibration occurring in heat exchangers as a result of vortex shedding has long been recognised. Despite this, there remains a shortage of basic design data for predicting reliably the flow conditions at which vortex induced resonance will occur. The Strouhal number correlations of Chen (1) and Fitzhugh (2) are probably the best available, but even they are contradictory and inconsistent with results from elsewhere. This situation is illustrated in Figure 1 for in line tube banks. Plots of Strouhal number against longitudinal pitch (X_L) are presented for four ranges of transverse pitch (X_T), together with an approximate representation of Fitzhugh's correlation. Data shown (o) is "new" data not used by Fitzhugh in deriving his correlation and has been taken from refs. 3 to 6. Large scatter is evident on the experimental points from closely packed banks of say X_L or X_T less than 2.0.

The discrepancies highlighted in this way appear too large to be explained by experimental errors, nor can they be explained by variations in Reynolds number between experiments and no systematic variation of Strouhal number with transverse pitch can be found within the ranges plotted. Thus, while the Fitzhugh chart probably represents the best summary currently available, it remains unsatisfactory for design purposes.

It is the aim of this paper first to present recent experimental results from the Author's Company and then to show how this may resolve some of the anomalies in published data.

2. EXPERIMENTAL RESULTS.

Figures 2 and 3 illustrate the principal results of a study of the occurrence of acoustic resonances in a variety of model heat exchangers. (The results of this study are reported more fully in ref. (7)). Tests were carried out on a model of a coiled heat exchanger, the essential features of which are shown in the Chart. When exposed to an atmospheric air flow it was found that, as the air velocity was increased to a critical value, a dramatic increase in the SPL was encountered, corresponding to aerodynamic excitation of an acoustic mode. Measurements confirmed that the mode encountered was principally the first annular Bessel mode of the cylindrical cavity, i.e. transverse to the flow direction. When the length of the coil (in the flow direction) was varied, the velocity at which this resonance occurred was found to vary considerably as shown in Figure 2. Thus, as the length of model exposed to gas flow was reduced from 80 tube rows to 40 rows, the velocity at which the first mode was encountered was found to increase by a factor of approximately two. As the row depth was further decreased, the first mode failed to be excited, and resonance first occurred in the second mode of the annular cavity.

When the turbulence spectrum in the bank was examined, a sharp peak was found varying linearly with gas velocity up to the point of onset of acoustic resonance, varying from 0.4 to 0.8 times the acoustic frequency at the onset of velocity.

Figure 3 presents results obtained from similar tests carried out on a cross-inclined bank of straight tubes, illustrating the effect of tube fixity on the onset velocity. The geometry of this bank is again illustrated in the Chart. Two cases are presented. In the first case, with the tubes welded into their tube plates, the first, second and third modes were excited successively as the velocity was increased over the

ranges shown in Figure 3. In the second case where the tubes were simply wedged into the tube plates, the first mode failed to be excited, and the onset velocity for the second mode was slightly higher than in the welded bank.

The significance of these results will be discussed further at a later stage but three conclusions are quite clear from these results.

(i) In the bank geometries studied, it is not possible to characterise the onset of acoustic resonance by a simple Strouhal number as a function of array geometry since the apparent Strouhal number varies as a function of row depth and tube fixity.

(ii) The effective Strouhal number range over which the resonance occurs is quite different from the Strouhal number as determined from turbulence spectra.

(iii) Under certain conditions the fundamental acoustic mode failed to be excited and first resonance is encountered in the second or higher mode.

Finally, it may be noted that although the present results relate to rather specialised geometries (coiled and cross-inclined heat exchanger banks) similar results have been noted for in line banks. Specifically, Bai(4) note the non-equivalence of acoustic and spectral Strouhal numbers and Fitzpatrick (3) noted the variation of effective Strouhal number with the length of the test bank.

A programme of work has also been carried out to determine the flow induced tube vibration characteristics of a bank of identical pitch arrangement to that of Figure 3. This bank was constructed with a few isolated tubes along its length having carefully controlled natural frequency and damping (the natural frequencies of the remaining tubes was kept high such that they may effectively be considered rigid). When this bank was exposed to gas flow, a clear peak was again found in the turbulence spectrum and the value of the Strouhal number calculated on this basis was found to agree well with that found in the earlier work. When the test bank was exposed to high density gas flow (around 25 kg/m3) significant amplitudes of tube vibration were encountered when the vortex frequency was in the vicinity of the natural frequency of the tube. This is illustrated in Figure 4, comparing on a plot of frequency against velocity the frequencies of the turbulence peak and the velocity and frequency at which peak vibration responses were encountered. The coincidence of Strouhal numbers indicated by turbulence spectra and by vibration measurements is quite evident. Moreover, the Strouhal number was found to be constant as gas density and damping was varied over a wide range.

Thus, contrary to the experience with acoustic resonances typified by Figure 2 it is concluded that vortex induced vibration can indeed occur deep in a tube bank and that it is usefully characterised by means of a Strouhal number.

3. DISCUSSION.

Figure 1 showed the uncertainty of Strouhal number data as presently correlated. Figure 5 shows by comparison the corresponding plots when all data pertaining to acoustic resonances has been removed, leaving only

Strouhal numbers obtained directly from tube vibration measurements or via measurements of turbulence spectra. The data comes principally from references 3 to 9. Since Clasen and Gregorig (8) quoted an upper critical Strouhal number corresponding to the velocity at which resonance was first detected rather than the velocity at which peak response occurred, the Strouhal numbers of (8) have been reduced by 20% in Figure 5, this being typically half of the range of velocity over which resonance occurs. On this basis, data from these various sources appears fairly consistent, although clearly sparse. Generally, a Strouhal number close to 0.2 appears to exist over a wide range of geometries, decreasing slightly at the lowest transverse and longitudinal pitches. An exception to this is the practically important range of closely packed geometries where there is considerable scatter on the data. There remains a need for the development of a reliable set of Strouhal numbers based directly on tube vibration measurements.

Figure 6 shows a conservative value of Strouhal number for preliminary design purposes based on Figure 5. Thus, over much of the domain of longitudinal and transverse pitch, a value of 0.2 appears quite appropriate, with a lower value of 0.15 appearing justifiable at the lowest longitudinal or transverse pitches. However, in the practically important range of X_L and X_T less than 1.75, data remains contradictory and the only safe figure on present data would appear to be 0.5. This is unsatisfactory since some evidence suggests this may be pessimistic by a factor of 5. Again the need for more, reliable Strouhal number data in this range is clear.

In section 2 the difficulty of reconciling recent experimental results concerning the onset of acoustic resonances with a simple vortex shedding model was indicated and similarly any attempt to correlate data on this basis of Strouhal number as a function of array geometry will be inadequate. In the following an alternative model of flow induced acoustic resonance is presented which has the merit of accommodating the main features of experimental results and providing a basis on which data can be sensibly correlated. Essentially, the acoustic resonance is considered to occur as a form of instability analogous in principle to the well established Connors instability in the sense that it results from positive feedback of the vibratory motion to the exciting force. In common with most other dynamic instability problems it may be shown that damping plays a crucial role in determining whether or not the instability occurs.

Considering a tube bank at the onset of acoustic instability, there exists an acoustic standing wave in the cavity between tube rows, in a direction transverse to the flow. It appears highly plausible that the interaction of this standing wave with the flow around the tube could deflect the flow as it separates from the tube, for example by changing the angular position of the separation points, resulting in a transverse velocity fluctuation which could oppose or reinforce the local acoustic velocity. Now, such a transverse velocity fluctuation will be carried downstream, across the cavity, by the mean flow, such that at a distance x downstream, the local velocity will lag that at the separation point by a phase angle $\frac{2\pi f x}{u}$ (where u is the mean velocity through the bank and f is the frequency of vibration). Figure 7 illustrates the situation. If a denotes the effective width of the cavity from the separation point to the reattachment point on the downstream tube, then clearly at small values of $\frac{u}{fa}$, the effect of these velocity fluctuations is largely self cancelling. However, at large $\frac{u}{fa}$ the velocity fluctuations approach an in-phase condition and reinforce. Its easily shown that $\frac{u}{fa} = 2$ represents the threshold condition where the net effect changes from negative to positive

By including a model of the flow/acoustic interaction hypothesis above in the one-dimensional wave equation, it may be shown that unstable feedback will, in principle, occur for $u/fa \geq 2$ This value therefore represents a threshold below which acoustic instability cannot occur. Above this threshold, the occurrence of instability is determined by the damping of the acoustic mode in question, although clearly as u/fa is increased, progressively more damping may be overcome as the levels of correlation and hence feedback increase as shown in Figure 7.

Before proceeding to compare this prediction with experimental results, it remains to define the effective width of the cavity "a". Clearly, this must be more than the distance between tubes $X_L - d$ but less than the full longitudinal pitch X_L . In the absence of any better information, a reasonable compromise is $a = X_L - d/2$ which leads to

$$\text{for resonance} \quad u/fd > 2.0(X_L - 0.5) \qquad (1)$$
$$\text{where } X_L = x_L/d$$

Figure 8 compares this prediction with a considerable quantity of data for in-line tube banks. It may be seen that equation (1) does indeed represent a reasonable lower bound to the experimental data over a wide range of X_L. A few points lying outside this bound at high X_L probably result from true vortex shedding. Moreover, the theory is capable of accommodating the effects of row depth and tube fixity noted experimentally. First, the increase in onset velocity with decreasing row depth may be interpreted as being the result of the increased acoustic damping which may be expected in shallow banks. Similarly, the effect of altering tube fixity can easily be explained in terms of resulting changes in acoustic damping. The failure of acoustic modes to be excited can also be accommodated within the theory since it may be shown that there is a critical value of damping above which instability cannot occur at any velocity.

Clearly the theory outlined above is at an early stage of development and more exhaustive testing and refinement must be carried out. It is presented at this time because of the promise shown by this generic type of model in accommodating experimental results and the practical usefulness of the correlation equation (1) as a preliminary design method.

4. CONCLUSIONS.

1. Existing Strouhal number correlations form an inadequate basis for design of in-line heat exchanger geometries since much of the experimental data on which they are based appear quite contradictory.

2. From our practical experience of testing model heat exchangers, supported by other published data, it appears that the Strouhal number characterising the occurrence of acoustic resonances in heat exchangers differs from that characterising tube vibration and cannot be expressed as a function of array geometry alone. For this reason, it appears essential to correlate separately vortex induced tube vibration data and the acoustic phenomena.

3. When considered on this basis, tube vibration data appears fairly consistent although there remains a need for more, reliable Strouhal number measurements based directly on tube vibration measurements, particularly for closely packed banks.

4. Experimental results appear consistent with a model which considers the acoustic phenomena observed to result from a flow/acoustic instability.

5. Thus, it is recommended that separate methods be used for predicting tube vibration and acoustic vibration in closely packed in-line tube banks. For tube vibration, a simple vortex shedding model appears appropriate, using the Strouhal number correlation shown in Figure 6. For acoustic vibration, the instability model will provide a lower velocity limit that vortex shedding over a considerable range of geometries and Figure 8 defines the safe operating range.

REFERENCES

1. Chen, Y.N. — Trans ASME series B 90 p134 (1968)
2. Fitzhugh, J.S. — International Symposium: Vibration Problems in Industry, Keswick (1973)
3. Fitzpatrick, J.H. — Ph.D Thesis Queens University, Belfast (1976)
4. Bai, D — Stress and Materials in Reactor Technology Conf. London (1975)
5. Batham, J.P. — International Symposium: Vibration Problems in Industry, Keswick (1973)
6. Funakawa — " " " "
7. Bryce, W.B, Wharmby, J.S. & Fitzpatrick J.A. — Converence "Vibration in Nuclear Plant" Keswick, (1978)
8. Clasen and Gregorig — Chemie Ing. Tech. 43 p982 (1971)
9. Donaldson, I.S. & McKnight, W — To be published ASME Symposium San Francisco (1979)

HEAT EXCHANGER - FLOW INDUCED VIBRATION

PROBLEM How to design heat exchangers to avoid vortex induced vibration - published data are contradictory and incomplete.

GEOMETRY Helically coiled and straight tubed heat exchangers with closely pitched arrays of tubes.

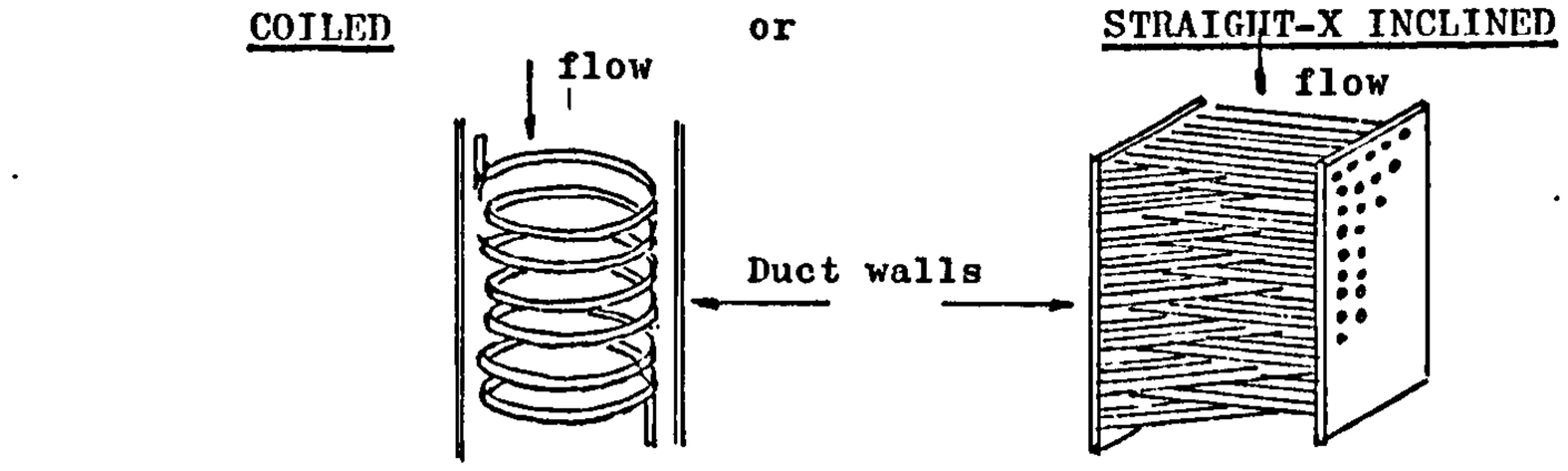

TUBE VIBRATION AND DUCT ACOUSTIC RESONANCES SHOULD BE CONSIDERED SEPARATELY

1. 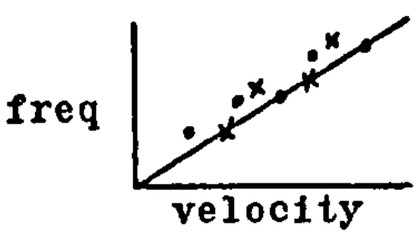

Vortex shedding drives tubes if frequencies match

Vortex frequency measured by hot wires
Tube response measured by accelerometers

2. 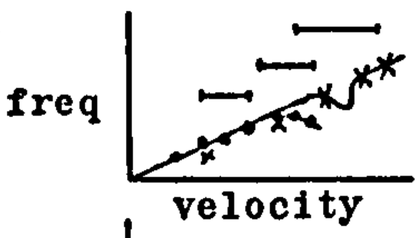

Acoustic resonances occur independently of vortex shedding

——Ranges of acoustic resonances
• Vortex shedding frequencies

3. 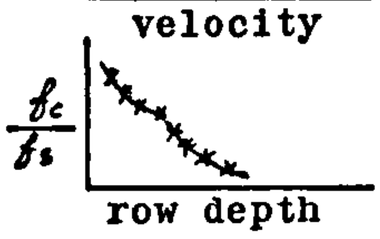

f_c is cavity resonant frequency
f_s is strouhal frequency measured by hot wires

2. and 3. demonstrate that STROUHAL NUMBERS deduced from acoustic responses are dependent on ACOUSTIC DAMPING and TUBE ROW DEPTH and are therefore inappropriate for generalisation.

DESIGN RECOMMENDATIONS

1. To avoid acoustic resonances

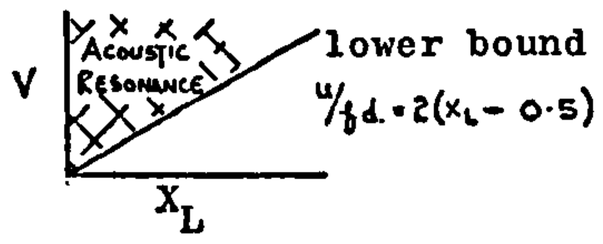

2. To deduce STROUHAL NUMBER for tube excitation

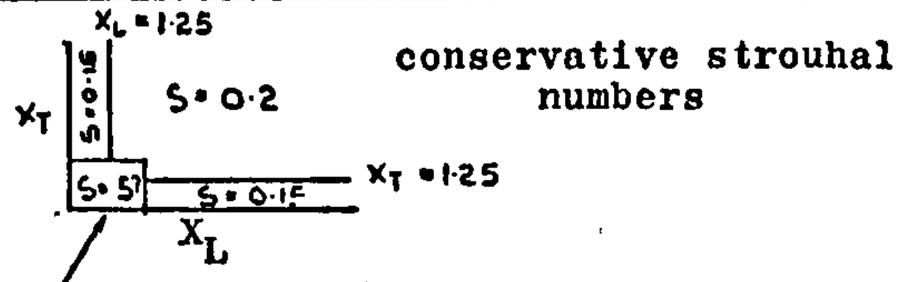

conservative strouhal numbers

more data required particularly here

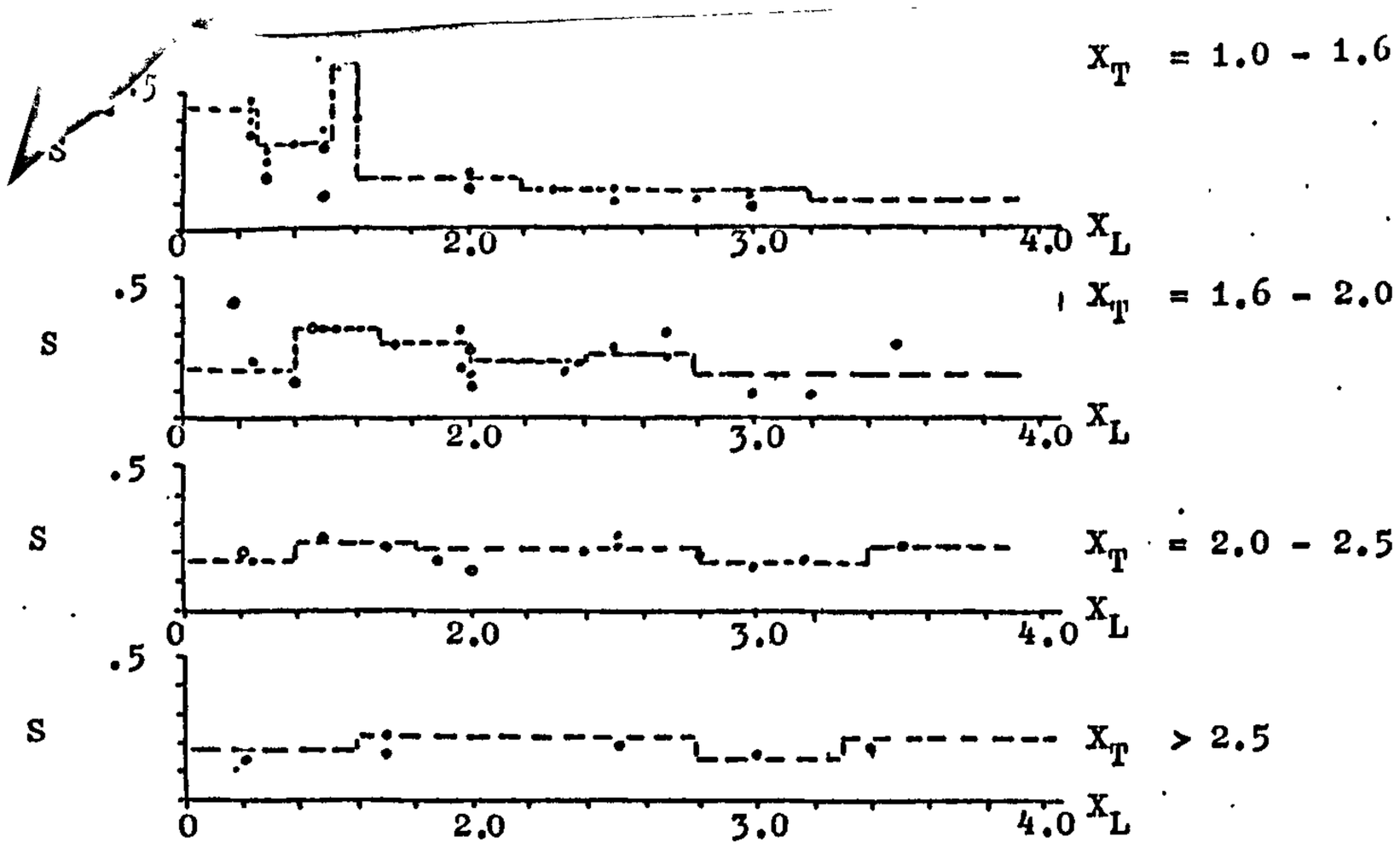

STROUHAL NUMBERS BASED ON ACOUSTIC AND TUBE RESPONSES

FIG.1

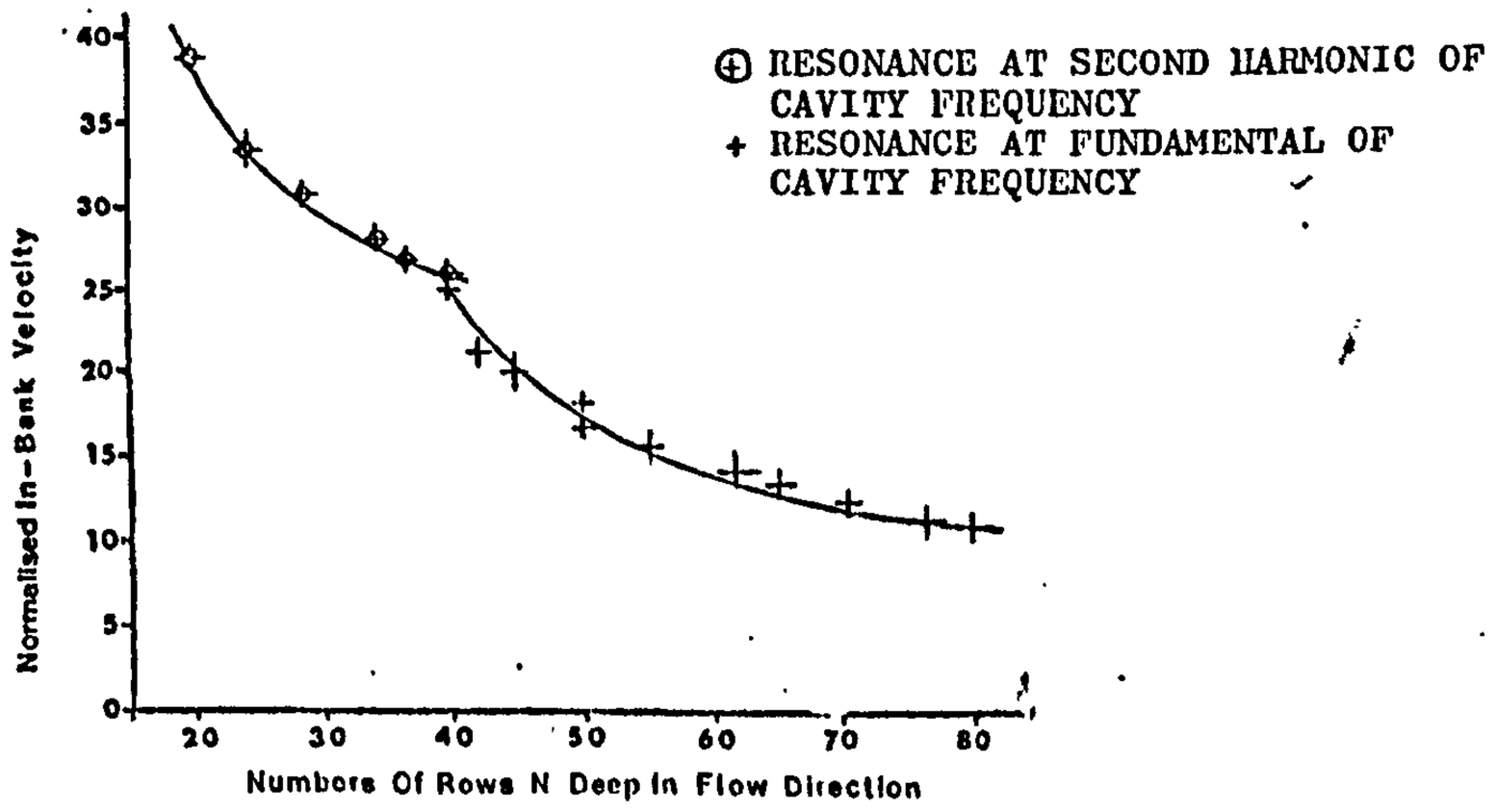

EFFECT OF ROW DEPTH ON VELOCITY TO EXCITE ACOUSTIC RESONANCE IN COILED HEAT EXCHANGER BANK

FIG.2

SERIES 2 - Tube ends wedged
SERIES 1 - Tube ends welded
——— Acoustic Resonant Zones

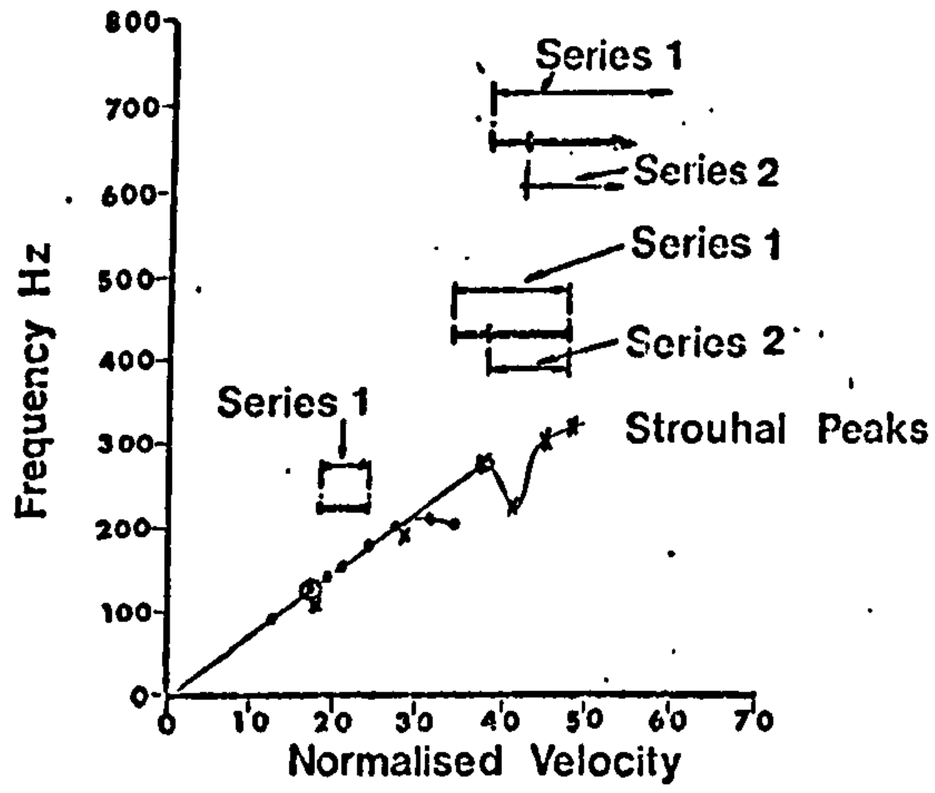

STROUHAL LINE AND ACOUSTIC RESONANCE ZONES FOR STRAIGHT TUBES BUNDLE WITH VARIOUS TUBE FIXINGS

FIG. 3

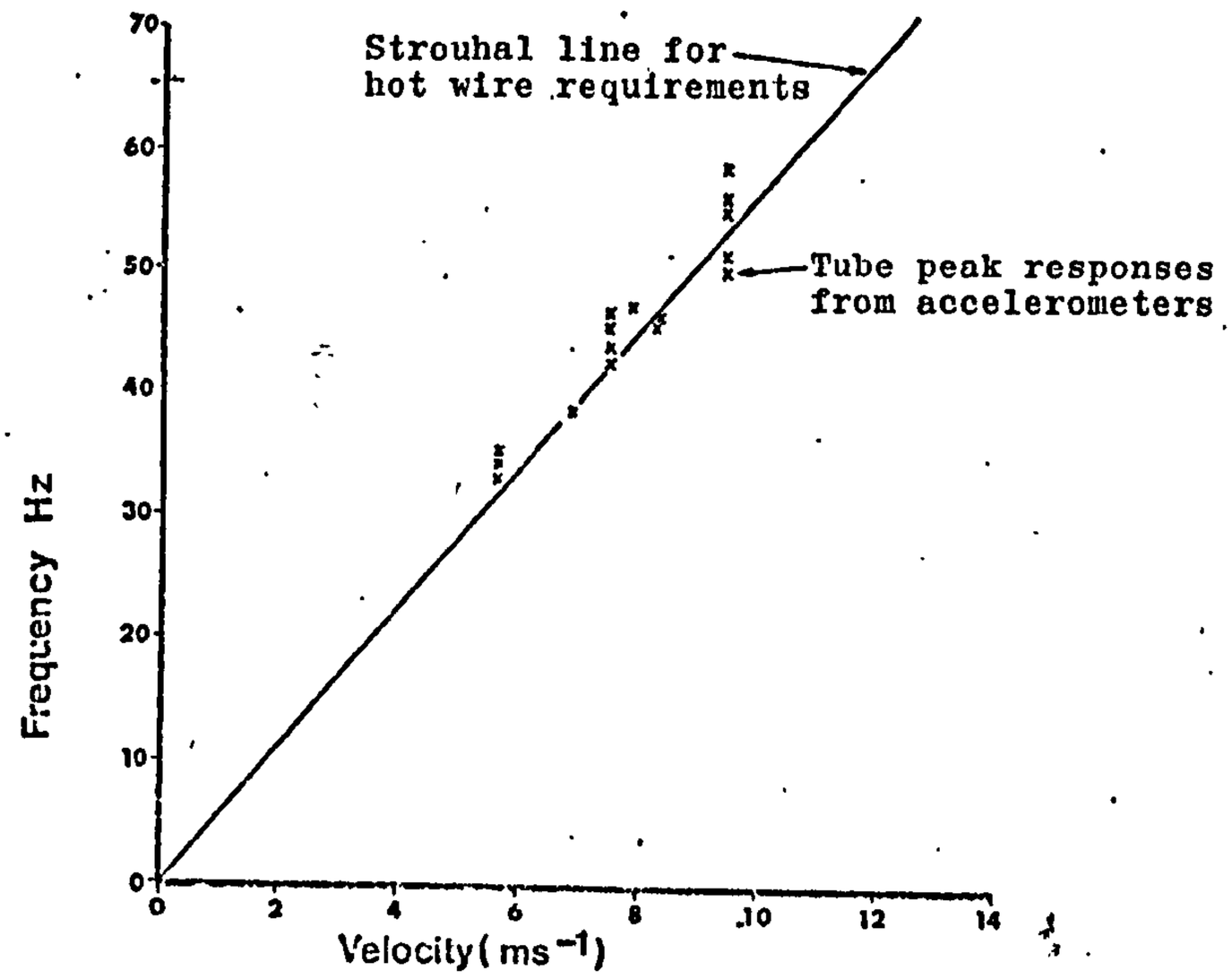

EQUIVALENCE OF HOT WIRE AND TUBE RESPONSES

FIG. 4

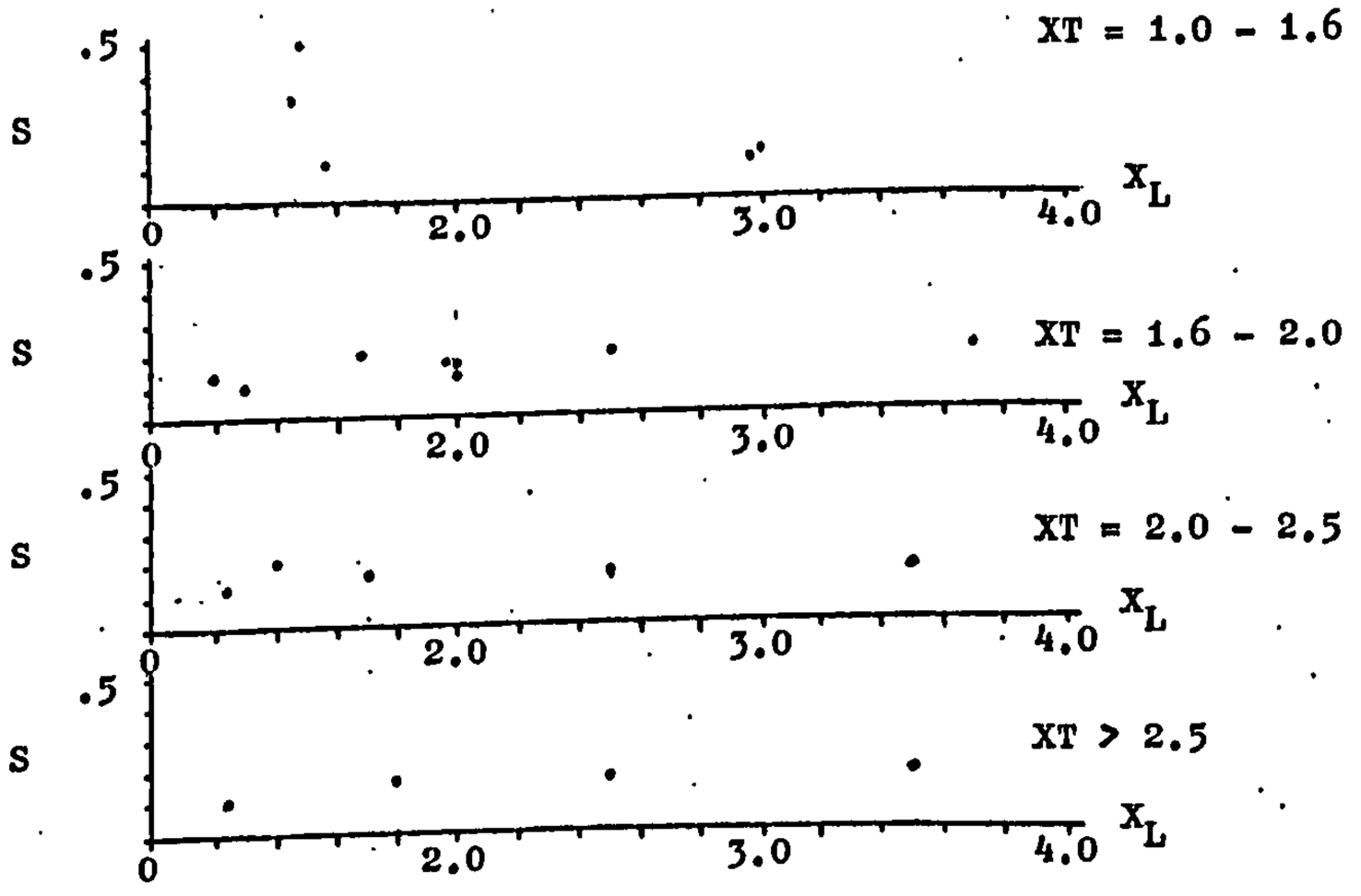

STROUHAL NUMBERS BASED ON TUBE AND HOT WIRE RESPONSES

FIG. 5

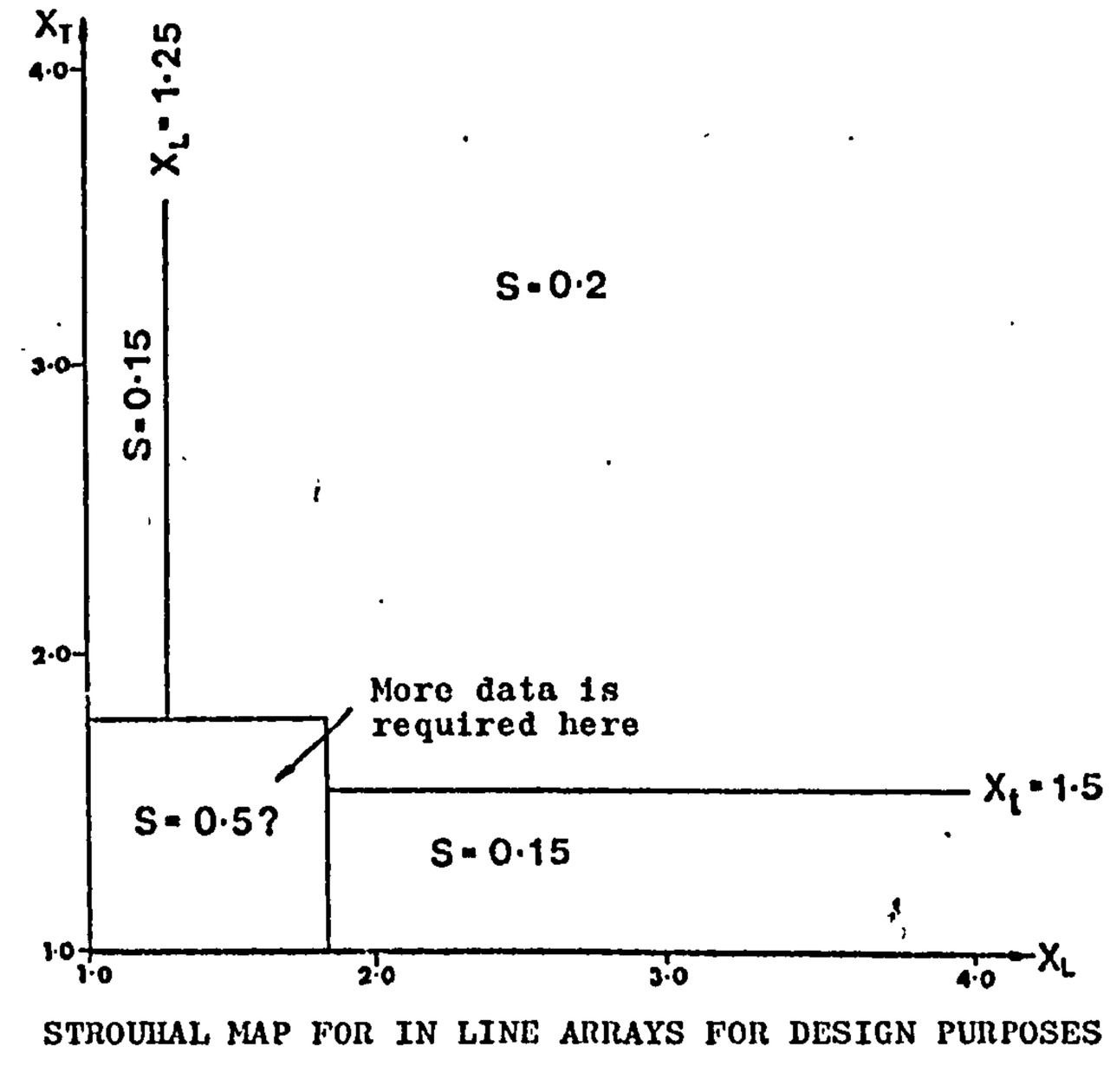

STROUHAL MAP FOR IN LINE ARRAYS FOR DESIGN PURPOSES

FIG. 6

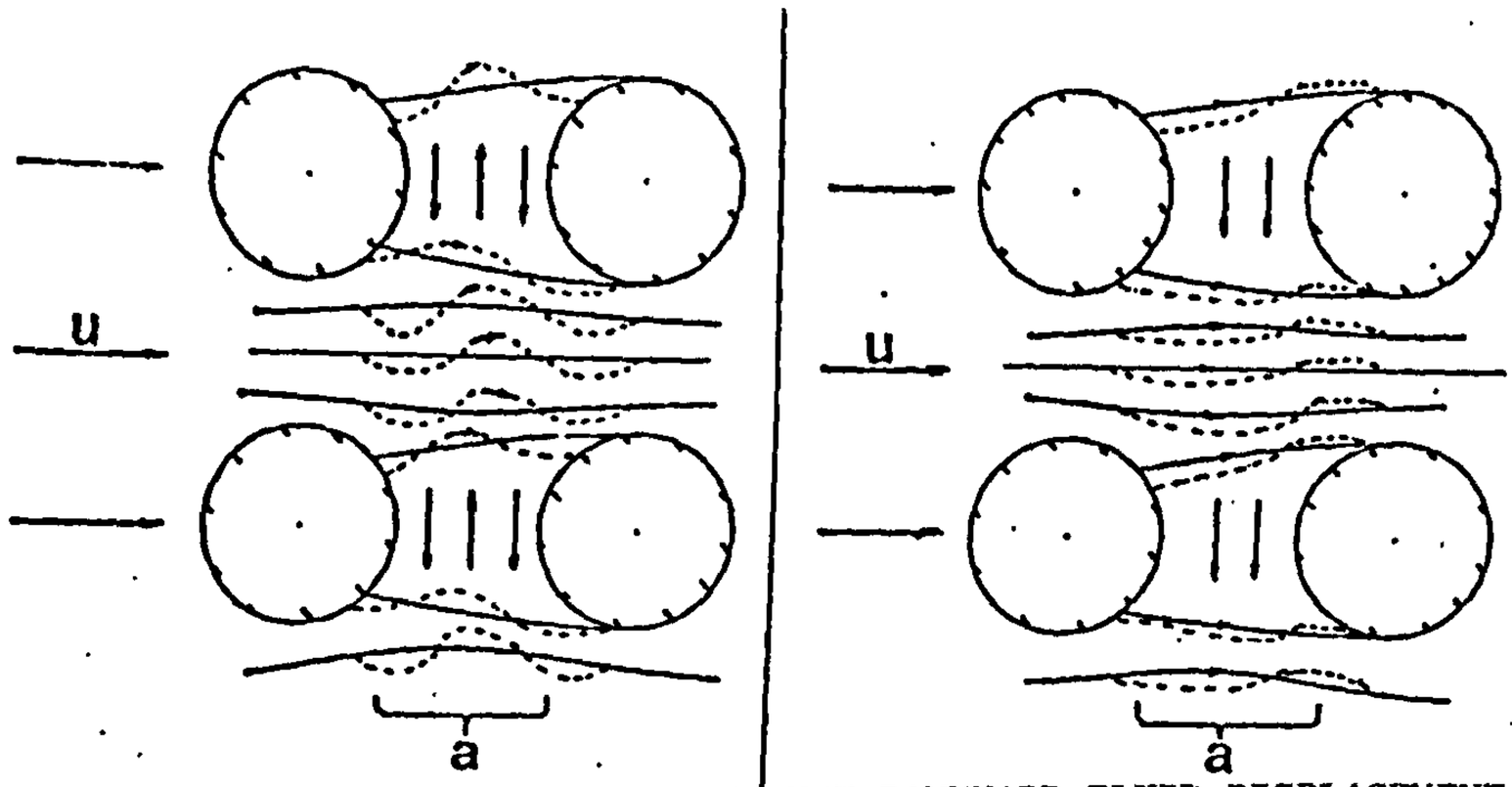

LITTLE OR NO NET FLUID DISPLACEMENT

Low Velocity $\frac{u}{a} = f$

Velocity fluctuation a distance X downstream to that leaving the separation point x/u ago. This phase shift across cavity causes cancellation of local velocity fluctuations

NET DOWNWARD FLUID DISPLACEMENT

High Velocity $\frac{u}{a} > f$

Transverse velocity fluctuations in phase across the cavity width.

——— Notional time averages streamlines
– – – -Instantaneous streamlines

NOTIONAL FLOW PATTERNS

FIG. 7

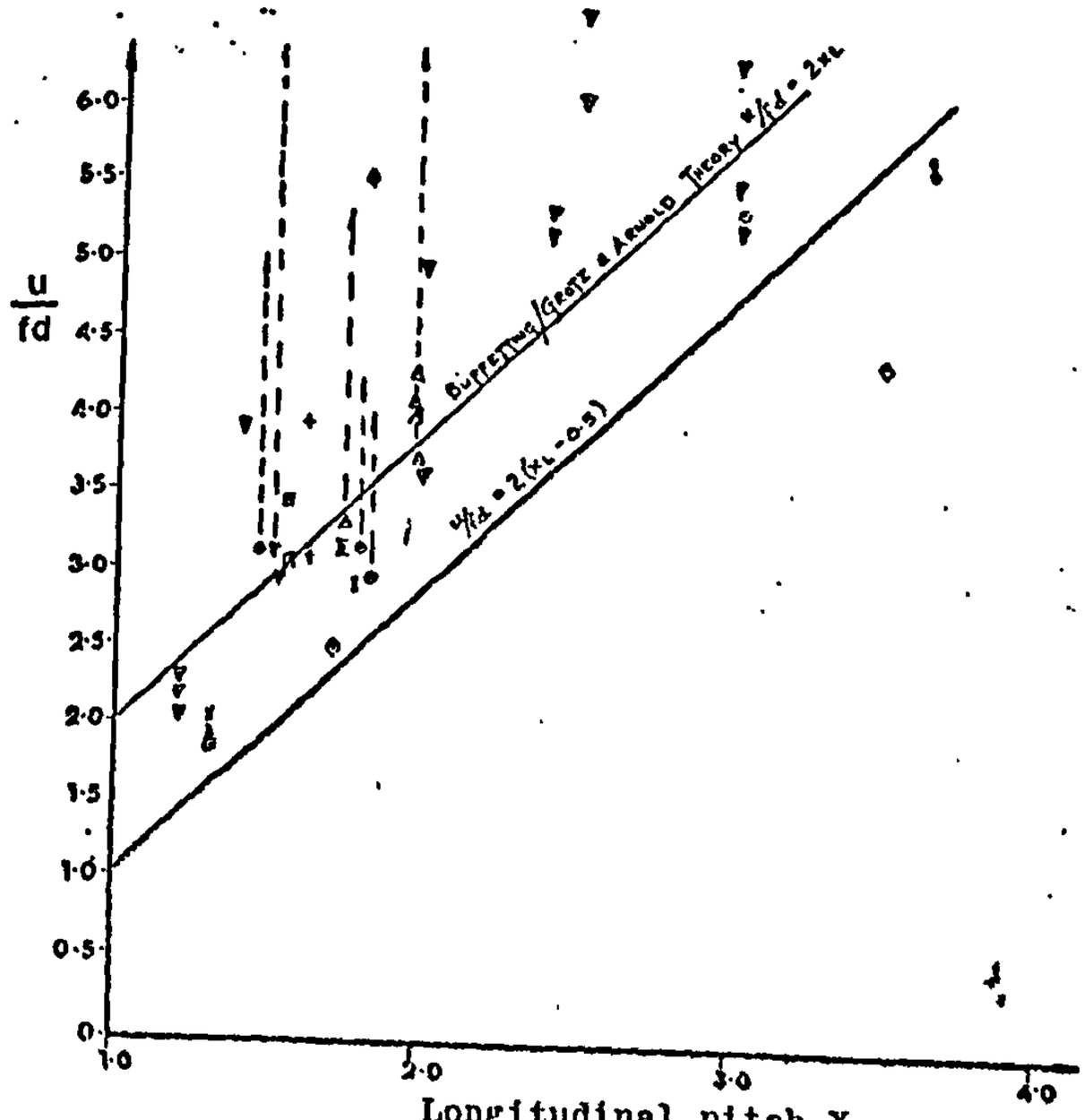

FIG. 8

LOWER BOUND CORRELATION TO AVOID FLOW INDUCED ACOUSTIC RESONANCES